

Targeted tumor cell elimination by redirecting  
vaccination-induced CD8<sup>+</sup> T cells in vivo with novel  
bifunctional peptide-MHC class I-IgG antibody fusions

von Cornelia Gertrud Fischer

Inaugural-Dissertation zur Erlangung der Doktorwürde  
der Tierärztlichen Fakultät der Ludwig-Maximilians-Universität  
München

Targeted tumor cell elimination by redirecting  
vaccination-induced CD8<sup>+</sup> T cells in vivo with novel  
bifunctional peptide-MHC class I-IgG antibody fusions

von Cornelia Gertrud Fischer

aus Regensburg

München 2017

Aus dem Veterinärwissenschaftlichen Department der Tierärztlichen Fakultät  
der Ludwig-Maximilians-Universität München

Lehrstuhl für Molekulare Tierzucht und Biotechnologie

Arbeit angefertigt unter der Leitung von: Univ.-Prof. Dr. Eckhard Wolf

Angefertigt bei: Roche Diagnostics GmbH  
Mentor: Dr. Hendrik Knötgen

**Gedruckt mit Genehmigung der Tierärztlichen Fakultät  
der Ludwig-Maximilians Universität München**

**Dekan:** Univ.-Prof. Dr. Joachim Braun

**Berichterstatter:** Univ.-Prof. Dr. Eckhard Wolf

**Korreferent/en:** Univ.-Prof. Dr. Heidrun Potschka

**Tag der Promotion:** 11. Februar 2017

Für meine Eltern

in Dankbarkeit

# TABLE OF CONTENTS

<b>1</b>	<b>LIST OF TABLES AND FIGURES .....</b>	<b>10</b>
1.1	TABLES.....	10
1.2	FIGURES .....	11
<b>2</b>	<b>ABBREVIATIONS .....</b>	<b>12</b>
<b>3</b>	<b>SUMMARY .....</b>	<b>17</b>
<b>4</b>	<b>ZUSAMMENFASSUNG .....</b>	<b>19</b>
<b>5</b>	<b>INTRODUCTION .....</b>	<b>21</b>
5.1	CHARACTERISTICS AND STRATEGIES OF CANCER DEVELOPMENT .....	21
5.2	THE INNATE AND ADAPTIVE IMMUNE SYSTEM.....	24
5.3	CANCER IMMUNOEDITING AND IMMUNE ESCAPE MECHANISMS OF TUMORS .....	27
5.4	DIFFERENT APPROACHES IN CANCER IMMUNOTHERAPY .....	29
5.5	AIM OF THE STUDY .....	31
<b>6</b>	<b>MATERIAL.....</b>	<b>34</b>
6.1	LABORATORY EQUIPMENT .....	34
6.1.1	<i>Devices .....</i>	<i>34</i>
6.1.2	<i>Consumables .....</i>	<i>35</i>
6.1.3	<i>Chemicals .....</i>	<i>36</i>
6.2	MATERIALS FOR DIFFERENT PROCEDURES.....	36
6.2.1	<i>Molecular biological procedures.....</i>	<i>36</i>
6.2.2	<i>Transfection of production cell line and protein purification.....</i>	<i>37</i>
6.2.3	<i>Cells, media, supplements and antibiotics for cell culture .....</i>	<i>37</i>
6.2.4	<i>In vivo procedures .....</i>	<i>39</i>
6.2.5	<i>Quantitative real-time polymerase chain reaction .....</i>	<i>40</i>
6.2.6	<i>Flow cytometry .....</i>	<i>40</i>
6.2.7	<i>Immunohistochemistry and ultramicroscopy.....</i>	<i>43</i>
<b>7</b>	<b>METHODS .....</b>	<b>44</b>
7.1	DESIGN AND CONSTRUCTION OF SURROGATE FUSION MOLECULES AND ANTIBODIES .....	44
7.1.1	<i>DNA expression vector construction .....</i>	<i>44</i>
7.1.2	<i>Restriction enzyme DNA fragmentation .....</i>	<i>44</i>
7.1.3	<i>Agarose gel electrophoresis .....</i>	<i>45</i>

7.1.4	<i>Agarose gel extraction of DNA</i> .....	45
7.1.5	<i>Dephosphorylation of vector fragments</i> .....	45
7.1.6	<i>Ligation of DNA fragments</i> .....	45
7.1.7	<i>Bacterial transformation</i> .....	46
7.1.8	<i>Plasmid DNA isolation and further proliferation</i> .....	46
7.1.9	<i>DNA purification by ethanol precipitation</i> .....	47
7.1.10	<i>Transient transfection of HEK293-F cells</i> .....	47
7.1.11	<i>Protein purification</i> .....	48
7.1.12	<i>Protein fusion by enzymatic sortase coupling</i> .....	48
7.2	CELL CULTURE TECHNIQUES.....	49
7.2.1	<i>Cell culture conditions</i> .....	49
7.2.2	<i>Thawing, subculturing and freezing of cells</i> .....	50
7.2.3	<i>Cell counting</i> .....	51
7.2.4	<i>Development and maturation of bone marrow-derived dendritic cells</i> .....	51
7.2.5	<i>Peptide-loading of cells</i> .....	51
7.2.5.1	Bone marrow-derived dendritic cells.....	51
7.2.5.2	Splenocytes.....	52
7.2.5.3	Tumor cells.....	52
7.3	IN VIVO PROCEDURES.....	52
7.3.1	<i>General modalities</i> .....	52
7.3.1.1	Animal facility.....	52
7.3.1.2	Laboratory animals.....	53
7.3.1.3	Anesthesia of mice.....	53
7.3.1.4	Euthanasia of mice.....	54
7.3.2	<i>Vaccination methods</i> .....	54
7.3.2.1	Vaccination with peptide-loaded, bone marrow-derived dendritic cells.....	54
7.3.2.2	DNA vaccination with electroporation.....	55
7.3.2.3	XCR1-targeted vaccination.....	56
7.3.3	<i>Tumor models</i> .....	57
7.3.3.1	Experimental lung metastasis model.....	57
7.3.3.2	Subcutaneous tumor model.....	58
7.3.3.3	Treatment with fusion molecules.....	58
7.3.4	<i>Harvest of sample material</i> .....	59
7.3.4.1	Blood sampling and preparation of blood samples.....	59
7.3.4.2	Harvest of organs and tissue.....	59
7.3.4.2.1	Harvest and processing of spleens.....	59
7.3.4.2.2	Harvest and processing of lungs.....	60

7.3.4.2.3	Harvest and processing of tumors .....	60
7.3.4.2.4	Harvest and processing of bone marrow .....	61
7.4	EX VIVO PROCEDURES.....	61
7.4.1	<i>Quantitative real-time polymerase chain reaction for evaluation of lung metastasis burden</i> .....	61
7.4.1.1	RNA isolation .....	62
7.4.1.2	Reverse transcription of RNA.....	62
7.4.1.3	Quantitative real-time polymerase chain reaction (qPCR) .....	63
7.4.1.4	Evaluation of qPCR.....	64
7.4.2	<i>Flow cytometry analyses</i> .....	65
7.4.2.1	Settings of flow cytometry.....	65
7.4.2.2	Preparation of samples for flow cytometry .....	65
7.4.2.3	Detection, quantification and characterization of specific CD8 <sup>+</sup> T cells.....	66
7.4.2.4	Confirmation of peptide-loading of cells .....	67
7.4.2.5	IFN- $\gamma$ activation of CD8 <sup>+</sup> T cells .....	67
7.4.2.6	Internalization and binding of fusion molecules to the target FAP.....	67
7.4.2.7	Confirmation of binding of fusion molecules after labelling.....	68
7.4.2.8	Detection of PD-L1 expression in tumors .....	68
7.4.3	<i>Immunohistochemistry</i> .....	68
7.4.3.1	Sample preparation .....	68
7.4.3.2	Target expression of tumor cells in vivo .....	69
7.4.3.3	Quantification of CD8 <sup>+</sup> T cells in the tumor .....	69
7.4.4	<i>Ultramicroscopy</i> .....	70
7.4.4.1	Treatment of animals and processing of tumors .....	70
7.4.4.2	Acquisition and quantification of labelled molecule in the tumors.....	70
7.4.4.3	Immunohistochemistry of ultramicroscopy samples.....	71
7.5	IN VITRO PROCEDURES.....	71
7.5.1	<i>Cytotoxicity analysis</i> .....	71
7.5.1.1	xCELLigence assay .....	71
7.5.1.2	Evaluation of cytotoxicity mediated by fusion molecules in the xCELLigence system .....	72
7.5.2	<i>IFN-<math>\gamma</math> activation of CD8<sup>+</sup> T cells</i> .....	73
7.6	STATISTICAL ANALYSES.....	73
<b>8</b>	<b>RESULTS</b> .....	<b>74</b>
8.1	CHARACTERIZATION OF SURROGATE FUSION MOLECULES AND ANTIBODIES.....	74
8.1.1	<i>Structure of peptide-MHC class I-antibody (pMHCI-IgG) fusion proteins</i> .....	74
8.1.1.1	Design of the molecule and transfection vectors .....	74
8.1.1.2	Disulfide-stabilization of the peptide-MHC class I complex in the fusion molecule .....	75
8.1.1.3	Modifications of the molecule for increased harvest of protein .....	75

8.1.1.4	Introduction of a silent Fc-part .....	76
8.1.1.5	Specifications of the molecules .....	76
8.1.2	<i>Structure of the T cell bispecific (TCB) antibody</i> .....	77
8.1.2.1	Design and modifications of the molecule.....	77
8.1.2.2	Design of transfection vectors .....	78
8.1.2.3	Specifications of the molecule .....	78
8.1.3	<i>Structure of the anti-mouse XCR1 antibody</i> .....	79
8.1.3.1	Design of the molecule and transfection vectors .....	79
8.1.3.2	Specification of molecules .....	80
8.1.4	<i>Yield and purity of recombinant proteins</i> .....	80
8.2	IN VITRO EVALUATION OF SURROGATE PEPTIDE–MHC CLASS I-ANTIBODY FUSION MOLECULES.....	81
8.2.1	<i>Binding of molecules to their target FAP</i> .....	81
8.2.2	<i>In vitro IFN-<math>\gamma</math> activation of CD8<sup>+</sup> T cells mediated by compounds</i> .....	84
8.2.3	<i>In vitro cytotoxicity mediated by compounds</i> .....	86
8.3	COMPARISON OF DIFFERENT VACCINATION METHODS FOR GENERATION OF EFFECTOR CELLS IN MICE.....	89
8.3.1	<i>Vaccination with peptide-loaded, bone marrow-derived dendritic cells</i> .....	90
8.3.2	<i>DNA vaccination with electroporation</i> .....	91
8.3.3	<i>XCR1-targeted vaccination</i> .....	92
8.3.4	<i>Comparison of vaccination methods</i> .....	92
8.4	IN VIVO EFFICACY EVALUATION OF SURROGATE PEPTIDE–MHC CLASS I-ANTIBODY FUSION MOLECULES.....	95
8.4.1	<i>Experimental lung metastasis model</i> .....	95
8.4.1.1	Anti-tumor efficacy of molecules in the experimental lung metastasis model.....	95
8.4.1.1.1	Preventive treatment setting.....	95
8.4.1.1.2	Therapeutic treatment setting.....	98
8.4.1.2	FAP expression in B16 lung metastases .....	106
8.4.2	<i>Solid subcutaneous tumor model</i> .....	108
8.4.2.1	Anti-tumor efficacy of molecules in the solid subcutaneous tumor model .....	108
8.4.2.2	FAP expression in MC38 tumors .....	110
8.4.2.3	Penetration of the MCMV m38-MHCI-IgG fusion molecule into tumors.....	112
8.4.2.4	Infiltration of tumors with CD8 <sup>+</sup> T cells .....	114
8.4.2.5	Characterization of T cells in tumors and blood .....	116
8.4.2.6	PD-L1 expression in tumors .....	118
<b>9</b>	<b>DISCUSSION</b> .....	<b>119</b>
9.1	COMPARISON OF DIFFERENT VACCINATION METHODS FOR GENERATION OF EFFECTOR CELLS IN MICE.....	119
9.2	COMPARISON OF PEPTIDE-MHC CLASS I-ANTIBODY FUSION MOLECULES WITH OTHER PEPTIDE- MHC CLASS I-RETARGETING MOLECULES.....	124

9.3	IN VITRO EVALUATION OF PEPTIDE-MHC CLASS I-ANTIBODY FUSION MOLECULES .....	127
9.4	IN VIVO EVALUATION OF PEPTIDE-MHC CLASS I-ANTIBODY FUSION MOLECULES.....	131
9.4.1	<i>Experimental lung metastasis model</i> .....	131
9.4.2	<i>Solid subcutaneous tumor model</i> .....	134
9.5	COMPARISON OF PEPTIDE-MHC CLASS I-ANTIBODY FUSION MOLECULES WITH CD3-BASED T CELL ENGAGERS .....	141
<b>10</b>	<b>REFERENCES.....</b>	<b>144</b>
<b>11</b>	<b>APPENDIX .....</b>	<b>154</b>
<b>12</b>	<b>DANKSAGUNG .....</b>	<b>159</b>

# 1 LIST OF TABLES AND FIGURES

## 1.1 TABLES

<b>Table 6.1:</b> Cell lines .....	38
<b>Table 6.2:</b> Cell culture media .....	39
<b>Table 6.3:</b> Primer for qPCR.....	40
<b>Table 6.4:</b> Primary antibodies for flow cytometry.....	41
<b>Table 6.5:</b> Dextramers for flow cytometry.....	42
<b>Table 6.6:</b> Secondary antibodies for flow cytometry.....	42
<b>Table 6.7:</b> Isotype control antibodies for flow cytometry .....	42
<b>Table 6.8:</b> Primary antibodies for immunohistochemistry .....	43
<b>Table 6.9:</b> Secondary antibodies for immunohistochemistry.....	43
<b>Table 7.1:</b> Injections of peptide-loaded dendritic cells.....	54
<b>Table 7.2:</b> Electric pulses for electroporation.....	55
<b>Table 7.3:</b> Steps of XCR1-targeted vaccination.....	57
<b>Table 7.4:</b> Reverse transcription protocol .....	63
<b>Table 7.5:</b> Reverse transcription reaction mix.....	63
<b>Table 7.6:</b> qPCR reaction mix .....	64
<b>Table 7.7:</b> qPCR protocol .....	64
<b>Table 8.1:</b> Classification of groups and treatment schedule in the experimental lung metastasis model. ....	102
<b>Table 8.2:</b> Classification of groups and treatment schedule in the solid subcutaneous tumor model. ....	110

## 1.2 FIGURES

<b>Figure 5.1:</b> Mechanism of action for peptide-MHC class I-IgG fusion molecules.....	33
<b>Figure 8.1:</b> Schematic illustration of the peptide-MHC class I-IgG fusion molecules.....	77
<b>Figure 8.2:</b> Schematic illustration of the T cell bispecific IgG. ....	79
<b>Figure 8.3:</b> Schematic illustration of the sortase-tagged anti-XCR1 antibody.....	80
<b>Figure 8.4:</b> Binding of pMHCI-IgG and TCB molecules and delivery of pMHCI complexes to the tumor cell surface .....	83
<b>Figure 8.5:</b> In vitro IFN- $\gamma$ activation of CD8 <sup>+</sup> T cells mediated by pMHCI-IgG and TCB molecules.....	86
<b>Figure 8.6:</b> In vitro cytotoxicity mediated by pMHCI-IgG and TBC molecules.....	89
<b>Figure 8.7:</b> Flow cytometry analysis of blood for detection and quantification of specific CD8 <sup>+</sup> T cells.....	90
<b>Figure 8.8:</b> CD8 <sup>+</sup> T cell responses in the blood after application of different vaccination methods. .	94
<b>Figure 8.9:</b> Time line for the experimental lung metastasis model. ....	101
<b>Figure 8.10:</b> Assessment of metastasis burden after preventive treatment of experimental lung metastases. ....	103
<b>Figure 8.11:</b> Assessment of metastasis burden after therapeutic treatment of experimental lung metastases. ....	106
<b>Figure 8.12:</b> FAP expression of experimental lung metastases. ....	107
<b>Figure 8.13:</b> Time line for the solid subcutaneous tumor model. ....	109
<b>Figure 8.14:</b> Growth kinetics of solid subcutaneous tumors after treatment with pMHCI-IgG or TCB molecules. ....	110
<b>Figure 8.15:</b> FAP expression of solid subcutaneous tumors. ....	111
<b>Figure 8.16:</b> Tumor penetration and accumulation of pMHCI-IgG molecules. ....	113
<b>Figure 8.17:</b> CD8 <sup>+</sup> T cell infiltration in the tumors. ....	115
<b>Figure 8.18:</b> Characterization of T cells in tumors and blood. ....	117
<b>Figure 8.19:</b> PD-L1 expression in tumors escaping therapy.....	118

## 2 ABBREVIATIONS

3D	Three-dimensional
4-1BB	Tumor necrosis factor receptor superfamily member 9 (TNFRSF9)
AAALAC	Association for Assessment and Accreditation of Laboratory Animal Care
Ab	Antibody
ADAS	“Antigen dependent amplification system” (XCR1-targeted vaccination)
ADCC	Antibody-dependent cellular cytotoxicity
ADCP	Antibody-dependent cellular phagocytosis
Amp <sup>+</sup>	Containing ampicillin
APC	Allophycocyanin
APC	Antigen presenting cell
BCR	B cell receptor
BGHpA	Bovine growth hormone polyadenylation
BiTE	Bispecific T cell engager
bp	Base pairs
C1q	Protein complex of the complement system
C57BL/6N(Crl)	Immunocompetent mouse strain
CAR	Chimeric antigen receptor
CCR4	C-C chemokine receptor type 4
CD	Cluster of differentiation
CDC	Complement-dependent cellular cytotoxicity
cDNA	Complementary desoxyribonucleic acid
CDR3	Complementarity-determining region 3
CEA	Carcinoembryonic antigen
CH	Constant domain of the antibody heavy chain
CMV	Cytomegalovirus
CO <sub>2</sub>	Carbon dioxide
CP	Crossing point
CpG ODN	CpG oligodeoxynucleotides

CSC	Cancer stem cell
CTL	Cytotoxic T lymphocytes
CTLA-4	Cytotoxic T lymphocyte-associated protein 4
cxIL-2	Complexed interleukin-2
Ck	Constant domain of the antibody light chain
DAPI	4',6-diamidin-2-phenylindol
DC	Dendritic cell
DICOM	Digital Imaging and Communications in Medicine
DMSO	Dimethyl sulfoxide
DNA	Desoxyribonucleic acid
dsRNA	Double-stranded ribonucleic acid
E:T	Effector to target
EDIM/MRV	Mouse Rotavirus
EDTA	Ethylenediaminetetraacetic acid
ELISA	Enzyme-linked immunosorbent assay
EpCAM	Epithelial cell adhesion molecule
Fab'	Fragment antigen binding
FAP	Fibroblast activation protein
FasL	Fas ligand
FasR	Fas receptor
Fc	Fragment crystallizable
FcRn	Neonatal Fc-receptor
FCS	Fetal calf serum
FcγR	Fc-gamma receptor
Fe	Iron
FELASA	Federation of Laboratory Animal Science Associations
FITC	Fluorescein isothiocyanate
FoxP3	Forkhead box P3
FV	Friend virus
G	Gauge

GAPDH	Glycerinaldehyd-3-phosphat-dehydrogenase
GLUT1	Glucose transporter 1
GM-CSF	Granulocyte macrophage colony-stimulating factor
HBSS	Hank's Balanced Salt Solution
HER2	Human epidermal growth factor receptor 2
HLA	Human leukocyte antigen
i.d.	Intradermal
i.p.	Intraperitoneal
i.v.	Intravenous
IFN- $\gamma$	Interferon- $\gamma$
IgG	Immunoglobulin G
IHC	Immunohistochemistry
IL-2	Interleukin-2
IL7R- $\alpha$	Interleukin-7 receptor subunit alpha
LB	Lysogeny broth
LCMV	Lymphochoriomeningitis Virus
LP	Long pass filter
LPS	Lipopolysaccharide
MAV	Mouse Adenovirus
MCMV	Murine Cytomegalovirus
MDSC	Myeloid-derived suppressor cells
MgCl <sub>2</sub>	Magnesium chloride
MHC	Major histocompatibility
MHV	Mouse Hepatitis Virus
MNV	Murine Norovirus
MPV	Mouse Parvovirus
mRNA	Messenger ribonucleic acid
MVM	Minute virus of mice
NK	Natural killer
NLR	Nucleotide-binding domain, leucine-rich repeat-containing receptor

NSCLC	Non-small cell lung cancer
OVA	Ovalbumin
P-value	Probability-value
PAMP	Pathogen-associated molecular pattern
PBMC	Peripheral blood mononuclear cell
PBS	Phosphate-buffered saline
PCR	Polymerase chain reaction
PD-1	Programmed cell death protein 1
PD-L1	Programmed cell death ligand 1
PEI	Polyethylenimine
PES	Polyethersulfone
PFA	Paraformaldehyde
pMHC-I-IgG	peptide-MHC class I-antibody
Poly(I:C)	Polyinosinic-polycytidylic acid
PRR	Pattern-recognition receptor
PVM	Pneumonia Virus of Mice
qPCR	Quantitative polymerase chain reaction
RCC	Renal cell carcinoma
REO-3	Reovirus
RLR	RIG-I-like receptor
RNA	Ribonucleic acid
s.c.	Subcutaneous
scFv	Single-chain variable fragment
SDS-PAGE	Sodium dodecyl sulfate polyacrylamide gel electrophoresis
$\beta_2$ M	Beta-2-microglobulin
TAA	Tumor-associated antigen
TBE	Tris-borate-EDTA
TBST	Tris-buffered saline with Polysorbate 20
TCB	T cell bispecific
TCR	T cell receptor

TIFF	Tagged image file format
Tim-3	T-cell immunoglobulin and mucin-domain containing-3
TLR	Toll-like receptor
TMEV	Theiler's Murine Encephalomyelitis Virus
TNF- $\alpha$	Tumor necrosis factor- $\alpha$
T <sub>reg</sub> cells	Regulatory T cells
TRP-2	Tyrosinase-related protein 2
VEGF-A	Vascular endothelial growth factor A
VH	Variable domain of the antibody heavy chain
VL	Variable domain of the antibody light chain
VPA	Valproic acid

### 3 SUMMARY

As part of the adaptive immune system cytotoxic, effector memory CD8<sup>+</sup> T cells patrol through the body and screen cells with their T cell receptor for peptide-major histocompatibility (MHC) class I complexes. Upon encounter of foreign or mutated self-peptides displayed on MHC class I molecules they rapidly expand and trigger elimination of the target cell. Tumors can evade the immune surveillance by reducing immunogenicity including down-regulation of MHC class I molecule expression. Antibody-mediated delivery of recombinant peptide-MHC class I complexes to tumor cells can overcome this and induce potent tumor cell lysis after recruitment and activation of specific, cytotoxic CD8<sup>+</sup> T cells. Schmittnaegel et al. successfully produced fully recombinant fusion proteins comprising a full length human IgG antibody and a MHC class I complex carrying an immunodominant epitope of the human Cytomegalovirus (CMV) and confirmed potent tumor cell killing capacity with pre-existing CMV-specific CD8<sup>+</sup> T cells from human donor-derived lymphocytes in vitro [1, 2]. Due to the polymorphism of MHC complexes the in vivo efficacy can only be tested in syngeneic, immunocompetent mouse models using surrogate molecules characterized in this study. Fully recombinant surrogate fusion proteins containing a full length murine IgG antibody directed against the murine fibroblast activation protein (FAP) and a murine MHC class I complex (H-2K<sup>b</sup>) carrying an immunodominant epitope of either the murine Cytomegalovirus (MCMV m38: "SSPPMFRV") or ovalbumin (OVA<sub>257-264</sub>: "SIINFEKL") were designed. For generation of MCMV m38- or OVA<sub>257-264</sub>-specific CD8<sup>+</sup> T cells in immunocompetent mice different vaccination methods were tested. In cytotoxicity assays with splenocytes from vaccinated mice the surrogate molecules mediated IFN- $\gamma$ -activation of CD8<sup>+</sup> T cells and eradication of tumor cells in vitro. Experimental lung metastasis in vivo studies with FAP-transfected B16 melanoma cells were performed to assess tumor burden after pMHCI-IgG treatment by counting of visible metastasis and real time-PCR. In a preventive setting pMHCI-IgG fusions mediated complete elimination of tumor cells in the circulation before settlement in the lung. In a therapeutic setting pMHCI-IgG molecules engaged T cells in a peptide-specific mode and induced delayed metastasis growth. A solid subcutaneous tumor model with FAP-transfected MC38 colorectal cancer cells represented a greater hurdle for pMHCI-IgG proteins. In this case no tumor growth inhibition under pMHCI-IgG treatment could be achieved. Basic prerequisites, like penetration of effector molecules and effector cells into the tumor and binding of pMHCI-IgG fusions to their target on the tumor cell surface, were accomplished as confirmed by immunohistochemistry and ultramicroscopy. Lack of tumor growth

inhibition was more likely due to inactivation of cytotoxic CD8<sup>+</sup> T cells by PD-1 / PD-L1 (programmed cell death protein 1 / Programmed cell death ligand 1) interactions with tumor cells and suppressive influences on the basis of regulatory T cells (T<sub>reg</sub> cells) as revealed by flow cytometry analysis of tumors. To remove those inhibitory influences on T cells, blockage of the PD-1 / PD-L1 axis in combination with T<sub>reg</sub> depletion could be applied. The study also compared the anti-tumor efficacy mediated by pMHC-IgG molecules and CD3-based T cell recruiters. The T cell bispecific (TCB) antibody and the pMHC-IgG molecule showed comparable outcomes in both the experimental lung metastasis and the solid subcutaneous tumor model.

## 4 ZUSAMMENFASSUNG

### Zielgerichtete Eliminierung von Tumorzellen *in vivo* durch Rekrutierung von Vakzin-induzierten CD8<sup>+</sup> T-Zellen mit Hilfe von bispezifischen Peptid-MHC Klasse I-IgG-Antikörper Fusionen

Als Teil des adaptiven Immunsystems patrouillieren zytotoxische CD8<sup>+</sup> T-Gedächtniszellen durch den Körper und überprüfen peptidbeladene MHC-Komplexe (engl. *major histocompatibility class I complex*) anderer Zellen mit ihrem T-Zell-Rezeptor. Erkennen sie ein fremdes oder ein mutiertes Eigenantigen auf einem MHC-Komplex expandieren sie clonal und eliminieren die Zielzelle. Tumore können der Überwachung durch das Immunsystem entgehen, indem sie ihre Immunogenität reduzieren, was unter anderem durch verringerte Expression von MHC-Molekülen erreicht wird. Durch Antikörper-vermittelte Beladung von Tumorzellen mit rekombinanten Peptid-MHC-Komplexen kann dies umgangen und eine effiziente Lyse der Tumorzellen durch Rekrutierung und Aktivierung von spezifischen, zytotoxischen CD8<sup>+</sup> T-Zellen ausgelöst werden. Schmittnaegel et al. konnten erfolgreich komplett rekombinante Fusionsproteine herstellen, die aus einem ganzen humanen IgG Antikörper und einem MHC-Komplex bestehen, der mit einem immundominanten Epitop des humanen Zytomegalievirus (engl. *Cytomegalovirus: CMV*) beladen ist. In *in vitro* Zytotoxizitätsexperimenten mit CMV-spezifischen CD8<sup>+</sup> T-Zellen von Lymphozyten, die aus Spenderblut isoliert wurden, konnten die Fusionsmoleküle eine potente Lyse der Tumorzellen induzieren [1, 2]. Aufgrund des Polymorphismus von MHC Komplexen kann die *in vivo* Wirksamkeit solcher Proteine nur in syngenen, immunkompetenten Mausmodellen mit Surrogatmolekülen, die in dieser Arbeit charakterisiert werden, getestet werden. Für diesen Zweck wurden komplett rekombinante Surrogat-Fusionsproteine hergestellt, die aus einem ganzen murinen IgG Antikörper, der gegen murines FAP (engl. *fibroblast activation protein*) gerichtet ist, und einem murinen MHC-Komplex (H-2K<sup>b</sup>), der ein immundominantes Epitop des murinen Zytomegalievirus (MCMV m38: "SSPPMFRV") oder von Ovalbumin (OVA<sub>257-264</sub>: "SIINFEKL") trägt, aufgebaut sind. Zur Erzeugung von MCMV m38- oder OVA<sub>257-264</sub>-spezifischen CD8<sup>+</sup> T-Zellen in den Versuchstieren wurden verschiedene Vakzinierungsmethoden getestet. In *in vitro* Zytotoxizitätsexperimenten mit Splenozyten von immunisierten Mäusen konnten die Surrogatmoleküle eine IFN- $\gamma$ -Aktivierung von CD8<sup>+</sup> T-Zellen erzeugen und eine potente Eliminierung von Tumorzellen hervorrufen. In einem experimentellen Lungenmetastasenmodell mit FAP-transfizierten B16 Melanomzellen wurde die Metastasenlast nach Behandlung mit den Fusionsmolekülen durch RT-PCR und durch Zählen der sichtbaren Metastasen auf der Lungenoberfläche ermittelt. Bei präventiver Behandlung mit pMHC-IgG

Molekülen konnten alle Tumorzellen im Blutkreislauf abgetötet werden, bevor sie sich in der Lunge ansiedeln konnten. Bei der therapeutischen Behandlung von Lungenmetastasen konnte gezeigt werden, dass die pMHC-IgG Fusionen peptid-spezifisch CD8<sup>+</sup> T-Zellen aktivieren und das Metastasenwachstum verzögern. Das solide subkutane Tumormodell mit FAP-transfizierten MC38 Kolonkarzinomzellen stellte eine größere Hürde für die pMHC-IgG Moleküle dar. Hier konnte bei der Behandlung mit pMHC-IgG Fusionsproteinen keine Hemmung des Tumorwachstums erzielt werden. Durch Immunhistochemie und Ultramikroskopie konnte bestätigt werden, dass grundlegende Voraussetzungen, wie Penetration der Moleküle und der Effektorzellen in den Tumor und Bindung der pMHC-IgG Moleküle an die Zielstruktur an der Oberfläche der Tumorzellen, gegeben waren. Mit durchflusszytometrischen Analysen der Tumore konnte schließlich gezeigt werden, dass die fehlende Wirksamkeit der Therapie sehr wahrscheinlich auf eine Inaktivierung der zytotoxischen CD8<sup>+</sup> T-Zellen durch PD-1 / PD-L1 (engl. *programmed cell death protein 1 / Programmed cell death ligand 1*) Interaktionen mit den Tumorzellen und auf den suppressiven Einfluss von regulatorischen T-Zellen (T<sub>reg</sub> Zellen) zurückzuführen ist. Um diesen inhibitorischen Einflüssen entgegenzuwirken, könnte eine Blockade der PD-1 / PD-L1 Achse in Kombination mit der Depletion von regulatorischen T-Zellen angewendet werden. In dieser Arbeit wurde außerdem die anti-tumorale Wirksamkeit der pMHC-IgG Fusionen mit der der CD3-basierten bispezifischen T-Zell-Antikörper (engl. *T cell bispecific antibody: TCB*) verglichen. Beide Moleküle zeigten vergleichbare Ergebnisse sowohl im experimentellen Lungenmetastasenmodell als auch im soliden subkutanen Tumormodell.

## 5 INTRODUCTION

### 5.1 CHARACTERISTICS AND STRATEGIES OF CANCER DEVELOPMENT

Tumors are not simply a homogeneous mass of cells derived from a mutated, abnormal cell, whose cell cycle got out of control. Instead, they consist of multiple cell types and an established tumor microenvironment influencing each other and can be compared with organs of high complexity. For development and maintenance of tumors several factors play a crucial role and there are a number of characteristics, which define a cell as cancerous (reviewed in [3]). Normal cells control production and secretion of growth-promoting signals in such a way that homeostasis of cell number and conservation of tissue architecture is sustained. By dysregulation of these control signals cancer cells are able to proliferate without control and affect other cell-biological processes such as cell survival and energy catabolism [3]. In addition tumor cells can produce growth factor ligands themselves and, by simultaneous expression of cognate receptors, trigger their own proliferation by autocrine proliferative stimulation [4]. Another way is to stimulate normal cells in the surrounding, which in the turn provide different growth factors for proliferation of cancer cells [5]. Alterations in number of growth factor ligand receptors expressed on the tumor cell surface and structure of receptor proteins enabling ligand-independent activation can make tumor cells hyperresponsive and contribute to enhanced proliferation of cancer cells [3]. Interruption of negative feedback loops, which normally attenuate proliferative signaling to avoid excessive proliferation, can also lead to increased proliferative signaling and is often used by tumor cells [6]. On the other hand tumor cells have to evade growth suppression by typical tumor suppressors, that decide whether a cell can proceed to another growth-and-division cycle or goes into apoptosis [7]. Another strategy of tumor cells is to escape programmed cell death by inactivation of transcription factors that induce apoptosis or senescence of cells in response to cellular stress like DNA (Desoxyribonucleic acid) damage, hypoxia or nutrient deprivation, which are circumstances often present in tumor cells [8, 9]. Necrotic cells frequently found in large tumor masses release proinflammatory signals into the surrounding. This recruits inflammatory cells of the immune system, which remove necrotic debris, but also promote tumor proliferation by enhancement of angiogenesis, cell proliferation and invasiveness [10]. Gaining capabilities like replicative immortality is also a strategy of cancer cells for enabling unlimited proliferation. The vast majority of tumor cells aberrantly upregulates telomerase, a DNA polymerase that fuses telomeres to the ends of chromosomes. Telomeres shorten over live time of a cell and in this way regulate cell aging

and viability by inhibiting cells from passing through a new growth-and-division cycle, if telomeres are too short. By overexpression of telomerase cancer cells prevent shortening of telomeres and consequently senescence and apoptosis of cells [11]. Genome instability and mutation in general is a characteristic that enables cancer cells to emerge, proliferate and adapt to new conditions. By enhanced sensitivity to mutagenic agents or impairment of the system that is responsible for genomic integrity, tumor cells increase the rates of mutations and in that way gain properties needed for tumorigenesis [12].

To continuously get access to oxygen and nutrients in a growing tumor new vessels are built in the process of angiogenesis. In contrast to normal tissue, where angiogenesis is turned on only transiently during e.g. wound healing, tumors activate an “angiogenic switch” that causes chronically activated angiogenesis promoting continuous sprouting and production of new, partially abnormal vessels [13, 14].

One further characteristic of advanced cancer is invasive and metastatic growth. Beginning with local invasion of thin-walled venules and lymphatic channels of the host, tumor cells or aggregates of them traffic through the lymphatic and hematogenous system and arrest in capillary beds of distant tissues. After extravasation cancer cells form micrometastases applying similar mechanisms as those used for initial tissue invasion. Finally proliferation and vascularization of metastatic foci lead to colonization of macroscopic tumors, which in turn reinitiate the development of new metastases [15]. After dissemination from the primary tumor some micrometastases in distant tissues may also adopt a state of dormancy and resume activation long time or directly after removal of the primary tumor. This micrometastatic dormancy can be mediated by the primary tumor itself via release of systemic suppressor factors, nutrient starvation, anti-growth signals from normal tissue or suppression of the immune system [16-19]. When changes in the microenvironment occur, dormant micrometastases regain activity and start to proliferate. Certain tissue microenvironments also seem to provide more favorable preconditions for metastasis formation than others [20]. Also the site of the primary tumor is a hospitable site for colonization of circulating tumor cells, so that returning tumors at the site of primary tumors often originate from reseeding and not from classical tumor progression [21].

Another characteristic of cancer cells is their reprogrammed energy metabolism first observed by Otto Warburg [3]. Even if oxygen is provided cancer cells pull the vast majority of energy from glycolysis. At first sight this seems surprising as glucose metabolism via glycolysis is much less

efficient compared to mitochondrial oxidative phosphorylation. However, glycolytic fueling is associated with activated oncogenes and mutant tumor suppressors [22] and provides particularly energy for generation of nucleosides and amino acids, which are needed for synthesis of new cells [23]. By upregulation of glucose transporters such as GLUT1 (glucose transporter 1) tumor cells compensate poor efficiency of their reprogrammed glucose metabolism [22]. In addition symbiosis of two cancer cell subpopulations, in which one population produces lactate via glycolysis, whereas the other one uses it as main energy source, can lead to maximal exploitation of resources [24].

The tumor has to be seen in context of its microenvironment. An assemblage of distinct cell types including cancer cells, cancer stem cells, immune inflammatory cells, cancer-associated fibroblasts, pericytes and endothelial cells constitutes most solid tumors [3]. Cancer cells build the basis of the disease and initiate tumors, while in the established tumor a great heterogeneity with cancer cells showing various degrees of differentiation, proliferation, vascularity, inflammation and invasiveness can be found. A special role is awarded to the cancer stem cells (CSCs), which represent a small population of cancer cells within the tumor that is suggested to display increased tumorigenic potential and possess a self-renewal capacity [15]. Endothelial cells and pericytes collaborate particularly in angiogenesis and maintenance of tumor vasculature, while cancer-associated fibroblasts contribute to cell proliferation and invasion and are involved in the formation of a desmoplastic stroma [3]. The tumor microenvironment consists of multiple stromal cell types and the extracellular matrix and interacts in complex processes with neoplastic and stromal cells within the tumor [3]. It enables primary, invasive and metastatic growth of tumor cells by reciprocal signaling interactions between cancer cells and stromal cells changing phenotype and histologic organization of supportive stroma during tumor progression [25]. Furthermore it is likely that also normal cells in the surrounding influence the character of the tumor microenvironment.

Some tumors and their microenvironment are infiltrated by immune cells from both the innate and the adaptive immune system. While cells belonging mainly to the adaptive immune system like cytotoxic T cells, T-helper Type I cells and mature dendritic cells (DCs) induce tumor regression, inflammatory cells such as M2 macrophages, mast cells, neutrophils and T regulatory ( $T_{reg}$ ) cells, which are largely associated with the innate immune system, mediate tumor-promoting effects [10, 26]. Inflammation in tumors can, as partly already mentioned before, contribute to tumor proliferation by secretion of growth, signaling, survival and proangiogenic factors and extracellular-matrix modifying enzymes resulting in limitation of cell death, invasion, metastasis and

angiogenesis. In addition escape of tumor cells from the control of the immune system is achieved by various complex mechanisms and promotes tumor formation and progression [27]. In this sense the immune system plays a critical role in cancerogenesis and tumor progression and is therefore an interesting platform for the development of new and innovative approaches in cancer therapy.

## 5.2 THE INNATE AND ADAPTIVE IMMUNE SYSTEM

The immune system has the task to protect the organism from pathogens like viruses, bacteria or parasites. To fulfill this mission different specialized compartments of the immune system interact with each other (reviewed in [28]). In general the immune system can be divided into the innate and the adaptive arm, the latter consists of a humoral and cellular part. The innate immune system includes macrophages, dendritic cells (DCs), neutrophil granulocytes, and natural killer (NK) cells. Upon encounter of a pathogen cells of the innate immune system are rapidly and non-specifically activated and provide immediate effector functions. In this sense they represent the first line of defense in the organism. Recognition of pathogens is thereby mediated by pattern-recognition receptors (PRRs), which detect conserved pathogen-associated molecular patterns (PAMPs). Most PAMPs can be detected both by cell-extrinsic pathways and by cell-intrinsic pathways. There are several classes of PRRs such as Toll-like receptors (TLRs) recognizing common components of bacterial and fungal cell walls, like lipopolysaccharides (LPS), bacterial lipopeptides, flagellin and  $\beta$ -glucans, or nucleotide-binding domain, leucine-rich repeat-containing receptors (NLRs) and RIG-I-like receptors (RLRs), sensing PAMPs in the cytosol like viral RNA (ribonucleic acid) or peptidoglycan fragments and flagellin. In addition cells of the innate immune system are capable to activate cells of the adaptive immune system. If professional antigen presenting cells (APCs) like DCs are activated via PRRs and take up pathogens, they process the foreign protein in the cytosol and display parts of it as immunogenic peptides on MHC (major histocompatibility) complexes, which activates T cells belonging to the adaptive part of the immune system. Besides presentation of pathogen-derived immunogenic peptides on MHC complexes, the expression of costimulatory molecules like CD80 and CD86 is enhanced and secretion of proinflammatory cytokines is induced. Pathogen-derived peptides are presented on MHC class II complexes for activation of  $CD4^+$  T cells. Via cross-presentation of peptides on MHC class I complexes also  $CD8^+$  T cells can be primed. This process takes place in secondary lymphoid organs like lymph nodes and spleen, to where DCs migrate after encounter of antigen.

The adaptive immune system includes B cells and T lymphocytes and is, in contrast to the innate immune system, able to specifically eliminate pathogens and build up an immunological memory. After priming of naïve CD8<sup>+</sup> T cells in the secondary lymphoid organs via T cell receptor / peptide-MHC class I complex interactions, CD8<sup>+</sup> T cells differentiate into effector cells, which specifically recognize the combination of peptide and MHC class I complex that they were primed for. Once activated they expand and patrol through the body searching for infected cells bearing the appropriate peptide-MHC class I complex. By secretion of cytotoxic granules containing granzymes and perforin antigen-specific CD8<sup>+</sup> T cells finally mediate killing of infected cells. In addition they can mediate apoptosis of target cells via Fas-ligand (FasL) / Fas-receptor (FasR) interaction and release pro-inflammatory cytokines like IFN- $\gamma$ , IL-2 and TNF- $\alpha$ , which activate cells of the innate immune system such as macrophages. After clearance of the infection most effector cells die, but a small population of memory cells remains building an immunological memory that can very quickly mount an effective immune response upon reencounter of the same antigen. Sometimes CD8<sup>+</sup> T cells are divided into two subtypes. In this case Tc1 cells represent the classical cytotoxic CD8<sup>+</sup> T cells, which mediate pro-inflammatory immune responses via release of IFN- $\gamma$ , and Tc2 cells contribute to anti-inflammatory immune reactions with IL-4 secretion [29].

B cells belong to the humoral part of the adaptive immune system as they produce antibodies against cell surface proteins and pathogens. They recognize specific antigens with their B cell receptor (BCR), which is a membrane bound antibody molecule. Once a B cell encounters its specific antigen it engulfs and digests it and displays parts of it on MHC class II complexes. This attracts and activates matching specific CD4<sup>+</sup> T cells, which secrete cytokines that help the B cell to multiply and differentiate into an effector cell, called plasma cell. Plasma cells produce and release antibodies, which specifically bind to antigens and mark them as targets for phagocytosis and clearance by the complement cascade.

As already partly mentioned above CD4<sup>+</sup> T cells are most notably responsible for the help of other immune cells to perform their tasks. In this sense they are immune mediators, which have rare cytotoxic activity, but rather a managing function for the immune response. By interaction of their T cell receptor (TCR) with antigens bound to MHC class II complexes on the surface of APCs they get activated and secrete cytokines, which influence many cell types including B cells, macrophages, neutrophils, cytotoxic lymphocytes and also APCs, that originally activated the CD4<sup>+</sup> T cell. In addition they activate other cells via direct cell-to-cell contact by CD40 / CD40 ligand-interactions.

There are two types of helper T cell responses. CD4<sup>+</sup> Th1 cells release proinflammatory cytokines like IFN- $\gamma$ , IL-2 and TNF- $\alpha$  and activate mainly macrophages and cytotoxic CD8<sup>+</sup> T cells, which eliminate viruses and intracellular pathogens. CD4<sup>+</sup> Th2 cells play a critical role in defense against extracellular pathogens and parasites and activate eosinophils and B cells via secretion of anti-inflammatory cytokines such as IL-4, IL-5, IL-6, IL-10 and IL-13. Also CD4<sup>+</sup> T cells can build an immunological memory after resolution of the infection. A special kind of CD4<sup>+</sup> T cells are T<sub>reg</sub> cells, which constitutively express CD25 and are positive for FoxP3 (Forkhead box P3). They are immunosuppressive T cells, which reduce proinflammatory and enhance anti-inflammatory processes, i. a. via secretion of IL-10, and in this way control autoimmunity. Other subtypes of CD4<sup>+</sup> T cells are Th9 cells, which contribute to defense against parasites and Th17 cells, which play a role in defense against extracellular bacteria and fungi. Both subtypes also seem to be able to activate CD8<sup>+</sup> T cells via release of cytokines like IL-9 and IL-21. In addition cytotoxic CD4<sup>+</sup> T cells (ThCTL) represent a small population, which can directly induce apoptosis of target cells via cytotoxic granules or FasL / FasR interaction [30].

Another subset of T cells are  $\gamma\delta$  T cells, which possess an alternative TCR that is able to recognize pathogens independent from MHC complexes. Those cells are involved in the epithelial and mucosal defense of the organism and have characteristics of both innate and adaptive immunity.

T cells go through different stages of differentiation during their development. In the thymus, hematopoietic precursors from the bone-marrow, referred to as thymocytes, undergo a procedure of selection that eliminates autoreactive cells and conserves only functional cells, that bind strongly or medium to MHC complexes or peptide molecules with their TCR. This selection process establishes a functional and self-tolerant repertoire of naïve T cells, which patrol between secondary lymphoid organs searching for their specific antigen. Once the naïve T cell has recognized its antigen as processed peptide loaded on a MHC complex on the surface on an APC, it gets activated and clonal expansion and differentiation of the T cell is induced. For activation and priming of naïve T cells a costimulatory signal via interaction of CD28 on the T cell surface and CD80 or CD86 on the APC is obligatory. The majority of activated T cells differentiate into effector T cells (T<sub>E</sub>), which provide immediate effector functions. Simultaneously a small population of activated T cells differentiates into long-lived memory T cells, which can be divided into central memory T cells (T<sub>CM</sub>), effector memory T cells (T<sub>EM</sub>) and effector memory RA T cells (T<sub>EMRA</sub>) [31, 32]. Memory T cells can get activated directly by TCR / peptide-MHC complex interactions without a

costimulatory signal via CD28.  $T_{EM}$  cells patrol through peripheral tissues and organs and provide immediate protection upon reencounter with their antigen. However, their proliferation capacity is very poor. In contrast,  $T_{CM}$  cells, which lack direct effector functions, reside in secondary lymphoid organs and mount effective recall responses following antigen stimulation by massive proliferation.  $T_{EMRA}$  cells show same characteristics as  $T_{EM}$  cells and provide immediate effector functions. After clearance of antigen they seem to develop from  $T_{EM}$  cells and represent the real long-lived memory T cells [33].

### 5.3 CANCER IMMUNOEDITING AND IMMUNE ESCAPE MECHANISMS OF TUMORS

In the last decades immuno-oncology research provided solid evidence that the immune system can recognize tumors and plays a critical role in cancer protection but also tumor progression. Those immune system - tumor interactions including host-protective and tumor shaping processes are called cancer immunoediting and composed of three sequential phases: Elimination, equilibrium and escape (reviewed in [34-37]). Unedited cancer cells express tumor-specific antigens, which emerge from mutations and are therefore exclusively expressed on those transformed cells [38]. In the elimination phase cells of the innate immune system recognize those specific ligands as foreign, destroy cancer cells and present tumor-derived peptides to T and B cells. This leads to production of tumor-specific, cytotoxic T cells and tumor-specific antibodies and finally the raised adaptive immune response eliminates remaining tumor cells and induces immune memory preventing tumor recurrence. However, if the immune system is not able to completely eradicate tumors cells, some cancer cells remain and the tumor enters a state of functional dormancy. In this phase called equilibrium repeated cycles of tumor regrowth and immune-mediated destruction occur, whereby the tumor does not progress or metastasize [39]. However, during this process the adaptive immune system edits tumor cell immunogenicity resulting in a selection pressure, which promotes capacities of tumor cells that enable them to escape the control of the immune system. The escape phase represents the final phase of cancer immunoediting, where edited tumors of reduced immunogenicity begin to grow progressively, become clinically apparent and establish an immunosuppressive tumor microenvironment [27]. Escape from immunosurveillance can thereby occur through many different mechanisms.

One mechanism of immune escape is loss of HLA (human leukocyte antigen) expression of tumors [40-43]. MHC molecules can thereby be lost during steps required for HLA synthesis, transport or

expression on the cell surface, by genetic mutation regarding heavy chain or beta-2-microglobulin ( $\beta_2M$ ), or by alterations in glycosylation or regulatory factors (reviewed in [40]). Reduced presentation of tumor-associated peptides on MHC complexes leads to decreased immunogenicity of tumors. This altered phenotype of tumor cells can be found in many human cancers like melanomas, head-neck, colorectal, prostate and breast tumors [44].

Besides reduction of immunogenicity tumors evade control of the immune system by formation of an immunosuppressive tumor microenvironment. Tumors can release immunosuppressive factors like TGF- $\beta$  or IL-10 [45, 46], which leads among other things to reduced CD28-signaling and IL-2 secretion of APCs and subsequently direct to decreased T cell activation. The recruitment of  $T_{reg}$  cells into the tumor induces suppression of cytotoxic lymphocytes [47]. Normally those cells are involved in the control of autoimmunity [48], but in this case the tumor exploits them for inhibition of tumor-specific T cell immunity [49]. Myeloid-derived suppressor cells (MDSCs) inhibit both the innate and adaptive immunity and can also be attracted by the tumor [50, 51]. They are induced by proinflammatory mediators released by the tumor and suppress cytotoxic T lymphocytes (CTL) and NK cell activity. In addition cancer-associated fibroblasts can actively recruit monocytes via secretion of growth factors and drive their polarization to M2 macrophages. This leads to increased tumor cell motility resulting in dissemination from the primary tumor and metastatic spread [52].

Furthermore cancer cells influence T cell activity via expression or down-regulation of surface molecules. For full activation of resting T cells a costimulatory signal by CD80/CD86 - CD28 interaction between APC and T cell is needed. If TCR engagement occurs in the absence of the second signal, T cells cannot develop full effector function and become anergic. In this case T cells also fail to provide effector function after a second encounter with antigen, even if both signals are delivered then [53]. This mechanism ensures tolerance to self-antigens, which are not able to provide a costimulatory signal. As most tumor cells are poor APCs, levels of CD80 and CD86 expression are low resulting in anergy of tumor-antigen-specific T cells due to absence of a costimulatory signal [54]. In addition CTLA-4 (cytotoxic T lymphocyte-associated protein 4), an inhibitory ligand on cytotoxic T cells, binds with higher affinity to CD80/CD86 than the engaging ligand CD28 [55, 56], which leads to further inhibition of tumor-antigen-specific T cells. Another strategy of tumor cells for immune escape is expression of the Programmed cell death ligand 1 (PD-L1). In a physiological immune reaction PD-L1 suppresses T cell activity via binding to the programmed cell death protein 1 (PD-1) on the T cell surface and in this way controls the immune

response. By upregulation of PD-L1 on cancer cells tumor-antigen-specific T cells are inhibited by tumor cells [57-59]. Not only the cancer cells but also other cell types associated with the tumor can express immunosuppressive surface molecules. For example endothelial cells in the vasculature of tumors express FasL in response to VEGF-A (vascular endothelial growth factor A) and IL-10, which is a death mediator for effector CD8<sup>+</sup> T cells [60].

Taken together tumors exploit a plethora of mechanisms to evade the control of the immune system, which enables them to promote proliferation, invasion and metastatic spread without immunologic constraint.

#### **5.4 DIFFERENT APPROACHES IN CANCER IMMUNOTHERAPY**

In the last decades immunotherapy of cancer has become a clinically validated treatment for many types of tumors. In general the idea is to specifically target and eliminate tumor cells, while leaving healthy cells unaffected, which can be successfully accomplished by exploiting the host's immune system. Several promising immunotherapeutic strategies are recently approved for the treatment of cancer or are in clinical trials (reviewed in [61-63]).

For activation of the host's innate and adaptive immune system cytokine therapies have been applied to enhance the patient's anti-tumor immune response [64]. Administration of IL-2 was used for example for the treatment of renal cell carcinoma (RCC) and IFN- $\alpha$  for the treatment of melanoma [65, 66]. The major disadvantages of cytokine therapies are low response rates, high toxicity and no tumor specificity.

A more specific approach constitute cancer vaccines, which specifically activate host T cells against tumor antigens (reviewed in [61, 67]). Prophylactic as well as therapeutic vaccines are in use. For defense against cancer-causing infectious diseases like hepatitis B virus and human papillomavirus preventive vaccines are approved [68, 69]. Therapeutic anti-cancer vaccines are developed to prime or boost tumor-specific immune responses. Thereby the identification of the most suitable antigens is a main hurdle. Cancer vaccines should contain a wide variety of tumor-associated antigens (TAAs), thus tumor lysates, purified tumor antigens, weakened whole tumor cells, tumor cells genetically engineered to secrete immunostimulatory cytokines as well as TAA-encoding recombinant DNA/RNA molecules formulated in various delivery systems were evaluated for treatment of established tumors [61, 67]. DC-based vaccines seem to be the most promising

approach in this field. For this vaccination DCs are isolated from the patient's peripheral blood mononuclear cells (PBMCs), loaded with tumor antigens ex vivo, activated and then reinfused into the patient. Sipuleucel-T is such a cell-based vaccine and is approved for the treatment of metastatic prostate cancer. Unfortunately, this approach is often associated with complications in production and administration of antigen-loaded DCs and only moderate clinical effectiveness, resulting in low application rates [61].

Besides that, various monoclonal antibodies targeting surface proteins on cancer cells are in use (reviewed in [63, 70]). Rituximab, a chimeric human-mouse monoclonal antibody, targets CD20 on B cells and is approved for the treatment of Non-Hodgkin's lymphoma. Herceptin (also known as Trastuzumab) is a recombinant humanized monoclonal antibody that is directed against HER2 (Human epidermal growth factor receptor 2) which was found to be overexpressed in breast cancer. Applying monoclonal antibodies for cancer treatment, tumor cell killing is achieved by different mechanisms (reviewed in [70]). By binding of the antibody to its target dimerization, downstream signaling and kinase activation can be blocked resulting in reduced proliferation and, finally, apoptosis. This antagonist activity is applied for example by Herceptin. Also agonist activities leading directly to apoptosis of tumor cells can be mediated by antibodies. Immune-mediated tumor cell killing can be achieved with antibodies as well. With binding of the antibody to the tumor cell surface antibody-dependent cellular cytotoxicity (ADCC), antibody-dependent cellular phagocytosis (ADCP) or complement-dependent cellular cytotoxicity (CDC) can be mediated by the Fc (fragment crystallizable)-part of the antibody [71]. This mechanism is exploited applying Rituximab. Also conjugated antibodies are in use to deliver a payload, such as a drug, a toxin or a radioisotope, which induces tumor cell killing.

As CD8<sup>+</sup> T cells represent the natural defense against mutated cells in the immune system, many approaches are aimed at initiating, retargeting or enhancing the tumor-specific cytotoxic T cell response.

Various immunomodulating antibodies, called checkpoint inhibitors, which enhance tumor-specific T cell activation via binding to costimulatory receptors or blockage of inhibitory receptors are approved or in clinical trials so far. Antibodies blocking the PD-1 receptor on T cells, like Nivolumab or Pembrolizumab, or its ligand PD-L1 on tumor cells, such as Atezolizumab, showed improvement of outcome in melanoma, RCC, non-small cell lung cancer (NSCLC), colorectal cancer, bladder cancer or Hodgkin's lymphoma [72-79]. Ipilimumab or Tremelimumab, antibodies blocking CTLA-4,

which is an inhibitory receptor on T cells that down-regulates their activation, are approved for the treatment of melanoma [80]. Antagonistic antibodies targeting costimulatory receptors on T cells, like 4-1BB (tumor necrosis factor receptor superfamily member 9 (TNFRSF9)), are also in clinical trials to test anti-tumor efficacy [81, 82].

Adoptive cell therapy is another strategy to broaden tumor-specific T cell response in the host. For this approach lymphocytes are isolated from patients' peripheral blood, tumor-draining lymph nodes or tumor tissue, expanded *ex vivo*, and reinfused back into the patient [83]. In clinical trials this therapy showed encouraging results in melanoma patients [84]. To enable this approach also for patients lacking MHC molecules on tumor cells, genetically engineered T cells, which express a chimeric antigen receptor (CAR) were developed. CARs consist of an IgG variable extracellular domain fused to a TCR constant domain. Thus the engineered T cells can directly bind to any potential tumor cell surface target antigen [85]. Administration of engineered T cells has been successful in B-cell malignancies, melanoma and synovial sarcoma and trials in other cancer types are ongoing [86].

Another approach is to redirect cytotoxic T cells independent from their specificity to eliminate tumor cells. This is accomplished by development of bispecific molecules consisting of a tumor targeting moiety and a second domain, which recruits T cells via CD3. At the moment two T cell engagers recruiting and activating T cells via CD3 are approved. Catumaxomab is a T cell bispecific (TCB) molecule that targets the epithelial cell adhesion molecule (EpCAM) for the treatment of malignant ascites [87, 88]. Blinatumomab targets CD19 and is approved for treatment of refractory B-cell acute lymphocytic leukemia [89, 90]. A novel IgG-based TCB, which targets carcinoembryonic antigen (CEA)-expressing solid tumors, is currently in phase I clinical trials [91]. However, redirection and activation of cytotoxic T cells via CD3 is often associated with toxicity due to severe cytokine releases and has to be handled with care [92].

## 5.5 AIM OF THE STUDY

One mechanism for immune escape of tumors is loss of HLA expression [40-43]. Antibody-mediated delivery of viral peptide-MHC class I complexes is an auspicious approach to enhance immunogenicity of tumor cells. Applying this strategy, a viral infection of target cells can be mimicked and thus tumor cell lysis is induced after recruitment of virus-specific, cytotoxic CD8<sup>+</sup> T cells (Fig. 5.1). In contrast to classical T cell recruiters based on CD3 involvement (TCBs), the

engagement of T cells via MHC class I complexes activates only a peptide-specific subpopulation of CD8<sup>+</sup> T cells. This may have the advantage of a lower risk of side effects due to inappropriate T cell activation, which may lead to a favorable safety profile. Several molecules have been developed to meet this strategy, but until now those bifunctional molecules could not be produced as a full monoclonal antibody in the IgG format, which would be associated with an improved pharmacokinetic profile [93-105]. Schmittnaegel et al. were the first ones to successfully produce a fully recombinant fusion protein comprising a full length IgG antibody and a MHC class I complex carrying an immunodominant epitope of the human Cytomegalovirus [1, 2]. The peptide-MHC class I-IgG (pMHCI-IgG) fusion proteins could successfully recruit pre-existing virus-specific CD8<sup>+</sup> T cells from human donor-derived lymphocytes and effectively trigger eradication of the targeted tumor cells in vitro [2]. Due to the polymorphism of MHC complexes the in vivo efficacy can only be tested in syngeneic immunocompetent mouse models using surrogate molecules. This study pursues following objectives:

- Design and production of functional surrogate pMHCI-IgG fusion proteins
- Establishment of a tunable and reproducible vaccination method for generation of effector cells in mouse tumor models
- In vitro evaluation of biological activity and cytotoxicity mediated by surrogate pMHCI-IgG fusion molecules
- Anti-tumor efficacy evaluation of surrogate pMHCI-IgG fusions in an experimental lung metastasis model and a solid subcutaneous tumor model
- Investigation of penetration profile and T cell recruitment capabilities of surrogate pMHCI-IgG fusion proteins in the solid subcutaneous tumor model and characterization of redirected effector cells
- Comparison of pMHCI-IgG molecules with CD3-based TCB antibodies regarding recruitment and activation of effector cells and mediation of tumor cell killing

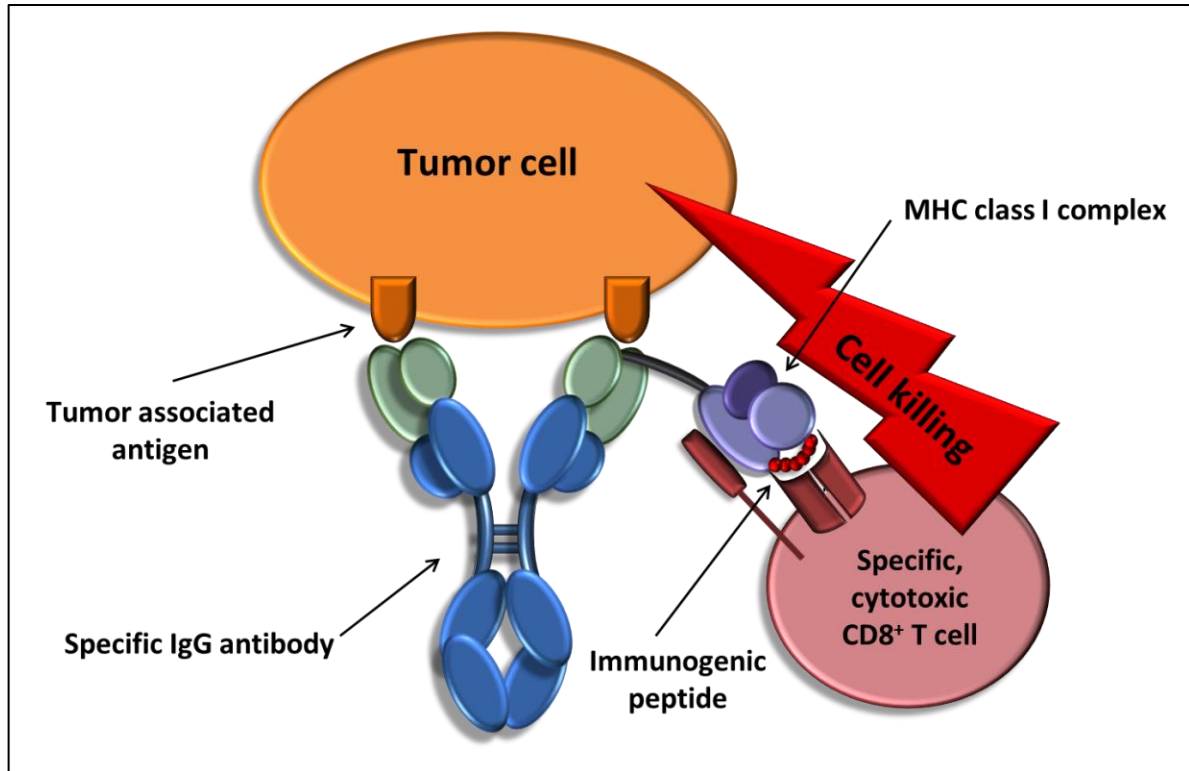


**Figure 5.1: Mechanism of action for peptide-MHC class I-IgG fusion molecules.**

PMHCI-IgG molecules selectively recruit peptide-specific, cytotoxic CD8<sup>+</sup> T cells via their peptide-MHCI complex. Upon binding of the antibody to target-specific tumor cells cytotoxic CD8<sup>+</sup> T cells mediate tumor cell lysis.

## 6 MATERIAL

### 6.1 LABORATORY EQUIPMENT

#### 6.1.1 Devices

Incubator Cytoperm 2	Heraeus Instruments
Vortex-Genie 2	Scientific Industries
Evacuator Vacusafe	INTEGRA Biosciences
Microscope Axiovert 135	Carl Zeiss International
Fluorescent microscope DM IL LED microscope	Leica Instruments
Centrifuge Multifuge 4 KR	Heraeus Holding
Rotixa 500 RS	Hettich Lab Technology
Centrifuge 5417R	Eppendorf
Centrifuge Megafuge 1.0 R	Thermo Fisher Scientific
Vi-Cell XR Cell Viability Analyzer	Beckman Coulter Biomedical
Fluorescence-Scanner Panoramic 250 Flash III	3D Histech
Isofluran-vaporizer	Eickenmeyer Medizintechnik
Laboratory scale	Sartorius
Cooling plate TES 99	MEDITE
AutostainerPlus	Dako
Microtome Microm HM 560	Thermo Fisher Scientific
Microtome Microm HM 355S	Thermo Fisher Scientific
Paraffin-deflasking station	Vogel
Laminar flow hood	Weiss Pharmatechnik
Tissue-Tek VIP Vacuum Infiltration Processor	Sakura Finetek
Ultramicroscope MVX10 Fluoreszenz MacroZoom	OLYMPUS CORPORATION
3QE Kamera	LaVision BioTec
SuperK EXTREME supercontinuum laser	NKT Photonics A/S
Water bath Julabo 5A	Julabo
MACSQuant Analyzer 10	Miltenyi Biotec
BTX Electroporation device ECM 830	Harvard Apparatus
2 Needle Array	Harvard Apparatus

FastPrep 24 homogenizer	MP Biomedicals
MagNA Pure LC 1.0	Roche
Veriti 96 Well Thermal Cycler	Applied Biosystems
LightCycler Carousel-Based System	Roche
LightCycler Sample Carousel	Roche
LightCycler Carousel Centrifuge	Roche
LightCycler instrument	Roche
xCELLigence RTCA SP	ACEA Biosciences
Eppendorf Thermomixer comfort	Eppendorf
NanoDrop Spectrophotometer ND-1000	Thermo Scientific
GelDOC-XR+System	Bio-Rad
Pipetboy acu 2	INTEGRA Biosciences
2.5 µl / 10 µl / 100 µl / 200 µl / 1 000 µl / 5 ml pipettes	Eppendorf

### 6.1.2 Consumables

Cell culture flasks (T175)	Greiner-bio-one
96-deepwell-plates	Eppendorf
96-well-plates	Brand, R&D Systems
E-Plate 96	ACEA Biosciences
6-well-plates (non-tissue culture treated)	Thermo Fisher Scientific
Erlenmeyer cell culture flasks	Corning
0.5 / 1.5 / 2 ml Eppendorf Safe-Lock Tubes	Eppendorf
50 ml tubes	Greiner-bio-one
15 ml tubes	Greiner-bio-one
250 ml tubes	Corning
70 µm cell strainer	FALCON, a Corning Brand
FACS tubes	FALCON, a Corning Brand
Reservoirs	Corning
2 ml / 5 ml / 10 ml syringes	Omnifix
Petri dishes	Corning
Pipette tips	Eppendorf

### 6.1.3 Chemicals

70 / 80 / 90 / 100 % ethanol	Roche
Isopropyl alcohol	Sigma Aldrich
Benzyl alcohol	Sigma Aldrich
Benzyl benzoate	Sigma Aldrich
Formalin (10 %)	VWR International
Histoplast Paraffin	Thermo Fisher Scientific
Xylene	Merck
Acetone	Merck
Methanol	Merck
TBST 10x	Roche
DMSO (Dimethyl sulfoxide)	Sigma Aldrich
Sucrose	Sigma Aldrich
Aqua bidest	SERAG-WIESSNER
Sodium acetate solution	Sigma Aldrich

## 6.2 MATERIALS FOR DIFFERENT PROCEDURES

### 6.2.1 Molecular biological procedures

Restriction enzymes and corresponding buffers	New England BioLabs
Bromophenol blue	Sigma Aldrich
Ficoll Plaque PLUS	GE Healthcare
EDTA	Sigma Aldrich
Agarose	Sigma Aldrich
TBE Buffer (Tris-borate-EDTA) (10X)	Thermo Fisher Scientific
SYBR Safe DNA Gel Stain	Thermo Fisher Scientific
QIAquick Gel Extraction Kit	Qiagen
Alkaline Phosphatase	Roche
Rapid DNA Ligation Kit	Roche
E.coli strain NEB 5-alpha F' lq	New England BioLabs
SOC Outgrowth Medium	New England BioLabs
QIAprep Spin Miniprep Kit	Qiagen

NucleoBond PC 2000 Kit

Macherey-Nagel

**6.2.2 Transfection of production cell line and protein purification**

FreeStyle F17	Gibco by Life Technologies
Glutamax	Gibco by Life Technologies
10 % Pluronic F-68	Gibco by Life Technologies
PEIpro	Polyplus-transfection SA
Valproic acid sodium	Sigma Aldrich
D-glucose	Merck
L-glutamine	Life Technologies
L-asparagine	Sigma Aldrich
Ethanolamine	Sigma Aldrich
HyPep 1510	Kerry
Ammonium-Fe(III)-citrate	Roche
HiTrap MabSelect SuRe columns	GE Healthcare
HiLoad 16/60 Superdex 200 pg columns	GE Healthcare
Amicon Ultra – 15 Centrifugal Filter Units	Merck Millipore
Sortase	Roche

**6.2.3 Cells, media, supplements and antibiotics for cell culture**

HBSS	Life Technologies
DPBS	PAN Biotech
FCS	PAN Biotech
RPMI-1640	PAN Biotech
DMEM	PAN Biotech
CTS AIM-V Medium	Gibco by Life Technologies
L-Glutamine	PAN Biotech
NEAA (non-essential amino acids)	PAN Biotech
Sodium pyruvate	PAN Biotech
2-Mercaptoethanol	Gibco by Life Technologies
Accutase solution	Sigma Aldrich

LB Broth Sigma Aldrich

GM-CSF R&D Systems

LPS Sigma Aldrich

**Antibiotics:**

Puromycin Gibco by Life Technologies

Zeocin Invitrogen

Ampicillin Gibco by Life Technologies

Penicillin-Streptomycin Gibco by Life Technologies

**Peptides:**

Peptide MCMV m38 (“SSPPMFRV”) BIOSYNTAN

Peptide OVA<sub>257-264</sub> (“SIINFEKL”) IBA

**Cell lines:**

Cell line	Species	Tissue	Disease	Growth properties	Stable transfections	Antibiotic	H-2K <sup>b</sup>	Vendor
<b>B16-muFAP:</b> B16-F10 _PHOPY_LUC _MUSMU_FAP	C57BL/6 (mouse)	Skin	Melanoma	adherent	FAP (fibroblast activation protein)	Puromycin	+	Perkin Elmer
					Luciferase	Zeocin		
<b>MC38-muFAP:</b> MC38 _MUSMU_FAP	C57BL/6 (mouse)	Colon	Adeno-carcinoma	adherent	FAP (fibroblast activation protein)	Puromycin	+	City of Hope
<b>HEK293-F</b>	Human	Embryonic kidney	Production cell line	suspension			-	Invitrogen

Table 6.1: Cell lines

**Cell culture media:**

<b>Cells</b>	<b>Cell culture medium</b>
<b>B16-muFAP</b>	RPMI 1640 supplemented with: - 10 % FCS - 0.75 µg/ml puromycin - 250 µg/ml zeocin
<b>MC38-muFAP</b>	Dulbecco's Modified Eagle's Medium (DMEM) supplemented with: - 10 % FCS - 2 mM L-Glutamine - 1 mM sodium pyruvate - 0.1 mM NEAA - 6 µg/ml puromycin
<b>HEK293-F</b>	FreeStyle F17 supplemented with: - 20 ml/L Glutamax - 2.5 ml/L Pluronic F-68
<b>Bone marrow-derived dendritic cells</b>	RPMI 1640 supplemented with: - 10 % FCS, - 2 mM L-Glutamine, - 1 mM sodium pyruvate, - 50 mM β-Mercaptoethanol, - 100 units/ml penicillin + 100 µg/ml streptomycin
<b>Freshly isolated splenocytes</b> (R10F <sup>+</sup> /β-Me medium)	RPMI 1640 supplemented with: - 10 % FCS - 1 mM sodium pyruvate - 0.1 mM NEAA - 50 mM β-Mercaptoethanol - 100 units/ml penicillin + 100 µg/ml streptomycin

**Table 6.2: Cell culture media****6.2.4 In vivo procedures**

C57BL/6NCrl mice	Charles River Laboratories
Bedding	Ssniff
Cages	Tecniplast
Drink bottle	Tecniplast
Pelleted standard diet	ProvimiKliba
Isofluran CP (Isofluran)	CP-Pharma
Ketavet (ketamine)	Pfizer Deutschland
Rompun (xylazine)	Bayer Pharma
ODN 1585 VacciGrade	InvivoGen
Poly(I:C) HMW	InvivoGen
Recombinant Murine IL-2	PeptoTech
Purified anti-mouse IL-2 Antibody (JES6-5H4)	BioLegend
Shaver	Harotec
Caliper	Mitutoyo Messgeräte

Surgical instruments	B. Braun Melsungen
27 G / 25 G needles STERICAN	B. Braun Melsungen
BD Microfine+ U100 Insulin syringes	Becton, Dickinson and Company
SOLOFIX blood lancets	B. Braun Melsungen
Blood capillaries	Hirschmann Laborgeräte
Microvette tubes 100 LH	Sarstedt

### 6.2.5 Quantitative real-time polymerase chain reaction

RNA later	Qiagen
Lysing matrix tubes	MP Biomedicals
MagNA Pure LC RNA Isolation Kit III	Roche
iScript Select cDNA Synthesis Kit	Bio-Rad
LightCycler FastSart DNA Master SYBR Green I Kit	Roche
LightCycler Capillaries	Roche

#### Primer:

Gene	Primer sense	Primer antisense	Company
TRP-2	5'-TTAGGTCCAGGACGCCCC-3'	5'-CTGTGCCACGTGACAAAGGC-3'	Metabion International AG
GAPDH	5'-CAATGTGTCCGTCGTGGA-3'	5'-GATGCCTGCTTACCACC-3'	Metabion International AG

Table 6.3: Primer for qPCR

### 6.2.6 Flow cytometry

MACSQuant Running buffer	Miltenyi Biotec
MACSQuant Washing solution	Miltenyi Biotec
MACSQuant Storage solution	Miltenyi Biotec
MACS Bleach solution	Miltenyi Biotec
MACSQuant Calibration Beads	Miltenyi Biotec
Compensation Particles Set (Anti-Mouse, Hamster, Rat)	BD Biosciences
Cell Staining Buffer	BioLegend
Fixation Buffer	BioLegend
Intracellular Staining Perm Wash Buffer (10x)	BioLegend
RBC Lysis Buffer 10x	BioLegend
TruStain fcX antibody	BioLegend

DAPI (4',6-diamidin-2-phenylindol)	Roche
DNase I solution	StemCell Technologies
Dispase	StemCell Technologies
Collagenase D	Roche

**Flow cytometry antibodies:****Primary antibodies**

Antigen	Fluorochrome	Source	Reactivity	Clone	Isotype	Manufacturer
CD45	PerCP	Rat	Mouse	30-F11	IgG2b, κ	BioLegend
CD3ε	Brilliant Violet 421	Hamster	Mouse	145-2C11	IgG	BioLegend
CD3ε	APC-Cy7	Hamster	Mouse	145-2C11	IgG	BioLegend
CD3ε	FITC	Hamster	Mouse	145-2C11	IgG	BioLegend
CD4	FITC	Rat	Mouse	GK1.5	IgG2b, κ	BioLegend
CD4	APC-Cy7	Rat	Mouse	GK1.5	IgG2b, κ	BioLegend
CD8a	Brilliant Violet 510	Rat	Mouse	53-6.7	IgG2a, κ	BioLegend
CD8a	PerCP	Rat	Mouse	53-6.7	IgG2a, κ	BioLegend
CD44	PE	Rat	Mouse	IM7	IgG2b, κ	BioLegend
CD62L	PE-Cy7	Rat	Mouse	MEL-14	IgG2a, κ	BioLegend
CD127	PE-Cy7	Rat	Mouse	A7R34	IgG2a, κ	BioLegend
PD-1	PE	Rat	Mouse	29F.1A12	IgG2a, κ	BioLegend
PD-L1	PE	Rat	Mouse	10F.9G2	IgG2b, κ	BioLegend
CD25	PE-Cy7	Rat	Mouse	PC61	IgG1, λ	BioLegend
FoxP3	PE	Rat	Mouse	MF-14	IgG2b, κ	BioLegend
IFN-γ	PE	Rat	Mouse	XMG1.2	IgG1, κ	BioLegend
CD40	PerCP-Cy5.5	Rat	Mouse	3/23	IgG2a, κ	BioLegend
CD80	PE-Cy7	Hamster	Mouse	16-10A1	IgG	BioLegend
CD86	Brilliant Violet 510	Rat	Mouse	GL-1	IgG2a, κ	BioLegend
I-A/I-E	FITC	Rat	Mouse	M5/114.15.2	IgG2b, κ	BioLegend
CD11c	APC	Hamster	Mouse	N418	IgG	BioLegend
"SIINFEKL" on H-2K <sup>b</sup>	PE	Mouse	Mouse	25-D1.16	IgG1, κ	BioLegend

Table 6.4: Primary antibodies for flow cytometry

**Dextramers for detection of specific CD8<sup>+</sup> T cells**

Antigen	Fluorochrome	Source	Reactivity	Manufacturer
"SSPPMFRV" / H-2K <sup>b</sup>	APC	Synthetic production	MCMV m38-specific T cell receptor (murine)	Immudex
"SIINFEKL" / H-2K <sup>b</sup>	APC	Synthetic production	OVA <sub>257-264</sub> -specific T cell receptor (murine)	Immudex

Table 6.5: Dextramers for flow cytometry

**Secondary antibodies**

Antigen	Fluorochrome	Source	Reactivity	Clone	Isotype	Manufacturer
Mouse IgG2c	FITC	Goat	Mouse	Polyclonal	-	LifeSpan BioSciences
H-2K <sup>b</sup>	APC	Mouse (BALB/c)	Mouse (C57BL/6)	AF6-88.5	IgG2a, κ	BioLegend

Table 6.6: Secondary antibodies for flow cytometry

**Isotype control antibodies**

Fluorochrome	Source	Clone	Isotype	Manufacturer
PE-Cy7	Rat	G0114F7	IgG1, λ	BioLegend
PE	Rat	RTK2071	IgG1, κ	BioLegend
Brilliant Violet 510	Rat	RTK2758	IgG2a, κ	BioLegend
PE	Rat	RTK2758	IgG2a, κ	BioLegend
PerCP	Rat	RTK2758	IgG2a, κ	BioLegend
PerCP-Cy5.5	Rat	RTK2758	IgG2a, κ	BioLegend
PE-Cy7	Rat	RTK2758	IgG2a, κ	BioLegend
FITC	Rat	RTK4530	IgG2b, κ	BioLegend
PE	Rat	RTK4530	IgG2b, κ	BioLegend
PerCP	Rat	RTK4530	IgG2b, κ	BioLegend
APC-Cy7	Rat	RTK4530	IgG2b, κ	BioLegend
Brilliant Violet 421	Hamster	RTK888	IgG	BioLegend
FITC	Hamster	RTK888	IgG	BioLegend
APC	Hamster	RTK888	IgG	BioLegend
APC-Cy7	Hamster	RTK888	IgG	BioLegend
PE-Cy7	Hamster	RTK888	IgG	BioLegend
PE	Mouse	MOPC-21	IgG1, κ	BioLegend
APC	Mouse	MOPC-173	IgG2a, κ	BioLegend

Table 6.7: Isotype control antibodies for flow cytometry

## 6.2.7 Immunohistochemistry and ultramicroscopy

Richard-Allan Scientific NEG 50 Frozen Section Medium	Thermo Scientific
Microscope slides	Thermo Scientific
Coverslips	Carl Roth
Microtome blades A35	FEATHER Safety Razor
Microtome blades C35	FEATHER Safety Razor
Dako Pen	Dako
Protein Block Serum-Free	Dako
Antibody Diluent, Dako REAL	Dako
Discovery Antibody Diluent	Ventana
ProLong Gold antifade reagent with DAPI	Life Technologies
Eukitt	Fluka

### Immunohistochemistry antibodies:

#### Primary antibodies

Antigen	Conjugate	Source	Reactivity	Clone	Concentration	Manufacturer
CD8a	-	Rabbit	Mouse	Polyclonal	1 mg/ml	Synaptic Systems
FAP	Alexa 647	Human	Human Mouse	28H1sf W(3a) IgG1	0.96 mg/ml	Roche Glycart

Table 6.8: Primary antibodies for immunohistochemistry

#### Secondary antibodies

Antigen	Conjugate	Source	Reactivity	Clone	Concentration	Manufacturer
IgG (H+L)	Alexa 488	Goat	Rabbit	Polyclonal	2 mg/ml	Thermo Fisher Scientific

Table 6.9: Secondary antibodies for immunohistochemistry

## 7 METHODS

### 7.1 DESIGN AND CONSTRUCTION OF SURROGATE FUSION MOLECULES AND ANTIBODIES

#### 7.1.1 DNA expression vector construction

For production of the plasmids needed for DNA vaccination and expression of peptide-MHC class I-IgG fusion proteins, T cell bispecific and anti-XCR1 antibodies already established standard protocols were used. Plasmid maps of the cloned DNA vectors with amino acid sequences were designed with the program *Vector NTI* (Invitrogen) and can be found in the appendix. Plasmids were cloned by inserting new sequences into already existing standard expression vectors. All expression vectors contained a CMV-promoter, Intron A, start codon and signal peptide for secretion and a bovine growth hormone polyadenylation (BGHpA). New sequences were designed and then purchased from *GeneArt* as gene synthesis. Gene synthesis were provided as lyophilisate and reconstituted in PCR-grade water to a concentration of 0.1 µg/µl.

#### 7.1.2 Restriction enzyme DNA fragmentation

DNA fragments for recombinant cloning were generated with restriction enzyme cleavage. Two restriction enzymes were used to cut out DNA sequences. For both donor plasmid and receiving plasmid, identical enzymes were used to generate matching DNA ends. 2 to 3 µg DNA of each plasmid were digested with 20 U of each restriction enzyme in a buffer and at a temperature suitable for both enzymes. Afterwards DNA fragments were separated with gel electrophoresis.

For analytical digestions two to three restriction enzymes, which cut the destination vector in another pattern as the new subcloned vector, were chosen. As a result destination and subcloned vector show different gel electrophoresis lanes. Analytical digestions were performed for one hour with 200 ng DNA and 5 U of each restriction enzyme in a buffer and at a temperature suitable for all used enzymes.

### **7.1.3 Agarose gel electrophoresis**

For gel electrophoresis DNA samples were diluted with a gel loading buffer containing 0.125 % (w/v) bromophenol blue, 25 % (w/v) Ficoll and 100 mM EDTA and loaded to an agarose gel (1 % agarose, TRIS-Borat-EDTA-buffer, 10 µg/ml *SYBR Safe DNA Gel Stain* (Thermo Fisher Scientific)). Gels were run at a constant voltage of 7 V/cm for 30 to 60 minutes. By excitation of the *SYBR Safe DNA Gel Stain* intercalated in the DNA with ultraviolet light, DNA got visible and could be recovered from the gel.

### **7.1.4 Agarose gel extraction of DNA**

For extraction of DNA from the agarose gel the *QIAquick Gel Extraction Kit* (Qiagen) was used. DNA fragments of interest were cut out of the gel and transferred into a 2 ml Eppendorf tube. Then DNA was isolated according to the manufacturer's instructions. Gel slides were dissolved in a buffer and then applied to a column which binds nucleic acids to a silica membrane at high-salt conditions. Finally pure DNA was eluted with water. DNA concentration was measured with a spectral photometer.

### **7.1.5 Dephosphorylation of vector fragments**

In order to prevent re-ligation of the digested destination vector, phosphate groups of the linearized plasmid DNA were removed with *Alkaline Phosphatase* (Roche). Therefore up to 1 pM 5' terminal phosphorylated DNA fragments were incubated with 1 U *Alkaline Phosphatase* for 10 minutes at 37°C. Afterwards the enzyme was inactivated at 65°C for 10 minutes.

### **7.1.6 Ligation of DNA fragments**

Ligation of insert and dephosphorylated vector fragment was performed using the *Rapid DNA Ligation Kit* (Roche). Vector fragment and insert were mixed at a molar ratio of 1:5 not exceeding the maximum amount of 200 ng DNA. Then DNA solution was filled up to 10 µl with *DNA Dilution Buffer* and 10 µl *Ligation buffer* and 1 µl *T4 DNA Ligase* were added. After 10 minutes of incubation at 25°C ligated plasmid DNA could be stored at -20°C without heat inactivation of enzyme or directly used for transformation of competent E.coli cells.

### 7.1.7 Bacterial transformation

For amplification of plasmid DNA the chemically competent *E.coli* strain *NEB 5-alphaF'*<sup>q</sup> from NEB was used. 50 µl of cells were thawed on ice for 10 minutes and 100 ng of plasmid DNA was added. After incubation of the mixture on ice for 30 minutes a heat shock was performed placing the vial in a 42°C water bath for exactly 30 seconds. Then cells were put back on ice for 5 minutes and resuspended in 200 µl *SOC Outgrowth Medium* (NEB). After incubation with shaking at 350 rpm for 30 to 60 minutes at 37°C the mixture was spread on a LB agar plate (LB medium: 5 g Trypton, 10 g yeast extract, 10 g sodium chloride in 1 L water) containing ampicillin (100 µg/ml) as selection antibiotic. Agar plates were placed into the brood chamber at 37°C overnight and the day later single colonies on the agar plate were picked and incubated in 3 ml LB medium containing ampicillin (*amp*<sup>+</sup>) for another 24 hours.

Genotype *NEB 5-alphaF'*<sup>q</sup>: ***fhuA2 Δ(argF-lacZ)U169 phoA glnV44 Φ80 Δ(lacZ)M15  
gyrA96 recA1 relA1 endA1 thi-1 hsdR17***

### 7.1.8 Plasmid DNA isolation and further proliferation

To verify the right assembling of the subcloned vector, plasmid DNA was isolated from *E.coli* clones with the *QIAprep Spin Miniprep Kit* (Qiagen) and used for analytical restriction enzyme cleavage. With the kit plasmid DNA is prepared by alkaline lysis of bacterial cells and adsorption of plasmid DNA to silica matrices. DNA sequence of plasmids was additionally confirmed by Sanger sequence analysis performed by the company *Sequiserve*. If correct assembling of the subcloned vector was confirmed in one of the Mini-Preps, the same clone was picked again from the agar plate, propagated in 3 ml LB medium (*amp*<sup>+</sup>) for 12 hours and inoculated into 800 ml LB medium (*amp*<sup>+</sup>) in a ratio of 1:1 000. After 12 to 16 hours of incubation in the brood chamber with shaking at 300 rpm at 37°C, plasmid DNA was extracted with the *NucleoBond PC 2000 Kit* (Macherey-Nagel). Cells are lysed under alkaline conditions and plasmid DNA is isolated via anion-exchange chromatography. DNA extracted from Mega-Preps was used for transfection of HEK293-F cells and therefore had to be sterilized by ethanol precipitation.

### **7.1.9 DNA purification by ethanol precipitation**

For ethanol precipitation plasmid DNA was mixed with sodium acetate solution (3 M, pH 5.2) in a ratio of 1:10 and precipitated by addition of 2.5 volume ethanol. The pellet was washed with 70 % ethanol, centrifuged and resuspended in sterile water. Yield and concentration of DNA was determined with a spectral photometer.

### **7.1.10 Transient transfection of HEK293-F cells**

Peptide-MHC class I-IgG fusion proteins, T cell bispecific and anti-XCR1 antibodies were transiently expressed in HEK293-F cells (Invitrogen). The transfection reagent *PEIpro* (Polyplus) was used. It is based on poly-cationic PEI polymers, which build so called polyplexes with the negative charged DNA. Production of antibodies and fusion molecules for in vivo use was accomplished in 2 to 6 L shake flasks scale to yield enough protein for this purpose. Transfection of HEK293-F cells was performed at a cell density of 20 to 25 x 10<sup>5</sup> cells/ml. For each liter of HEK293-F culture volume 0.5 mg DNA was diluted with 40 ml PBS and 1.25 ml *PEIpro* transfection reagent was added. When more than one plasmid was used for transfection, the equimolar amount of DNA depending on the size of plasmid (bp) was calculated and accordingly used. For production of pMHCI-IgG fusion proteins a molar ratio of 3:2:1 for peptide-MHCI-antibody heavy chain:antibody heavy chain:antibody light chain was applied. For the TCB antibody a molar ratio of 1:1:1:1 for all of the 4 plasmids was used. The normal anti-XCR1 antibody was produced with a molar ratio of 1:2 for antibody heavy chain:antibody light chain. For complex building the DNA/*PEIpro* mixture was incubated at room temperature for 8 to 15 minutes. Then it was added to the HEK293-F culture incubated in shake flasks in a humidified incubator at 120 rpm, 36.5°C temperature and 7% CO<sub>2</sub>. Three hours after transfection VPA (valproic acid) solution was added to a final concentration of 4 mM in the shake flask. VPA is a histon-deacetylase inhibitor, which was used for enhancement of protein expression. Special attention was paid to the right dilution of VPA as it induces apoptosis and contributes to a premature cell death. Until harvest, cell number and viability was checked daily. 24 hours after transfection supplementary feeding of cells was started. Therefore a 6 ml glucose bolus (Stock solution: 500 g/L glucose) was added once per liter HEK293-F transfection culture and additionally 120 ml Feed7 (Stock solution: 6.5 g/L D-glucose, 3 g/L L-glutamine, 2 g/L L-asparagine, 0.3 ml/L ethanolamine, 30 g/L soy peptone (*HyPep 1510*), 85.5 mg/L ammonium-Fe(III)-citrate) was administered daily per liter HEK293-F transfection culture. Harvest of

transfection culture was performed when viability of cells dropped to 50 % or on day 7 after transfection. Cell suspension was centrifuged first at 2 000 rpm for 30 minutes to deplete cells from the supernatant containing the protein and then at 3 500 rpm for 90 minutes for optimal removal of remaining cell fragments. The supernatant was pre-filtrated over a PES filter with pore size 0.45 µm and then filtered through a 0.22 µm sterile filter. Afterwards the sterile harvest was stored at -20°C or directly used for purification of protein.

#### **7.1.11 Protein purification**

Protein purification was carried out by the department for Biochemistry (Large Molecule Research, Roche Diagnostics GmbH). Proteins were purified from supernatant by Protein A affinity chromatography with *HiTrap MabSelect SuRe columns* (GE Healthcare). After a wash step antibodies were eluted with 50 mM sodium citrate (pH 3.2). To remove aggregates and byproducts a preparative size-exclusion chromatography was performed with *HiLoad 16/60 Superdex 200 pg columns* (GE Healthcare). Purified proteins were buffered in 20 mM Histidine and 140 mM sodium chloride at pH 6.0. The concentration of purified proteins was determined with a calculation of the extinction coefficient according to the protein sequence and measurements of the optical density at 280 nm. Purified proteins were concentrated to 2 to 6 mg/ml with *Amicon Ultra – 15 Centrifugal Filter Units* (Merck Millipore) with a molecular cut off of 30 000. Purity of protein was assessed by SDS-PAGE (sodium dodecyl sulfate polyacrylamide gel electrophoresis) and western blotting and protein identity by mass spectroscopy.

#### **7.1.12 Protein fusion by enzymatic sortase coupling**

The anti-XCR1 antibody MARX10 used for vaccination was produced with a C-terminally fused sortase tag followed by a poly-histidine tag. This has the advantage that any peptide, which should be used as antigen for vaccination, can be fused to the antibody via enzymatic sortase coupling. The sortase A peptide recognition motif “LPXTG” (amino acid sequence: Leu–Pro–any–Thr–Gly) was added to the C-terminus of the antibody (sortase tag) and an oligo-glycine motif was fused to the N-terminus of the peptide. For linking the immunodominant epitope m38 of the murine Cytomegalovirus (MCMV) to the MARX10 antibody, an amino acid sequence consisting of the complete m38 peptide (“SSPPMFRV”) and the ten amino acids naturally occurring N-terminally of the peptide in the protein sequence was used. This ensures that the m38 epitope is normally

processed inside the cell after internalization and correctly presented in MHC class I complexes on the cell surface. The following amino acid sequences were fused to the heavy chain of the antibody (C-terminal) and the peptide (N-terminal):

#### Antibody:

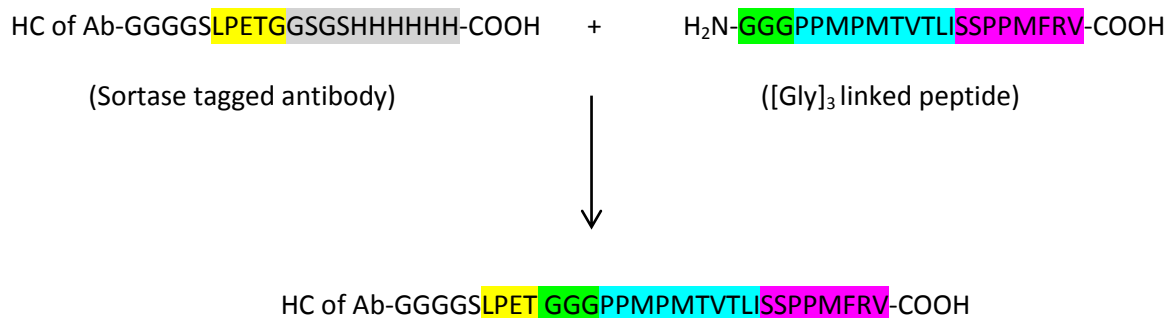
Antibody heavy chain-GGGGSLPETGGSGSHHHHHH-COOH      sortase motif      poly-histidine-tag

#### Peptide:

H<sub>2</sub>N-GGGPPMPMTVTLISSPPMFRV-COOH      (Gly)<sub>3</sub> motif      10 previous AA      m38 peptide

For enzymatic reaction 20 mg of the sortase tagged MARX10 antibody were incubated with (Gly)<sub>3</sub>-fused peptide and sortase A in sortase buffer at a molar ratio of 0.8:1:15 (sortase A:antibody:peptide). After 3 hours of incubation in a 37°C water bath the peptide was C-terminally fused to the MARX10 antibody.

#### Enzymatic reaction:



After sortase coupling affinity purification was performed with poly-histidine-tag columns to deplete non- or single-coupled protein. After purification antibodies were concentrated to 2 to 6 mg/ml with *Amicon Ultra – 15 Centrifugal Filter Units* (Merck Millipore) with a molecular cut off of 30 000. Purity of protein was assessed by SDS-PAGE and western blotting.

## 7.2 CELL CULTURE TECHNIQUES

### 7.2.1 Cell culture conditions

All adherent tumor cell lines (table 6.1: B16-muFAP and MC38-muFAP) were grown on polystyrene dishes in a humidified incubator at 37°C supplied with 5% CO<sub>2</sub>. Bone marrow-derived dendritic cells were cultured under same conditions in non-tissue culture treated 6-well-plates to avoid

attachment of the cells to the dish. Production cell line HEK293-F (table 6.1: Human embryonic kidney 293-FreeStyle) was cultured in shake flasks in a humidified incubator at 120 rpm, 36.5°C temperature and 7% CO<sub>2</sub>. All cells were grown in dedicated media as specified in table 6.2. To maintain selective pressure, permanently transfected tumor cell lines were cultured with addition of the respective antibiotic. Before in vivo inoculation the absence of murine pathogens like Mycoplasma Genus, Mousepox (Ectromelia), Mouse parvoviruses (MPV/MVM), Mouse Hepatitis Virus (MHV), Reovirus (REO-3), Lymphochoriomeningitis Virus (LCMV), Mouse Rotavirus (MRV (EDIM)), Theiler's Murine Encephalomyelitis Virus (TMEV), Hantavirus Hantaan, Mouse Adenoviruses (MAV 1 and 2), Murine Cytomegalovirus (MCMV), Pneumonia Virus of Mice (PVM), Sendai Virus and Murine Norovirus (MNV) in tumor cell lines was confirmed by PCR.

### **7.2.2 Thawing, subculturing and freezing of cells**

For cultivating cells stored in liquid nitrogen, cell suspension was briefly thawed in a water bath at 37°C until a little clump of frozen cells remained and then immediately mixed with preheated cell culture media. To remove DMSO the cell suspension was centrifuged at 300 x g for 5 minutes at room temperature and the supernatant was discarded. The remaining cell pellet was resuspended in cell culture medium and transferred to a culture dish.

When adherent cells (tumor cell lines) were 80 to 100 % confluent, cell culture medium was removed from the culture dish and the cell layer was washed with PBS and then covered with *Accutase Solution* (Sigma Aldrich) for cell detachment. After incubation with accutase at 37°C for 2 to 5 minutes detached cells were resuspended in cell culture medium containing FCS (fetal calf serum) to stop the enzymatic reaction. Cells were centrifuged at 300 x g for 5 minutes and the cell pellet was resuspended in the required volume of cell culture medium. Cells were counted and subcultured into new dishes in a ratio ranging from 1:3 – 1:10 depending on the cell type. If tumor cell lines were used for flow cytometry analysis, cells were resuspended in an appropriate volume of *Cell Staining Buffer* (BioLegend) after centrifugation and adjusted to  $10 \times 10^6$  cells/ml.

Suspension cells (HEK293-F and dendritic cells) were subcultured by addition or replacement of fresh cell culture medium. When HEK293-F cells reached a viable cell density of 40 to 45 x 10<sup>5</sup> cells/ml cells were subcultured in a ratio of 1:10. For transfection of HEK293-F cells a viable cell density of 20 to 25 x 10<sup>5</sup> cells/ml cells was preferred. Dendritic cells were subcultured only once in a ratio of 1:2 three days after cell culture start.

For permanent storage detached and resuspended cells were centrifuged at 300 x g for 5 minutes at room temperature. Then the cell pellet was resuspended in 1ml FCS containing 10% DMSO, frozen at - 80°C and transferred to liquid nitrogen for permanent storage the next day.

### **7.2.3 Cell counting**

Cell number was calculated with the *Vi-Cell XR Cell Viability Analyzer* (Beckman Coulter Biomedical). The device diluted the provided cell suspension with trypan blue and analyzed 50 aliquots of the suspension. Cellular viability and cell number were determined.

### **7.2.4 Development and maturation of bone marrow-derived dendritic cells**

After generating a single cell suspension, bone marrow cells were cultivated in a special medium (see table 6.2) supplemented with 0.05 µg/ml GM-CSF (granulocyte macrophage colony-stimulating factor) to induce development of dendritic cells out of bone marrow cells. After three days DCs were subcultured with the same medium in a ratio of 1:2. Another three days later LPS (Lipopolysaccharide; final concentration: 0.1 µg/ml) was added overnight for maturation of bone marrow-derived DCs. The day after maturation DCs could be used for peptide-loading.

### **7.2.5 Peptide-loading of cells**

Loading of cells was always performed with the peptides of the immunodominant epitopes of either the murine Cytomegalovirus (MCMV m38: “SSPPMFRV”) or ovalbumin (OVA<sub>257-264</sub>: “SIINFEKL”). The peptides were presented on the murine MHC class I complex H-2K<sup>b</sup>. All cells to be loaded were positive for expression of the murine H-2K<sup>b</sup> MHC class I complex.

#### **7.2.5.1 Bone marrow-derived dendritic cells**

For loading of mature bone marrow-derived DCs with peptide cells were resuspended in RPMI(-) and cell density was adjusted to 5 x 10<sup>5</sup> cells/ml. Peptide was added in a concentration of 2 µg/ml. After incubation for 1 to 2 hours at 37°C in the humidified incubator supplied with 5% CO<sub>2</sub> cells were washed twice with RPMI containing 10% FCS and finally resuspended in PBS for injection into

animals. Before administration, peptide-loading of bone marrow-derived DCs was confirmed by flow cytometry at least in the case of the peptide “SIINFEKL” (see chapter 7.4.2.4).

### 7.2.5.2 Splenocytes

Splenocytes were loaded with peptide at a cell density of  $5 \times 10^6$  cells/ml in R10F<sup>+</sup>/β-Me medium (see table 6.2). Cells were loaded for 1 – 2 hours at 37°C in a humidified incubator supplied with 5% CO<sub>2</sub> at a molar peptide concentration of 10 μM. To remove unbound peptide, splenocytes were washed two times with PBS and then resuspended in PBS for injection into mice. Before administration, peptide-loading of splenocytes was checked by flow cytometry at least in the case of the peptide “SIINFEKL” (see chapter 7.4.2.4).

### 7.2.5.3 Tumor cells

Peptide-loaded tumor cells served as positive control in in vitro assays. Tumor cell lines B16-muFAP and MC38-muFAP were loaded at different molar peptide concentrations. Peptide-loading was performed with cells adherent at the dish or in suspension after detachment at a cell density of  $5 \times 10^6$  cells/ml. After incubation in a humidified incubator at 37°C supplied with 5% CO<sub>2</sub> for 1 to 2 hours, unbound peptide was removed by washing of cells with plain medium or *Cell Staining Buffer* (BioLegend).

## 7.3 IN VIVO PROCEDURES

### 7.3.1 General modalities

#### 7.3.1.1 Animal facility

Animals were kept in the conventional area of the animal facility of the Roche Diagnostics GmbH in Penzberg. The facility is AAALAC accredited and therefore conform to the “Association for the Assessment and Accreditation of Laboratory Animal Care International”. Animals are tested quarterly for defined germs according to FELASA (Federation of Laboratory Animal Science Associations) guidelines. Mice were purchased from Charles River Laboratories. After an adaption period of one week after arrival, mice were used for experiments. A 12 hour dark/light-rhythm was used in the facility. Mice were housed in groups of six animals in M3 cages and fed with autoclaved

standard diet. As enrichment animals got hemp pads for nest-building and small pieces of wood for gnawing. Bedding, water bottles and food pellets were changed weekly by animal care takers. All animals were monitored daily for general health condition. The Veterinary Office of the administrative district examines the animal facility quarterly and all experiments conducted for this work were approved by the Government of Upper Bavaria.

### **7.3.1.2 Laboratory animals**

Due to the polymorphism of MHC complexes in vivo efficacy, tolerability and interaction with the immune system of peptide-MHC class I-IgG fusion proteins could only be tested in syngeneic immunocompetent mouse models using surrogate molecules. In the fusion molecules the murine MHC class I complex H-2K<sup>b</sup> carrying an immunodominant epitope of the murine Cytomegalovirus (m38: "SSPPMFRV") or ovalbumin (OVA<sub>257-264</sub>: "SIINFEKL") was used. Effector cells recruited by the fusion proteins for elimination of tumor cells were generated via vaccination. As C57BL/6N mice are immunocompetent and have the MHC haplotype H-2K<sup>b</sup> this mouse strain was the most appropriate one for the studies. There are also several established tumor models available for that mouse strain. The C57BL/6N strain is a black coated inbred strain broadly used for multiple purposes. It was developed by C.C. Little in 1921.

### **7.3.1.3 Anesthesia of mice**

For painful procedures such as opening of the thorax for final blood drawing from the heart mice were anesthetized with an intraperitoneal injection of 100 mg/kg ketamine (Ketavet) and 20 mg/kg xylazine (Rompun) in a total volume of 200 µl PBS. After 5 to 10 minutes surgical tolerance was reached, which could be proved by testing of reflexes such as the pedal withdrawal reflex of the hind limb. If animals were not euthanized during intervention (e.g. final blood draw from the heart) awakening after the procedure was monitored and heat source was provided. For short time anesthesia or anesthesia during less painful procedures inhalation anesthesia with Isofluran was used. Applying this method animals get anesthetized within a few minutes and awake easily without extended post-anesthetic sleep.

### 7.3.1.4 Euthanasia of mice

Mice were sacrificed by cervical dislocation, exposure to CO<sub>2</sub> or final blood draw from the heart under ketamine / xylazine anesthesia. When using CO<sub>2</sub> for euthanasia special attention was paid to a laminar flow rate, slowly rising concentration in the sealed cage and maintenance of accustomed groups of animals.

## 7.3.2 Vaccination methods

### 7.3.2.1 Vaccination with peptide-loaded, bone marrow-derived dendritic cells

After generation of peptide-loaded dendritic cells out of bone marrow from donor mice as described in chapters 7.3.4.3.4, 7.2.4 and 7.2.5.1, animals were injected with the cells for vaccination. Before injection into mice loading of DCs with peptide (OVA<sub>257-264</sub>: "SIINFEKL") was checked with flow cytometry (see chapter 7.4.2.4). OVA<sub>257-264</sub>-loaded DCs were injected into mice in four different application routes (i.v., i.p., i.d. and s.c.) with different cell numbers for each administration route. The following table describes the classification of animals and number of cells injected:

Group:	Route of administration of DC:	Number of cells injected:	Injected volume:
1	intravenous (i.v.)	$8 \times 10^5$	100 $\mu$ l
2	Intraperitoneal (i.p.)	$1.6 \times 10^6$	200 $\mu$ l
3	Intradermal (i.d.)	$2 \times 10^5$	20 $\mu$ l
4	Subcutaneous (s.c.)	$1.6 \times 10^6$	200 $\mu$ l

Table 7.1: Injections of peptide-loaded dendritic cells

For intradermal injection mice were anesthetized with Isofluran, other injections were performed without anesthesia. Intradermal and subcutaneous injection sites were shaved and disinfected with alcohol prior to injection. In total animals of all groups were injected 3 times at an interval of 7 days with the peptide-loaded DCs. Together with the first and the second immunization 20  $\mu$ g of CpG oligodeoxynucleotides (CpG ODN: *ODN 1585 VacciGrade*, InvivoGen) were administered subcutaneously. In bacterial DNA CpG motifs are 20 times more frequent compared to mammalian DNA. The motifs are recognized by TLR9, which leads to strong immunostimulatory effects on cells of the innate immune system [106]. After injection DCs presenting the peptide OVA<sub>257-264</sub> prime CD8<sup>+</sup> T cells and induce an OVA<sub>257-264</sub>-specific CD8<sup>+</sup> T cell response. Blood was drawn twice weekly from mice to evaluate CD8<sup>+</sup> T cell response with flow cytometry analysis (see chapter 7.4.2.3).

### 7.3.2.2 DNA vaccination with electroporation

Generation of standard vectors encoding for ovalbumin was described in chapters 7.1.1 to 7.1.9. Mice were anesthetized with Isofluran and shaved on the back or hind leg. Then 100 µg plasmid DNA was injected either intradermal (volume: 20 µl) on the back or intramuscular (volume: 30 µl) into the *M. tibialis anterior*. Immediately after injection of DNA the electroporation was performed with the *BTX Electroporation device ECM 830* (Harvard Apparatus) with a *2 Needle Array* (Harvard Apparatus; needle length: 20 mm, needle spacing: 10 mm). After intradermal injection electrodes were placed on the dry, shaved skin in such a way that they enclose the welt resulting from the intradermal injection. After intramuscular injection electrodes were inserted into the muscle to a depth of 5 mm so that they encompass the injection site of DNA. Following electric pulses were delivered for electroporation:

<b>Injection route of DNA:</b>	<b>intradermal</b>	<b>intramuscular</b>
Number of pulses:	2	6
Voltage:	500 V	75 V
Duration:	0.1 ms	20 ms
Interval:	0.125 s	200 ms
	followed by	
Number of pulses:	4	
Voltage:	144 V	
Duration:	10 ms	
Interval:	0.125 s	

**Table 7.2: Electric pulses for electroporation**

Injection of DNA with subsequent electroporation was performed two times at an interval of seven days. Together with every immunization 20 µg of the TLR9-agonist CpG ODN (InvivoGen) were administered subcutaneously. Electroporation enhances the uptake of the vector into the antigen presenting cells. Genes encoding for the antigen are expressed and produce a xenogeneic protein. This protein (ovalbumin) is processed inside the cell and immunogenic peptides (including OVA<sub>257-264</sub>) of the protein are displayed on MHC class I molecules on the cell surface of antigen presenting cells. Cells presenting the peptide OVA<sub>257-264</sub> prime CD8<sup>+</sup> T cells and induce an OVA<sub>257-264</sub>-specific CD8<sup>+</sup> T cell response. After vaccination blood was drawn twice weekly from mice to evaluate CD8<sup>+</sup> T cell response with flow cytometry analysis (see chapter 7.4.2.3).

### 7.3.2.3 XCR1-targeted vaccination

The XCR1-targeted vaccination was performed according to a modified and expanded protocol from Hartung et al. [107]. The anti-XCR1 antibody MARX10 was produced and recombinantly fused to an antigen as described in chapter 7.1. The entire ovalbumin protein or peptides of the immunodominant epitopes of either ovalbumin (OVA<sub>257-264</sub>: “SIINFEKL”) or the murine Cytomegalovirus (MCMV m38: “SSPPMFRV”) were used as antigens for fusion to the targeting antibody. Antibody fusion molecules OVA<sub>257-264</sub>-MARX10 and ovalbumin-MARX10 were kindly provided from Prof. Richard Krokzek from the Robert-Koch-Institute in Berlin, whereas the MCMV m38-MARX10 antibody fusion was produced in house (see chapter 7.1). Peptide-loaded splenocytes were generated as described in chapters 7.3.4.3.1 and 7.2.5.2. Vaccination was performed in three steps as shown in table 7.3. In the first step called “Prime” mice were injected intravenously with the XCR1-targeting antibody MARX10, which was C-terminally fused to the antigen, and polyinosinic-polycytidylic acid (*Poly(I:C)* HMW: InvivoGen). The MARX10 antibody targets cross-presenting DCs via binding to XCR1, which is exclusively expressed on those cells. The antigen gets internalized into cross-presenting DCs together with the antibody. In order to become degraded by the proteasome the antigenic fragments need to escape from the endosomal compartment. After reaching the cytoplasm the antigens become degraded at the proteasome and loaded onto MHC class I complexes after transport into the endoplasmic reticulum via the TAP-transporter. Cells presenting the peptide OVA<sub>257-264</sub> prime CD8<sup>+</sup> T cells and induce an OVA<sub>257-264</sub>-specific CD8<sup>+</sup> T cell response, cells presenting the peptide MCMV m38 prime CD8<sup>+</sup> T cells and induce a MCMV m38-specific CD8<sup>+</sup> T cell response. The TLR3-agonist *Poly(I:C)* was applied as adjuvant to enhance immune activation. It is a synthetic analog of double-stranded RNA (dsRNA) present in viruses that activates mainly cells of the innate immune system [108]. Five days after the “Prime” step the “Antigen dependent amplification system” (ADAS) was applied. Peptide-loaded splenocytes (OVA<sub>257-264</sub> or MCMV m38) from donor mice of the same mouse strain were administered intravenously together with *Poly(I:C)*. This step was performed to boost the specific CD8<sup>+</sup> T cell response elicited in the first step of vaccination. Prior to injection, peptide-loading of splenocytes was confirmed by flow cytometry at least in the case of OVA<sub>257-264</sub> (see chapter 7.4.2.4). The following two or three days complexed IL-2 (cxIL-2) was injected intraperitoneally for further amplification of specific CD8<sup>+</sup> T cells. Complexed IL-2 was prepared by adding the purified anti-mouse IL-2 antibody *JES6-5H4* (BioLegend) to Recombinant Murine IL-2 (PeproTec) the day before injection. Antibody and target got complexed overnight and could be further diluted with PBS and

administered the next day. To evaluate the contribution of every single step to the CD8<sup>+</sup> T cell response, three treatment groups were built for each antigen (OVA<sub>257-264</sub> and MCMV m38). One group was administered the “Prime” step only, the other group was given the “Prime” step followed by the “ADAS” step and the third group was treated with all three steps of the vaccination method. After vaccination blood was drawn twice weekly from mice to evaluate CD8<sup>+</sup> T cell response with flow cytometry analysis (see chapter 7.4.2.3).

Step:	Compounds administered:	Amount:	Injection route:	Injected volume:	Injection time point:
Step 1 Prime	MCMV m38-MARX10 or OVA <sub>257-264</sub> -MARX10 or ovalbumin-MARX10	5 µg/animal 5 µg/animal 2 µg/animal	intravenous	100 µl	Day 0
	Poly(I:C)	10 µg/animal			
Step 2 ADAS	MCMV m38- or OVA <sub>257-264</sub> - loaded splenocytes	1 x 10 <sup>7</sup> cells/animal	intravenous	100 µl	Day 5
	Poly(I:C)	50 µg/animal			
Step 3 cxIL-2	Complexed IL-2: -Recombinant Murine IL-2 -anti-mouse IL-2 Ab: JES6-5H4	2.5 µg/animal 10 µg/animal	intraperitoneal	200 µl	Day 6, 7 (and 8)

**Table 7.3: Steps of XCR1-targeted vaccination**

### 7.3.3 Tumor models

#### 7.3.3.1 Experimental lung metastasis model

In order to induce experimental lung metastasis, mice were injected intravenously into the lateral tail vein with 2 x 10<sup>5</sup> FAP-transfected B16 melanoma cells in a total volume of 100 µl Hank's Balanced Salt Solution (HBSS). For generation of effector cells, animals were immunized with the XCR1-targeted vaccination. In the preventive setting animals were pretreated with the therapeutic proteins 24 hours before tumor challenge followed by one therapeutic treatment three days later. In the therapeutic setting melanoma cells were allowed to grow in the lungs for nine days after intravenous injection. Then mice were treated twice at an interval of 3 days (see figure 8.9 and table 8.1). Animals were monitored daily for general health condition. When stopping criterion (such as bad health condition, bodyweight loss  $\geq$  20 %) was reached mice were sacrificed. After 21 days of metastasis growth animals were sacrificed by cervical dislocation under Isofluran anesthesia and lungs were removed for assessment of metastasis burden or confirmation of stable target expression in tumor cells with immunohistochemistry (IHC) staining of FAP.

### 7.3.3.2 Subcutaneous tumor model

Mice were anesthetized with Isofluran and shaved on the right flank. After disinfection of the skin with alcohol  $1 \times 10^6$  FAP-transfected MC38 colorectal cancer cells were injected subcutaneously in a total volume of 100  $\mu$ l PBS. Tumor volume was measured weekly with a caliper. After 2 to 3 weeks tumors reached an average volume of 75  $\text{mm}^3$  and animals were immunized with the XCR1-targeted vaccination. Finally animals included into the study were selected based on their blood level of specific  $\text{CD8}^+$  T cells and tumor volume. Four different groups were treated five times at an interval of 3 days during the  $\text{CD8}^+$  T cell peak after vaccination (see figure 8.13 and table 8.2). Tumor volume and bodyweight were assessed twice weekly during study. Animals were monitored daily for general health condition. When stopping criterion (such as bad health condition, bodyweight loss  $\geq 20$  % or tumor diameter  $\geq 2.0$  cm) was reached mice were sacrificed. Besides efficacy evaluation of pMHC1-IgG and TCB treatment, tumors were used for ultramicroscopy, flow cytometry and IHC analyses (see chapters 7.3.4.3.3 and 7.4.2 to 7.4.4).

Formula for calculation of ellipsoid tumor volumes:

$$\text{TV} = (l \cdot w^2)/2 [\text{mm}^3]$$

**TV = tumor volume in  $\text{mm}^3$**

**l = length of tumor in mm**

**w = width of tumor in mm**

### 7.3.3.3 Treatment with fusion molecules

After assignment to treatment and control groups animals were treated with compounds or PBS as shown in the tables 8.1 and 8.2. Peptide-MHC class I-IgG fusion (pMHC1-IgG) molecules were administered in a dosage of 5 mg/kg and T cell bispecific (TCB) antibodies were given with 2 mg/kg. All compounds were tested for endotoxin levels before injection (reference value:  $< 1$  EU/ml). Therapeutic proteins were diluted with PBS in such a way that they could be injected in a total volume of 100  $\mu$ l into the lateral tail vein of mice.

### **7.3.4 Harvest of sample material**

#### **7.3.4.1 Blood sampling and preparation of blood samples**

Blood samples were taken to determine blood levels of specific CD8<sup>+</sup> T cells. For evaluation of CD8<sup>+</sup> T cell response after vaccination blood was drawn twice weekly from mice over a period of three to four weeks. Blood sampling methods were changed for consecutive blood draws. Blood taking from the retrobulbar venous plexus was performed only once at every eye at an interval of at least two weeks and under Isofluran anesthesia. A non-heparinized glass capillary with an external diameter of 0.8 mm was used. Blood sampling from the tail vein and the facial vein was conducted without anesthesia. For drawing blood from the tail vein a 27 G needle was employed and the facial vein was punctured with a lancet. Maximally 7.5 % of the total blood volume was taken weekly, assuming that the total blood volume is about 7 % of bodyweight. When blood sampling was performed only once during the whole study (lung metastasis and subcutaneous tumor model) up to 10 % of the total blood volume was taken. For final blood drawings mice were anesthetized with an intraperitoneal injection of ketamine / xylazine. Thorax was opened and blood was drawn with a 25 G needle from the right ventricle of the heart.

For flow cytometry analysis 50 to 100 µl blood were collected in heparinized *Microvette tubes* (Sarstedt) and diluted with 50 µl PBS. Next lysis of blood was performed with 1 ml of 1x *RBC Lysis Buffer* (BioLegend) for 15 minutes at room temperature. After blood lysis erythrocytes were destroyed and only leukocytes remained. To remove cell debris after blood lysis, white blood cells were washed twice with *Cell Staining Buffer* (BioLegend) and could be used for flow cytometry afterwards (see chapters 7.4.2.2 and 7.4.2.3).

#### **7.3.4.2 Harvest of organs and tissue**

For harvesting of organs and tissue animals were sacrificed by cervical dislocation, CO<sub>2</sub> exposure or euthanasia by exsanguination under anesthesia.

##### **7.3.4.2.1 Harvest and processing of spleens**

Spleens were taken out for flow cytometry analysis of specific CD8<sup>+</sup> T cells, for preparation of peptide-loaded splenocytes applied during vaccination and for the use in in vitro assays. Organs were placed into ice cold PBS up to further processing and then mashed through a 70 µm cell strainer with the plunge of a syringe. After rinsing the mesh with PBS cell suspension was

centrifuged at 380 x g for 8 minutes at room temperature. The splenocyte pellet was resuspended in 5 ml of 1x *RBC Lysis Buffer* (BioLegend) for lysis of erythrocytes. After 5 minutes of incubation on ice lysis was stopped by addition of 30 ml PBS and the cell suspension was filtered again through a 70 µm cell strainer and centrifuged. For flow cytometry analysis splenocytes were resuspended in an appropriate volume of *Cell Staining Buffer* (BioLegend). For loading of splenocytes with peptide the cell pellet was resuspended in R10F<sup>+</sup>/β-Me medium (see table 6.2) and for the use in in vitro assays splenocytes were resuspended in *CTS AIM-V Medium* (Life Technologies).

#### **7.3.4.2.2 Harvest and processing of lungs**

After 21 days of metastasis growth lungs were taken out for assessment of metastasis burden and IHC analysis. After opening of thorax lungs were taken out properly and placed into *RNA later* (Qiagen). Then visible metastases were counted by two different experimenters under a binocular microscope. Afterwards RNA was prepared from lung tissue for qPCR (see chapter 7.4.1). For IHC analyses lungs were placed into *Richard-Allan Scientific NEG 50 Frozen Section Medium* (Thermo Scientific) on dry ice and then stored at -80°C until preparation of sections (see chapter 7.4.3).

#### **7.3.4.2.3 Harvest and processing of tumors**

In the subcutaneous tumor model tumors were excised and used for flow cytometry, ultramicroscopy and IHC analyses. For flow cytometry analysis tumors were harvested 48 hours after the second treatment for characterization of T cells present in the tumor or 31 days after the last treatment for detection of PD-L1 expression of tumor cells. Tumors were cut into small pieces and digested in 5 ml RPMI (-) with 1 mg/ml *Dispase* (StemCell Technologies), 0.8 mg/ml *Collagenase D* (Roche) and 0.01 mg/ml *DNase* (StemCell Technologies). After 20 minutes of incubation under rotation in a humidified incubator at 37°C supplied with 5% CO<sub>2</sub>, the digest was transferred over a 70 µm cell strainer by gently pressing the tumor pieces through the mesh with the plunge of a syringe. The mesh was rinsed with PBS and the tumor cell suspension was then centrifuged at 300 x g for 5 minutes at room temperature. After centrifugation the cell pellet was resuspended in an appropriate volume of *Cell Staining Buffer* (BioLegend) for flow cytometry analysis (see chapter 7.4.2). For IHC analyses of stable target expression of tumor cells, tumors were excised 18 days after the last treatment. For IHC staining of CD8<sup>+</sup> T cells recruited into the tumor, tumors were harvested 24 hours after the first treatment. After excision tumors were put immediately in liquid

nitrogen and then stored at -80°C until preparation of sections (see chapter 7.4.3). Explanting of tumors for ultramicroscopy analysis is described in chapter 7.4.4.1.

#### **7.3.4.2.4 Harvest and processing of bone marrow**

For generation of peptide-loaded DCs bone marrow from femur and tibia of mice was isolated. Therefore animals' fur was disinfected with 70 % ethanol and bones were prepared as clean as possible. Both hind limbs were cut off by cutting through the hip joint and placed into sterile PBS. Special care was taken not to open the bone cavity. Bones were washed with ethanol and placed in a new petri dish containing sterile PBS. Remnants of muscle tissue were removed by rubbing the bones in gauze. Then femur and tibia were separated by cutting through the knee joint. After another disinfection step with ethanol, single bones were placed in a new petri dish with sterile PBS. Then each bone was cut at both ends and the bone cavity was flushed with medium (see table 6.2) using a 27 G needle. Bone marrow of two femurs and two tibias each was collected in one tube and centrifuged at 400 x g for 4 minutes at room temperature. The cell pellet was resuspended in 6 ml of 1x *RBC lysis buffer* (BioLegend) and incubated at room temperature for two minutes to lyse erythrocytes. Reaction was stopped by filling up to 50 ml with sterile PBS and bone marrow cell suspension was filtered through a 70 µm cell strainer by mashing the cells through the sieve using the plunge of a syringe. After a second centrifugation step bone marrow cells were resuspended in medium (see table 6.2) supplemented with 0.05 µg/ml GM-CSF and cultivated in non-tissue culture treated 6-well-plates to differentiate into DCs.

## **7.4 EX VIVO PROCEDURES**

### **7.4.1 Quantitative real-time polymerase chain reaction for evaluation of lung metastasis burden**

Quantitative real-time polymerase chain reaction (qPCR) for quantification of tyrosinase-related protein 2 (TRP-2) expression in lungs was performed according to a modified protocol from Sorensen et al. [109].

#### 7.4.1.1 RNA isolation

RNA isolation from lungs was performed with the *MagNA Pure LC RNA Isolation Kit III* (Roche). Harvested lungs were fixed in *RNA later* (Qiagen) until processing. For tissue disruption and homogenization lungs were transferred to *Lysing Matrix Tubes* (MP Biomedicals) containing garnet matrix and a ceramic sphere and 1 ml *Tissue Lysis Buffer* (bottle 8) was added. Then tubes were placed into the FastPrep 24 homogenizer and 2 cycles of tissue disruption and homogenization were carried out at 6.5 M/S for 2 x 50 seconds. After every run samples were put on ice for a few minutes to avoid degradation of RNA by heat stress. After incubation for 30 minutes at room temperature samples were centrifuged at room temperature for 3 minutes at 13 000 x g and 350  $\mu$ l of the lysate supernatant were used for RNA isolation with the *MagNA Pure LC 1.0* instrument. Therefore all reagents provided with the kit (bottle 1 to 7) were filled into the reagent tubs in an appropriate volume as listed in the information screen of the instrument. Then RNA isolation procedure was started. In the first step *Binding Buffer* (bottle 3) and *Proteinase K* (bottle 6a reconstituted with buffer from bottle 6b) are added to the samples for complete cell lysis, digestion of proteins and release of RNA. Then *Magnetic Glass Particles* (bottle 5) are added and RNA binds to the silica surface of the particles. By incubation with *DNase I* (bottle 4a reconstituted with buffer from bottle 4b) genomic DNA is removed. *Magnetic Glass Particles* with bound RNA are magnetically separated from the residual lysed sample and washed with *Wash Buffer I* (bottle 1) several times to purify RNA from unbound substances. Then a second wash step is carried out with *Wash Buffer II* (bottle 2) to remove residual salts and cellular debris. Finally purified RNA is eluted from the *Magnetic Glass Particles* with 50  $\mu$ l *Elution Buffer* (bottle 7). The whole procedure is run and monitored by the *MagNA Pure LC Software V3.0*. After isolation of RNA, concentration was determined with a spectral photometer and adjusted to 25 ng/ $\mu$ l with PCR-grade water.

#### 7.4.1.2 Reverse transcription of RNA

For synthesis of first-strand complementary DNA (cDNA) from RNA the *iScript Select cDNA Synthesis Kit* (Bio-Rad) was used. 200 ng of RNA were mixed with following components of the kit and incubated in the *Veriti 96 Well Thermal Cycler* (Applied Biosystems) as follows:

Component:	Volume ( $\mu$ l):
RNA sample (25 ng/ $\mu$ l)	8
5x iScript select reaction mix	4
Random primer	2
iScript reverse transcriptase	1
Nuclease-free water	5
<b>Total:</b>	<b>20</b>

Table 7.5: Reverse transcription reaction mix

Temperature:	Incubation time:
25°C	5 min.
42°C	30 min.
85°C	5 min.

Table 7.4: Reverse transcription protocol

Using this method about 1  $\mu$ g/ $\mu$ l cDNA was yielded. One-tenth (2  $\mu$ l) of the reaction volume was used for quantitative real-time polymerase chain reaction.

#### 7.4.1.3 Quantitative real-time polymerase chain reaction (qPCR)

For qPCR the *LightCycler FastSart DNA Master SYBR Green I Kit* (Roche) and the *LightCycler Carousel-Based System* (Roche) was used. PCR primers for TRP-2 (tyrosinase-related protein 2) and GAPDH (glyceraldehyd-3-phosphat-dehydrogenase) were purchased from Metabion and reconstituted with PCR-grade water to 200  $\mu$ M. The melanocyte-specific gene TRP-2 was used as target gene and the housekeeping gene GAPDH served as reference gene. Tyrosinase-related protein 2 is involved in the synthesis of melanin and therefore specifically expressed in melanocytes. The detection of melanocyte-specific cDNA, or mRNA (messenger ribonucleic acid) respectively, encoding TRP-2 in lung tissue indicates the presence of B16-muFAP melanoma cells in the lung. During qPCR the desired PCR products are amplified and detected by measurement of a fluorescence signal. The fluorescent dye *SYBR Green I* intercalates into double stranded DNA. If *SYBR Green I* is in solution, it exhibits only very little fluorescence. Bound to DNA its fluorescence is greatly enhanced. Therefore the amount of intercalated dye is directly proportional to the amount of PCR product generated during PCR. 2  $\mu$ g of cDNA produced by reverse transcription as described above were used as template for quantitative real time PCR. *LightCycler FastStart DNA Master SYBR Green I* (10x conc.) was prepared by pipetting 10  $\mu$ l from vial 1a (*LightCycler FastStart Enzyme*) into one vial 1b (*LightCycler FastStart Reaction Mix SYBR Green I*, 10 x conc.) containing *FastSart Taq DNA Polymerase*, reaction buffer, dNTP mix, *SYBR Green I* dye and 10 mM  $MgCl_2$ . Total  $MgCl_2$  concentration in the reaction mix was raised to 1.5 mM by adding additional  $MgCl_2$  to ensure specific and efficient amplification of target DNA. Primer stock solutions (200  $\mu$ M) were diluted 1:40 to 5  $\mu$ M with PCR-grade water prior to use. All solutions were prepared and stored on ice during procedure and mixed gently by pipetting up and down before use. Components were mixed

together in pre-cooled *LightCycler Capillaries* as described in table 7.6 below. Then capillaries were put into the *LightCycler Sample Carousel*, centrifuged with the *LC Carousel Centrifuge* and transferred into the *LightCycler* instrument for qPCR applying the following protocol (see table 7.7):

Component:	Volume (µl):
cDNA sample (1 µg/µl)	2
LightCycler FastStart DNA Master SYBR Green I (10x conc.)	2
MgCl <sub>2</sub> (25 nM)	0.4
Primer sense (5 µM)	2
Primer antisense (5 µM)	2
PCR-grade water	11.6
<b>Total:</b>	<b>20</b>

Table 7.6: qPCR reaction mix

Segment:	Temperature:	Time:	Cycles:
<b>Pre-Incubation</b>			
Enzyme activation	95°C	5 min.	1
<b>Amplification</b>			
Denaturation	95°C	1 sec.	50
Annealing	58°C	9 sec.	
Elongation	72°C	9 sec.	
<b>Melting Curve</b>			
Denaturation	95°C	0 sec.	1
Annealing	65°C	15 sec.	
Melting	97°C	0 sec.	
<b>Cooling</b>			
Cooling	40°C	30 sec.	1

Table 7.7: qPCR protocol

For confirmation of specificity of PCR product a melting curve was applied. qPCR was monitored and recorded with the *LightCycler Software 3.5*.

#### 7.4.1.4 Evaluation of qPCR

For relative quantification of gene expression the crossing point (CP) values of samples were used. The CP values correspond to the number of PCR cycles needed for reaching a defined fluorescence signal. The more cycles are required to reach the defined fluorescence signal, the less amount of cDNA, or mRNA respectively, encoding the target gene was present in the sample at the beginning of PCR. Using relative quantification, not the absolute copy number of the target gene was defined, but the expression of the target gene was referred to a second gene, which is expressed ubiquitously and homogenously. In this case expression of the target gene TRP-2 was normalized to expression of the housekeeping gene GAPDH. As TRP-2 is specifically expressed in melanocytes, detection of cDNA, or mRNA respectively, encoding TRP-2 in lung tissue indicates the presence of B16-muFAP melanoma cells in lungs. By relative quantification of TRP-2 expression, metastasis burden in treatment and control groups can be quantified and compared, assuming that TRP-2 was expressed equally in treatment and control groups. All lung samples were measured as duplicates and the average value of CP was applied for relative quantification. As control samples lungs from

naïve mice were used. Relative expression of TRP-2 was calculated with the following formula [110]:

$$\text{Normalized TRP-2 expression} = 2^{-\Delta\Delta\text{CP}}$$

$$\Delta\Delta\text{CP} = \Delta\text{CP}_{\text{sample}} - \Delta\text{CP}_{\text{control}}$$

$$\Delta\text{CP} = \text{CP}_{\text{TRP-2}} - \text{CP}_{\text{GAPDH}}$$

## 7.4.2 Flow cytometry analyses

### 7.4.2.1 Settings of flow cytometry

Flow cytometry analyses were carried out with the *MACSQuant Analyzer 10* (Miltenyi Biotec). The device is equipped with three lasers: A violet one (405 nm) with two filters (450/50 nm and 525/50 nm), a blue one (488 nm) with four filters (525/50 nm, 585/40 nm, 655-730 nm and 750 nm LP) and a red one (635 nm) with two filters (655-730 nm and 750 nm LP). Consequently eight fluorescent channels and the forward scatter for size of cells as well as the side scatter for granularity of cells can be used for multi-color flow cytometry analysis. Cell surface antigens and intracellular antigens of cells can be detected by fluorescent dye-labeled antibodies binding to the antigen. For analysis the cell suspension is carried by a sheath fluid, which singularizes the cells and aligns them so that they pass the laser stream one after another. Thus every single cell can be analyzed by size and granularity as well as fluorescent pattern. For evaluation of flow cytometry analysis cells can be categorized into different populations according to their characters. Therefore the *FlowJo Software* (TreeStar) was used. Categorization into positive or negative populations was performed by reference to isotype controls of specific antibodies.

### 7.4.2.2 Preparation of samples for flow cytometry

For flow cytometry analyses a single cell suspension was generated and cells were adjusted to  $1 \times 10^6$  cells/well. After a wash step with *Cell Staining Buffer* (BioLegend), cells were resuspended in 100  $\mu\text{l}$  *Cell Staining Buffer* containing 1.0  $\mu\text{g}$  of *TruStain fcX antibody* (BioLegend) and incubated on ice for 5 to 10 minutes. This procedure was carried out for blockage of Fc $\gamma$  receptors IIa and III (CD32 and CD16) on the cell surface to avoid antigen independent binding of detection antibodies to Fc-receptors. After Fc-receptor block, fluorescent dye-conjugated detection antibodies or

purified primary antibodies (if a secondary antibody staining is necessary) were added at concentrations according to the manufacturer's instructions. Cells were incubated on ice in the dark for 20 minutes. If specific CD8<sup>+</sup> T cells should be detected, cells were pre-incubated with 10 µl of the appropriate *Dextramer* (Immudex) for 10 minutes at room temperature in the dark prior to cell surface staining with antibodies. After incubation cells were washed with 1 ml *Cell Staining Buffer* and centrifuged at 300 x g for 5 minutes at 4°C. If a purified primary antibody was used, cells were resuspended in 100 µl *Cell Staining Buffer* containing the appropriate amount of fluorochrome-conjugated secondary antibody, incubated on ice in the dark for 20 minutes and washed again with 1 ml *Cell Staining Buffer*. After washing cells were resuspended in 100 µl *Cell Staining Buffer* and analyzed with the flow cytometer. For exclusion of dead cells DAPI (4',6-diamidin-2-phenylindol), which binds to double stranded DNA in the nucleus and is therefore suitable for staining of dead cells, was used at a final concentration of 0.02 µg/ml. As DAPI penetration into the nucleus is time dependent and after longer time periods even live cells can be DAPI-positive, every sample on the 96-well-plate was incubated with DAPI for only a few minutes prior to measurement. This was accomplished by automated DAPI-labelling of every sample by the *MACSQuant Analyzer 10* prior to measurement.

If an intracellular target should be detected, cells were fixed and permeabilized with 1x *Fixation Buffer* (BioLegend) and 1x *Intracellular Staining Perm Wash Buffer* (BioLegend) after cell surface antigen staining. Then intracellular staining was performed with a fluorophore-conjugated antibody binding to the intracellular target. Cells were incubated at room temperature for 20 minutes in the dark and then washed two times with 1 ml of 1x *Intracellular Staining Perm Wash Buffer*. Finally cells were resuspended in 100 µl *Cell Staining Buffer* and analyzed with the flow cytometer. Using an intracellular staining no exclusion of dead cells was performed.

#### **7.4.2.3 Detection, quantification and characterization of specific CD8<sup>+</sup> T cells**

For detection and quantification of specific CD8<sup>+</sup> T cells in blood, spleen and tumors, cells were pre-stained with the appropriate *Dextramer* (OVA<sub>257-264</sub>: "SIINFEKL" on H-2K<sup>b</sup> or MCMV m38: "SSPPMFRV" on H-2K<sup>b</sup>) and afterwards labelled with fluorochrome-conjugated antibodies specific for murine CD8a, CD4, CD3ε and CD45. To characterize the phenotype of specific T cells fluorochrome-conjugated antibodies directed against murine PD-1, CD44, CD62L, CD127, CD25 and

FoxP3 were used in different combinations. For staining of FoxP3 an intracellular staining was performed.

#### 7.4.2.4 Confirmation of peptide-loading of cells

For confirmation of peptide-loading of bone marrow-derived DCs, splenocytes or tumor cells a commercially available fluorochrome-conjugated antibody recognizing the peptide "SIINFEKL" on H-2K<sup>b</sup> was used. As only for this combination of peptide and MHC class I complex a detection antibody is available, the MCMV-derived m38 peptide "SSPPMFRV" on H-2K<sup>b</sup> could not be checked for proper loading. In the case of bone marrow-derived DCs a costaining with fluorochrome-conjugated antibodies detecting murine CD40, CD80, CD86, I-A/I-E and CD11c was performed to determine activation status of DCs.

#### 7.4.2.5 IFN- $\gamma$ activation of CD8<sup>+</sup> T cells

For analysis of in vitro IFN- $\gamma$  activation of CD8<sup>+</sup> T cells an intracellular staining for IFN- $\gamma$  of splenocytes applied in the activation assay was performed. Prior to the intracellular staining splenocytes were stained with fluorochrome-conjugated antibodies recognizing murine CD8a, CD4, CD3 $\epsilon$  and CD45.

#### 7.4.2.6 Internalization and binding of fusion molecules to the target FAP

For analysis of binding and internalization of peptide-MHC class I-IgG fusion proteins on the cell surface of tumor cell lines, a staining with secondary antibodies was carried out. Therefore tumor cell lines B16-muFAP and MC38-muFAP were pre-incubated with fusion molecules functioning as primary antibodies at different concentrations. For confirmation of molecule binding, incubation was carried out for 1 hour at 4°C at a cell density of  $2 \times 10^6$  cells/ml. To check internalization of molecules, tumor cells were coincubated with the fusion molecules for 1, 6 or 24 hours at 4°C or 37°C at a cell density of  $2 \times 10^6$  cells/ml. After incubation cells were washed two times with 1 ml *Cell Staining Buffer* and incubated with a FITC-conjugated secondary antibody against murine IgG2c to detect the antibody part of the fusion molecule and an APC-conjugated secondary antibody recognizing H-2K<sup>b</sup> to detect the MHC class I complex of the fusion molecule. At least in the case of the OVA<sub>257-264</sub>-H-2K<sup>b</sup>-IgG fusion protein the APC-conjugated antibody recognizing "SIINFEKL" on

H-2K<sup>b</sup> could be used to detect the peptide-MHC class I part of the fusion construct on the cell surface. "SIINFEKL" peptide-loaded tumor cells served as a positive control.

#### **7.4.2.7 Confirmation of binding of fusion molecules after labelling**

In order to confirm that peptide-MHC class I-IgG fusion proteins still bind to their target FAP on the cell surface of tumor cell lines after in house Alexa 647-conjugation for ultramicroscopy, flow cytometry was applied. MC38-muFAP tumor cells were incubated with Alexa 647-labeled fusion molecules at a concentration of 2.0 µg/ml for 1 hour at 4°C at a cell density of 2 x 10<sup>6</sup> cells/ml. Then cells were washed with 1 ml *Cell Staining Buffer* and analyzed with the flow cytometer. In the channel detecting APC (red laser [635 nm], 655-730nm filter) cells carrying the Alexa 647-conjugated fusion molecule could be detected.

#### **7.4.2.8 Detection of PD-L1 expression in tumors**

For detection of PD-L1 upregulation in tumors, cells of digested tumors were stained with fluorochrome-conjugated antibodies specific for murine CD45 and PD-L1.

### **7.4.3 Immunohistochemistry**

#### **7.4.3.1 Sample preparation**

Frozen tumors or lungs embedded in *Richard-Allan Scientific NEG 50 Frozen Section Medium* (Thermo Scientific) were used for immunohistochemical analysis. Therefore 10 to 14 µm frozen sections of tissues were prepared using a pre-cooled cryostat. Before sectioning, tissue stored at -80°C was equilibrated to -20°C for approximately 15 minutes to prevent cracking of the tissue block while cutting. Then frozen sections were cut and mounted to adhesive glass slides. After drying of sections for a few minutes at room temperature, slides were stored at -80°C or directly used for staining.

First tissue was fixed for 10 minutes in 4 % paraformaldehyde (PFA) containing 5 mM sucrose at room temperature. Then slides were washed twice with deionized water for five minutes. Afterwards samples were blocked with *Protein Block Serum-Free* (Dako) for 10 minutes to avoid

non-specific binding of detection antibodies. After blocking of reactive sites, staining with detection antibodies was performed.

#### **7.4.3.2 Target expression of tumor cells in vivo**

To confirm maintenance of target expression of tumor cells in subcutaneous tumors and lung metastasis in vivo, IHC was applied. Sections of tumors and lung tissue containing metastases were stained with an antibody detecting the target FAP. Therefore the antibody *28H1sf W(3a)* (Roche Glycart), which is directly labeled with Alexa 647, was applied to the tissue section slides in a dilution of 1:900 for 60 minutes (see table 6.8 for concentration of antibody stock solution). Afterwards slides were washed two times with TBST for two minutes. After sealing of slides by mounting a coverslip with *ProLong Gold antifade reagent with DAPI* (Life Technologies), samples could be evaluated under the fluorescent microscope.

#### **7.4.3.3 Quantification of CD8<sup>+</sup> T cells in the tumor**

For illustration and quantification of CD8<sup>+</sup> T cell recruitment into the tumor after treatment, tumor sections were stained with an antibody specific for CD8a. Therefore slides were incubated with an unlabeled *polyclonal rabbit anti-mouse CD8a antibody* (Synaptic Systems) for 60 minutes at a dilution of 1:200 (see table 6.8 for concentration of antibody stock solution). Slides were washed three times with TBST for two minutes and then incubated with a secondary antibody. An *Alexa 488-labelled goat anti-rabbit antibody* (Invitrogen) was applied for 30 minutes in a dilution of 1:400 (see table 6.9 for concentration of antibody stock solution). After washing of slides with TBST for two minutes for three times, slides were mounted with a coverslip with *ProLong Gold antifade reagent with DAPI* (Life Technologies) and finally evaluated under the fluorescent microscope. For quantification of CD8<sup>+</sup> T cells present in the tumor, the average signal for each slide was quantified as positive stained area per five randomly selected tumor areas of 2 000 x 1 000 µm by automated analysis with the *Image Intensity Threshold Tool* (Roche).

#### 7.4.4 Ultramicroscopy

##### 7.4.4.1 Treatment of animals and processing of tumors

To analyze molecule penetration into solid subcutaneous tumors fluorescence ultramicroscopy was applied as described in Dobosz et al. [111]. Mice were injected intravenously into the lateral tail vein with Alexa 647-labelled MCMV m38-MHCI-IgG fusion protein (5 mg/kg) in a volume of 100  $\mu$ l PBS. Alexa 647-labelling of fusion molecules was carried out by the department for Protein Chemistry (Roche Diagnostics GmbH). Prior to injection Alexa 647-labeled fusion proteins were checked for maintenance of binding capacity by flow cytometry analysis (see chapter 7.2.4.7). 12, 24 or 48 hours after administration of Alexa 647-labeled molecules, animals were injected intravenously with Alexa 750-labeled *Bandeiraea simplicifolia* lectin (4 mg/kg) in a total volume of 100  $\mu$ l PBS to stain vessels. After five minutes of lectin circulation mice were sacrificed. Tumors were explanted immediately and incubated overnight in 4% PFA at room temperature in the dark. Afterwards tumors were dehydrated in a graded ethanol series (3 x 70 %, 2 x 95 % and 2 x 100 % for 30 minutes each) using the *Tissue-Tek VIP Vacuum Infiltration Processor* (Sakura Finetek) and placed into a clearing solution consisting of one volume part benzylalcohol and two volume parts benzylbenzoate. After incubation for two days at 4°C in the dark the specimen became optically transparent and tumors could be scanned with the ultra-microscope.

##### 7.4.4.2 Acquisition and quantification of labelled molecule in the tumors

Optically transparent tumors with a diameter up to 5 mm were analyzed with the ultramicroscope *MVX10 Fluoreszenz MacroZoom* (OLYMPUS CORPORATION), which is equipped with a *3QE Kamera* (LaVision BioTec). A magnification of x0.63 in combination with a x2 objective lens was applied. This resulted in a final xy resolution of 5.1  $\mu$ m, to which step size was adjusted. Tumors were scanned with the integrated *SuperK EXTREME supercontinuum white light laser* (NKT Photonics A/S), which is able to excite every fluorophore used in this experiment. First autofluorescence of tissue was measured to illustrate tumor morphology (excitation range: 543/22 nm; emission range: 593/40 nm; Exposure time per slice: 300 ms). Then Alexa 647 (excitation range: 655/15 nm; emission range: 680/30 nm; Exposure time per slice: 200 ms) and Alexa 750 (excitation range: 747/33 nm; emission range: 786/22 nm; Exposure time per slice: 500 ms) signals were measured to assess molecule penetration into the tumor and visualize vessels. Depending on tumor size acquisition took about 1 to 1.5 hours. During acquisition a *tagged image file format* (TIFF) is created

for every slice. Those were converted into *Digital Imaging and Communications in Medicine* (DICOM) files and visualized with the *OsiriX Software* (Pixmeo) for further editing. After processing of images with the software to exclude minimal residual fat tissue or other components not belonging to the tumor, data sets of each tumor were quantified with a set of custom-developed image analysis algorithms to define molecule penetration into the tumor and vascularization.

#### **7.4.4.3 Immunohistochemistry of ultramicroscopy samples**

Following 3D scanning with the ultramicroscope tumor samples were shortly incubated first in 100 % xylene to remove clearing solution and then in paraffin (3 x 1 hour). Tumors were embedded in paraffin blocks and tissue slices with a thickness of 2  $\mu\text{m}$  were cut randomly from the middle of the tumors and mounted to glass slides. Sections were incubated at 37°C overnight and then stored at 4°C until further processing. After deparaffination and rehydration (xylene: 3 x 5 minutes, ethanol series two minutes each: 2 x 100 %, 1 x 90 %, 1 x 80 %, 2 x 70 %, deionized water: 2 x 20 seconds) of tissue sections using the *Tissue-Tek VIP Vacuum Infiltration Processor* (Sakura Finetek), slides were sealed by mounting a coverslip with *ProLong Gold antifade reagent with DAPI* (Life Technologies). Then slides were scanned with the Fluorescence scanner *Pannoramic 250 Flash III* (3D Hitech), detecting Alexa 647, Alexa 750 and DAPI signals, and fluorescent images from sections were taken.

## **7.5 IN VITRO PROCEDURES**

### **7.5.1 Cytotoxicity analysis**

#### **7.5.1.1 xCELLigence assay**

For in vitro cytotoxicity analysis the *xCELLigence system* (Roche) was applied. The system is based on measurement of electrical impedance. For this purpose interdigitated microelectrodes are integrated on the bottom of special flat bottom *E-Plate 96* well-plates (ACEA Biosciences) used for the assay. If contact between electrodes and medium is isolated by the cell layer of adherent cells on the well bottom, electrical impedance is high. When cells die, contact between electrodes and medium rises and therefore electrical impedance is reduced. The *xCELLigence system* measures electrical impedance every 5 to 15 minutes according to the settings. In this way cell growth or

elimination of cells can be displayed as variation of electrical impedance over time. For growing phase of tumor cells after inoculation into the plate, cell culture medium was used. During cytotoxicity assay serum free *CTS AIM-V Medium* (Gibco by Life Technologies) was applied to avoid loading of effector cells with foreign antigen from serum and potential mutual killing.

### 7.5.1.2 Evaluation of cytotoxicity mediated by fusion molecules in the xCELLigence system

At the beginning 50  $\mu$ l of cell culture medium was added to the wells and background measurement was performed. Then 20 000 adherent MC38-muFAP tumor cells in a volume of 50  $\mu$ l cell culture medium were added per well. One day after cell inoculation medium was changed. Another 24 hours later, when cell index exceeded 1, the assay was started. First of all tumor cells in the positive control wells were loaded with peptide. Therefore medium was removed from the wells and 100  $\mu$ l cell culture medium containing peptide in different concentrations was added. After one to two hours in the incubator at 37°C peptide-loaded tumor cells were washed with 100  $\mu$ l *CTS AIM-V Medium*. Then all wells were washed with 180  $\mu$ l *CTS AIM-V Medium* and 50  $\mu$ l *CTS AIM-V Medium* was pipetted in each well. Afterwards 50  $\mu$ l *CTS AIM-V Medium* containing effector molecules in different concentrations (pMHC-I-IgG fusion proteins or TCB antibodies) were administered. Then 50  $\mu$ l *CTS AIM-V Medium* with 300 000 freshly isolated splenocytes from vaccinated mice were added. Splenocytes from vaccinated mice varied in their percentage of specific CD8<sup>+</sup> T cells from 2.5 to 3.0 % (percentage of all lymphocytes), so that effector cell:target cell ratio was about 0.25:1 (specific CD8<sup>+</sup> T cells:tumor cells). Control wells containing peptide-loaded tumor cells or tumor cells without effector molecules and/or effector cells were filled up to 150  $\mu$ l with *CTS AIM-V Medium*. 100 units/ml penicillin and 100  $\mu$ g/ml streptomycin were added to all wells to avoid contamination from animal-derived splenocytes. After 40 to 55 hours of incubation under cell culture conditions cytotoxicity was analyzed. For determination of spontaneous lysis of tumor cells mediated by splenocytes without effector molecules, wells containing only tumor cells and splenocytes were analyzed. Evaluation of specific tumor cell lysis in percent was calculated with the following formula:

**Specific tumor cell lysis [%] =**

$$\frac{[\text{cell index spontaneous lysis} - \text{cell index sample}]}{[\text{cell index spontaneous lysis}]} \times 100$$

### **7.5.2 IFN- $\gamma$ activation of CD8<sup>+</sup> T cells**

For analysis of in vitro IFN- $\gamma$  activation of CD8<sup>+</sup> T cells normal flat bottom 96-well-plates were prepared in the same manner as used for the *xCELLigence* cytotoxicity assay (see chapter 7.5.1.2). However, starting cell number was raised to 30 000 MC38-muFAP tumor cells per well to ensure a dense cell layer when starting the assay. In this assay splenocytes from vaccinated mice varied in their percentage of specific CD8<sup>+</sup> T cells from 5.5 to 13.5 % (percentage of all lymphocytes), so that effector cell:target cell ratio was about 0.33 to 1:1 (specific CD8<sup>+</sup> T cells:tumor cells). After six hours of incubation under cell culture conditions, splenocytes were taken out of the wells, centrifuged, resuspended in *Cell Staining Buffer* (BioLegend) and used for flow cytometry analysis after intracellular staining for IFN- $\gamma$  (see chapter 7.4.2.5).

## **7.6 STATISTICAL ANALYSES**

All graphs were generated with *GraphPad Prism 6* (Graphpad Software, Inc.). For statistical analysis the *JMP Software* (SAS Institute) was used applying the two-sided t-test for significance evaluation in the in vitro cytotoxicity analyses and the Wilcoxon-test for significance evaluation in the in vivo efficacy analyses. P-values from 0.01 to 0.05 were considered as significant (\*), p-values from 0.001 to < 0.01 were considered as very significant (\*\*) and p-values < 0.001 were considered as extremely significant (\*\*\*)

## 8 RESULTS

### 8.1 CHARACTERIZATION OF SURROGATE FUSION MOLECULES AND ANTIBODIES

For generation of surrogate peptide-MHC class I-IgG fusion proteins, T cell bispecific and anti-XCR1 antibodies standard expression vectors encoding for amino acid sequences of light chains, heavy chains and modified heavy chains were cloned (see appendix for plasmid card and amino acid sequences). HEK293-F cells were transiently transfected with expression plasmids and the protein secreted into the supernatant was purified by Protein A affinity chromatography.

#### 8.1.1 Structure of peptide-MHC class I-antibody (pMHCI-IgG) fusion proteins

##### 8.1.1.1 Design of the molecule and transfection vectors

For production of surrogate peptide-MHC class I-antibody fusion molecules three expression plasmids were cloned. All expression vectors contained a CMV-promoter, Intron A, start codon and signal peptide for secretion and BGHpA. The first plasmid [1] encoded for the antibody heavy chain with N-terminal fusion of the peptide-MHC class I complex and was about 6400 bp. The second vector [2] encoded for the normal antibody heavy chain with approximately 5100 bp and the third plasmid [3] for the antibody light chain was about 4400 bp. Vectors were applied at a molar ratio of 3:2:1 (plasmid [1]:plasmid [2]:plasmid [3]) for transient transfection. Consequently the fusion protein consisted of an entire murine IgG antibody, of which one heavy chain was fused to a peptide-MHC class I complex (Fig. 8.1 A). The heavy chain fused to the peptide-MHC class I complex was composed of following components in N- to C-terminal direction (Fig. 8.1 B): The antigenic peptide was fused to the murine beta-2-microglobulin ( $\beta_2M$ ) with a GS-linker ( $[G_4S]_3$ ). The  $\beta_2M$  was linked to the  $\alpha_1$  domain of the murine MHC class I complex with a second GS-linker ( $[G_4S]_4$ ). The murine MHC class I complex lacked the transmembrane domain and ended after the  $\alpha_3$  domain. The N-terminus of the variable domain (VH) of the antibody heavy chain was fused to the C-terminus of the  $\alpha_3$  domain of the MHC class I complex with a short GS-linker (GS). The variable domain is followed by the constant part of the heavy chain consisting of CH1 and the Fc-part of the antibody (hinge, CH2 and CH3). The normal heavy chain of the antibody was composed of the variable domain (VH) and constant regions CH1, hinge, CH2 and CH3. The antibody light chain comprised a variable domain (VL) and a constant domain Ck.

### 8.1.1.2 Disulfide-stabilization of the peptide-MHC class I complex in the fusion molecule

The GS-linkers used in the peptide-MHC class I complex linked to the heavy chain consisted of  $[G_4S]_n$  sequences. The linkers should have the effect of proper assembling of the MHC class I complex, stabilizing the peptide in the groove of the MHC class I complex. This should result in higher stability of the entire molecule and higher production yield. Additional stabilization of the peptide-MHC class I complex could be achieved by introduction of a disulfide bond connecting the linker between peptide and  $\beta_2M$  with the  $\alpha_1$  domain of the MHC class I complex. Therefore the second glycine in the linker and the tyrosine at position 84 in the MHC class I complex (N- to C-terminal direction) was mutated to cysteine [1, 112].

### 8.1.1.3 Modifications of the molecule for increased harvest of protein

As surrogate pMHCI-IgG fusions were designed in a hetero-dimerized format only one of the heavy chains was fused to a peptide-MHC class I complex and the other one remained unfused. To avoid assembling of two unfused heavy chains the knob-into-hole-modification was introduced in the Fc-part of the antibody [113]. Therefore defined amino acids in the CH3 domain of the heavy chains were mutated, which leads to a structural formation in that region that promotes the assembling of unfused heavy chains together with peptide-MHC class I complex fused heavy chains. The hole-modification was introduced in the peptide-MHC class I complex fused heavy chain. Threonine was mutated to serine at position 366 (EU-Index Kabat numbering scheme [114]), methionine to alanine at position 368 and tyrosine to valine at position 407. To implement the knob-modification in the CH3 domain of the unfused heavy chain threonine was exchanged to tryptophan at position 366. For enhanced stabilization of the heterodimer an additional artificial disulfide bond was inserted in the CH3 domain of the heavy chains. Therefore tyrosine was mutated to cysteine at position 349 on the hole-side and proline was exchanged to cysteine at position 354 on the knob-side. Despite the introduction of the knob-into-hole-modification a certain proportion of knob-knob-side products can be present after purification. As formats consisting of the normal antibody without peptide-MHC class I complex should be excluded after purification, another mutation in the CH3 domain of the knob-antibody heavy chain (normal antibody heavy chain without peptide-MHC class I complex) was implemented. The histidine at position 435 was exchanged to arginine and the leucine at position 436 to phenylalanine (HL->RF mutation). The result of this mutation is that the knob-antibody heavy chain can no longer bind to Protein A. Consequently unwanted knob-knob-side

products do not bind to the Protein A column during purification process, while desired knob-hole-products (antibody fused to one peptide-MHC class I complex) can still bind to the column with the hole-antibody heavy chain. Hole-hole-side products (antibody fused to two peptide-MHC class I complexes) were expressed so poorly that they were negligible as side product.

#### **8.1.1.4 Introduction of a silent Fc-part**

The constant domain of the antibody fusion molecules was the murine isotype IgG2c. To abrogate binding to Fc-gamma receptors (FcγR) and complement components (C1q) modifications in the CH2 domains of the antibody were introduced. At position 270 (Kabat numbering scheme [114]) aspartic acid was exchanged to alanine and at position 329 proline was mutated to glycine (DAPG mutation). In addition the leucine amino acids at positions 234 and 235 were mutated to alanine amino acids (LALA mutation) [115]. The mutations led to loss of binding capacity to FcγRI, FcγRII and FcγRIII, whereas FcRn (neonatal Fc-receptor) binding was unchanged. The antibody fusions have IgG-like half-life and pharmacokinetic properties. Also binding to C1q was inhibited so that CDC and FcγR-mediated co-activation of innate immune effector cells such as ADCC or ADCP were prevented.

#### **8.1.1.5 Specifications of the molecules**

The target on the mouse tumor cells was murine FAP (fibroblast activation protein). The monoclonal antibody 28H1 was used to target murine FAP. It binds to murine and human FAP with high bivalent affinity (μFAP: < 1 pM, huFAP: 268 pM) [116, 117]. The non-binding control molecule contained an antibody based on the antibody germline sequence DP47 [118] with a modified complementarity-determining region 3 (CDR3). Lack of binding to any murine target structure and normal antibody pharmacokinetic properties in vivo were confirmed previous in various experiments (Roche unpublished). For the peptide-MHC class I part of the molecule peptides of the immunodominant epitopes of the murine Cytomegalovirus (MCMV m38: "SSPPMFRV" or MCMV IE3: "RALEYKNL") or ovalbumin (OVA<sub>257-264</sub>: "SIINFEKL") were applied. Peptides derived from both MCMV and ovalbumin are presented on the murine MHC class I complex H-2K<sup>b</sup> so that this MHC class I allotype was chosen for the fusion proteins.

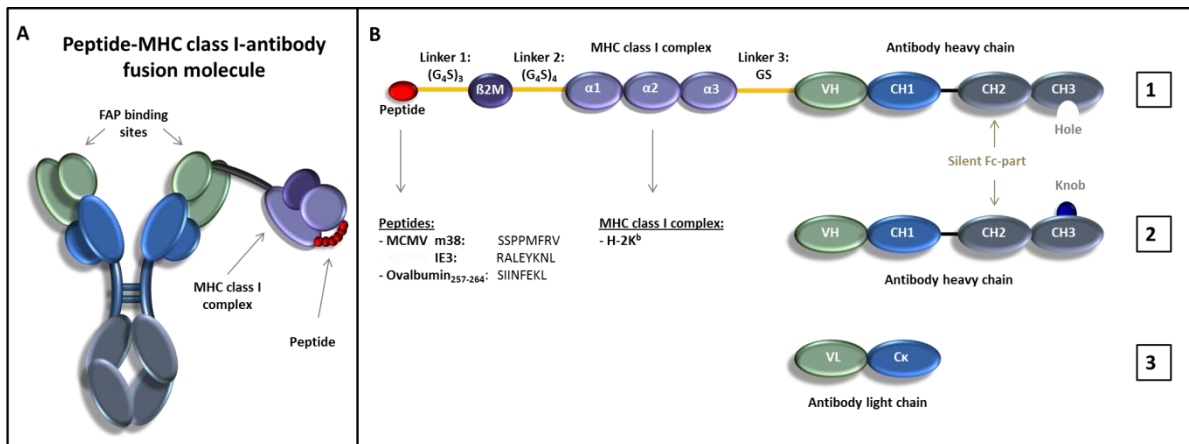


**Figure 8.1: Schematic illustration of the peptide-MHC class I-IgG fusion molecules.**

**(A)** pMHCI-IgGs comprise of a full murine monoclonal IgG2c antibody with two binding moieties for the target fibroblast activation protein (FAP). The N-terminus of one heavy chain is fused with the murine MHC class I complex H-2K<sup>b</sup> via a linker. The MHC class I complex carries a covalently fused, antigenic peptide. **(B)** N- to C-terminal drawing of antibody chains: pMHCI fused antibody heavy chain (1): Antigenic peptide (red), Linker 1: (G<sub>4</sub>S)<sub>3</sub> (orange), beta-2-microglobulin (dark purple), Linker 2: (G<sub>4</sub>S)<sub>4</sub> (orange), extracellular domain of H-2K<sup>b</sup> α1-α3 (light purple), Linker 3: GS (orange), variable (VH) (green) and constant (CH1) (blue) domain of murine IgG2c antibody heavy chain, hinge (black), effector-function free CH2 domain and CH3 domain with hole mutation of IgG2c antibody heavy chain (grey). Unfused antibody heavy chain (2): Variable (VH) (green) and constant (CH1) (blue) domain of murine IgG2c antibody heavy chain, hinge (black), effector-function free CH2 domain and CH3 domain with knob mutation of IgG2c antibody heavy chain (grey). Antibody light chain (3): Variable (VL) (green) and constant Ckappa (Cκ) (blue) domain of antibody light chain.

## 8.1.2 Structure of the T cell bispecific (TCB) antibody

### 8.1.2.1 Design and modifications of the molecule

Basis of the surrogate TCB antibody was the 2+1 format (Fig. 8.2 A). It comprised a full IgG with two binding moieties for the target and to the N-terminus of one of the antibody heavy chains a CD3ε-binding Fab (Fragment antigen binding) was fused. Consequently the molecule could bind bivalently to the antibody target on the tumor cell and monovalently to CD3ε on the T cell. The Fc-part of the heavy chains was engineered to promote heterodimerization. Proper assembling of light chains was forced by introducing a CH1-Cκ crossover in the CD3ε binding Fab in the CrossMAb format [119]. As CH1 and CH1 domains as well as Cκ and Cκ are repulsive and only CH1 and Cκ can form a heteromeric complex, light chains of CD3ε binding Fab and target binding Fab could only assemble to their corresponding part of the heavy chain (Fig. 8.2 B). The antibody was murine IgG1-based and the Fc-part was also silenced with the DAPG mutation as described in chapter 8.1.1.4.

### 8.1.2.2 Design of transfection vectors

To generate the surrogate TCB antibody 4 expression vectors were designed (Fig. 8.2 B). The first plasmid [1] was about 4400 bp and encoded for the variable region of the light chain (VL) of the CD3 $\epsilon$  binding domain followed by the CH1 domain crossed from the heavy chain. The second [2] vector encoded for the antibody heavy chain with both CD3 $\epsilon$  binding and target binding domain and was about 5800 bp. The third vector [3] encoded with about 5100 bp for the normal antibody heavy chain containing only the target binding domain (VH-CH1-hinge-CH2-CH3) and the fourth plasmid [4] encoded with about 4400 bp for the normal antibody light chain with the variable region (VL) of the target binding domain and the constant region (C $\kappa$ ). The heavy chain containing two binding domains (third vector) was composed of following components in N- to C-terminal direction: The VH domain binding to CD3 $\epsilon$  was followed by the C $\kappa$  domain crossed from the light chain. Next the VH domain binding to the target followed by the CH1 domain was attached and fused to hinge and CH2 and CH3 domain of the Fc-part. For transient transfection of HEK293-F cells vectors were applied at a molar ratio of 1:1:1:1.

### 8.1.2.3 Specifications of the molecule

The target binding variable domains of the surrogate TCB antibody were derived from the monoclonal antibody 28H1 which binds to murine FAP (see chapter 8.1.1.5). The CD3 $\epsilon$  binding Fab was derived from the monoclonal antibody 145-2C11 and targeted the epsilon chain of murine CD3 [120].

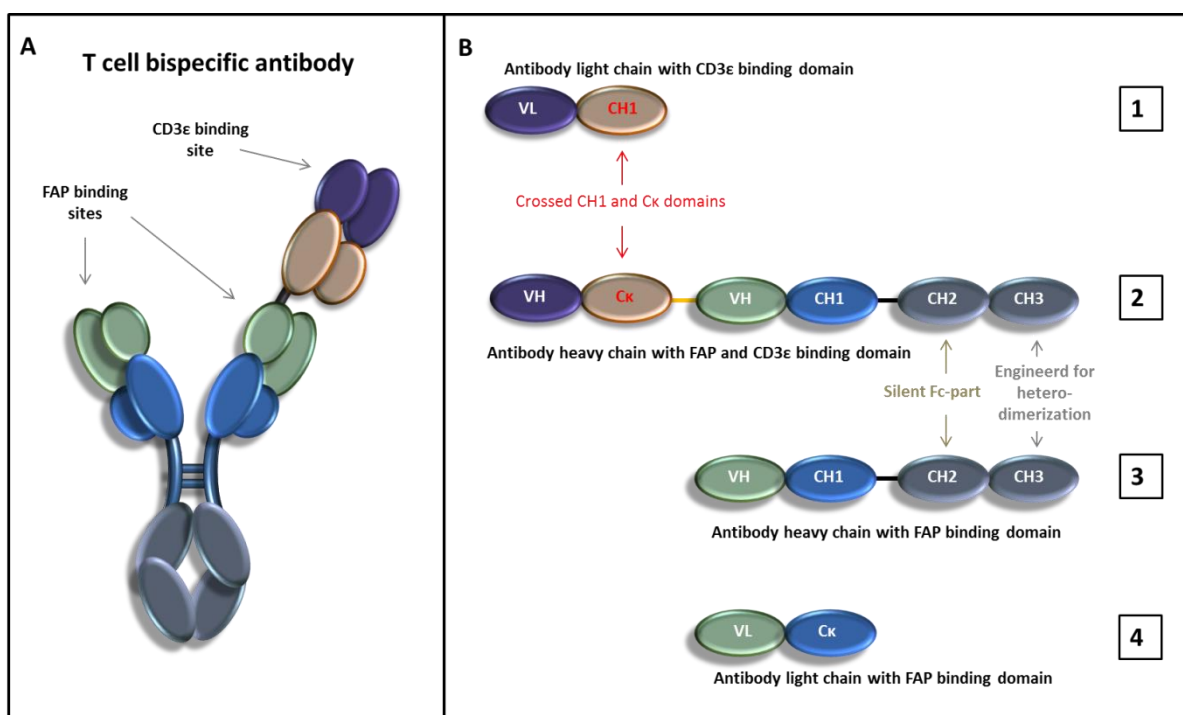


**Figure 8.2: Schematic illustration of the T cell bispecific IgG.**

(A) The T cell bispecific antibody (TCB) consists of a full murine monoclonal IgG1 antibody in a CrossMAb format with two binding moieties for the target FAP and one binding site for CD3 $\epsilon$ , linked to the N-terminus of one of the heavy chains. (B) N- to C-terminal drawing of antibody chains: Antibody light chain with CD3 $\epsilon$  binding domain (1): Variable (VL) (dark purple) and crossed constant (CH1) (bronze) domain of antibody light chain. Antibody heavy chain with one CD3 $\epsilon$  and one target binding domain (2): Variable (VH) (dark purple) and crossed constant Ckappa (C $\kappa$ ) (bronze) domain of the CD3 $\epsilon$  binding Fab, (G<sub>4</sub>S)<sub>2</sub> linker (orange), variable (VH) (green) and constant (CH1) (blue) domain of the target binding Fab, hinge (black), effector-function free CH2 domain and CH3 domain engineered for heterodimerization of IgG1 antibody heavy chain (grey). Antibody heavy chain with target binding domain (3): Variable domain (VH) (green) and constant domain (CH1) (blue), hinge (black), effector-function free CH2 domain and CH3 domain engineered for heterodimerization of IgG1 antibody heavy chain (grey). Antibody light chain with target binding domain (4): Variable (VL) (green) and constant Ckappa (C $\kappa$ ) (blue) domain of antibody light chain.

### 8.1.3 Structure of the anti-mouse XCR1 antibody

#### 8.1.3.1 Design of the molecule and transfection vectors

For generation of the monoclonal murine anti-XCR1 antibody two transfection vectors were cloned (Fig. 8.3). The first plasmid [1] encoded with about 5100 bp for the heavy chain of the antibody and the second vector [2] encoded for the antibody light chain with about 4400 bp. For transient transfection vectors were applied at a molar ratio of 1:2 (plasmid [1]:plasmid [2]). In N- to C-terminal direction the heavy chain of the antibody was composed of the variable domain (VH) followed by constant regions CH1, hinge, CH2 and CH3. The antibody light chain consisted of the variable domain (VL) and the constant domain C $\kappa$ . A sortase tag was fused to the C-terminus of the antibody to have the option to link an antigen to the protein. Therefore the sortase A recognition

motif “LPXTG” (amino acid sequence: Leu–Pro–any–Thr–Gly) followed by a poly-histidine–tag was added C-terminally to both antibody heavy chains of the molecule. The Fc-part of the antibody was the murine isotype IgG2c and lacked effector functions (described in chapter 8.1.1.4).

### 8.1.3.2 Specification of molecules

The anti-mouse XCR1 antibody was derived from the monoclonal antibody MARX10 and targeted the XCR1 receptor on cross-presenting DCs [121, 122].

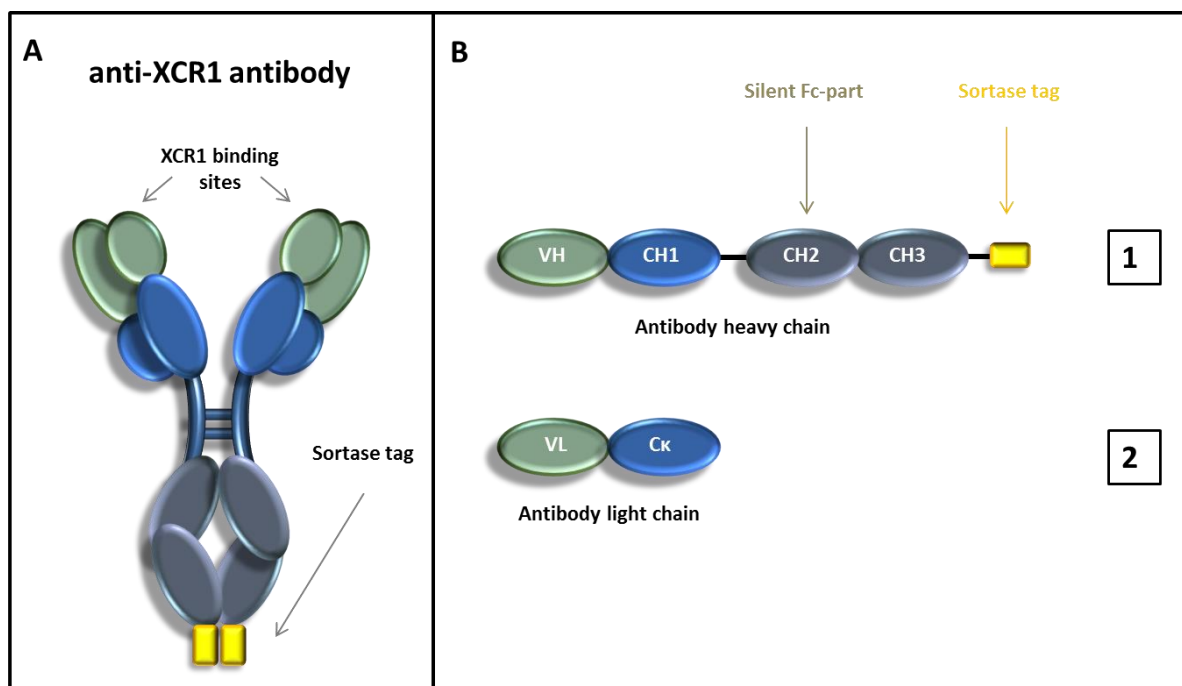


**Figure 8.3: Schematic illustration of the sortase-tagged anti-XCR1 antibody.**

**(A)** The antibody targeting the murine XCR1 receptor consists of a full murine monoclonal IgG2c antibody with two binding sites for the target. A sortase tag is fused to the C-terminus of each heavy chain. **(B)** N- to C-terminal drawing of antibody chains: Antibody heavy chain (1): Variable (VH) (green) and constant (CH1) (blue) domain of murine IgG2c antibody heavy chain, hinge (black), effector-function free CH2 domain and CH3 domain of IgG2c antibody heavy chain (grey), sortase tag (yellow). Antibody light chain (2): Variable (VL) (green) and constant Ckappa (Cκ) (blue) domain of antibody light chain.

### 8.1.4 Yield and purity of recombinant proteins

After purification by Protein A affinity chromatography yield and purity of molecules was determined. Peptide–MHC class I-IgG fusions, which had a molecular weight of about 190 kDa, were produced in a yield of 10 to 15 mg/l transfection culture. In some cases production yields up to 30 mg/l transfection culture could be achieved. After preparative size-exclusion chromatography

aggregates and byproducts could be removed so that the purified protein could be obtained in a purity of about 97 %. The surrogate TCB antibody had a molecular weight of about 170 kDa and was produced in a yield of about 10 mg/l transfection culture. The normal anti-XCR1 antibody with a molecular weight of 150 kDa reached about 100 mg/l transfection culture. After sortase coupling of the MCMV m38 peptide to the anti-XCR1 antibody, protein was purified again with poly-histidine-tag columns to remove non- or single-coupled protein. Thus protein yield was reduced by half, but finally 100 % of double-coupled antibody could be obtained.

## **8.2 IN VITRO EVALUATION OF SURROGATE PEPTIDE–MHC CLASS I-ANTIBODY FUSION MOLECULES**

### **8.2.1 Binding of molecules to their target FAP**

Both the peptide-MHC class I-IgG fusion molecule (pMHCI-IgG) and the T cell bispecific (TCB) antibody targeted the murine fibroblast activation protein (FAP). FAP is a 170 kDa membrane-bound glycoprotein, which is expressed on activated stromal fibroblasts and therefore involved in epithelial-mesenchymal interactions during development and tissue repair, but also in epithelial carcinogenesis [NCBI Gene ID: 14089]. Binding of the engineered pMHCI-IgG fusion and TCB antibody to their target was tested by an extracellular staining of tumor cell lines expressing FAP in flow cytometry analysis with a secondary antibody.

Figure 8.4 A shows the detection of the antibody-part of the pMHCI-IgG molecules on the cell surface of B16-muFAP melanoma cells by staining of the Fc-part of the antibody with a secondary antibody directed against murine IgG2c. The Fc-part of the TCB antibody was detected with a secondary antibody specific for murine IgG1. Binding patterns of both molecules were similar and confirmed binding of molecules in a concentration dependent manner. With a molecule concentration of 5 nM saturation of FAP binding sites on the tumor cell surface was reached and a maximum binding signal could be detected with secondary antibodies. With decreasing compound concentrations reduction of the binding signal was found. At a molecule concentration of 0.005 nM nearly no binding could be detected anymore. The pMHCI-IgG molecule containing the non-binding IgG DP47 showed no binding to tumor cells independent of compound concentration. In figure 8.4 A binding of molecules to FAP-transfected B16 melanoma cells is exemplarily shown. Same results could be found for FAP-transfected MC38 colorectal cancer cells (data not shown).

In figure 8.4 B internalization of pMHCI-IgG molecules into MC38-muFAP tumor cells is depicted. After one, six and 24 hours same amounts of molecules binding to FAP on the tumor cell surface could be detected at 4°C and 37°C. No internalization of pMHCI-IgG molecules could be shown at concentrations of 5 and 0.5 nM. The slight shifts of signals after six and 24 hours of incubation at 37°C at a molecule concentration of 0.5 nM indicate a minimal degree of internalization, which can be attributed to the normal turnover of surface proteins.

In figure 8.4 C the detection of the MHC class I-part of the pMHCI-IgG molecules with a secondary antibody against murine H-2K<sup>b</sup> is illustrated. Data are shown exemplarily for the B16-muFAP tumor cell line, but results also apply for the MC38-muFAP tumor cell line (data not shown). With binding of pMHCI-IgG molecules to their target FAP the murine MHC class I complex H-2K<sup>b</sup> could be delivered to the cell surface of the target cells. The red signals in the histograms show amounts of native H-2K<sup>b</sup> complexes present on the cell surface of syngeneic tumor cell lines. With binding of pMHCI-IgG molecules to tumor cells additional H-2K<sup>b</sup> complexes included in the fusion molecules were brought onto the cell surface, which is demonstrated by the green signals in the histograms. As green signals shift to the left and approach red signals with decreasing compound concentration, concentration dependent binding of molecules was confirmed in this experiment. The pMHCI-IgG molecule containing the non-binding IgG DP47 did not bring any additional H-2K<sup>b</sup> complexes onto the cell surface of the target cells indicating that there is no binding of those molecules.

In figure 8.4 D density of FAP surface proteins and H-2K<sup>b</sup> complexes on FAP-transfected B16 melanoma cells and MC38 colorectal cancer cells are compared. The red signals in histograms show that the MC38-muFAP tumor cell line has more native H-2K<sup>b</sup> complexes on the cell surface than the B16-muFAP tumor cell line. Upon binding of pMHCI-IgG molecules to tumor cells additional H-2K<sup>b</sup> complexes were delivered onto the cell surface (green signal). The shift of the green signal to the right found in the FAP-transfected B16-F10 melanoma cells is bigger than the one detected in FAP-transfected MC38 colorectal cancer cells, which demonstrates that B16-muFAP tumor cells have more FAP binding sites on the cell surface than the MC38-muFAP tumor cells. This is also confirmed in figure 8.4 E, where the detection of the OVA<sub>257-264</sub> peptide in the pMHCI-IgG molecule binding to the cell surface by a specific monoclonal antibody is shown. In this experiment the peptide in the groove of the MHC class I complex of the fusion molecule is detected. Such an antibody specific for the peptide within the MHC class I complex is only available for the immunodominant epitope of ovalbumin (OVA<sub>257-264</sub> "SIINFEKL" in the H-2K<sup>b</sup> complex). The light green signals show the native

H-2K<sup>b</sup> complexes of tumor cells loaded with the Ova-derived peptide “SIINFEKL” and the dark green signals show the “SIINFEKL”- H-2K<sup>b</sup> complexes delivered to the cell surface exclusively by the pMHC-IgG molecule. This experiment showed again that MC38-muFAP tumor cells have more native H-2K<sup>b</sup> complexes, but less expression of FAP on the cell surface than B16-muFAP tumor cells.

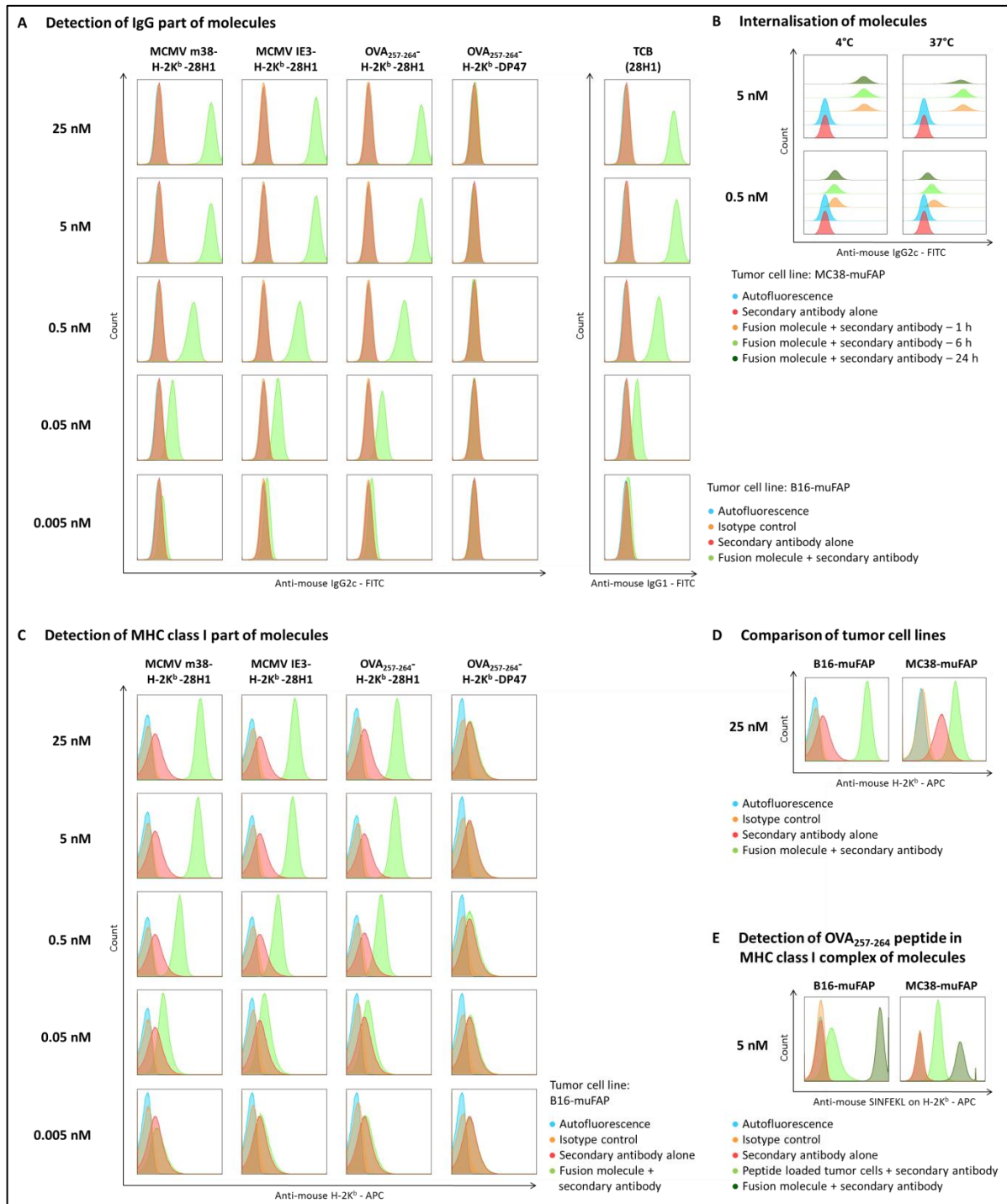


Figure 8.4: Binding of pMHC-IgG and TCB molecules and delivery of pMHC complexes to the tumor cell surface

**(A)** Flow cytometry analysis of binding of pMHCI-IgG and TCB molecules to the target FAP on the cell surface of the tumor cell line B16-muFAP at different concentrations (indicated on the left): MCMV m38-MHCI-28H1 (column 1), MCMV IE3-MHCI-28H1 (column 2), OVA<sub>257-264</sub>-MHCI-28H1 (column 3), OVA<sub>257-264</sub>-MHCI-DP47 (column 4) and TCB (column 5). Color code: Autofluorescence of cells (blue), isotype control antibody (orange), secondary antibody alone (red), pMHCI-IgG or TCB and secondary antibody (light green). **(B)** Flow cytometry analysis of internalization of pMHCI-IgG molecules into MC38-muFAP cells at 4°C (left column) or 37°C (right column) at different concentrations (indicated on the left). Color code: Autofluorescence of cells (blue), secondary antibody alone (red), secondary antibody after one hour of incubation with pMHCI-IgGs (orange), secondary antibody after six hours of incubation with pMHCI-IgGs (light green), secondary antibody after 24 hours of incubation with pMHCI-IgGs (dark green). **(C)** Flow cytometry analysis of delivery of pMHCI complexes to the cell surface of B16-muFAP cells with pMHCI-IgG molecules at different concentrations (indicated on the left): MCMV m38-MHCI-28H1 (column 1), MCMV IE3-MHCI-28H1 (column 2), OVA<sub>257-264</sub>-MHCI-28H1 (column 3) and OVA<sub>257-264</sub>-MHCI-DP47 (column 4). Color code: Autofluorescence of cells (blue), isotype control antibody (orange), secondary antibody alone (red), pMHCI-IgG and secondary antibody (light green). **(D)** Flow cytometry analysis of FAP and H-2K<sup>b</sup> density on the cell surface of B16-muFAP (left column) and MC38-muFAP (right column) cells. Color code: Autofluorescence of cells (blue), isotype control antibody (orange), secondary antibody alone (red), pMHCI-IgG and secondary antibody (light green). **(E)** Flow cytometry analysis of OVA<sub>257-264</sub>-H-2K<sup>b</sup> delivery to B16-muFAP (left column) and MC38-muFAP (right column) cells. Color code: Autofluorescence of cells (blue), isotype control antibody (orange), secondary antibody alone (red), peptide-loaded tumor cells and secondary antibody (light green), pMHCI-IgG and secondary antibody (dark green).

### 8.2.2 In vitro IFN- $\gamma$ activation of CD8<sup>+</sup> T cells mediated by compounds

The biological activity of pMHCI-IgG fusions and the TCB antibody was tested in vitro in an IFN- $\gamma$  activation assay. FAP-transfected MC38 colorectal cancer cells were coinubated with splenocytes from MCMV m38- or OVA<sub>257-264</sub>-vaccinated mice in the presence of effector molecules at various concentrations. After six hours of incubation splenocytes were analyzed with flow cytometry for IFN- $\gamma$  production.

Splenocytes applied in the IFN- $\gamma$  activation assay contained about 60 % lymphocytes, of which 25 to 33 % of lymphocytes were CD3<sup>+</sup> T cells. Splenocytes from mice vaccinated for MCMV m38 included 13.5 % MCMV m38-specific CD8<sup>+</sup> T cells out of all lymphocytes, which represented 62 % of MCMV m38-specific CD8<sup>+</sup> T cells out of all CD8<sup>+</sup> T cells. Splenocytes from mice vaccinated for OVA<sub>257-264</sub> contained 5.5 % OVA<sub>257-264</sub>-specific CD8<sup>+</sup> T cells out of all lymphocytes, which represented 42 % of OVA<sub>257-264</sub>-specific CD8<sup>+</sup> T cells out of all CD8<sup>+</sup> T cells. The TCB antibody activates effector cells via CD3 and the pMHCI-IgG molecule via peptide-MHC class I / T cell receptor interactions. In this respect 100 % of CD8<sup>+</sup> T cells could theoretically be activated by the TCB. 62 % for MCMV m38 and 42 % for OVA<sub>257-264</sub> of CD8<sup>+</sup> T cells could theoretically be activated by pMHCI-IgG molecules.

Figure 8.5 A shows the percentage of CD8<sup>+</sup> T cells activated by effector molecules in different concentrations when splenocytes derived from MCMV m38-vaccinated mice were used. With the TCB antibody (Fig. 8.5 A green) 4.9 % of CD8<sup>+</sup> T cells could be activated at a compound concentration of 0.1 nM. At a compound concentration of 1 nM, when nearly all FAP molecules on

the tumor cell surface are covered with a TCB molecule, 10.3 % of CD8<sup>+</sup> T cells produced IFN- $\gamma$ . With rising concentrations of the TCB antibody IFN- $\gamma$  activation of CD8<sup>+</sup> T cells slightly decreased to 7.5 % activated CD8<sup>+</sup> T cells at a molecule concentration of 100 nM. The pMHCI-IgG molecule (Fig. 8.5 A red) could mediate activation of 2.5 % of CD8<sup>+</sup> T cells at a compound concentration of 0.1 nM. At molecule concentrations ranging from 1 to 100 nM, when saturation is reached, between 5.3 and 6.4 % of CD8<sup>+</sup> T cells produced IFN- $\gamma$ . IFN- $\gamma$  activation induced by peptide (MCMV m38)-loading of target cells (Fig. 8.5 A blue) led to 4.7 % activated CD8<sup>+</sup> T cells at a peptide-loading concentration of 1 nM and 10.3 to 12.4 % activated CD8<sup>+</sup> T cells at peptide-loading concentrations of 5 to 1 000 nM. The pMHCI-IgG molecule containing the control peptide MCMV IE3 (Fig. 8.5 A pink) mediated almost no IFN- $\gamma$  activation of CD8<sup>+</sup> T cells. 0.6 to 1.5 % of CD8<sup>+</sup> T cells produced IFN- $\gamma$  upon exposure to molecule concentrations of 0.1 to 100 nM. By cocubation of splenocytes together with tumor cells in absence of effector molecules no IFN- $\gamma$  activation of CD8<sup>+</sup> T cells could be found (Fig. 8.5 A cyan). In summary the pMHCI-IgG molecule could activate 6.4 % of all CD8<sup>+</sup> T cells in maximum, which represents 10 % of the MCMV m38-specific CD8<sup>+</sup> T cell population. The TCB antibody could activate 10 % of all CD8<sup>+</sup> T cells. Peptide (MCMV m38)-loaded target cells mediated activation of 12.4 % of the entire CD8<sup>+</sup> T cell population, which represents 20 % of the MCMV m38-specific CD8<sup>+</sup> T cells. The pMHCI-IgG molecule containing the control peptide MCMV IE3 induced no activation of CD8<sup>+</sup> T cells indicating that IFN- $\gamma$  activation of CD8<sup>+</sup> T cells mediated by pMHCI-IgG molecules is specific.

Figure 8.5 B depicts the results of the IFN- $\gamma$  activation assay using splenocytes from OVA<sub>257-264</sub>-vaccinated mice. Here the TCB antibody (Fig. 8.5 B green) could induce IFN- $\gamma$  production in 7.8 % of CD8<sup>+</sup> T cells at a compound concentration of 0.1 nM. Increased concentrations of the molecule led to a peak of IFN- $\gamma$  activation with 17.2 % activated CD8<sup>+</sup> T cells at a compound concentration of 1 nM and slowly decreasing percentages (15.2 to 10.4 %) of activated CD8<sup>+</sup> T cells at molecule concentrations ranging from 5 to 100 nM. In comparison the pMHCI-IgG molecule (Fig. 8.5 B red) could only activate very few CD8<sup>+</sup> T cells with 1.6 to 2.4 % at compound concentrations of 0.1 to 100 nM. However, OVA<sub>257-264</sub> peptide-loaded tumor cells (Fig. 8.5 B blue) mediated IFN- $\gamma$  activation of 11.1 % of CD8<sup>+</sup> T cells at a peptide-loading concentration of 1 nM. With rising concentrations of peptide-loading more CD8<sup>+</sup> T cells get activated with about 16.0 % of CD8<sup>+</sup> T cells producing IFN- $\gamma$  at concentrations of 100 to 1 000 nM. Percentages of CD8<sup>+</sup> T cells activated by the pMHCI-IgG molecule containing the control peptide MCMV IE3 (Fig. 8.5 B pink) remained low with 0.8 to 1.7 % of activated CD8<sup>+</sup> T cells at compound concentrations ranging from 0.1 to 100 nM. Cocubation of

splenocytes together with tumor cells in the absence of effector molecules (Fig. 8.5 B cyan) showed no IFN- $\gamma$  activation of CD8<sup>+</sup> T cells. Using the pMHCI-IgG molecule containing the immunodominant epitope of ovalbumin (OVA<sub>257-264</sub>) nearly no activation of CD8<sup>+</sup> T cells could be found, whereas about 40 % of the MCMV m38-specific CD8<sup>+</sup> T cell population could be activated by loading of target cells with the OVA<sub>257-264</sub> peptide. The TCB antibody mediated IFN- $\gamma$  activation in about 20 % of CD8<sup>+</sup> T cells.

In addition it could be found that peptide-loading of tumor cells achieved only at higher concentrations (5 nM) the maximum of IFN- $\gamma$  activation compared to pMHCI-IgG coated tumor cells, which reached maximal IFN- $\gamma$  activation at lower concentrations (1 nM).

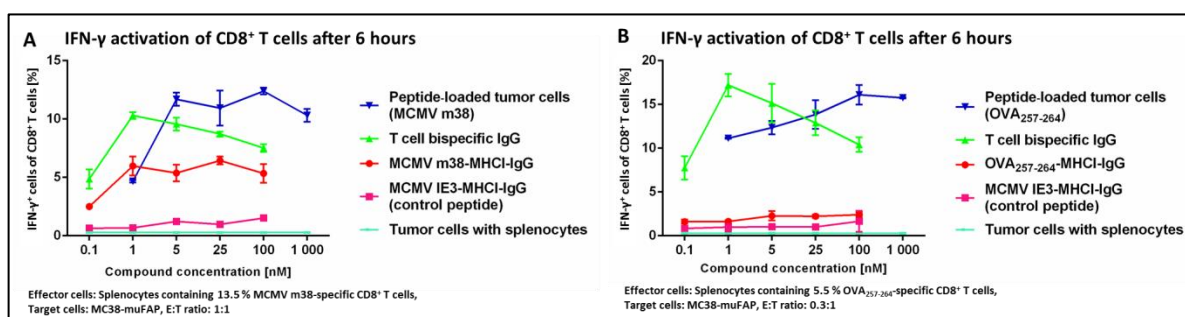


**Figure 8.5: In vitro IFN- $\gamma$  activation of CD8<sup>+</sup> T cells mediated by pMHCI-IgG and TCB molecules.**

Flow cytometry analysis of frequency of IFN- $\gamma$  expressing cells of all CD8<sup>+</sup> T cells after exposure to target cells loaded with different molecules. **(A)** Incubation of MC38-muFAP tumor cells loaded with MCMV m38 peptide (blue), TCB (green), MCMV m38-MHCI-IgG (red) or MCMV IE3-MHCI-IgG (pink) and unloaded tumor cells (cyan) together with freshly isolated splenocytes from MCMV m38-vaccinated mice. **(B)** Incubation of MC38-muFAP tumor cells loaded with OVA<sub>257-264</sub> peptide (blue), TCB (green), OVA<sub>257-264</sub>-MHCI-IgG (red) or MCMV IE3-MHCI-IgG (pink) and unloaded tumor cells (cyan) together with freshly isolated splenocytes from OVA<sub>257-264</sub>-vaccinated mice. **(A, B)** Compounds were added in different concentrations (0.1, 1.0, 5.0, 25.0, 100 and 1 000 nM) and after 6 hours of incubation flow cytometry analysis of splenocytes with intracellular staining for IFN- $\gamma$  was performed. Percentage of specific CD8<sup>+</sup> T cells out of lymphocytes and effector cell:target cell ratio are annotated below graphs. All graphs show mean of replicates (n=2) with error bars indicating standard deviation.

### 8.2.3 In vitro cytotoxicity mediated by compounds

Functionality of the pMHCI-IgG fusion and the TCB antibody was tested in an in vitro cytotoxicity assay based on the xCELLigence technology. FAP-transfected MC38 colorectal cancer cells were incubated together with splenocytes from vaccinated mice containing either MCMV m38- or OVA<sub>257-264</sub>-specific CD8<sup>+</sup> T effector cells. After addition of effector molecules in different concentrations, kinetics of target cell lysis were displayed over time and specific tumor cell elimination mediated by pMHCI-IgG molecules or TCB antibodies was analyzed.

Splenocytes applied in the cytotoxicity assay contained 60 to 70 % lymphocytes. 25 to 30 % of lymphocytes were CD3<sup>+</sup> T cells and 2.5 to 3.0 % of lymphocytes were specific CD8<sup>+</sup> T cells. Thus the amount of cells activated by the TCB antibody via CD3 is tenfold higher than the number of cells engaged by the pMHCI-IgG molecule via peptide-MHC class I / T cell receptor interaction.

In the assay using splenocytes containing MCMV m38-specific CD8<sup>+</sup> T cells a tumor cell lysis of 93 % could be achieved with the TCB antibody after 40 hours of incubation at a compound concentration of 25 or 5 nM as shown in figure 8.6 A on the right. 63 % of tumor cells could be eliminated with the pMHCI-IgG molecule under same conditions. At lower molecule concentrations of 1 and 0.1 nM target cell killing mediated by pMHCI-IgG molecules decreased to 52 and 30 %. Tumor cell elimination by means of TCB antibodies stayed at a high level of 95 % at a compound concentration of 1 nM and slightly decreased to 86 % only at a molecule concentration of 0.1 nM. Target cell death induced by pMHCI-IgG molecules containing the control peptide MCMV IE3 was very small with about 10 % at nearly all concentrations. Looking the positive control 86 % of peptide-loaded tumor cells were eliminated by MCMV m38-specific CD8<sup>+</sup> T cells at a peptide-loading concentration of 25 nM. When peptide-loading concentration was reduced, cell killing of peptide-loaded tumor cells decreased. Controls showed that tumor cell killing mediated by pMHCI-IgG molecules was specific.

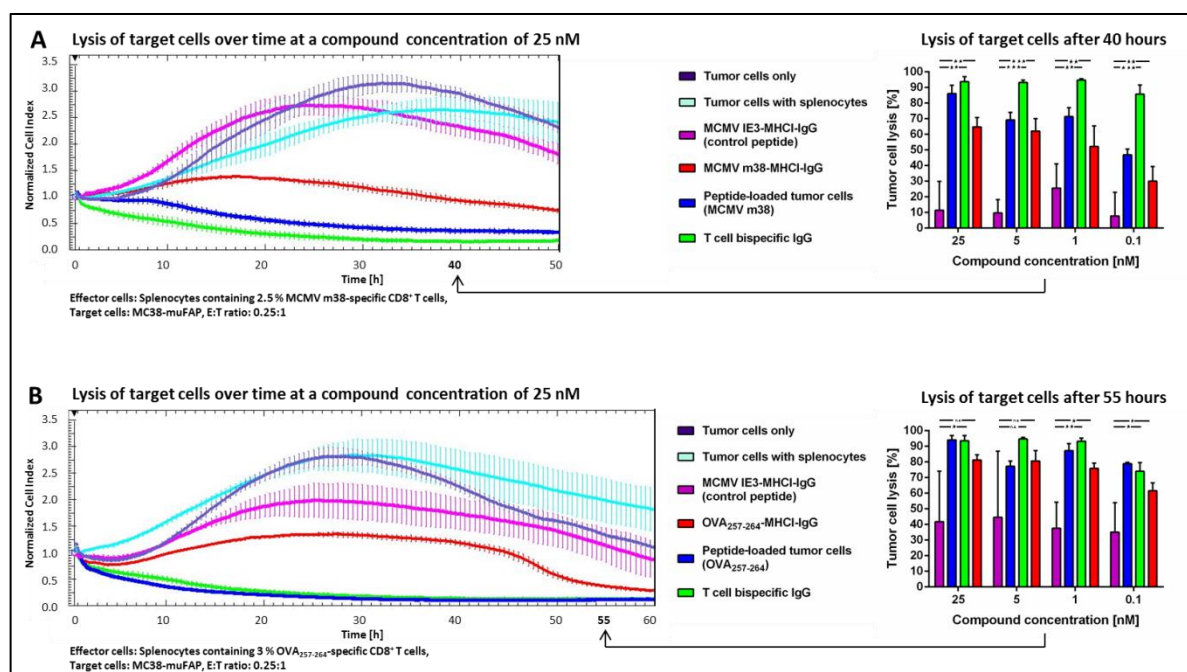
The TCB antibody led to an immediate reduction of target cells measured with the xCELLigence system in figure 8.6 A on the left. Peptide-loaded tumor cells were eliminated with similar kinetics. The results with the peptide-MHCI-IgG-loaded target cells showed a delayed onset of cell killing. After 10 hours of incubation cell killing started and continued to the end of the experiment. This indicated that tumor cells lysis induced by TCB antibodies happened more rapidly than the one mediated by pMHCI-IgG molecules. Control samples (tumor cells only, tumor cells with splenocytes and tumor cells loaded with the pMHCI-IgG molecule containing the control peptide MCMV IE3) were very similar to each other and increased constantly until viability of cells decreased due to lack of nutrients and space. pMHCI-IgG molecules containing the control peptide MCMV IE3 induced only weak target cell lysis showing that tumor cell killing is specifically mediated by molecules.

Figure 8.6 B shows the same assay with splenocytes containing OVA<sub>257-264</sub>-specific CD8<sup>+</sup> T cells. In this case both the pMHCI-IgG molecule and the TCB antibody induced efficacious tumor cell killing within 55 hours. At compound concentrations of 1 to 25 nM about 80 % target cell lysis could be

induced with the pMHCI-IgG fusion and about 94 % with the TCB antibody. However the percentage of target cells lysed with the pMHCI-IgG fusion containing the control peptide MCMV IE3 was very high with about 35 to 45 % at compound concentrations from 0.1 to 25 nM. 77 to 94 % of peptide-loaded tumor cells were eliminated in the assay.

Looking at the kinetics of target cell lysis displayed with the xCELLigence technology the pMHCI-IgG molecule was clearly inferior to the TCB antibody. Tumor cell lysis induced by pMHCI-IgG molecules began after 10 hours but could not control tumor cell growth completely as the slowly rising curve indicates. Only when curves of control samples containing exclusively tumor cells started to go down due to decreased cell viability, killing of tumor cells mediated by pMHCI-IgG fusions also became prevalent and the signals went down. Curves of peptide-loaded tumor cells and TCB antibodies overlapped and showed efficacious tumor cell killing within a few hours. Target cell death induced by pMHCI-IgG molecules containing the control peptide MCMV IE3 was relatively high so that results showing the MHC class I-IgG fusion molecules containing the right peptide (OVA<sub>257-264</sub>) and the control peptide lied close together. No lysis of target cells was induced without effector molecules.

Another aspect of the vitro cytotoxicity assay was to check functionality of specific CD8<sup>+</sup> T cells generated by vaccination. In this experiment splenocytes from mice immunized with the XCR1-targeted vaccination (see chapter 8.3.3) were applied. Figure 8.6 A and B show that tumor cells loaded with the peptide corresponding to vaccination (OVA<sub>257-264</sub> or MCMV m38) were nearly completely eliminated indicating that specific CD8<sup>+</sup> T cells generated by vaccination were functional. If splenocytes were applied to wells containing only tumor cells without effector molecules or peptide-loading, no target cell lysis was induced showing that target cell killing was exclusively mediated by specific CD8<sup>+</sup> T cells generated by vaccination.



**Figure 8.6: In vitro cytotoxicity mediated by pMHCI-IgG and TBC molecules.**

Induction of specific tumor cell lysis mediated by pMHCI-IgGs or TCB IgGs after incubation with freshly isolated splenocytes from vaccinated mice. **(A)** Analysis of target cells with the xCELLigence system: MC38-muFAP cells loaded with MCMV IE3-MHCI-IgG (purple), MCMV m38 peptide (blue), TCB IgG (green) or MCMV m38-MHCI-IgG (red) together with freshly isolated splenocytes from MCMV m38-vaccinated mice. **(B)** Analysis of target cells with the xCELLigence system: MC38-muFAP cells loaded with MCMV IE3-MHCI-IgG (purple), OVA<sub>257-264</sub> peptide (blue), TCB IgG (green) or OVA<sub>257-264</sub>-MHCI-IgG (red) together with freshly isolated splenocytes from OVA<sub>257-264</sub>-vaccinated mice. **(A, B)** Compounds were added in different concentrations (0.1, 1.0, 5.0 and 25.0 nM) and induced lysis of tumor cells was evaluated after 40 (A) or 55 hours (B) (right column). Lysis of target cells was displayed over time with the xCELLigence system and kinetics of cell lysis at a compound concentration of 25 nM is shown exemplarily (left column). Growing curves of tumor cells without compounds or splenocytes (dark purple) and spontaneous release by incubation of tumor cells with splenocytes but without compound (light blue) are depicted as reference. Percentage of specific CD8<sup>+</sup> T cells out of lymphocytes and effector cell:target cell ratio are annotated below xCELLigence curves. All graphs show mean of replicates (n=3) with error bars indicating standard deviation.

### 8.3 COMPARISON OF DIFFERENT VACCINATION METHODS FOR GENERATION OF EFFECTOR CELLS IN MICE

To evaluate pMHCI-IgG molecules in vivo, effector cells had to be generated in mice. Therefore three different vaccination methods were tested. All immunizations were performed with the immunodominant epitope of ovalbumin (OVA<sub>257-264</sub>) as antigen. After vaccination blood was drawn twice weekly from mice and OVA<sub>257-264</sub>-specific CD8<sup>+</sup> T cells were quantified with flow cytometry analysis. Figure 8.7 shows exemplarily the gating strategy of flow cytometry analysis for detection of specific CD8<sup>+</sup> T cells. OVA<sub>257-264</sub>-specific CD8<sup>+</sup> T cells were quantified as percentage of all CD8<sup>+</sup> T cells. The CD8<sup>+</sup> T cell response of the different vaccination methods was compared and the method

of choice for vaccination in further experiments was then also tested for the immunodominant epitope of the murine Cytomegalovirus (MCMV m38).

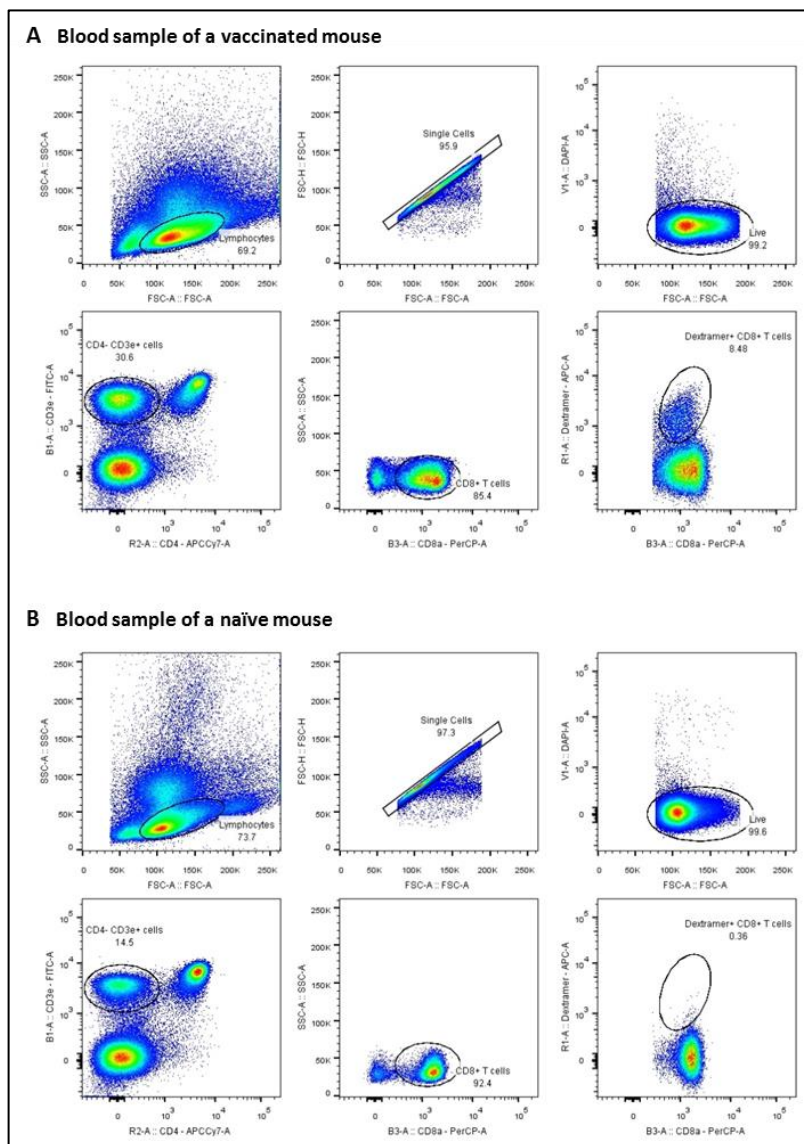


**Figure 8.7: Flow cytometry analysis of blood for detection and quantification of specific CD8<sup>+</sup> T cells.**

**Figure 8.7** shows the gating strategy for detection and quantification of specific CD8<sup>+</sup> T cells in blood samples. **(A)** Blood sample of a mouse immunized with the XCR1-targeted vaccination **(B)** Blood sample of a naïve mouse. Based on size (FSC: Forward scatter) and granularity (SSC: Side scatter) lymphocytes were selected. After discrimination of duplets applying FSC-Area versus FSC-Height, DAPI<sup>+</sup> dead cells were excluded (top row). Then cells were gated on CD3e<sup>+</sup> and CD4<sup>-</sup> cells to exclude B cells and CD4<sup>+</sup> T cells. Afterwards CD8a<sup>+</sup> cells were selected and OVA<sub>257-264</sub><sup>-</sup> or MCMV m38-Dextramer<sup>+</sup> cells as specific CD8<sup>+</sup> T cells out of all CD8<sup>+</sup> T cells were detected (bottom row).

### 8.3.1 Vaccination with peptide-loaded, bone marrow-derived dendritic cells

Figure 8.8 A shows the CD8<sup>+</sup> T cell response after vaccination with peptide-loaded DCs for four different application routes. The first group was injected intravenously with  $8 \times 10^5$  OVA<sub>257-264</sub> peptide-loaded DCs for three times at an interval of seven days (red curve). The CD8<sup>+</sup> T cell response constantly increased until a peak on day 13 after start of vaccination. At the peak levels of 1.9 to 6.0 % of OVA<sub>257-264</sub>-specific CD8<sup>+</sup> T cells could be detected. Then the curve decreased again to 0.7 to 1.9 % on day 20 and finally leveled out at an average percentage of 0.4 % OVA<sub>257-264</sub>-specific

CD8<sup>+</sup> T cells from the 25<sup>th</sup> day of vaccination. The second group was immunized intraperitoneally with  $1.6 \times 10^6$  OVA<sub>257-264</sub>-loaded DCs for three times at an interval of seven days (green curve). Applying this administration route for vaccination only a weak CD8<sup>+</sup> T cell response could be elicited. After a small increase to 0.3 to 3.8 % OVA<sub>257-264</sub>-specific CD8<sup>+</sup> T cells on day 13 it constantly dropped again. After day 25 an average basis level of 0.3 % OVA<sub>257-264</sub>-specific CD8<sup>+</sup> T cells was found. The third group was administered intradermally three times at an interval of seven days with  $2 \times 10^5$  OVA<sub>257-264</sub>-loaded DCs (blue curve). Here the CD8<sup>+</sup> T cell response showed two peaks on day 13 and day 20. On day 13 OVA<sub>257-264</sub>-specific CD8<sup>+</sup> T cell levels ranged from 0.2 to 8.3 %, on day 20 from 0.7 to 5.7 %. Afterwards the number rapidly decreased to a constant level of 0.3 % from day 25 on. The fourth group was injected subcutaneously three times at an interval of seven days with  $1.6 \times 10^6$  OVA<sub>257-264</sub>-loaded DCs (yellow curve). This application route of peptide-loaded DCs showed a CD8<sup>+</sup> T cell response with two peaks. The first peak on day 13 included OVA<sub>257-264</sub>-specific CD8<sup>+</sup> T cell levels in a range from 0.4 to 12.0 %. The second peak on day 20 was weaker with about 0.2 to 4.5 % of OVA<sub>257-264</sub>-specific CD8<sup>+</sup> T cells. After day 25 an average percentage of 0.2 % OVA<sub>257-264</sub>-specific CD8<sup>+</sup> T cells could be detected.

The i.d. and the s.c. injection of peptide-loaded DCs generated two CD8<sup>+</sup> T cell peaks whereas the systemic administration routes (i.v. and i.p.) only elicited one peak. After the first application CD8<sup>+</sup> T cell responses went up and the second injection further enhanced OVA<sub>257-264</sub>-specific CD8<sup>+</sup> T cell levels. The third administration of peptide-loaded DCs was applied without the TLR9-agonist CpG ODN and produced only in the i.d. and in the s.c. group a second augmentation of OVA<sub>257-264</sub>-specific CD8<sup>+</sup> T cells. In total the intradermal application of peptide-loaded DCs was clearly superior to the other administration routes, because it generated the highest specific CD8<sup>+</sup> T cell levels and only a fourth or an eighth of the cells used for i.v. or s.c./i.p. injection, respectively, was needed.

### **8.3.2 DNA vaccination with electroporation**

Figure 8.8 B depicts the CD8<sup>+</sup> T cell response after i.m. or i.d. DNA vaccination with subsequent electroporation. Only low frequencies of OVA<sub>257-264</sub>-specific CD8<sup>+</sup> T cells could be generated after intramuscular injection of plasmid vectors followed by electroporation. After two immunizations the number of specific CD8<sup>+</sup> T cells rose until day 15 and then decreased again to a constant level of 0.2 % OVA<sub>257-264</sub>-specific CD8<sup>+</sup> T cells from day 28 on. At the peak on day 15 0.14 to 2.76 % specific CD8<sup>+</sup> T cells could be detected. The intradermal injection of DNA with subsequent electroporation

elicited higher CD8<sup>+</sup> T cell responses with a range of 0.7 to 3.9 % of OVA<sub>257-264</sub>-specific CD8<sup>+</sup> T cells at the peak on day 15. Here the number also increased until day 15 and then dropped down to an average level of 0.2 % OVA<sub>257-264</sub>-specific CD8<sup>+</sup> T cells from day 28 on. Comparing the application routes of DNA vectors, the i.d. administration was marked superior to i.m. injection.

### **8.3.3 XCR1-targeted vaccination**

XCR1 is a chemokine receptor exclusively expressed on murine and human cross-presenting DCs [121]. Delivery of antigen via the XCR1-specific monoclonal antibody MARX10 (see chapter 8.1.3) elicited specific CD8<sup>+</sup> T cell responses, which could be further boosted by two amplification steps. Table 7.3 shows the three different steps of the vaccination method.

Figure 8.8 shows the frequencies of OVA<sub>257-264</sub>-specific CD8<sup>+</sup> T cells after vaccination. All groups generated a CD8<sup>+</sup> T cell response with a peak on day 9 of vaccination. The first group only treated with the “Prime” step had only 0.5 to 1.0 % OVA<sub>257-264</sub>-specific CD8<sup>+</sup> T cells on day 9. Afterwards frequencies of OVA<sub>257-264</sub>-specific CD8<sup>+</sup> T cells decreased to 0.15 %. Specific CD8<sup>+</sup> T cell levels of the group given the “Prime” and the “ADAS” step rose to 3.0 to 12.8 % on day 9 and then slowly decreased to a minimum of 1.5 % on day 44. The curve of the group treated with all steps (“Prime” + “ADAS” + “cxIL-2”) increased tremendously to a CD8<sup>+</sup> T cell peak of 19.6 to 48.7 % of OVA<sub>257-264</sub>-specific CD8<sup>+</sup> T cells on day 9. Then the amount of specific CD8<sup>+</sup> T cells slowly decreased to about 4 % between day 20 and 37 and finally went down to about 2.5 % on day 44.

The combination of all steps of the vaccination method generated the most potent CD8<sup>+</sup> T cell response, whereby the biggest part was contributed by the complexed IL-2, which was injected three times. Reduction of complexed IL-2 administration to two applications resulted in lower frequencies of OVA<sub>257-264</sub>-specific CD8<sup>+</sup> T cells on day 9, but still higher than combination of only “Prime” and “ADAS” step (data not shown). The “ADAS” step potentiated the CD8<sup>+</sup> T cell response elicited with the “Prime” step by ten.

### **8.3.4 Comparison of vaccination methods**

Figure 8.8 D shows the comparison of CD8<sup>+</sup> T cell responses of all tested vaccination methods. DNA vaccination with electroporation resulted in OVA<sub>257-264</sub>-specific CD8<sup>+</sup> T cell frequencies that remained always below 4.0 %. Vaccination with peptide-loaded DCs elicited CD8<sup>+</sup> T cell responses

up to 12 % in individual cases, but most of the time under 10 % depending on the administration route. Obviously targeting of antigen to the XCR1-receptor combined with further amplification steps generated the most potent CD8<sup>+</sup> T cell response with an average level of 34.0 % OVA<sub>257-264</sub>-specific CD8<sup>+</sup> T cells. By addition or omission of amplification steps the intended percentage of specific CD8<sup>+</sup> T cells was reasonably well controlled, so that this was the method of choice for generating effector cells in further efficacy studies. Keeping in mind that the vaccination method had to be applied in a large number of animals in the following experiments, other advantages of the immunization method were the simple technical implementation and the low number of animals needed as donors compared to the vaccination with peptide-loaded, bone marrow-derived DCs. To evaluate the potency of the vaccination method for other antigens, immunization for the immunodominant epitope m38 of the murine Cytomegalovirus was tested as shown in figure 8.8 E. Using the m38 peptide of MCMV as antigen, the XCR1-targeted vaccination generated less specific CD8<sup>+</sup> T cells than using OVA<sub>257-264</sub> as antigen. However, frequencies of MCMV m38-specific CD8<sup>+</sup> T cells ranged in a double-digit percentage when applying all steps of the vaccination, so that the method was considered the best one for further experiments. Functionality of specific CD8<sup>+</sup> T cells generated with the XCR1-targeted vaccination was tested in in vitro cytotoxicity assays before further application in in vivo efficacy studies (see chapter 8.2.3).

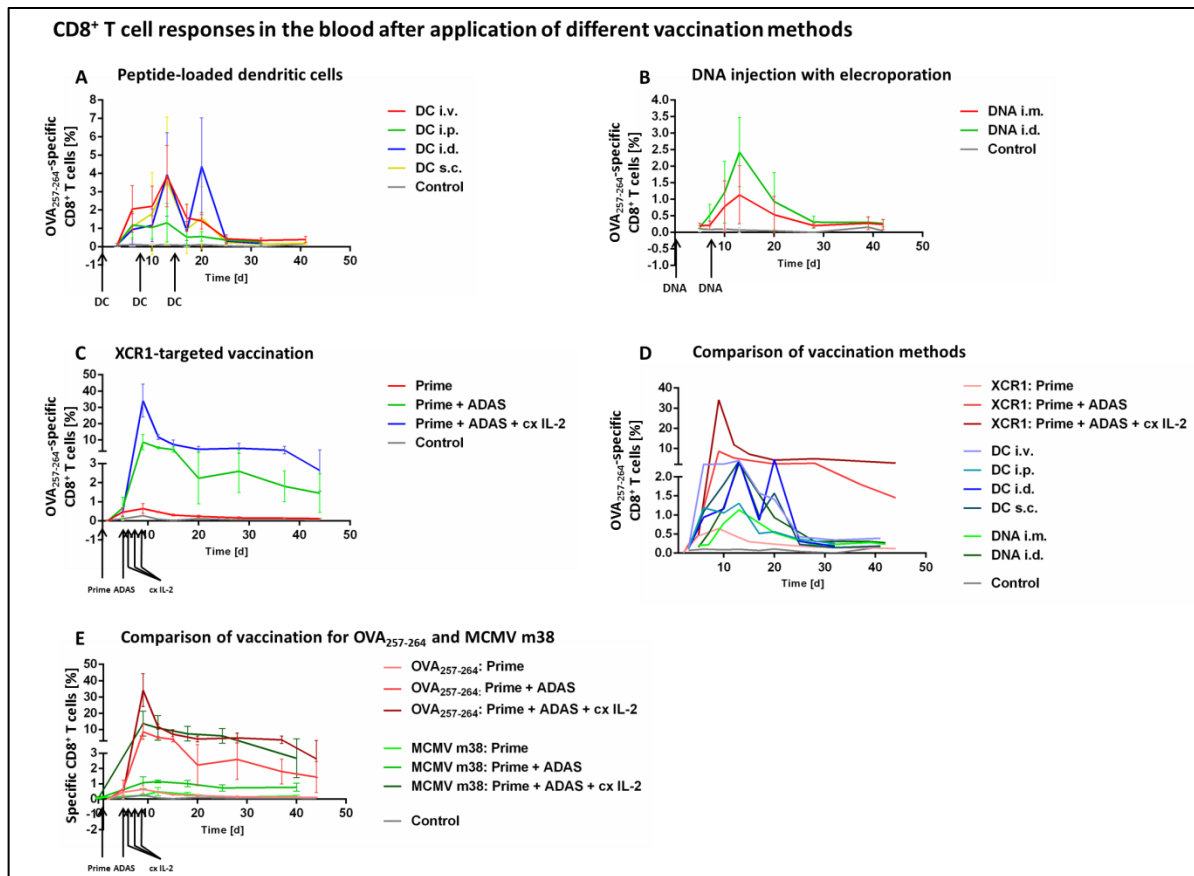


**Figure 8.8: CD8<sup>+</sup> T cell responses in the blood after application of different vaccination methods.**

Frequencies of specific CD8<sup>+</sup> T cells in the blood over time after different vaccination methods. Specific CD8<sup>+</sup> T cells in blood samples were quantified by flow cytometry analysis as percentage of all CD8<sup>+</sup> T cells. Time points of injections of compounds/cells are indicated below time axes. **(A)** CD8<sup>+</sup> T cell response after intravenous (red), intraperitoneal (green), intradermal (blue), subcutaneous (yellow) or no (grey) injection of OVA<sub>257-264</sub>-loaded DCs. **(B)** CD8<sup>+</sup> T cell response after intramuscular (red), intradermal (green) or no (grey) injection of DNA vectors encoding for ovalbumin with subsequent electroporation. **(C)** CD8<sup>+</sup> T cell response after the XCR1-targeted vaccination. Evaluation of three different steps of the vaccination method: “Prime” (red), “Prime” + “ADAS” (green), “Prime” + “ADAS” + “cxIL-2” [3 days] (blue), no vaccination (grey). **(D)** Comparison of the vaccination methods: XCR1-targeted vaccination (red panel), OVA<sub>257-264</sub>-loaded DCs (blue panel), DNA vaccination with electroporation (green panel), not vaccinated control (grey). **(E)** Comparison of XCR1-targeted vaccination for different antigens: Targeting of ovalbumin to the XCR1-receptor (red panel), Targeting of MCMV m38 to the XCR1-receptor (green panel). All graphs show mean of different animals per group (n=6-12) with error bars indicating standard deviation.

## 8.4 IN VIVO EFFICACY EVALUATION OF SURROGATE PEPTIDE–MHC CLASS I-ANTIBODY FUSION MOLECULES

### 8.4.1 Experimental lung metastasis model

#### 8.4.1.1 Anti-tumor efficacy of molecules in the experimental lung metastasis model

To evaluate anti-tumor efficacy of pMHCI-IgG molecules on single tumor cells or bigger tumor cell agglomerates in vivo an experimental lung metastasis model with FAP-transfected B16 melanoma cells was carried out. First a preventive treatment setting was used to examine, if the molecule could mediate elimination of single tumor cells in the circulation before they could settle down in the lung and cause lung metastasis. Second, the ability of the molecules to induce eradication of already established lung metastasis was tested in a therapeutic treatment setting. Lung metastasis burden was assessed by counting of visible metastasis on the lung surface and qPCR for TRP-2. TRP-2 is involved in the synthesis of melanin and therefore specifically expressed in melanocytes. In the healthy lung melanin is not produced. The detection of melanocyte-specific mRNA encoding TRP-2 indicated the presence of B16 melanoma cells in the lung. Counting of metastasis on the lung surface was carried out by two different experimenters under a binocular microscope, whereby treatment and control groups were blinded.

##### 8.4.1.1.1 Preventive treatment setting

Figure 8.9 depicts the time line of the preventive setting of the B16 lung metastasis model in purple. For generation of MCMV m38- or OVA<sub>257-264</sub>-specific CD8<sup>+</sup> T cells, animals were immunized with the XCR1-targeted vaccination as described in chapter 7.3.2.3. After vaccination blood was drawn from mice and analyzed with flow cytometry for detection and quantification of specific CD8<sup>+</sup> T cells. Based on their blood level of specific CD8<sup>+</sup> T cells animals were assigned to treatment or control groups with the aim of having an equal average blood level of specific CD8<sup>+</sup> T cells in every group at start of treatment. Mice which were vaccinated for MCMV m38 had an average blood level of 3.2 % specific CD8<sup>+</sup> T cells in every group at start of treatment, whereby the highest value included into the study was 5.7 % and the lowest one was 1.4 % (data not shown). Blood levels of animals vaccinated for OVA<sub>257-264</sub> averaged 5.7 % specific CD8<sup>+</sup> T cells with 12.9% for maximum and 2.3 % for minimum (data not shown). Table 8.1 A shows the different groups of the study and the treatment schedule. Groups 1 to 3 were vaccinated for MCMV m38 and treated with either the pMHCI-IgG molecule containing the MCMV m38 peptide, the TCB antibody or PBS.

Groups 4 and 5 were not vaccinated and treated with the TCB antibody or PBS. Groups 6 to 8 were vaccinated for OVA<sub>257-264</sub> and treated with the pMHCI-IgG molecule containing the OVA<sub>257-264</sub> peptide, with the pMHCI-IgG molecule containing the control peptide MCMV IE3 or with PBS. As the TCB recruits effector cells via CD3, it should show efficacy both with and without vaccination. The pMHCI-IgG molecule recruits only specific CD8<sup>+</sup> T cells and can therefore only work in combination with previous vaccination. After assignment to treatment and control groups animals were treated prophylactically with the molecules (see time line in figure 8.9). One day after treatment mice were challenged with the B16-muFAP tumor cells. Two days after i.v. injection of tumor cells animals were given a second treatment with the molecules. The pMHCI-IgG molecule was dosed with 5 mg/kg and the TCB antibody with 2 mg/kg. On day 21 of metastasis growth lungs were taken out and tumor burden was assessed by counting of visible metastasis on the lung surface and quantifying expression of TRP-2 by qPCR.

Figure 8.10 shows the results of the preventive treatment of B16 lung metastases. In figure 8.10 A the number of visible lung metastases in the MCMV m38-vaccinated groups is depicted in green. In the MCMV m38-vaccinated vehicle group all of the seven lungs showed metastasis with a range of 17 to 125 and a median value of 58 counted spots per lung. Six MCMV m38-vaccinated animals were treated with the TCB antibody and had no metastasis after treatment except for two mice which had one single spot on the lung. Here the median metastasis load was 0. In the MCMV m38-vaccinated group treated with the pMHCI-IgG molecule three out of seven animals were metastasis free and the other ones showed metastases in a range of 1 to 8 spots per lung, which resulted in a median value of 1 metastasis per lung. Representative example pictures of lungs are shown in figure 8.10 C. In the lung of the MCMV m38-vaccinated vehicle group a lot of metastasis could be recognized, whereas lungs of pMHCI-IgG and TCB treatment groups showed no metastases. Data from counting of lung metastases correlated well with the data of qPCR for TRP-2 expression in lungs depicted in figure 8.10 B in green. TRP-2 expression in lungs of the MCMV m38-vaccinated vehicle group was very high with values up to 3 000 and a median TRP-2 expression level of 1571. Treatment groups had very low levels of TRP-2 expression. In the vaccinated TCB treatment group levels stayed below 2 with one exception with a value of 12. Median TRP-2 expression level was 1. The peptide-MHCI-IgG treatment group included four lungs with a value below 3, two lungs in the double digit range and one outlier with a value of 605, which resulted in a median TRP-2 expression level of 2. Data of metastases counting and qPCR suggested that preventive treatment with the

pMHCI-IgG molecule or the TCB antibody could prevent metastasis growth in lungs with a slightly better outcome for the TCB antibody.

Figure 8.10 A shows also the number of lung metastases counted in lungs of the not-vaccinated groups in blue. Those groups included ten animals per group. In the vehicle group six animals had over 230 lung metastasis, two animals showed only 7 spots on the lung surface and another two animals lied in-between. A median metastasis count of 254 spots per lung could be found. In the treatment group with the TCB all animals except two ones which had a single spot on the lung were free of metastasis, which resulted in a median metastasis count of 0 spots per lung. TRP-2 expression levels in lungs of the not-vaccinated vehicle group ranged from 6 to about 6600 with a median TRP-2 expression level of 6506, whereby all lungs except two had a level over 1 000 (Fig. 8.10 B in blue). In the not-vaccinated TCB treatment group TRP-2 expression levels stayed in the one-digit range except one outlier with a value of 41. Here the median TRP-2 expression level was 2.5. Figure 8.10 C shows also example pictures of the not-vaccinated groups, which visualize the results of metastasis counting and quantification for TRP-2. The TCB antibody could mediate nearly complete protection of mice from lung metastasis in a preventive setting also without vaccination.

Counting of lung metastases in groups vaccinated for OVA<sub>257-264</sub> is illustrated in figure 8.10 D in red. In the OVA<sub>257-264</sub>-vaccinated vehicle group containing six animals between 8 and 104 spots per lung could be found with a median value of 31 metastases per lung. The OVA<sub>257-264</sub>-vaccinated group treated with the pMHCI-IgG molecule containing the control peptide MCMV IE3 consisted of seven animals and showed lung metastasis in a range from 30 to 124 spots per lung. In this group 59 metastases could be detected in median. In the vaccinated group treated with the OVA<sub>257-264</sub>-MHCI-IgG four out of six animals had no metastasis, one animal had one and another one counted 28. This resulted in a median value of 0 metastases per lung. Expression of TRP-2 in lungs showed in figure 8.10 E correlated well with the data of counting the lung metastases. The OVA<sub>257-264</sub>-vaccinated vehicle group included two lungs with values over 2 500 and two lungs with levels about 66. One lung of the group was between them with a value of 714 and one lung had a level of 4. The median TRP-2 expression level of the group was 393. All lungs of the MCMV IE3-MHCI-IgG-treated group showed TRP-2 expression levels over 1 000 except one with a value of 744. Here the median TRP-2 expression level was 1911. The TRP-2 expression levels of the OVA<sub>257-264</sub>-MHCI-IgG-treated group were all below 3 except one lung with a value of 23 and another one with a value of 164. The

median TRP-2 expression level of the group was 1.5. Figure 8.10 F depicts representative example pictures of lungs where lung metastases in vehicle and control groups can be perceived and the lung of the treatment group shows no metastases. Also when the OVA<sub>257-264</sub> peptide is applied for vaccination mice could be protected from lung metastases by treatment with pMHCI-IgG fusion molecules.

Figures 8.10 A, B, D and E contain graphs of the not-vaccinated vehicle group in blue and graphs of the vaccinated vehicle groups in green (MCMV m38) or red (OVA<sub>257-264</sub>). Compared to each other a big influence of vaccination on metastasis growth can be noticed. This is also obvious in the example pictures of lungs in figures 8.10 C and F.

In summary the experimental set up showed that both pMHCI-IgG fusion molecules and TCB antibody induced efficacious and specific elimination of B16 tumor cells in the circulation before settlement in the lung and could protect mice from lung metastasis. Antitumor efficacy of the pMHCI-IgG fusion molecule was thereby successful for both peptides (MCMV m38 or OVA<sub>257-264</sub>).

#### **8.4.1.1.2 Therapeutic treatment setting**

Figure 8.9 shows the time line of the therapeutic setting of the B16 lung metastasis model in green. Vaccination, determination of blood levels of specific CD8<sup>+</sup> T cells and assignment of animals to treatment or control groups were performed in the same way as in the preventive setting of the lung metastasis model (see chapter 8.4.1.1.1). In this experiment MCMV m38-vaccinated mice had an average blood level of 11.8 % specific CD8<sup>+</sup> T cells in every group at start of treatment, whereby the highest frequency included into the study was 20.5 % and the lowest one was 5.0 %. Blood levels of animals vaccinated for OVA<sub>257-264</sub> averaged 16.6 % specific CD8<sup>+</sup> T cells with 27.1 % for maximum and 9.8 % for minimum (data not shown). Table 8.1 B shows the different groups and the treatment schedule of the lung metastasis study with the therapeutic setting. Groups in the therapeutic setting were similar to those in the preventive setting (see chapter 8.4.1.1.1) except two alterations. One control group treated with the pMHCI-IgG molecule containing the control peptide MCMV IE3 was added to the MCMV m38-vaccinated groups and the control peptide group in the OVA<sub>257-264</sub>-vaccinated groups was replaced by a group treated with the pMHCI-IgG molecule containing the non-binding IgG DP47. In the therapeutic setting mice were injected with the B16-muFAP tumor cells nine days before treatment so that tumor cells could migrate to the lung, settle down there and cause lung metastases (see time line in figure 8.9). Established lung

metastases were treated two times at an interval of three days with the test molecules. Molecules were dosed in the same manner as in the preventive setting with 5 mg/kg for the pMHC1-IgG molecule and 2 mg/kg for the TCB antibody. On day 21 after injection of tumor cells lungs were taken out and tumor burden was assessed by counting of visible metastases on the lung surface and quantification of TRP-2 expression by qPCR.

Figure 8.11 depicts the results of the therapeutic treatment of experimental lung metastasis. In green counting of lung metastases (Fig. 8.11 A) and TRP-2 expression levels (Fig. 8.11 B) of the MCMV m38-vaccinated groups are shown. The MCMV m38-vaccinated vehicle group was very heterogeneous with 4 counted spots on the lung surface as minimum and 122 counted spots as maximum as shown in figure 8.11 A. The group included ten animals and 43 metastases per lung were counted in median. In the MCMV m38-vaccinated group treated with the TCB one out of eight animals was metastasis free and the other ones had lung metastases in a range of 3 to 32 spots per lung. Here the median value of counted lung metastases was 13. The MCMV m38-vaccinated group treated with the pMHC1-IgG molecule containing the control peptide MCMV IE3 consisted of ten animals per group and had a median lung metastasis burden of 45 spots per lung. Minimum count of lung metastasis was 1 and maximum count of lung metastasis was 157. The MCMV m38-MHC1-IgG-treated group had 16 lung metastases in median, whereby seven out of ten animals showed less than 20 spots per lung. Results of metastases counting can be verified with example pictures of lungs shown in figure 8.11 C. On the left lungs of MCMV m38-vaccinated groups can be found showing multiple metastases in the control groups (vehicle and MCMV IE3-MHC1-IgG) and reduced metastasis burden in the treatment groups (TCB and MCMV m38-MHC1-IgG). Data of qPCR for TRP-2 expression in lungs is depicted in figure 8.11 B. TRP-2 expression in lungs of the MCMV m38-vaccinated vehicle group ranged from 2 to 700, whereby half of the group had a value over 140 and the median value was 103. The MCMV m38-vaccinated group treated with the TCB had a median TRP-2 expression level of 26. Four animals were in the single-digit range, three ones in the double-digit range and one outlier showed a value of 347. TRP-2 expression levels of the MCMV m38-vaccinated group treated with the pMHC1-IgG molecule containing the control peptide MCMV IE3 were in a range of 225 to 2102 except two lungs with only a value of 4 and 6. In this group the median TRP-2 expression level was 439. The MCMV m38-MHC1-IgG-treated group showed TRP-2 expression levels in a double-digit range except two lungs with a value of 1 and 5 and one lung with a value of 100. The median TRP-2 expression level was 43. Comparing median values of metastasis counting and qPCR, metastasis burden of the vaccinated vehicle group and the vaccinated control

group (MCMV IE3-MHCI-IgG) was 2.5-fold higher than tumor burden of vaccinated groups treated with pMHCI-IgG molecules or the TCB antibody.

Figures 8.11 A and B show also blue graphs, which depict results of the therapeutic treatment of experimental lung metastasis in the not-vaccinated groups. Here the vehicle group counted 463 metastases per lung in median with a range of 60 to 676 spots per lung. The TCB-treated group had 19 to 80 spots per lung with a median count of 55 metastases per lung. TRP-2 expression levels in the vehicle group ranged from 125 to 8379 with a median value of 3049. In the TCB-treated group the median TRP-2 expression level was 150 and values ranged from 35 to 338. Figure 8.11 C shows corresponding example pictures of the not vaccinated groups on the right with reduced metastasis burden in the treatment group (TCB) compared to the vehicle group. In not-vaccinated animals the TCB antibody could reduce metastases burden tenfold. Still tumor burden in the not-vaccinated, TCB-treated group was higher than in the MCMV m38-vaccinated vehicle group.

Figure 8.11 D depicts counts of metastases in lungs of OVA<sub>257-264</sub>-vaccinated groups in red. The vaccinated vehicle group consisted of ten animals and had 58 metastases per lung in median. Counted spots on the lung surface ranged from 4 to 124. The OVA<sub>257-264</sub>-vaccinated control group treated with the pMHCI-IgG molecule containing the non-binding IgG DP47 showed lung metastasis in a range of 2 to 178 with a median count of 41 spots per lung. The group also included ten animals. Lung metastasis numbers of the group treated with the OVA<sub>257-264</sub>-MHCI-IgG fusion molecule fell all below 57 counts with one out of nine metastasis free animal and a median count of 12 spots per lung. Figure 8.11 F shows representative example pictures of lungs from the study, where lung metastasis can be found in all groups, but overall metastasis burden was slightly reduced in the treatment group. Expression of TRP-2 in lungs of OVA<sub>257-264</sub>-vaccinated groups is shown in figure 8.11 E in red. The OVA<sub>257-264</sub>-vaccinated vehicle group had TRP-2 expression levels in a range of 3 to 531 with a median value of 156. Seven lungs lied over a value of 100, the other three ones were below 30. TRP-2 expression levels of the control group treated with the pMHCI-IgG molecule containing the non-binding IgG DP47 showed a median value of 131 with a huge range from 1 to 1302. The same applied to the group treated with the OVA<sub>257-264</sub>-MHCI-IgG fusion molecule. Here TRP-2 expression levels were between 0.5 and 905 with a median of 62. Comparing all OVA<sub>257-264</sub>-vaccinated groups, treatment with the pMHCI-IgG molecule showed a trend towards reduction of metastasis load, but no significant difference between control and treatment groups could be found.

Besides green graphs for the MCMV m38-vaccinated groups and red graphs for the OVA<sub>257-264</sub>-vaccinated groups, figures 8.11 A, B, D and E show also blue graphs with the results of the not-vaccinated groups. Compared to each other metastasis burden of vehicle groups was already reduced by vaccination. This is also visible, when example pictures of vehicle lungs of the vaccinated and not-vaccinated group in figures 8.11 C and F are compared.

When tumor cells have already settled in the lung metastasis growth can be delayed with both pMHC-IgG molecules and TCB antibodies. In this case the MCMV m38 peptide was more potent than the OVA<sub>257-264</sub> peptide.

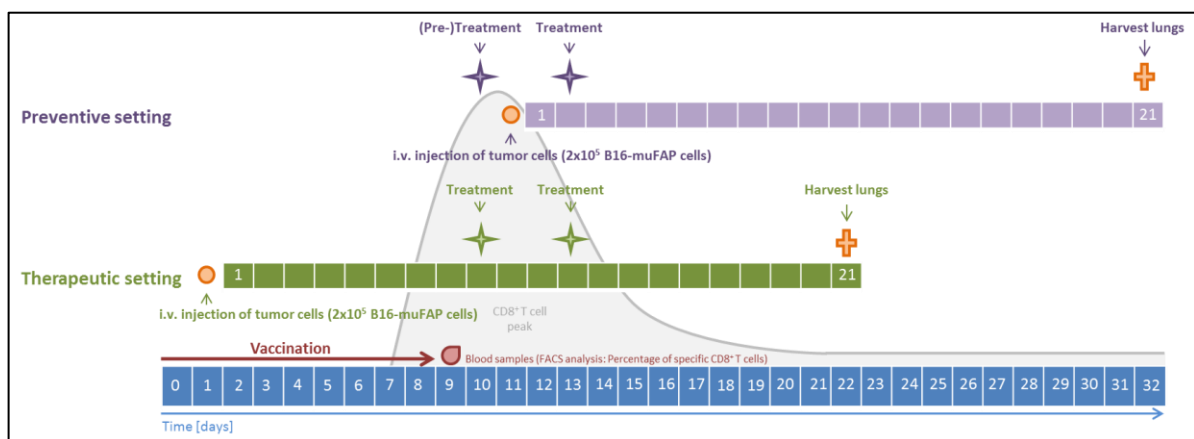


**Figure 8.9: Time line for the experimental lung metastasis model.**

Experimental setting: Time line for the preventive treatment in the experimental lung metastasis model in purple and timeline for the therapeutic treatment setting in the experimental lung metastasis model in green. The blue bar shows time in single days. Duration of the XCR1-targeted vaccination is depicted with a red arrow. One day after vaccination blood sampling from mice is illustrated with a red drop and time window of CD8<sup>+</sup> T cell peak after vaccination is outlined with a grey curve. Orange points indicate intravenous injection of  $2 \times 10^5$  B16-muFAP melanoma cells. Purple or green stars show time points of treatments in each setting. Orange crosses demonstrate euthanasia of mice and harvest of lungs for assessment of metastasis burden.

<b>A: Preventive setting</b>						
Group	Number of animals	Vaccination	Compound	Dosage (mg/kg)	Preventive treatment	Therapeutic treatment
1	6	MCMV m38	PBS	-	x	x
2	6	MCMV m38	T cell bispecific IgG	2	x	x
3	7	MCMV m38	MCMV m38-MHCI-IgG	5	x	x
4	10	-	PBS	-	x	x
5	10	-	T cell bispecific IgG	2	x	x
6	6	OVA <sub>257-264</sub>	PBS	-	x	x
7	7	OVA <sub>257-264</sub>	MCMV IE3-MHCI-IgG	5	x	x
8	6	OVA <sub>257-264</sub>	OVA <sub>257-264</sub> -MHCI-IgG	5	x	x
<b>B: Therapeutic setting</b>						
Group	Number of animals	Vaccination	Compound	Dosage (mg/kg)	Therapeutic treatment 1	Therapeutic treatment 2
1	10	MCMV m38	PBS	-	x	x
2	8	MCMV m38	T cell bispecific IgG	2	x	x
3	10	MCMV m38	MCMV IE3-MHCI-IgG	5	x	x
4	10	MCMV m38	MCMV m38-MHCI-IgG	5	x	x
5	10	-	PBS	-	x	x
6	8	-	T cell bispecific IgG	2	x	x
7	10	OVA <sub>257-264</sub>	PBS	-	x	x
8	10	OVA <sub>257-264</sub>	OVA <sub>257-264</sub> -MHCI-DP47	5	x	x
9	9	OVA <sub>257-264</sub>	OVA <sub>257-264</sub> -MHCI-IgG	5	x	x

**Table 8.1: Classification of groups and treatment schedule in the experimental lung metastasis model.**

Classification of treatment and control groups in the experimental lung metastasis model and the treatment schedule of each group. **(A)** Classification of groups and treatment schedule in the preventive treatment setting of experimental lung metastasis with B16-muFAP melanoma cells. **(B)** Classification of groups and treatment schedule in the therapeutic treatment setting of experimental lung metastasis with B16-muFAP melanoma cells. **(A, B)** In the column "Group" the number of each group in the study is listed. In the following column the number of animals included in each group is noted. The column "Vaccination" indicates if the group was vaccinated and which epitope was used for vaccination. In the fourth column compounds for treatment of each group are listed and in the fifth column dosage of molecules is shown in mg/kg. The last two columns in the table indicate the time points and number of treatments given.

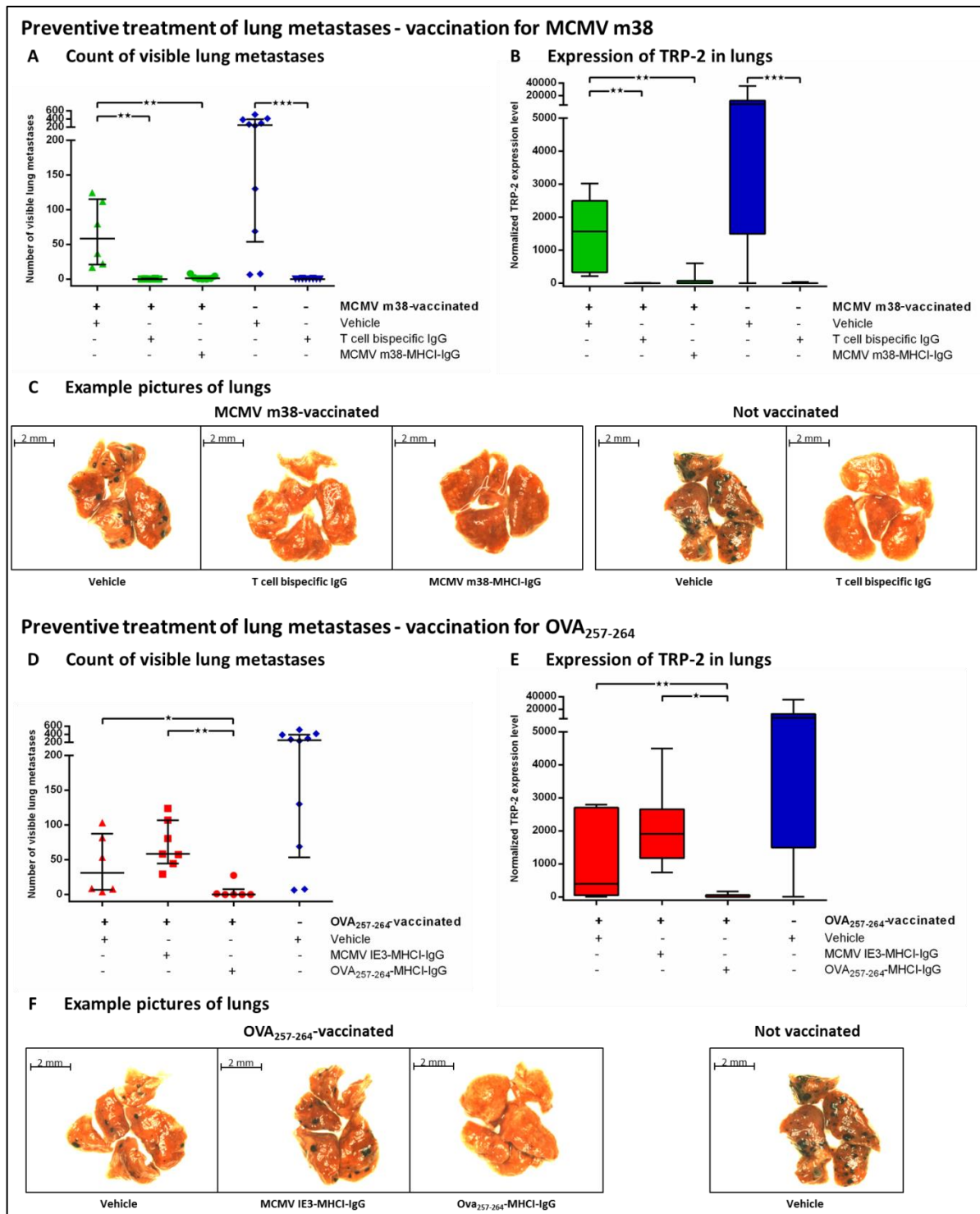


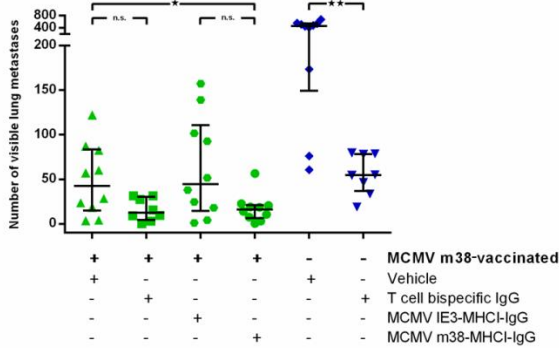
**Figure 8.10: Assessment of metastasis burden after preventive treatment of experimental lung metastases.**

(A) Visible lung metastases were counted under a binocular after harvest of lungs on day 21 of metastasis growth. MCMV m38-vaccinated (green) and non-vaccinated (blue) mice were either treated with PBS (green triangles/blue hashes), TCB (green squares/blue inverted triangles) or MCMV m38-MHCI-IgG (green dots) 24 hours before i.v. injection of  $2 \times 10^5$  B16- $\mu$ FAP melanoma cells and two days after tumor challenge. All graphs show median of different animals per group ( $n=6-10$ ) with error bars indicating interquartile range. (B) Assessment of TRP-2 expression with qPCR in lungs harvested on day 21 of metastasis growth. MCMV m38-vaccinated (green bars) and non-vaccinated (blue bars) mice were either treated

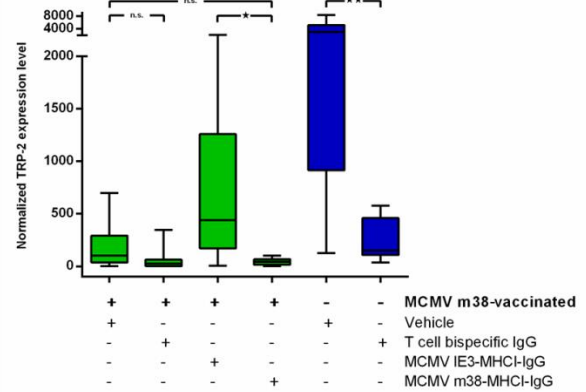
with PBS, TCB or MCMV m38-MHCI-IgG 24 hours before i.v. injection of  $2 \times 10^5$  B16-muFAP melanoma cells and two days after tumor challenge. All graphs show box plots with median of different animals per group ( $n=6-10$ ) with whiskers indicating maximum and minimum value. **(C)** Representative example pictures of lungs taken out on day 21 of metastasis growth. MCMV m38-vaccinated mice were treated with PBS (first picture in the left section), TCB (second picture in the left section) or MCMV m38-MHCI-IgG (third picture in the left section) and non-vaccinated mice were treated with PBS (first picture in the right section) or TCB (second picture in the right section) 24 hours before i.v. injection of  $2 \times 10^5$  B16-muFAP melanoma cells and two days after tumor challenge. **(D)** Visible lung metastases were counted under a binocular after harvest of lungs on day 21 of metastasis growth. OVA<sub>257-264</sub>-vaccinated (red) and non-vaccinated (blue) mice were either treated with PBS (red triangles/blue hashes), MCMV IE3-MHCI-IgG (red squares) or OVA<sub>257-264</sub>-MHCI-IgG (red dots) 24 hours before i.v. injection of  $2 \times 10^5$  B16-muFAP melanoma cells and two days after tumor challenge. All graphs show median of different animals per group ( $n=6-10$ ) with error bars indicating interquartile range. **(E)** Assessment of TRP-2 expression with qPCR in lungs harvested on day 21 of metastasis growth. OVA<sub>257-264</sub>-vaccinated (red bars) and non-vaccinated (blue bars) mice were either treated with PBS, MCMV IE3-MHCI-IgG or OVA<sub>257-264</sub>-MHCI-IgG 24 hours before i.v. injection of  $2 \times 10^5$  B16-muFAP melanoma cells and two days after tumor challenge. All graphs show box plots with median of different animals per group ( $n=6-10$ ) with whiskers indicating maximum and minimum value. **(F)** Representative example pictures of lungs taken out on day 21 of metastasis growth. OVA<sub>257-264</sub>-vaccinated mice were treated with PBS (first picture in the left section), MCMV IE3-MHCI-IgG (second picture in the left section) or OVA<sub>257-264</sub>-MHCI-IgG (third picture in the left section) and non-vaccinated mice were treated with PBS (picture in the right section) 24 hours before i.v. injection of  $2 \times 10^5$  B16-muFAP melanoma cells and two days after tumor challenge.

**Therapeutic treatment of lung metastases - vaccination for MCMV m38**

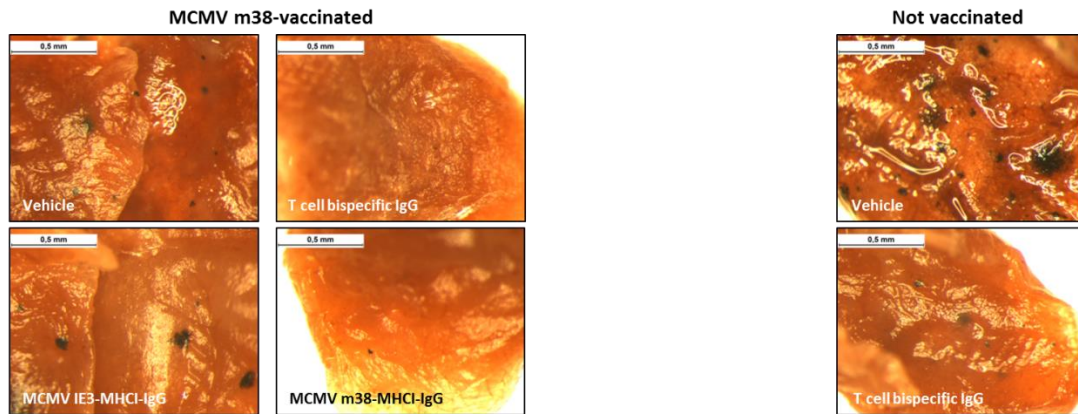
**A** Count of visible lung metastases



**B** Expression of TRP-2 in lungs

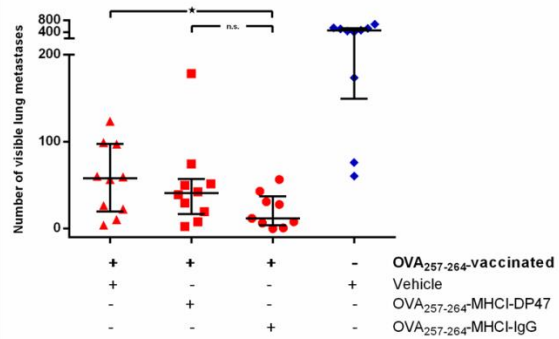


**C** Example pictures of lungs

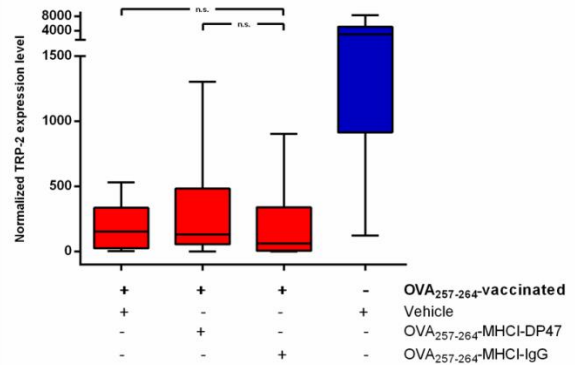


**Therapeutic treatment of lung metastases - vaccination for OVA<sub>257-264</sub>**

**D** Count of visible lung metastases



**E** Expression of TRP-2 in lungs



**F** Example pictures of lungs

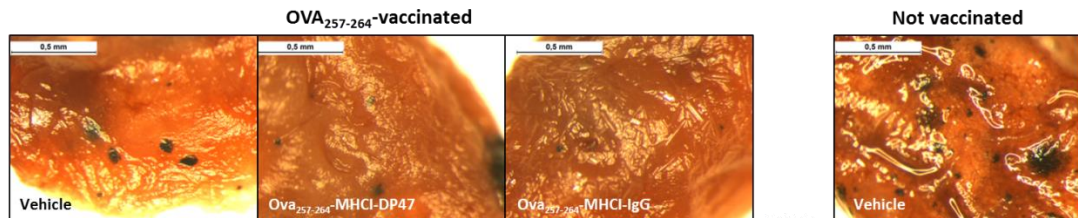


**Figure 8.11: Assessment of metastasis burden after therapeutic treatment of experimental lung metastases.**

**(A)** Visible lung metastases were counted under a binocular after harvest of lungs on day 21 of metastasis growth. MCMV m38-vaccinated (green) and non-vaccinated (blue) mice were either treated with PBS (green triangles/blue hashes), TCB (green squares/blue inverted triangles), MCMV IE3-MHCI-IgG (green hexagons) or MCMV m38-MHCI-IgG (green dots) for two times at an interval of three days starting nine days after i.v. injection of  $2 \times 10^5$  B16-muFAP melanoma cells. All graphs show median of different animals per group (n=8-10) with error bars indicating interquartile range. **(B)** Assessment of TRP-2 expression with qPCR in lungs harvested on day 21 of metastasis growth. MCMV m38-vaccinated (green bars) and non-vaccinated (blue bars) mice were either treated with PBS, TCB, MCMV IE3-MHCI-IgG or MCMV m38-MHCI-IgG for two times at an interval of three days starting nine days after i.v. injection of  $2 \times 10^5$  B16-muFAP melanoma cells. All graphs show box plots with median of different animals per group (n=8-10) with whiskers indicating maximum and minimum value. **(C)** Representative example pictures of lungs taken out on day 21 of metastasis growth. MCMV m38-vaccinated mice were treated with PBS (picture in the left section, top row left), TCB (picture in the left section, top row right), MCMV IE3-MHCI-IgG (picture in the left section, bottom row left) or MCMV m38-MHCI-IgG (picture in the left section, bottom row right) and non-vaccinated mice were treated with PBS (picture in the right section, top row) or TCB (picture in the right section, bottom row) for two times at an interval of three days starting nine days after i.v. injection of  $2 \times 10^5$  B16-muFAP melanoma cells. **(D)** Visible lung metastases were counted under a binocular after harvest of lungs on day 21 of metastasis growth. OVA<sub>257-264</sub>-vaccinated (red) and non-vaccinated (blue) mice were either treated with PBS (red triangles/blue hashes), OVA<sub>257-264</sub>-MHCI-DP47 (red squares) or OVA<sub>257-264</sub>-MHCI-IgG (red dots) for two times at an interval of three days starting nine days after i.v. injection of  $2 \times 10^5$  B16-muFAP melanoma cells. All graphs show median of different animals per group (n=9-10) with error bars indicating interquartile range. **(E)** Assessment of TRP-2 expression with qPCR in lungs harvested on day 21 of metastasis growth. OVA<sub>257-264</sub>-vaccinated (red bars) and non-vaccinated (blue bars) mice were either treated with PBS, OVA<sub>257-264</sub>-MHCI-DP47 or OVA<sub>257-264</sub>-MHCI-IgG for two times at an interval of three days starting nine days after i.v. injection of  $2 \times 10^5$  B16-muFAP melanoma cells. All graphs show box plots with median of different animals per group (n=9-10) with whiskers indicating maximum and minimum value. **(F)** Representative example pictures of lungs taken out on day 21 of metastasis growth. OVA<sub>257-264</sub>-vaccinated mice were treated with PBS (first picture in the left section), OVA<sub>257-264</sub>-MHCI-DP47 (second picture in the left section) or OVA<sub>257-264</sub>-MHCI-IgG (third picture in the left section) and non-vaccinated mice were treated with PBS (picture in the right section) for two times at an interval of three days starting nine days after i.v. injection of  $2 \times 10^5$  B16-muFAP melanoma cells.

#### 8.4.1.2 FAP expression in B16 lung metastases

Maintenance of a stable target expression of tumor cells in vivo is a prerequisite for successful treatment of lung metastases. To address this question, the FAP-transfected B16 melanoma cell line was tested for stable FAP expression in vivo. Therefore mice were injected intravenously with  $2 \times 10^5$  tumor cells and lung metastasis could grow for 21 days. Three animals were injected with FAP-transfected B16 melanoma cells, another three ones with non-transfected B16 melanoma cells. On day 21 lungs were taken out and used for IHC staining for detection of FAP-transfected B16 lung metastases. Figure 8.12 shows the IHC staining of a lung from a mouse injected with non-transfected B16 melanoma cells on the left and the IHC staining of a lung from a mouse injected with FAP-transfected B16 melanoma cells on the right. Cell nuclei of normal lung tissue and lung metastases were stained with DAPI and are depicted in blue. Cell nuclei of tumor cells are bigger and less bright than cell nuclei of normal lung tissue. This is due to a higher mitotic rate of tumor cells and to the fact that B16 melanoma cells contain melanin, which quenches the DAPI fluorescence signal. Taking advantage of this, lung metastases can be detected in normal lung tissue without an additional marker for B16 tumor cells. In addition metastases in lung sections can

be localized by matching the tissue section with the end of the cut cryo-section tissue block. B16 lung metastases on the right show FAP expression of tumor cells in cyan. Control lungs containing metastases with non-transfected B16 melanoma cells show no cyan signal confirming the absence of FAP expression. Even after 21 days of tumor cell growth in vivo FAP-transfected B16 melanoma cells still express their recombinant target FAP so that effector molecules applied in the in vivo efficacy study can bind to their target in lung metastases.

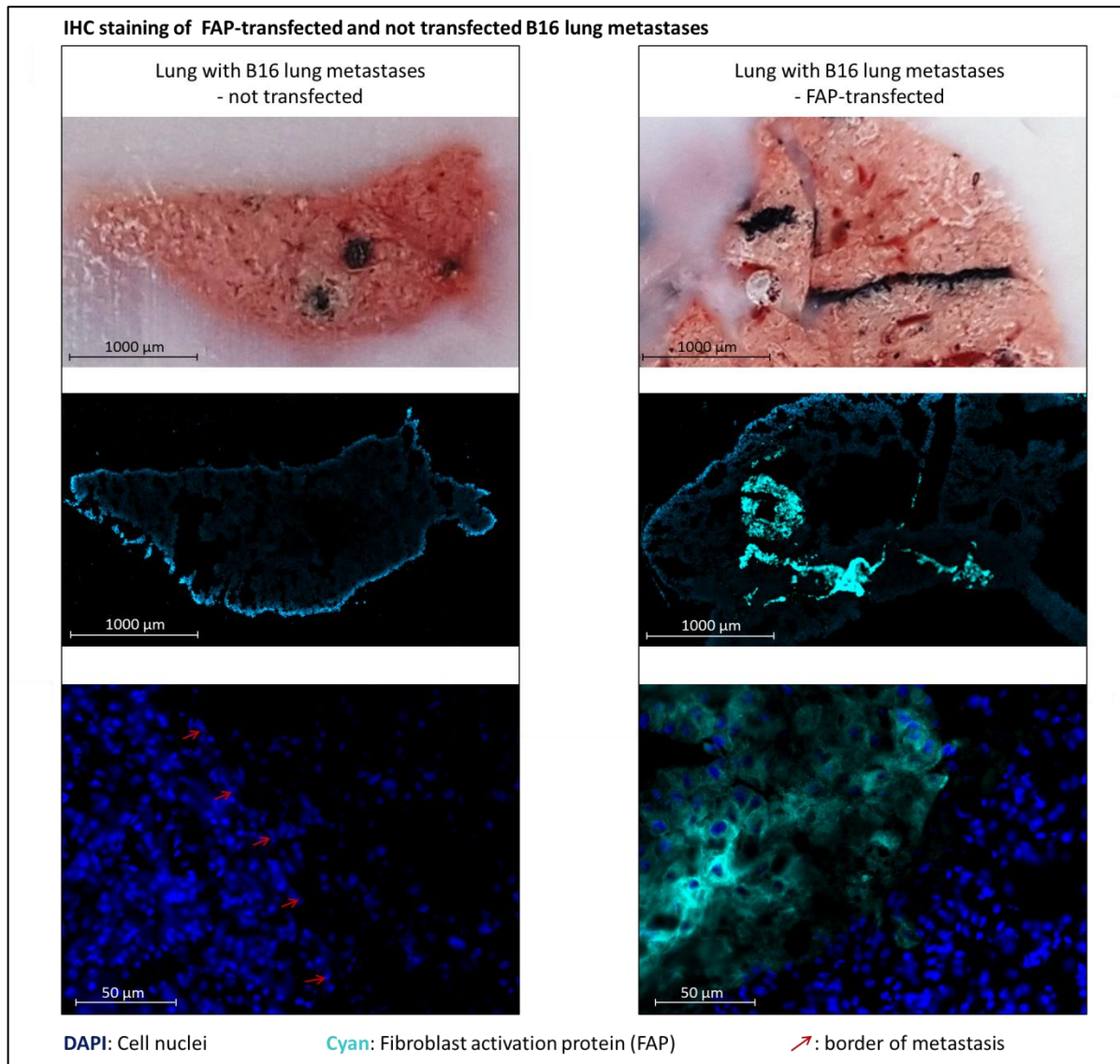


**Figure 8.12: FAP expression of experimental lung metastases.**

Immunofluorescence staining for murine FAP expression in lungs containing metastases of either murine FAP-transfected (right) or non-transfected (left) B16 melanoma cells. In the top row cut ends of cryo-section tissue blocks are depicted so that metastases can be localized in the corresponding stained cryo-sections below (middle row). The close-up images (bottom row) show normal lung tissue and parts of metastases. Cell nuclei are stained with DAPI and depicted in blue. Murine FAP located on the cell surface is depicted in cyan. Red arrows indicate borders of metastases.

## 8.4.2 Solid subcutaneous tumor model

### 8.4.2.1 Anti-tumor efficacy of molecules in the solid subcutaneous tumor model

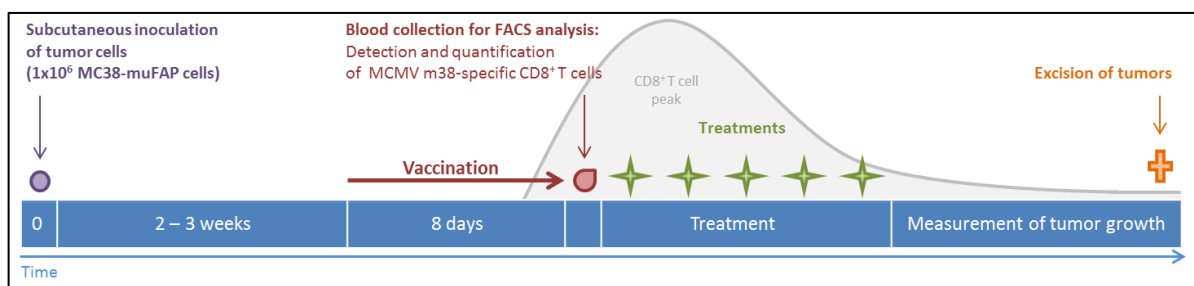
To evaluate anti-tumor efficacy of pMHCI-IgG molecules on solid tumors in vivo a subcutaneous tumor model with FAP-transfected MC38 colorectal cancer cells was carried out. In figure 8.13 the time line of the study is depicted. When solid subcutaneous tumors were established 2 to 3 weeks after subcutaneous inoculation of tumor cells, XCR1-targeted vaccination for MCMV m38 as described in chapter 7.3.2.3 was started. After vaccination blood was drawn from mice and analyzed with flow cytometry for detection and quantification of specific CD8<sup>+</sup> T cells. Based on their blood level of MCMV m38-specific CD8<sup>+</sup> T cells and tumor volume animals were assigned to treatment or control groups with the aim of having an equal average blood level of specific CD8<sup>+</sup> T cells and an equal average tumor volume in every group at start of treatment. Mice had an average blood level of 4.8 % MCMV m38-specific CD8<sup>+</sup> T cells and an average tumor volume of 97 mm<sup>3</sup> in every group at start of treatment. Frequencies of MCMV m38-specific CD8<sup>+</sup> T cells ranged from 1.4 to 15.3 % and tumor volume from 55 to 142 mm<sup>3</sup> (data not shown). Table 8.2 shows the different groups of the study and the treatment schedule. All groups consisted of eight animals and were treated with either the MCMV m38-MHCI-IgG fusion molecule, the MCMV IE3-MHCI-IgG fusion control molecule, the TCB antibody or PBS. Animals were treated five times at an interval of three days with the compounds. Molecules were dosed with 5 mg/kg for the pMHCI-IgG molecule and 2 mg/kg for the TCB antibody. During and after treatment tumor volume was measured with a caliper.

Figure 8.14 shows the results of the treatment of solid subcutaneous FAP-transfected MC38 tumors with pMHCI-IgG molecules or the TCB antibody. The red curve in figure 8.14 A depicts the growth kinetics of the MCMV m38-MHCI-IgG fusion molecule-treated group. Three out of eight animals were tumor free nine days after start of treatment, whereas tumor volumes of the other ones increased constantly and reached 380 to 1063 mm<sup>3</sup> on day 26 after start of treatment. This resulted in a median tumor volume of 428 mm<sup>3</sup> at the end of study. In the group treated with the TCB (Fig. 8.14 A green curve) two out of eight animals were tumor free 13 days after start of treatment. The other ones had tumor volumes in a range of 550 to 1882 mm<sup>3</sup> on day 26 after start of treatment. In the end median tumor volume of the group was 789 mm<sup>3</sup>. The group treated with the pMHCI-IgG molecule containing the control peptide MCMV IE3 is depicted in pink and showed two tumor free animals on day nine after start of treatment. Tumor volumes of the other ones

constantly rose to 534 to 1660 mm<sup>3</sup>, which resulted in a median tumor volume of 598 mm<sup>3</sup> on day 26. Also in the vehicle group (Fig. 8.14 A blue curve) two tumor free animals could be found on day nine and remaining animals reached tumor volumes of 431 to 1294 mm<sup>3</sup>. The median tumor volume of the group was 437 mm<sup>3</sup> on day 26. In total there was one more tumor free animal in the MCMV m38-MHCI-IgG fusion molecule-treated group than in the others, but in the end median tumor volumes in all groups increased constantly to high values with no significant difference between groups.

Figure 8.14 B shows the results of the time-to-event analysis of the study, when the event is defined as a tumor volume  $\geq 500$  mm<sup>3</sup>. In the vehicle group (Fig. 8.14 B blue line) some animals successively reached the event, but others showed complete tumor regression. Those animals never reached the event. Same results could be found in treatment groups. At the beginning MCMV m38-MHCI-IgG-treated animals (Fig. 8.14 B red line) needed more time to reach a tumor volume of 500 mm<sup>3</sup>, but finally on day 26 the same number of animals in the treatment group as in the vehicle group (Fig. 8.14 B blue line) reached the event. Animals in the MCMV IE3-MHCI-IgG- or TCB-treated group (Fig. 8.14 B pink and green lines) reached the event as quickly as mice in the vehicle group. In the end in those two groups more animals had a tumor volume  $\geq 500$  mm<sup>3</sup> than in the vehicle or MCMV m38-MHCI-IgG fusion molecule-treated groups. Ultimately none of the effector molecules could induce reduction or stasis of tumor growth and prevent tumors from reaching the event.

In summary, neither the pMHCI-IgG molecule nor the TCB antibody could induce tumor growth inhibition. No significant difference between treatment and control groups and no specific tumor cell killing could be found.



**Figure 8.13: Time line for the solid subcutaneous tumor model.**

Experimental setting for the solid subcutaneous tumor model. The blue bar shows the time. The purple dot indicates the subcutaneous inoculation of  $1 \times 10^6$  MC38-muFAP colorectal cancer cells. Duration of the XCR1-targeted vaccination is depicted with a red arrow. One day after vaccination blood sampling from mice is illustrated with a red drop and time window of CD8<sup>+</sup> T cell peak after vaccination is outlined with a grey curve. Green stars show time points of treatments during the CD8<sup>+</sup> T cell peak. The orange cross demonstrates euthanasia of mice and harvest of tumors for further investigations.

Group	Number of animals	Vaccination	Compound	Dosage (mg/kg)	Treatments				
					d 0	d 3	d 6	d 9	d 12
1	8	MCMV m38	PBS	-	x	x	x	x	x
2	8	MCMV m38	T cell bispecific IgG	2	x	x	x	x	x
3	8	MCMV m38	MCMV IE3-MHCI-IgG	5	x	x	x	x	x
4	8	MCMV m38	MCMV m38-MHCI-IgG	5	x	x	x	x	x

**Table 8.2: Classification of groups and treatment schedule in the solid subcutaneous tumor model.**

Classification of treatment and control groups in the solid subcutaneous tumor model and the treatment schedule of each group. In the column “Group” the number of each group in the study is listed. In the following column the number of animals included in each group is noted. The column “Vaccination” indicates which epitope was used for vaccination. In the fourth column compounds for treatment of each group are listed and in the fifth column dosage of molecules is shown in mg/kg. The last five columns in the table indicate the time points and number of treatments given.

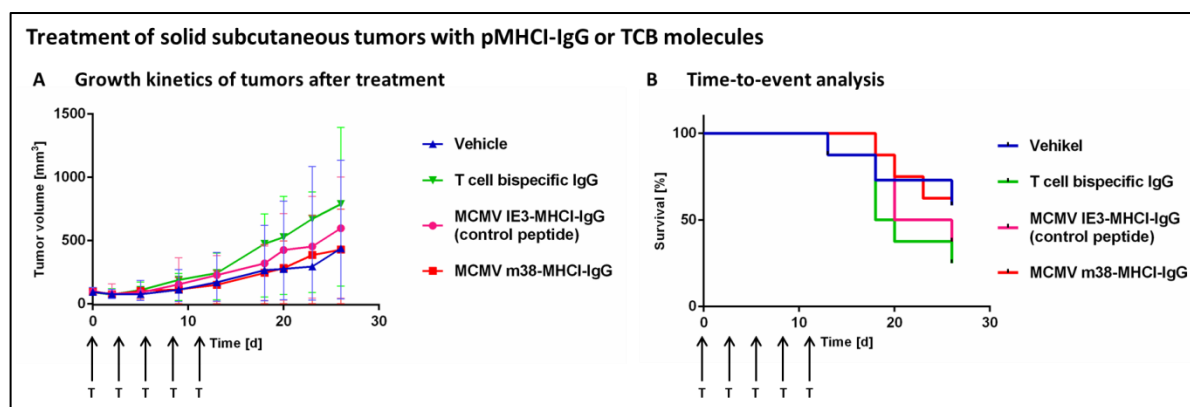


**Figure 8.14: Growth kinetics of solid subcutaneous tumors after treatment with pMHC-IgG or TCB molecules.**

**(A)** Growing curves of tumors after treatment with TCB (green), MCMV IE3-MHCI-IgG (pink), MCMV m38-MHCI-IgG (pink) or without treatment (blue). On day 0 treatments were started at an average tumor volume of  $97 \text{ mm}^3$  in every group. Time points of treatments are indicated with arrows below time axis. All graphs show median of different animals per group ( $n=8$ ) with error bars indicating interquartile range. **(B)** Time-to-event analysis of groups treated with TCB (green), MCMV IE3-MHCI-IgG (pink), MCMV m38-MHCI-IgG (pink) or without treatment (blue) starting with an average tumor volume of  $97 \text{ mm}^3$ . A tumor volume  $\geq 500 \text{ mm}^3$  was defined as event. Time points of treatments are indicated with arrows below time axis.

#### 8.4.2.2 FAP expression in MC38 tumors

Also in the case of a solid subcutaneous tumor maintenance of stable target expression of tumor cells in vivo is a prerequisite for successful treatment of tumors with effector molecules. Tumor cells can lose their target expression when growing in vivo, which in this case leads to inability of effector molecules to bind to tumor cells and mediate tumor cell killing. MC38 tumors were harvested after several weeks of in vivo growth with or without treatment and checked for stable expression of their target FAP. Figure 8.15 depicts representative pictures of IHC stainings of MC38 tumors for detection of FAP expression. The illustration at top left shows the IHC staining for FAP of a tumor with non-transfected MC38 colorectal cancer cells. The other three pictures show tumors with FAP-transfected MC38 colorectal cancer cells after treatment with effector molecules or PBS.



### 8.4.2.3 Penetration of the MCMV m38-MHCI-IgG fusion molecule into tumors

For successful treatment of solid tumors, it is a requirement that effector molecules penetrate into the tumor tissue and bind to their target on the surface of tumor cells. To confirm penetration of the test molecules ultramicroscopy analyses of tumors treated with Alexa 647-labelled pMHCI-IgG molecules were carried out.

Figure 8.16 A shows the penetration profile of the Alexa 647-labelled MCMV m38-MHCI-IgG fusion molecule. The bigger the distance to the vessels got, the less fusion molecule could be found in the tumor tissue. This applies to tumors excised 12, 24 and 48 hours after application. 12 and 24 hours after injection the highest amount of molecule could be found at a distance of about 50  $\mu\text{m}$  around the vessels. With increasing distance from the vessel the amount of molecule quickly decreased almost by half. In distances to vessels exceeding 50  $\mu\text{m}$  amounts of molecule present in the tumor tissue remained constant 12 and 24 hours after application. 48 hours after injection much less of the molecule could be found in the tumor regardless of distance to vessels. However in larger distances to vessels curves go up again indicating increasing quantities of the molecule in the tumor. This finding might be due to accumulation of molecule in non-vascularized, necrotic areas of the tumor with no possibility of clearance.

In figure 8.16 B the accumulation of the Alexa 647-labelled MCMV m38-MHCI-IgG fusion molecule is depicted. The highest amount of molecule could be detected 12 hours after injection. Clearance was obvious after 24 hours and the bulk was cleared after 48 hours. This is also reflected by images in figure 8.16 C, which depict representative sections of tumors used for ultramicroscopy analysis. Overview images in the top row show that after 12 hours the Alexa 647-labelled MCMV m38-MHCI-IgG fusion molecule penetrated into the tumor. Distribution pattern was spotty with areas containing more and areas containing less labelled molecule, whereby particularly in marginal regions and in areas, where vessel density was high, the highest amount of labelled fusion molecule could be found. As also shown in figure 8.16 B most of the molecule could be detected 12 hours after application. After 24 and 48 hours decreasing quantities of the molecule were visible in the tissue due to clearance from tumor. The close-up image of a section in the bottom row on the right shows that the Alexa 647-labelled MCMV m38-MHCI-IgG fusion molecule can be found especially near the vessels (as also demonstrated in the penetration profile in figure 8.16 A) and that the labelled molecule binds to its target on the tumor cell surface. In the bottom row on the left an overview image of a non-treated control tumor is depicted, showing no Alexa 647 signal.

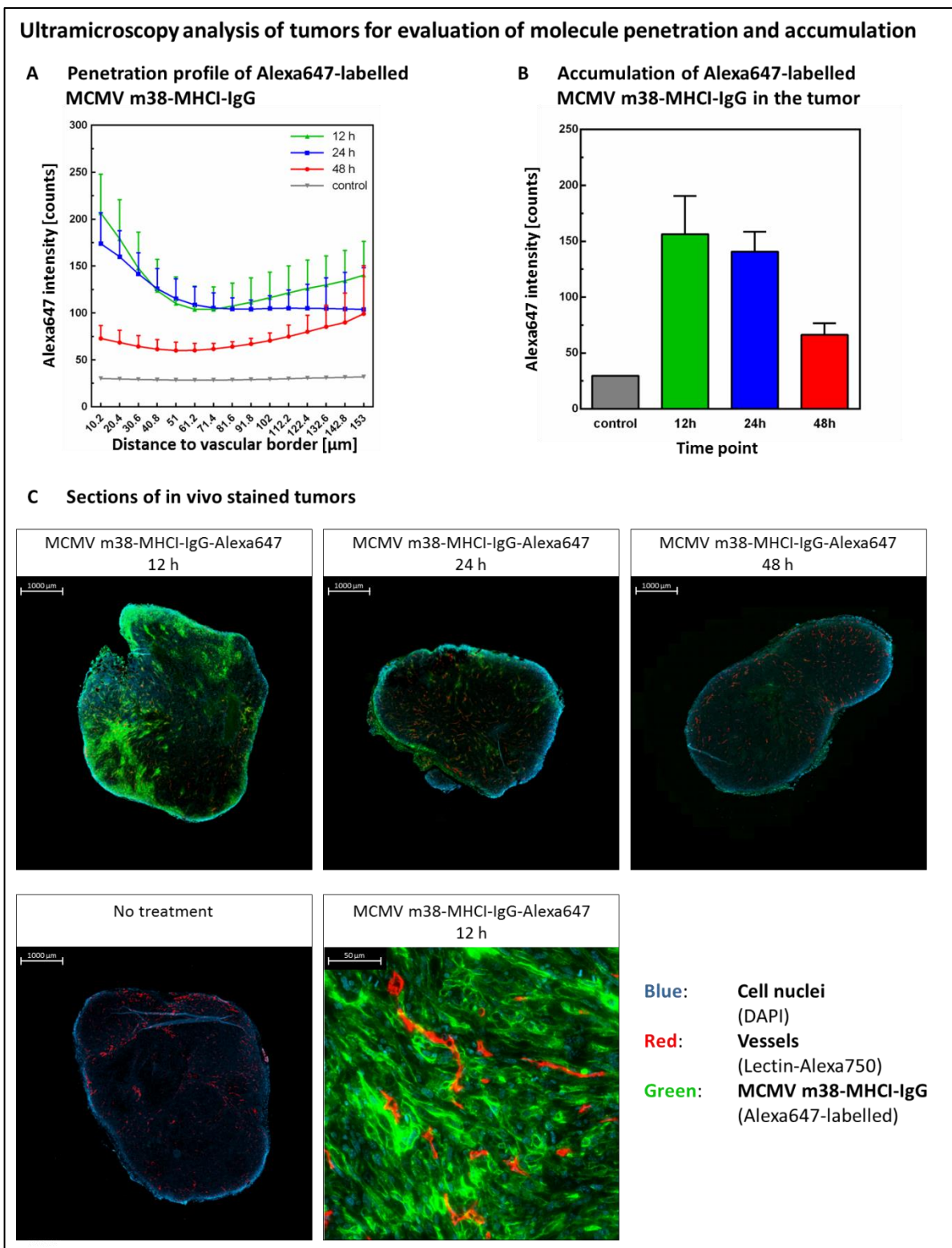


**Figure 8.16: Tumor penetration and accumulation of pMHC-IgG molecules.** (A) Penetration profile of Alexa 647-labelled MCMV m38-MHCI-IgG molecule. Tumors were excised 12 (green), 24 (blue) and 48 (red) hours after injection of molecule or without injection of labelled molecule (grey). Amount of MCMV m38-MHCI-IgG molecule present in the tumor is depicted in relation to distance to vessel borders. All graphs show mean of different animals per group (n=4) with error bars indicating standard deviation. (B) Accumulation of Alexa 647-labelled

MCMV m38-MHCI-IgG molecule in the tumor. Total amounts of MCMV m38-MHCI-IgG molecule present in the tumor 12 (green), 24 (blue) and 48 (red) hours after injection of molecule or without injection of labelled molecule (grey) are shown. All graphs show mean of different animals per group (n=4) with error bars indicating standard deviation. **(C)** Sections of in vivo stained tumors excised 12 (upper left), 24 (upper middle) and 48 (upper right) hours after injection of Alexa 647-labelled MCMV m38-MHCI-IgG molecule or without injection of labelled molecule (lower left). Close-up image of tumor tissue with high penetration of Alexa 647-labelled MCMV m38-MHCI-IgG molecule shows binding of labelled molecule to tumor cells (lower middle). Color code: Cell nuclei (blue), vessels (red), MCMV m38-MHCI-IgG (green).

#### 8.4.2.4 Infiltration of tumors with CD8<sup>+</sup> T cells

Another prerequisite for successful treatment of solid subcutaneous tumors with T cell recruiters is the penetration of effector cells into the tumor mass. To check this, tumor bearing mice were vaccinated and treated with effector molecules as depicted in figure 8.13. 24 hours after the first treatment with pMHCI-IgG or TCB molecules tumors were excised and used for IHC staining detecting CD8<sup>+</sup> T cells.

Figure 8.17 shows representative example pictures of tumor cryo-sections stained for CD8a (Fig 8.17 A) and a quantification analysis of CD8<sup>+</sup> T cells infiltrating the tumor (Fig. 8.17 B). The tumor samples from not vaccinated animals showed only poor CD8<sup>+</sup> T cell infiltration, while in tumors from MCMV m38-vaccinated mice markedly more CD8<sup>+</sup> T cells could be detected. The amount of tumor infiltrating CD8<sup>+</sup> T cells could be even slightly increased by treatment with pMHCI-IgGs or TCBs. The molecules function as CD8<sup>+</sup> T cell recruiters and attract effector cells via the pMHC class I complex (pMHCI-IgG) or via CD3 (TCB). With this staining it could only be proven that CD8<sup>+</sup> T cells are recruited into the tumor after treatment with CD8<sup>+</sup> T cell recruiters, but not that MCMV m38-specific CD8<sup>+</sup> T cells are attracted, as needed for the anti-tumor activity of pMHCI-IgGs. It is however not unreasonable to assume that the proportion of MCMV m38-specific CD8<sup>+</sup> T cells present in the pMHCI-IgG-treated tumors correlates with or even exceeds the amount of MCMV m38-specific CD8<sup>+</sup> T cells found in the blood.

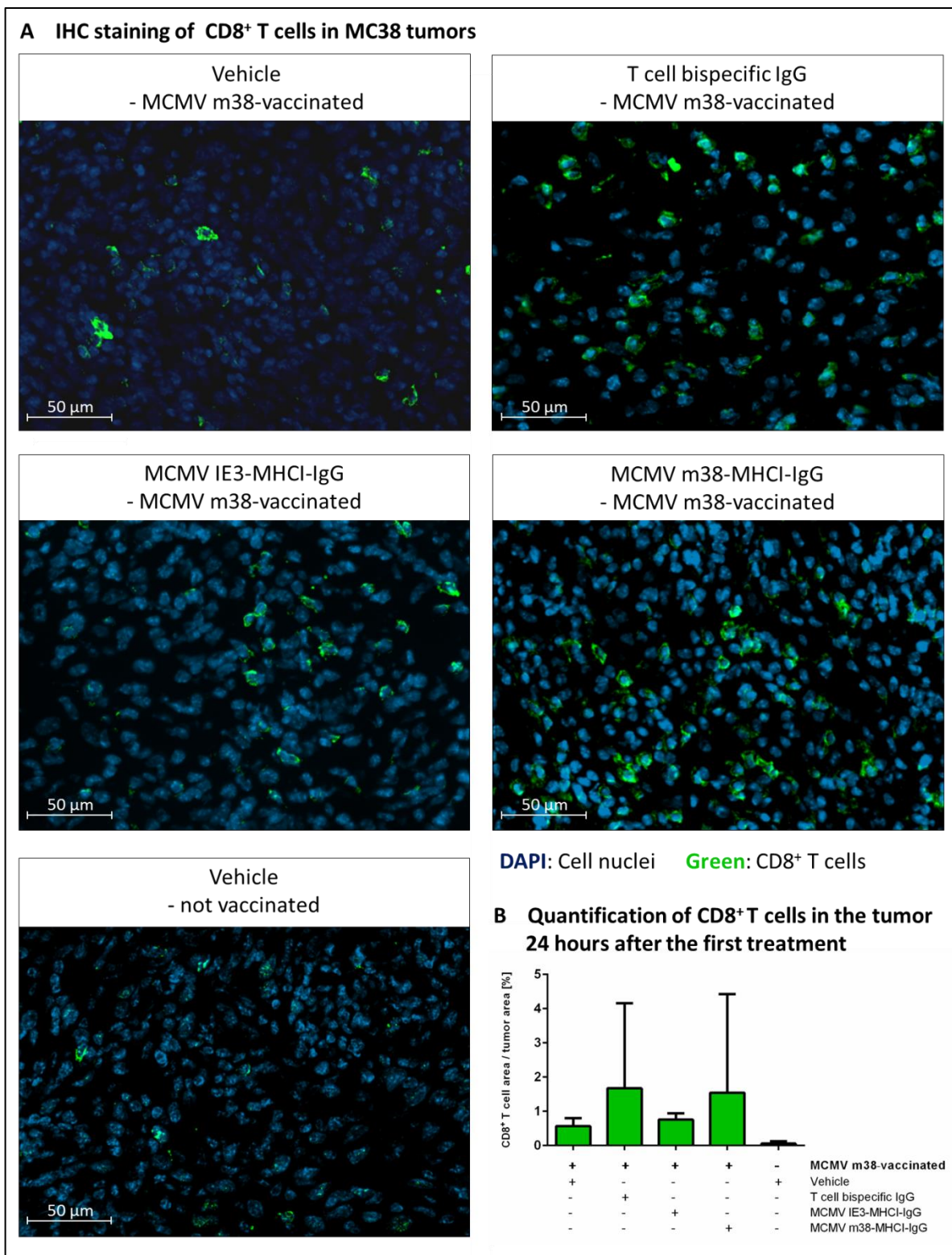


**Figure 8.17: CD8<sup>+</sup> T cell infiltration in the tumors.**

(A) Immunofluorescence staining for murine CD8a of tumors without vaccination and without treatment (lower left) or MCMV m38 vaccination and TCB (upper right), MCMV IE3-MHCI-IgG (middle left), MCMV m38-MHCI-IgG (middle right) treatment or without treatment (upper left). Cell nuclei are stained with DAPI and depicted in blue. Murine CD8a<sup>+</sup> cells are depicted in green. (B) Quantification of CD8<sup>+</sup> T cells in the tumor. Area covered by CD8<sup>+</sup>T cells in relation to tumor

area is depicted for MCMV m38-vaccinated/untreated, MCMV m38-vaccinated/TCB-treated, MCMV m38-vaccinated/MCMV IE3-MHCI-IgG-treated, MCMV m38-vaccinated/MCMV m38-MHCI-IgG-treated and not vaccinated/untreated tumors. All graphs show mean of different animals per group (n=4) with error bars indicating standard deviation.

#### 8.4.2.5 Characterization of T cells in tumors and blood

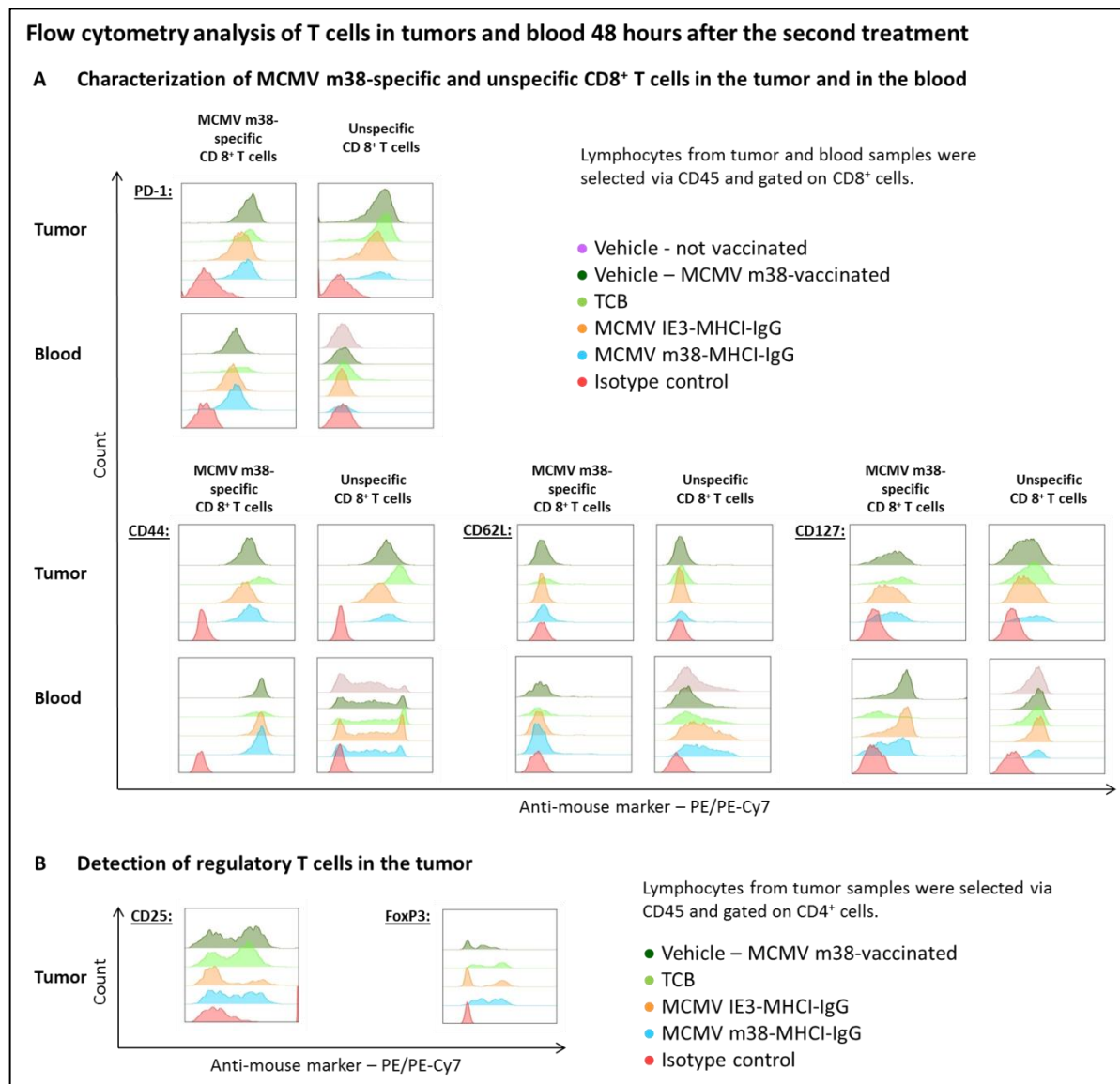
To determine the phenotype of T cells recruited into the tumor and in the blood flow cytometry analyses were applied. Tumor bearing mice were vaccinated and treated with effector molecules as depicted in figure 8.13 and 48 hours after the second treatment tumors were taken out and blood was drawn.

Figure 8.18 A shows the characterization of MCMV m38-specific and unspecific CD8<sup>+</sup> T cells in the tumor and in the blood. CD8<sup>+</sup> T cells were checked for expression of CD44 (bottom left), CD62L (bottom middle), CD127 (bottom right) and PD-1 (top left). As can be seen in the left histograms for each marker MCMV m38-specific CD8<sup>+</sup> T cells were CD44<sup>+</sup>/CD62L<sup>-</sup>/CD127<sup>+</sup> both in the tumor and in the blood. Unspecific CD8<sup>+</sup> T cells depicted in the right histograms for each marker were CD44<sup>+</sup>/CD62L<sup>-</sup>/CD127<sup>+</sup> in the tumor and CD44<sup>+</sup> or <sup>-</sup>/CD62L<sup>+</sup>/CD127<sup>+</sup> in the blood. Those phenotypes were independent from treatment except from CD44 expression in pMHCI-IgG- or TCB-treated tumors, where CD44 expression was slightly higher. Evaluating the marker expression MCMV m38-specific CD8<sup>+</sup> T cells generated by vaccination could be characterized as effector cells (CD44<sup>+</sup>/CD62L<sup>-</sup>/CD127<sup>+</sup>) both in the tumor and in the blood. Unspecific CD8<sup>+</sup> T cells in the tumor were effector cells as well and unspecific CD8<sup>+</sup> T cells in the blood could be divided into naïve (CD44<sup>-</sup>/CD62L<sup>+</sup>/CD127<sup>+</sup>) or memory (CD44<sup>+</sup>/CD62L<sup>+</sup>/CD127<sup>+</sup>) cells, whereby also cells in the transition state could be found. In not vaccinated vehicle mice nearly no CD8<sup>+</sup> T cells could be found in the tumor so that characterization of CD8<sup>+</sup> T cells was only possible in the blood. They were also characterized as naïve or memory cells.

MCMV m38-specific CD8<sup>+</sup> T cells in the tumor and in the blood expressed PD-1. With pMHCI-IgG or TCB treatment PD-1 expression was a little bit higher. In the tumor expression of PD-1 could be found on all CD8<sup>+</sup> T cells, regardless of whether they were MCMV m38-specific or unspecific. Unspecific CD8<sup>+</sup> T cells in the blood showed no PD-1 expression.

Figure 8.18 B shows the detection of regulatory T cells (T<sub>reg</sub> cells: CD4<sup>+</sup>/CD25<sup>+</sup>/FoxP3<sup>+</sup>) in the tumor. In the left histogram the detection of CD25<sup>+</sup> and CD25<sup>-</sup> CD4<sup>+</sup> T cells in tumors independent from treatment is shown. The same applied to the marker FoxP3 analyzed in the right histogram. A

FoxP3<sup>+</sup> and a FoxP3<sup>-</sup> population of CD4<sup>+</sup> T cells could be found in the tumors of every treatment or control group.



**Figure 8.18: Characterization of T cells in tumors and blood.**

**(A)** Flow cytometry analysis for PD-1 (top row), CD44 (bottom row left), CD62L (bottom row middle) and CD127 (bottom row right) of MCMV m38-specific (left column each marker) and unspecific (right column each marker) CD8<sup>+</sup> T cells in tumor (top row each marker) and blood (bottom row each marker) samples 48 hours after the second treatment. Color code for treatment: Not vaccinated/vehicle (markers only detectable for unspecific CD8<sup>+</sup>T cells in the blood) (purple), MCMV m38-vaccinated/vehicle (dark green), MCMV m38-vaccinated/TCB (light green), MCMV m38-vaccinated/MCMV IE3-MHCI-IgG (orange), MCMV m38-vaccinated/MCMV m38-MHCI-IgG (blue), Isotype control antibody (red). **(B)** Flow cytometry analysis for CD25 (left) and FoxP3 (right) of CD4<sup>+</sup> T cells in tumor samples 48 hours after the second treatment. Color code for treatment: MCMV m38-vaccinated/vehicle (dark green), MCMV m38-vaccinated/TCB (light green), MCMV m38-vaccinated/MCMV IE3-MHCI-IgG (orange), MCMV m38-vaccinated/MCMV m38-MHCI-IgG (blue), Isotype control antibody (red).

### 8.4.2.6 PD-L1 expression in tumors

PD-L1 expression is often found in human and murine tumors and influences effector functions of cytotoxic T cells via binding to PD-1 on those cells. To determine whether this is the case in the present tumor model, tumors which escaped pMHCI-IgG or TCB therapy were excised 31 days after the last treatment and used for flow cytometry analysis of PD-L1 expression.

Figure 8.19 shows the flow cytometry analysis of tumors for PD-L1. While tumors of the vehicle group showed only little PD-L1 expression with 4.9 to 5.9 % PD-L1<sup>+</sup> tumor cells out of all tumor cells, upregulation of PD-L1 could be found in treatment groups. In tumors of the TCB-treated group 24.2 to 30.5 % PD-L1<sup>+</sup> tumor cells out of all tumor cells could be detected and in the pMHCI-IgG-treated group about 20.8 % of all tumor cells were positive for PD-L1.

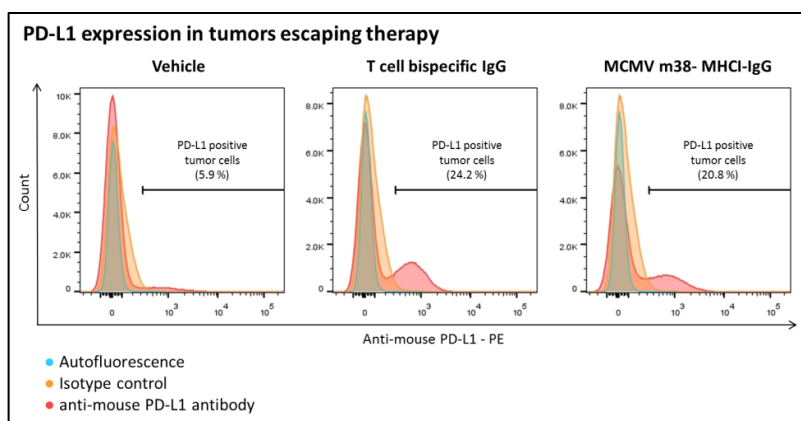


**Figure 8.19: PD-L1 expression in tumors escaping therapy.**

Flow cytometry analysis of tumors, which escaped pMHCI-IgG or TCB therapy. Tumors of the untreated (left), TCB treated (middle), MCMV m38-MHCI-IgG treated (right) groups were analyzed for PD-L1 expression on the cell surface. Color code: Autofluorescence of cells (blue), isotype control antibody (orange), anti-PD-L1 antibody (red).

## 9 DISCUSSION

### 9.1 COMPARISON OF DIFFERENT VACCINATION METHODS FOR GENERATION OF EFFECTOR CELLS IN MICE

For in vivo characterization of pMHC-IgG molecules a surrogate mouse model with endogenous T cell recruitment should be applied. Generation of effector cells should be accomplished by vaccination of mice. Therefore three different vaccination methods were tested. The aim was to establish a reproducible immunization, which is tunable, predictable and also flexible regarding level of effector cells generated. For proof of concept relatively high levels and for final efficacy studies considerable low levels of effector cells, reflecting frequencies of effector cells in patients, should be elicited.

In the adaptive immune response naïve CD8<sup>+</sup> T cells get primed upon encounter of their antigen on DCs. In the following primary response primed CD8<sup>+</sup> T cells differentiate into effector CD8<sup>+</sup> T cells and expand up to 50 000-fold to complete killing of infected cells [123, 124]. After the peak of the primary CD8<sup>+</sup> T cell response most of the effector cells die and only few continue to differentiate into memory CD8<sup>+</sup> T cells [125]. Upon rechallenge with the same pathogen the long lived memory CD8<sup>+</sup> T cells can mount very quickly and effectively a secondary immune response against the previously encountered antigen [124].

In the present experiments the primary response of effector CD8<sup>+</sup> T cells after vaccination should be used for endogenous T cell recruitment. The magnitude of the primary CD8<sup>+</sup> T cell response is dependent on the duration of the TCR stimulus during initial antigen encounter [126] and therefore influenced by availability and amount of antigen at first contact with precursor cells [125]. Thus delivery of antigen via different vaccination methods and application routes results in different frequencies of effector CD8<sup>+</sup> T cells during the primary response. Three different vaccination methods, resulting in presentation of antigen on MHC complexes of DCs, were tested. First, differentiated and activated DCs, already loaded with antigen in vitro, were injected into mice via different administration routes. Second, DNA vectors encoding for the antigen were introduced into DCs of animals with DNA injection and following in vivo electroporation. As a third method antigen was targeted to DCs in mice via antibody-delivery of antigen to the XCR1-receptor of DCs with following internalization and cross-presentation of antigen.

For the vaccination with peptide-loaded DCs (see chapter 8.3.1), matured bone marrow-derived DCs were loaded with the OVA-derived peptide "SIINFEKL" and injected into mice to induce a "SIINFEKL"-specific CD8<sup>+</sup> T cell response. As "SIINFEKL"-pulsed DCs showed superior efficacy compared to OVA-protein pulsed DCs [127], the decision was made in favour of the peptide-pulsed DCs. With this strategy no CD4<sup>+</sup> T cell response is expected, but priming of CD8<sup>+</sup> T cells for expansion and development of effector functions like cytotoxicity or cytokine secretion during primary response is feasible in the absence of CD4<sup>+</sup> T cell help [128]. Indeed, secondary immune response is impaired as no second round of clonal expansion is possible upon restimulation [128]. It was found that vaccination with mature DCs is superior regarding migration, accumulation in lymph nodes and expansion of CD8<sup>+</sup> T cells [129]. Hence vaccination was performed with LPS-treated DCs. LPS-activated DCs are able to secrete MHC class I-bearing exosomes, which can be uptaken by autochthonous DCs in secondary lymphoid organs [130, 131]. Those DCs can then present the antigen themselves without having got in touch with the original antigen source. Thereby exosomes bearing antigen / MHC class I complexes can get to secondary lymphoid organs via migration of peptide-loaded, injected DCs or via transport of exosomes with the lymphatic fluid or blood stream [130, 131]. This exosomal way of antigen distribution results in an increase of antigen presentation and therefore augments antigen-specific CD8<sup>+</sup> T cell response (discussed in [132]).

Depending on how good preconditions like migration and accumulation of APCs in lymph nodes and availability and amount of antigen during initial antigen encounter are satisfied, antigen-specific CD8<sup>+</sup> T cell response will turn out correspondingly. In the present experiment with peptide-loaded DCs the i.d. and the s.c. administration of cells seemed to fulfill those requirements best. Peptide-loaded DCs provided with those injection routes elicited antigen-specific CD8<sup>+</sup> T cell responses of about 3 to 4 % after two administrations at interval of one week. After a third injection a second peak could be triggered, which was marked higher with i.d. administration of cells. By contrast i.p. or i.v. injection of peptide-loaded DCs was clearly inferior to i.d. or s.c. administration with the i.p. administration route only inducing very low levels of antigen-specific CD8<sup>+</sup> T cells in general and the i.v. injection missing the second peak after the third administration of DCs.

The normal localisation of DCs is the skin or other surface tissues, where the primary contact with pathogens takes place. Antigens are taken up by DCs via endocytosis and DCs migrate to draining secondary lymphatic organs. If antigen uptake took place in the periphery DCs migrate to draining lymph nodes, if pathogens entered blood stream antigens are trapped in the spleen and uptaken by

DCs there. In the secondary lymphatic organs DCs present peptides of the antigen on MHC complexes and prime naïve CD8<sup>+</sup> T cells. With injection of already peptide-loaded DCs this procedure is mimicked. By i.p. or i.v. injection of DCs a very broad distribution pattern in various organic systems can be found [133, 134]. It is likely that many peptide-loaded DCs die or get stuck after i.p. or i.v. injection before they can enter the spleen or a lymph node and induce CD8<sup>+</sup> T cell priming there. The final amount of antigen presented during initial antigen encounter may be strongly reduced compared to the amount injected at the beginning. As the physiological localisation of DCs is the skin, it is probably argumentative that i.d. and s.c. injection of peptide-loaded DCs worked better. The exosomal way of antigen distribution as described before with secretion of peptide-MHC class I-bearing exosomes, which can be uptaken by other DCs located in the skin, is likely to contribute to the success of those application routes. The amount of antigen presented during initial antigen encounter in the lymph nodes is probably higher than the one in the spleen after i.p. or i.v. injection. The amount of peptide-loaded DCs which can be injected also depends on the volume, that can be administered using a certain application route. Applying i.d. injection only 20 µl are allowed to be administered, so that only  $2 \times 10^5$  cells could be injected, which is a fourth or an eighth of the cells used for i.v. or s.c./i.p. injection, respectively. In this respect, the i.d. injection of peptide-loaded DCs was the most effective one in inducing an antigen-specific CD8<sup>+</sup> T cell response, which can be due to the “most physiological” introduction of peptide-loaded DCs into the organism. In the past years also others compared different administration routes of peptide-loaded DCs for generation of an antigen-specific CD8<sup>+</sup> T cell response. However, in most cases indirect parameters such as outgrowth of tumor cells were used for efficacy evaluation of induced antigen-specific CD8<sup>+</sup> T cell responses. Challenge of mice with tumor cells after immunization with peptide-loaded DCs led to better tumor rejection after i.d. or s.c. injection of cells than systemic administration of peptide-loaded DC [129, 135, 136], whereby Okada et al. also showed a superior efficacy of i.d. administration in an in vitro lysis assay with splenocytes of vaccinated mice [135]. Huck et al. and Okada et al. demonstrated that the route of DC administration affects site of DC accumulation, time of DC persistence and relating efficacy of vaccination in vivo [129, 135]. It was shown that after s.c./i.d. injection DCs accumulate in draining lymph nodes for a much longer time than DCs accumulate in the spleen after i.v. injection resulting in a better outcome for s.c./i.d. administration of peptide-loaded DCs. These results are reflecting the findings in the present study.

Applying DNA injection with following in vivo electroporation as vaccination (see chapter 8.3.2), vectors encoding for the antigen are brought into murine cells. Genes of plasmid DNA are expressed and a xenogeneic protein is produced, which is processed inside cells. As a result immunogenic peptides of the protein are presented on MHC class I complexes on the cell surface. DCs present an immunogenic peptide prime naïve CD8<sup>+</sup> T cells and a primary response of antigen-specific effector CD8<sup>+</sup> T cells is induced. In the present experiment the DNA vector injected into mice encoded for the whole OVA-protein to ensure correct processing and MHC class I-presentation of the OVA-derived "SIINFEKL"-peptide. Two administration routes, i.d. and i.m. injection of DNA vectors, were tested. Crucial factors for success of DNA vaccination is a high level of antigen expression at the site of application [137] and the initiation of a T cell response by DCs [138]. After intramuscular injection of DNA myocytes and keratinocytes express the antigen, but also DCs, the professional APCs, can be directly transfected or take up antigen that is secreted by other cell types or released by apoptotic cells [138, 139]. Electroporation may contribute to this process, as death of some transfected cells after electroporation could supply danger signals, which activate DCs [139]. For a long time it was suggested that striated muscle is the only tissue to be capable of taking up and expressing genes that are transferred in the form of plasmid DNA [140]. However, it was found that also DCs located in the skin can be successfully transfected with plasmid DNA [141, 142]. After transfection they migrate to draining lymph nodes and prime naïve T cells [142].

In the present study vaccination via DNA injection with following electroporation elicited only low numbers of specific CD8<sup>+</sup> T cells in general. In addition the number of non-responders and heterogeneity of specific CD8<sup>+</sup> T cell levels was very high, making the method not applicable for studies requiring high animal numbers with relatively homogenous distributions of specific CD8<sup>+</sup> T cell levels. Comparing the application routes, the i.d. administration of DNA vectors was marked superior to i.m. injection of plasmids, which was also found by Raz et al. [141]. Condon et al. could establish a protective tumor immunity by cutaneous genetic immunization with naked DNA [142], implicating the generation of a potent, antigen-specific, cytotoxic T cell response. In most cases i.m. injection of DNA with following electroporation was used for immunization [137-139, 143-147]. Paster et al. and Peng et al. could generate specific CD8<sup>+</sup> T cell frequencies of 10 % to 25 % [139, 147]. A result, which could not be achieved in the present experiments. Paster et al. engineered the vaccination-epitope in-frame into the human HLA-Cw3 molecule [139], an antigen, which is exceptional in provoking immunogenicity [148]. This modification of the vector led to increased

frequencies of epitope-specific CD8<sup>+</sup> T cells, which could mediate delayed tumor outgrowth in experiments of Kalat et al. [143]. Other groups also tested i.m. injection of DNA with subsequent electroporation and evaluated efficacy of vaccination only with indirect parameters like tumor growth. In several studies i.m. application of DNA vectors with following electroporation could mediate protection of mice from tumor outgrowth or reduction of tumors [139, 143, 145-147]. Electric pulses delivered for electroporation were different to the ones delivered in the present experiment, which can alter permeabilization of cells during electroporation. Also diverse vectors were used for DNA delivery, whereby most of the time a CMV promotor was included, but nevertheless this can also influence antigen expression. This alterations could explain reduced specific CD8<sup>+</sup> T cell frequencies in the present experiment compared to others.

As a third immunization method the XCR1-targeted vaccination was tested (see chapter 8.3.3). XCR1 is exclusively expressed on cross-presenting DCs and no other tissues in mice and humans [121] and therefore optimal for specific targeting of cross-presenting DCs. In this experiment the OVA-protein and later the MCMV m38 peptide were targeted to the XCR1 receptor with the antibody MARX10. This antibody specifically binds to murine XCR1 [121] without altering the activation status of XCR1<sup>+</sup> DCs [107]. Applying this method a large number of DCs is presenting the antigen in the secondary lymphoid organs, resulting in a high amount of antigen at first contact with precursor cells and a strong TCR stimulus during initial antigen encounter, which are prerequisites for a strong primary CD8<sup>+</sup> T cell response [125, 126]. Hartung et al. showed that in an in vivo cytotoxicity assay and in an in vivo tumor protection experiment vaccination with the MARX10-OVA antibody could induce “SIINFEKL”-specific CD8<sup>+</sup> T cells, which eliminate target cells in vivo [107]. After immunization with the MARX10-OVA antibody low frequencies of “SIINFEKL”-specific CD8<sup>+</sup> T cells could be detected in the present study. The laboratory of R. Kroczeck developed further amplification steps to enhance antigen-specific CD8<sup>+</sup> T cell response after injection of the targeting antibody coupled to the antigen. By addition of a boost step, constituted of an i.v.-injection of antigen-loaded cells, and an amplification step with administration of half-life extended IL-2, high frequencies with up to 50 % “SIINFEKL”-specific CD8<sup>+</sup> T cells could be generated. Corresponding levels of MCMV m38-specific CD8<sup>+</sup> T cells could not achieve such high frequencies, but keeping in mind that for MCMV 38 immunization only the peptide and not the whole protein, as applied for “SIINFEKL”-vaccination, was fused to the targeting antibody (see chapter 7.1.12) MCMV m38-specific CD8<sup>+</sup> T cell response was still very high with up to 20 % specific CD8<sup>+</sup> T cells.

Another contributing factor for the varying CD8<sup>+</sup> T cell responses for the epitopes is the high immunogenicity of ovalbumin.

As mentioned before a reproducible immunization method, which is tunable, predictable and also flexible regarding level of effector cells, should be established for efficacy evaluation of pMHCI-IgG molecules. Obviously targeting of antigen to the XCR1-receptor of cross-presenting DCs combined with further amplification steps generated the most potent CD8<sup>+</sup> T cell response in our hands. By addition or omission of amplification steps the intended percentage of specific CD8<sup>+</sup> T cells was reasonably well steerable, so that this was the method of choice for generating effector cells in further efficacy studies. The amplification steps could have also been combined with DNA vaccination or immunization with peptide-loaded DCs, but as the XCR1 targeting vaccination was the best established one the choice finally was in favor of this immunization method. Keeping in mind that large numbers of animals had to be vaccinated for efficacy studies with pMHCI-IgG molecules, this method was also the most feasible one regarding effort.

## **9.2 COMPARISON OF PEPTIDE-MHC CLASS I-ANTIBODY FUSION MOLECULES WITH OTHER PEPTIDE- MHC CLASS I-RETARGETING MOLECULES**

Several studies focused on the recruitment of CTL with antibody-targeted peptide-MHC class I complexes for elimination of tumor cells in recent years [1, 2, 93-105, 149-151]. None of the molecules were developed for clinical testing up to now because the antibody-MHC fusion proteins are technically difficult to produce and in vivo potency of these molecules is difficult to prove. Basically the molecules consist of two parts, the peptide-MHC class I part, binding to CD8<sup>+</sup> T cells, and the targeting moiety, a monoclonal antibody or antibody-derived fragment, which binds to the tumor cells. For the targeting part, single chain variable fragments (scFvs) [99, 100, 102, 103] or fragment antigen binding portions (Fab') [98, 101, 104] of antibodies were applied. The molecule used in the present study contained a full monoclonal antibody in the IgG format as described and applied in previous research work [1, 2, 151]. The size and properties of the molecule are crucial for tumor penetration and half-life of the molecule. Fusion proteins containing a scFv have a molecular mass of about 65 to 67 kDa [99, 100, 103], molecules with a Fab' weigh about 95 kDa [98, 101] and the molecular weight of fusion proteins comprising a full IgG is about 190 kDa (see chapter 8.1.4). With respect to tumor penetration the smaller molecules constructed with a scFv or a Fab' may have an advantage over the ones containing a full IgG. However, earlier work showed that

microvascular permeability varied only twofold for proteins between 25 and 160 kDa [152]. Regarding pharmacokinetic properties full IgG-fusions with a half-life of about three to six days in mice (and 10 to 21 days in humans) are superior to molecules with smaller antibody fragments, which have only a half-life of about 24 to 48 hours [99] due to lack of FcRn binding properties and fast renal clearance. Zahnd et al. postulated that either very small, soluble proteins with high affinity or very large proteins such as full IgG antibodies achieve the best tumor accumulation, while intermediate size molecules like scFv fragments show lower tumor accumulation. The very small molecules achieve this by a significantly greater capillary extravasation and the very large molecules by exceeding the renal filtration cutoff resulting in long circulation. Intermediate size molecules lack both favorable properties and thus tumor accumulation is reduced [153]. As shown in chapter 8.4.2.3 the surrogate peptide-MHCI- IgG fusion molecules penetrate fairly well into the tumor. The early clearance from the tumor is likely owed to the special surrogate isotype used for the antibody (see chapter 8.1.1.4). In the surrogate model no further pharmacokinetic studies were carried out, but recent pharmacokinetic experiments with human peptide MHC class I-IgG fusions in a xenograft model showed accumulation of the molecule in the tumor for over 72 hours and a blood half-life of the fusion protein of three to six days [154]. Some groups promoted antibody-streptavidin-MHC tetramers for redirection of CTL [93, 94, 97, 102, 104, 150], which imply advantages but also several limiting factors for the use in vivo. If applied in a two-step process with biotinylated peptide-MHC class I complexes and a scFv genetically fused to streptavidin [97, 102, 104], higher flexibility for patients with different HLA types could be enabled and molecular weight of the two proteins would be relatively low with about 85 kDa for the SA-scFv and about 45 kDa for the biotinylated peptide-MHC class I part indicating an adequate penetration profile. However, streptavidin for in vivo use is still a matter of debate, as antibody responses could be developed against this immunogenic protein [155, 156]. If Ab-streptavidin-MHC tetramers would be applied as pre-formed complexes, molecular weight would rise to about 400 kDa predicting poor tissue penetrance. An additional disadvantage of tetramers is the possibility of T cell activation in the circulation [157, 158], as they provide four sites for peptide-MHC class I / T cell receptor interaction, which can lead to cross-linking and following activation of T cells in the periphery. Another aspect regarding the antibody part of the CTL recruiters is the number of target binding sites. As shown by previous research bivalent binding to tumor cells elicits a more effective tumor cell killing than monovalent binding [1, 2, 105]. If using a monomer with a scFv or a Fab' fragment as targeting moiety [98-101, 103] only monovalent binding to target cells is possible.

With respect to the stability of peptide-MHC class I complexes included in the molecules, covalent linkage of peptides to the MHC complex is preferable to loading of peptides by refolding of MHC class I heavy chain and  $\beta_2M$  around the peptide. Loaded peptide can disassociate from the MHC complex, which leads to loss of recruitment function of the molecule and probably non-specific activation of T cells and non-specific elimination of non-targeted cells due to loading of peptide onto other cells expressing the appropriate MHC class I complex [96, 101, 105, 150, 159]. To overcome those issues covalent cross-linking of the peptide to the MHC class I complex by photoactivation [101] or connection of the peptide to the MHC class I complex with a flexible linker in various formats were promoted [95, 100, 112, 160, 161].

Summing up all aspects regarding construction of molecules, pMHCI-IgG molecules seem to be the optimal format for the use in patients. Applying a full IgG enables binding to target cells via avidity and half-life extension of the molecule due to FcRn recycling with still good tumor penetration properties. Fusion of the peptide, the  $\beta_2M$ , the heavy chain of the MHC class I complex and the antibody is all recombinant (see chapter 8.1.1.1), which results in a very stable protein with reduced immunogenicity risk compared to approaches using a biotin-streptavidin complex for linkage or loading of peptide into the groove of the MHC class I complex. An alternative option is the chemical conjugation of the targeting moiety to the peptide-MHC class I complex [98, 101, 105, 150], which is less preferred for large scale production as it involves significant effort for synthesis of the molecules. Applying pMHCI-IgG molecules involves no risk of disassociation of the peptide from the MHC complex, as the peptide, the  $\beta_2M$  and the heavy chain of the MHC class I complex are fused with two flexible linkers. Additional stabilization of the peptide-MHC class I complex could be achieved by introduction of a disulfide bond connecting the linker between peptide and  $\beta_2M$  with the  $\alpha_1$  domain of the MHC class I complex (see chapter 8.1.1.2) [112]. It is also very unlikely that T cells in the periphery get activated by pMHCI-IgG molecules, as the fusion protein contains only one peptide-MHC class I complex and activates T cells only when cross-linking with target cells is taking place as shown in in vitro assays [1]. For further stabilization of the molecule and enhancement of production yield several modifications were induced (see chapter 8.1.1). The use of a full monoclonal antibody in the IgG format as targeting moiety may raise the question for Fc $\gamma$ R and C1q binding. To avoid CDC and Fc $\gamma$ R-mediated co-activation of innate immune effector cells such as ADCC or ADCP a silent Fc-part was introduced into the molecules (see chapter 8.1.1.4).

### 9.3 IN VITRO EVALUATION OF PEPTIDE-MHC CLASS I-ANTIBODY FUSION MOLECULES

Before evaluation of the in vivo efficacy of pMHCI-IgG molecules and TCB antibody, binding of surrogate fusion molecules to their target on tumor cell lines was tested (see chapter 8.2.1). With flow cytometry analysis could be shown that the fusion molecules bind to their target and that binding of the antibody is not impaired by N-terminal fusion of the peptide-MHC class I complex. This has been shown before for N-terminal fusions [1, 2, 162]. At molecule concentrations of 5 nM or more saturation is reached and all FAP proteins on the surface of tumor cell lines are bound. With decreasing compound concentrations fewer molecules are bound to tumor cells with no more molecule binding detected at a concentration of 0.005 nM. This applies to both tumor cell lines (B16-muFAP and MC38-muFAP) and both pMHCI-IgG molecules and TCB antibody. With a secondary antibody detecting the murine MHC class I complex H-2K<sup>b</sup> it could be demonstrated, that pMHCI-IgG molecules deliver H-2K<sup>b</sup> complexes onto the cell surface of tumor cell lines. Also in this case a concentration dependent manner of molecule binding with saturation at 5 nM could be found. The antibody detecting the OVA<sub>257-264</sub> peptide on the H-2K<sup>b</sup> complex, demonstrated that the peptide together with the MHC class I complex could be brought onto the cell surface of tumor cell lines by means of pMHCI-IgG molecules. Thus all components of the fusion molecule could be detected on tumor cell lines with flow cytometry, which justified further testing of the molecules. Also internalization of molecules could be excluded, constituting another pre-requisite for functionality of molecules. Regarding density of native H-2K<sup>b</sup> complexes and FAP molecules on the cell surface of the different tumor cell lines, it could be found that B16-muFAP cells express more FAP but less H-2K<sup>b</sup> complexes on their cell surface than MC38-muFAP cells. The density of target molecules on the tumor cell surface plays a crucial role in tumor cell killing as shown for the TCB antibodies before [91], but in this case the difference in target expression between both tumor cell lines is very small and both tumor cell lines show a high density of target molecules, so that tumor cell killing should be possible in both cases. This could be also confirmed in in vitro and in vivo studies (see chapters 8.2.3 and 8.4.1).

Before evaluation of the in vivo efficacy of pMHCI-IgG molecules and TCB antibodies, IFN- $\gamma$  activation of CD8<sup>+</sup> T cells and cytotoxicity induced by fusion proteins was analyzed in vitro (see chapters 8.2.2 and 8.2.3). Oved et al. measured activation of specific CD8<sup>+</sup> T cells mediated by sHLA-A2/EBV tetramers by determination of IFN- $\gamma$  release into the culture supernatant with an

ELISA (enzyme-linked immunosorbent assay) assay and could demonstrate that CD8<sup>+</sup> T cells are specifically activated by scHLA-A2/EBV tetramers in a concentration dependent mode [100]. <sup>51</sup>Cr release [93, 97, 98, 101, 102, 105, 150] or [<sup>35</sup>S]methionine release [96, 99, 100, 103] assays were used by several groups for cytotoxicity analyses and showed that peptide-MHCI-antibody conjugates could mediate in vitro tumor cell elimination in a concentration- and effector to target (E:T) ratio- dependent manner. In this study intracellular IFN- $\gamma$  production of specific CD8<sup>+</sup> T cells upon exposure to effector molecules bound to target cells was measured with flow cytometry analysis. For evaluation of cytotoxicity mediated by fusion molecules the xCELLigence technology was applied as also used by Schmittnaegel et al. to determine in vitro cytotoxicity mediated by human pMHCI-IgG fusions compared to BiTEs (bispecific T cell engagers) with donor-derived PBMCs [2]. Schmittnaegel et al. could show that CMV pp65-MHC class I-IgG fusion molecules achieved a comparable absolute target cell killing as the BiTEs (recruiting T cells via CD3) even at low frequencies of specific CD8<sup>+</sup> T cells, whereby pMHCI-IgG molecules needed more time than BiTEs to complete absolute tumor cell elimination.

The MCMV m38-MHCI-IgG fusion molecule as well as the TCB antibody used in this surrogate model could induce IFN- $\gamma$  activation of only 10 % of CD8<sup>+</sup> T cells available for activation. However, target cell elimination could be completed up to 93 % with the TCB antibody and up to 63 % with the MCMV m38-MHCI-IgG fusion molecules. Also the surrogate pMHCI-IgG molecules needed more time than the TCB antibody to complete tumor cell killing. Additionally tumor cell lysis induced by the TCB is more effective than the one induced by pMHCI-IgGs. This is due to the fact that CD3-based T cell recruiters can recruit a substantially larger number of T cells within CTL than pMHCI-IgG molecules, which recruit only specific CD8<sup>+</sup> T cells via T cell receptor / peptide-MHC class I complex interaction. Consequently T cells redirected by pMHCI-IgG molecules have to eliminate more target cells per effector cell than T cells redirected by CD3-based T cell recruiters. This was shown by Schmittnaegel et al. before [154] and explains the longer time needed to complete target cell killing and the less effective tumor cell lysis mediated by pMHCI-IgG molecules. Nevertheless, keeping in mind that pMHCI-IgG molecules had tenfold less effector cells available for target cell killing than TCB antibodies they could still eliminate two-thirds of the amount of tumor cells lysed with TCB antibodies. PMHCI-IgG molecules containing the control peptide MCMV IE3 showed same results as controls (tumor cells only, tumor cells with splenocytes) and induced no IFN- $\gamma$  activation of specific CD8<sup>+</sup> T cells or cytotoxicity. This demonstrated that IFN- $\gamma$  activation of specific CD8<sup>+</sup> T cells and cytotoxicity is specifically mediated by pMHCI-IgG molecules and that other

components of splenocytes such as NK cells or macrophages barely induce molecule independent and unspecific elimination of tumor cells. However, 20 % of CD8<sup>+</sup> T cells available for activation were activated by peptide-loading of target cells and lysis of peptide-loaded tumor cells was completed by 86 %. IFN- $\gamma$  activation of CD8<sup>+</sup> T cells induced by peptide-loaded tumor cells was higher than the one mediated by pMHCI-IgG coated tumor cells. Additionally more tumor cells were killed when loaded with peptide as when coated with pMHCI-IgGs. This indicates that not all MCMV m38-specific CD8<sup>+</sup> T cells detecting the natural peptide-loaded MHC class I-complex on the tumor cell surface recognized the recombinant MCMV m38-MHCI-complex delivered to the target cell surface with pMHCI-IgGs.

With respect to the OVA<sub>257-264</sub>-MHCI-IgG fusion molecule results were comparable. However, for OVA<sub>257-264</sub> nearly no IFN- $\gamma$  activation of CD8<sup>+</sup> T cells could be induced by the pMHCI-IgG. Nevertheless up to 80 % of tumor cells could be lysed by means of the fusion molecule, while time interval needed to complete target cell killing was again very large compared to TCB or peptide-loaded tumor cells. Also in this case peptide-loaded tumor cells induced higher IFN- $\gamma$  activation of CD8<sup>+</sup> T cells and more effective target cell lysis than pMHCI-IgG coated tumor cells.

Keeping in mind that there are even less H-2K<sup>b</sup> complexes on the tumor cell surface for peptide-loading than FAP molecules for pMHCI-IgG binding (see chapter 8.2.1), this indicates that the less efficient target cell killing or IFN- $\gamma$  activation of CD8<sup>+</sup> T cells mediated by pMHCI-IgGs is caused by the molecule itself and not by reduced functionality of specific CD8<sup>+</sup> T cells generated by vaccination. Reasons for that could be incorrect folding of peptide-MHC class I complex, impurity of molecules in the fashion of side products lacking the peptide-MHC class I complex, aggravated accessibility of the peptide-MHC class I complex for CD8<sup>+</sup> T cells due to steric hindrance or suboptimal distance between target cell surface and peptide-MHC class I complex brought onto the cell surface by pMHCI-IgGs.

Impurity of protein can be excluded as SDS-PAGE and western blotting were applied to prove that only knob-hole-products (antibody fused to one peptide-MHC class I complex) were obtained after the purification process (see chapter 8.1.4).

Incorrect folding of the peptide-MHC class I complex can be partially excluded, because some portions of the MHC complex and the peptide could be detected in the right formation with secondary antibodies (see chapter 8.2.1). Still it is possible that the N-terminus or C-terminus of the peptide is not formatted optimally in the groove of the MHC class I complex despite the disulfide

bond connecting the linker between peptide and  $\beta_2M$  with the  $\alpha_1$  domain of the MHC class I complex (see chapter 8.1.1.2), which can cause poor recognition by specific  $CD8^+$  T cells. To verify this, a crystal structure analysis could be carried out, but this is very time consuming and expensive, so that this technology was not applied here.

The accessibility of the peptide-MHC class I complex on the target cell surface is difficult to prove, but could be a reason for less efficient target cell killing or  $IFN-\gamma$  activation of  $CD8^+$  T cells mediated by pMHCI-IgGs. If pMHCI-IgG molecules bind to the cell surface target in such a way that the peptide-MHC class I complex is not or only difficult to access for specific  $CD8^+$  T cells due to steric hindrance, efficacy of fusion proteins will be impaired. Thus functionality of pMHCI-IgG molecules is also dependent on the cell surface target chosen for the fusion protein. Schmittnaegel et al. showed that human pMHCI-IgG fusions delivered peptide-MHC class I complexes to the target cell surface, that were recognized just as well as native MHC class I complexes loaded with peptide by specific  $CD8^+$  T cells, resulting in equal  $IFN-\gamma$  activation of specific  $CD8^+$  T cells and tumor cell lysis [1]. According to this every newly designed pMHCI-IgG fusion protein has to be tested for those properties before further development.

Another aspect is the distance between tumor cell surface and peptide-MHC class I complex. By means of the pMHCI-IgG molecule an artificial peptide-MHC class I complex is delivered to the target cell surface, which is located further away from the cell surface than a native MHC class I complex loaded with peptide. With 170 kDa the fibroblast activation protein (FAP) is a fairly large surface protein. If the antibody included in pMHCI-IgG fusions binds to a part of the protein, which is located at the very outer end of the surface molecule, the distance between target cell surface and peptide-MHC class I complex delivered to the cell surface by pMHCI-IgGs is relatively large. Consequently the distance between target cell and effector cell recognizing to the peptide-MHC class I complex is also enlarged. This can have a considerable influence on effectiveness of target cell killing mediated by effector cells. The larger the distance between target cell and effector cell is the less effective is killing activity mediated by effector cells. This issue was also described for CARs (T cells genetically modified to express chimeric antigen receptors) [163, 164].

Another finding was that peptide-loading of tumor cells achieved only at higher concentrations the maximum of  $IFN-\gamma$  activation, whereas pMHCI-IgG coating of tumor cells reached maximal  $IFN-\gamma$  activation already at lower concentrations. This is likely due to the fact that the antibody constructs bind very fast and with high affinity ( $< 1$  pM: see chapter 8.1.1.5) to their target on the tumor cell

surface, while affinity of peptides to MHC class I complexes is comparably weak (<1 nM to >20 000 nM) [165]. Thus at lower concentrations more peptide-MHC class I complexes are present on the tumor cell surface when delivered by pMHCI-IgGs than with peptide-loading, because the antibody constructs bind to the tumor cell surface very fast and with high affinity, while peptides bind more slowly to the MHC class I complexes and disassociate again easily.

## **9.4 IN VIVO EVALUATION OF PEPTIDE-MHC CLASS I-ANTIBODY FUSION MOLECULES**

In vivo studies with CTL recruiters for antibody-targeted tumor cell elimination have been carried out before [2, 96-99, 101, 103-105]. Many experiments were performed as pre-treatment models, in which tumor cells were already pre-incubated with the targeting molecule in vitro before injection into mice [97, 101, 104, 105]. In other low bar models tumor cells were injected subcutaneously together with effector cells and effector molecules [96] or systemic treatment with effector molecules was started at the day of tumor cell inoculation or one day later [2, 98, 101, 103]. As effector cells genetically engineered T cell clones or expanded CTLs from patient-derived PBMCs were applied in immunodeficient mice [2, 96, 97, 99, 103], which lack an immune system. Others used vaccination strategies which mostly targeted OVA as antigen and in some cases included adoptive transfer of OVA-specific H-2K<sup>b</sup>-restricted TCR transgenic T cells from OT-1 mice [98, 104, 105]. This approach with endogenous T cell recruitment rather meets the conditions in patients, but is still artificial as OVA is an exceptional antigen in provoking immunogenicity resulting in very high and unphysiological levels of specific CD8<sup>+</sup> T cells. Cesson et al. used a model with Lymphochoriomeningitis Virus (LCMV)-infected mice [101], which reflects the situation in patients best. Effector cells are generated in a physiological way resulting in physiological levels of specific CD8<sup>+</sup> T cells. In this study endogenous T cell recruitment after vaccination for OVA or MCMV is applied.

### **9.4.1 Experimental lung metastasis model**

Syngeneic models comparable to the preventive setting of the experimental lung metastasis model carried out with pMHCI-IgGs (see chapter 8.4.1.1.1) were performed by Cesson et al., Savage et al. and King et al. [101, 104, 105]. They showed killing capacity of pMHCI-retargeting conjugates on single tumor cells in the circulation using lung metastasis models with B16 melanoma cells

transfected for a target surface protein and endogenous T cell recruitment. Savage et al. and King et al. immunized mice for OVA<sub>257-264</sub> as also done in studies with pMHCI-IgG fusions [104, 105], whereas Cesson et al. used mice acutely infected with influenza [101]. Comparing studies regarding numbers of effector cells available at tumor challenge, animals had levels of 10 % to 15 % influenza-specific CD8<sup>+</sup> T cells in the bronchoalveolar lavage [101], 1 % to 2 % OVA<sub>257-264</sub>-specific CD8<sup>+</sup> T cells in the spleen [105] or 6 % OVA<sub>257-264</sub>-specific CD8<sup>+</sup> T cells and 3 % MCMV m38-specific CD8<sup>+</sup> T cells, respectively, in the blood in the present study. Savage et al. and King et al. targeted human CD20 on B16 melanoma cells [104, 105], whereby King et al. used tumor cells expressing very low levels of target antigen [105]. Cesson et al. used HER2 as target on B16 melanoma cells, which was expressed in high frequencies comparable to FAP expression of B16 cells used in the present study [101]. Different to described experiments, in which tumor cells were coated with effector molecules in vitro before intravenous injection into mice [101, 104, 105], in the present study mice were treated systemically (intravenously) with effector molecules 24 hours before tumor challenge. As a result of all protection assays mice treated with a pMHCI-retargeting molecule showed significantly fewer or no lung metastases compared to control groups. The different experiments with variable preconditions regarding expression of target antigen, generation, epitope and levels of specific CD8<sup>+</sup> T cells, effector molecules and target cells (in vitro before injection or in vivo after administration) led to similar results with respect to protection from lung metastases. To prove that elimination of tumor cells is mediated by recruitment of specific CD8<sup>+</sup> T cells and not by other effects associated with the molecules (e.g. ADCC by FcγR-mediated co-activation of innate immune effector cells) one group in the present study was treated with a pMHCI-IgG molecule containing the control peptide MCMV IE3. For this MCMV epitope mice do not have specific CD8<sup>+</sup> T cells so no killing of tumor cells was observed as expected. This is in line with the results on non-immunized mice with pMHCI-conjugates from King et al. [105]. King et al. also compared retargeting conjugates with one or two binding sites for hCD20, whereby the molecule with two binding sites was the more effective one, indicating that avidity binding of retargeting molecules is important for a better outcome. Additionally this is the only previous in vivo study, which compares pMHCI-retargeting conjugates with bispecific molecules recruiting CTL via CD3. For this purpose heterodimers targeting muCD3 and hCD20 with one Fab' each were engineered [166, 167]. In the lung metastases protection assay the bispecific antibody could protect naïve mice completely from lung metastases and also immunized mice treated with the retargeting conjugates showed almost complete inhibition of metastases formation, with the retargeting conjugate containing two binding

sites for hCD20 being more effective. This results match with the findings in the this study. King et al. also performed a surrogate lymphoma model with human CD20-transfected EL4 cells and endogenous T cell recruitment after vaccination for OVA<sub>257-264</sub> [105], in which systemic molecule administration was started three days after tumor cell inoculation. In this survival experiment mice treated with the bispecific antibody survived as long as animals treated with the retargeting conjugates with one binding moiety for hCD20. Retargeting conjugates binding the target via avidity showed the best results regarding survival of mice and hence were prior to the bispecific antibody containing only one target binding site. Vaccination had a significant impact on tumor growth, as immunized mice showed increased survival compared to naïve mice. This finding corresponds to the result of the experimental lung metastasis model carried out here for evaluation of pMHC-IgG fusions. Vaccinated control groups showed markedly fewer B16 colonies than not-vaccinated vehicle groups. Tumor growth inhibition mediated only by vaccination may be an effect of activation of innate immune cells due to cytokine release during primary immune reaction. In the present study it is probably owed to the administration of complexed IL-2 during immunization, whereas King et al. might elicit a weak anti-tumor response induced by the anti-CD40 antibody injected as part of vaccination [105]. Nevertheless in both experiments a marked tumor growth inhibition mediated by pMHC-retargeting molecules could be observed beyond immunisation alone.

So far no study evaluating the therapeutic treatment of already established lung metastasis with pMHC-retargeting molecules was described. In the present experiment B16 melanoma cells were injected intravenously so that tumor cells could migrate to the lung, settle down there and cause lung metastases. After nine days, when lung metastases were established, mice were treated intravenously twice with pMHC-IgG fusions. Effector cells in mice were generated with the XCR1-targeted vaccination as described before (see chapter 7.3.2.3.). In this experimental setup neither the pMHC-IgG nor the TCB could completely eliminate tumor cells, but a significant, delayed metastasis growth could be achieved with both molecules in a similar fashion. One group of animals vaccinated for MCMV m38 was treated with the pMHC-IgG molecule containing the control peptide MCMV IE3 resulting in strong metastasis growth. This showed that elimination of tumor cells was specifically mediated by redirection of specific CTL with pMHC-IgG fusions. Conspicuously the MCMV m38 system showed a clearly better outcome than the OVA<sub>257-264</sub> system. This may be caused by impaired activation capability of the OVA<sub>257-264</sub>-MHC-IgG fusion molecule, which is likely due to the fact that the recombinant pMHC-IgG was not fully achieving the potency

of the peptide-loading of the endogenous MHC class I complexes already obvious from the in vitro assays. As part of this issue there is no significant difference in metastasis burden between control groups treated with the non-binding control molecule or PBS and the OVA<sub>257-264</sub>-MHCI-IgG treatment group. Loss of target expression of tumor cells can be excluded as reason for missing efficacy as stable FAP expression in metastases could be demonstrated by immunohistochemistry (see chapter 8.4.1.2).

Again vaccination had marked influence on metastasis growth as already described by others before [98, 105]. Furthermore it is interesting to note that activation of effector cells by immunization also seems to support function of the TCB. Metastasis burden of the not-vaccinated, TCB-treated group is outstandingly reduced compared to the not-vaccinated vehicle group, but still comparable to the number of metastases found in the vaccinated vehicle group. TCB treatment combined with immunization reduces metastasis burden further more.

Summing up the pMHCI-IgG molecule as well as the TCB antibody could protect mice from lung metastasis in a preventive setting and reduce metastasis burden in a therapeutic setting. Keeping in mind that B16 is a very aggressive growing and immune suppressive tumor a notable tumor growth inhibition could be induced by only two systemic treatments with the molecules. This could be proven by two different evaluation methods (counting of visible metastasis on the lung surface and quantitative PCR), whereby results correlated very well.

#### **9.4.2 Solid subcutaneous tumor model**

Donda et al., Lev et al. and Novak et al. were the first ones to treat already established subcutaneous tumors with peptide-MHCI-antibody conjugates [98, 99, 103].

Yoram Reiter's group performed xenograft models with human tumors and human CTL in Balb/C nude mice [99, 103]. Human tumor cell lines were injected subcutaneously into mice and after 4 to 7 days tumor volume reached 40 to 50 mm<sup>3</sup> and therapeutic treatment was started. Therefore effector molecules and CTL were injected intravenously with a time interval of about six hours. The injections were repeated three times every other day. With this experimental set up Lev et al. and Novak et al. could achieve marked tumor growth inhibition and tumor regression mediated by retargeting molecules, which lasted even ten days after the last treatment [99, 103].

A syngeneic model with endogenous T cell recruitment was performed by Donda et al. [98]. Also in this case ovalbumin was used as antigen for generation of specific effector cells. Mice were adoptively transferred with splenocytes derived from OT-1 mice, which have a transgenic T cell receptor that recognizes ovalbumin residues 257 to 264 ("SIINFEKL") in the context of H-2K<sup>b</sup>, and afterwards immunized by subcutaneous injection of ovalbumin emulsified in an adjuvant. This raised a CD8<sup>+</sup> T cell response of 12 to 40 % OVA<sub>257-264</sub>-specific CD8<sup>+</sup> T cells in the blood at the peak and about 15 % at the time point when tumor cells were grafted subcutaneously. Eight days after subcutaneous inoculation of CEA-transfected MC38 colon carcinoma cells, when all mice had palpable nodules, systemic treatment with effector molecules was started and continued until end of experiment with administration of retargeting conjugates every second day. In this experiment a significant tumor growth inhibition under continuous treatment with retargeting molecules could be achieved. However, the therapeutic effect showed only a temporary nature as ultimately tumors developed despite treatment with effector molecules.

In the present study a surrogate model with endogenous T cell recruitment was applied to scrutinize efficacy of pMHC-IgG retargeting molecules in a solid subcutaneous tumor. For generation of effector cells mice were immunized. As the OVA system is artificial, the immunodominant epitope m38 of the murine Cytomegalovirus was chosen as antigen for vaccination. For generation of a solid subcutaneous tumor FAP-transfected MC38 colorectal cancer cells were injected subcutaneously into mice. At start of treatment with the retargeting molecules mice had an average blood level of about 5 % MCMV m38-specific CD8<sup>+</sup> T cells (which equals the level of CMV pp65-specific CD8<sup>+</sup> T cells in chronically CMV-infected humans) and an average tumor volume of 97 mm<sup>3</sup>. Effector molecules were administered systemically five times at an interval of three days. Afterwards tumor volume was measured twice weekly. As a result no difference regarding tumor growth inhibition between treatment and control groups could be found. In the group treated with the pMHC-IgG three out of eight animals were tumor free and in the group treated with the TCB two out of eight animals had complete tumor regression, while tumor volumes of the other animals constantly increased. However, control groups treated with PBS or the pMHC-IgG molecule containing the control peptide MCMV IE3 showed same results with two out of eight tumor free animals and the rest of the tumors constantly growing. Tumor free mice in control groups are very likely caused by immune activation during vaccination as also observed in the experimental lung metastasis model and by others before [98, 105]. In this case especially administration of complexed IL-2 during vaccination seemed to be the main driver of unspecific

tumor regression. With the IL-2 being half-life extended by binding to a full IgG, effects lasted for about one week and were able to influence tumors in such a way that they completely disappear in some cases. Conversely, this also reveals that tumor free animals in the treatment groups may potentially not be induced by treatment with the pMHCI-IgG or the TCB, but by immune activation during immunization. In the time-to-event analysis tumor growth is slightly retarded by treatment with the pMHCI-IgG fusion molecule, but overall no significant tumor growth inhibition could be found in treatment groups. Tumor volume of the remaining tumor bearing mice in treatment groups constantly increased as in the control groups without delayed tumor growth kinetics.

This exhibits a certain resemblance to the findings made by Donda et al., where a significant tumor growth inhibition could be achieved in the retargeting conjugate treatment group compared to the control group, but finally MC38 tumors also grew despite continuous systemic treatment with retargeting conjugates every second day [98]. Compared to the present study minor barriers had to be broken down as treatment interval was closer and sustained until end of experiment and at start of treatment blood levels of specific CD8<sup>+</sup> T cells were higher and volume of tumors was smaller. In the xenograft models performed by Lev et al. and Novak et al. significant tumor growth inhibition and tumor regression could be achieved with only three systemic injections of retargeting molecules [99, 103]. However, effector cells were not recruited endogenously, but injected systemically within a short time period after every administration of effector molecules. This provides a higher amount of specific CD8<sup>+</sup> T cells available for retargeting after treatment and simplifies preconditions for effective tumor growth inhibition mediated by retargeting molecules. In addition tumor volume at start of treatment was only half as large as in the present efficacy study. Considered in this context hurdles in the present experiment were quite high.

Causes for missing tumor growth inhibition mediated by pMHCI-IgG fusion molecules can be due to a multifold of factors. One prerequisite for successful treatment of tumors with targeted effector molecules is the maintenance of stable target expression of tumor cells in vivo. Recombinant cells are usually kept under selection pressure to force expression of the transgene (e.g. antibiotics). In the absence of the selection pressure in vivo and the new cellular environment, engineered cells may quickly adapt and lose the expression of the transgene. This may lead to loss of transgene expression in some tumor cells, which generate subpopulations of cells that do no longer express the target protein. Elimination of those tumor cells mediated by effector molecules is not possible as fusion proteins are not able to bind to the tumor cell surface. As shown in chapter 8.4.2.2 target

expression of tumor cells was still maintained independent from treatment after several weeks of tumor growth in vivo. Consequently loss of target expression in the solid tumor can be excluded as reason for missing tumor growth inhibition mediated by pMHCI-IgG fusion molecules.

Donda et al. mentioned poor vascularization causing low penetration of effector molecules into the tumor and dropping blood levels of specific CD8<sup>+</sup> T cells at later time points as reasons for reduced efficacy of effector molecules [98]. Different to the MC38 tumors applied by Donda et al. the MC38 tumors used in the present study showed good vascularization and moderate molecule penetration as shown in chapter 8.4.2.3. The highest amount of the labelled fusion protein could be found near the vessels and with rising distance to vessels quantity of the molecule in the tumor tissue decreased. Consequently distribution of the fusion molecule in the tumor was not even, but rather patchy. Also binding of pMHCI-IgG molecules to tumor cells could be proved. Clearance of the protein from the tumor started quite early with obvious reduction of molecule amount after 24 hours and clearance of the bulk after 48 hours. Overall, ultramicroscopy analysis showed that tumors were well vascularized and that fusion molecules were able to penetrate into the tumor tissue and bind to their target on the tumor cells. Even though distribution pattern was spotty, fusion proteins covered widespread areas of the tumor, which should have been at least sufficient for induction of stasis of tumor growth. As the bulk of the molecule is cleared from the tumor after 48 hours, the treatment interval with systemic injections only every third day might have been a bit too infrequent. Shortening of the treatment interval to molecule administrations every second day might improve constant penetration of the tumor with effector molecules. In summary the penetration profile of the pMHCI-IgGs is not optimal and leaves room for improvement, but indeed shows widespread molecule distribution in the tumor, so that this issue should not be the reason for missing tumor growth inhibition in solid tumors under pMHCI-IgG treatment.

Decrease of specific CD8<sup>+</sup> T cell levels in the blood at later time points as mentioned by Donda et al. [98] could also be observed in the present study. Looking at the vaccination experiments in chapter 8.3.3 the peak of the MCMV m38-specific CD8<sup>+</sup> T cell response after the XCR1-targeted vaccination was on day nine after start of vaccination. Afterwards levels of specific CD8<sup>+</sup> T cells slowly decreased until day 25 and then started to drop more significantly. In the present study animals were treated five times at an interval of three days with treatment starting on day ten after start of vaccination (see figure 8.13 and table 8.2). Thus all treatments fell into the time frame of the CD8<sup>+</sup> T cell peak or in the phase of only slowly dropping CD8<sup>+</sup> T cell levels. In this sense MCMV m38-specific

CD8<sup>+</sup> T cells should have been available as effector cells at every time point of treatment with fusion molecules. Still no tumor growth inhibition could be observed, as tumors in the treatment groups started to grow as fast as tumors in the control groups. This is different to Donda et al., where tumor growth could be delayed at the beginning of treatment and only at later time points, when blood levels of specific CD8<sup>+</sup> T cells dropped, no more tumor growth inhibition could be induced with retargeting molecules [98].

Another aspect is the infiltration of tumors with CD8<sup>+</sup> T cells. If effector cells found in the blood are not able to infiltrate the tumor, no tumor cell elimination mediated by pMHCI-IgG fusions is possible. As shown in chapter 8.4.2.4 CD8<sup>+</sup> T cells could be found in the tumor during treatment. Compared to tumors of not-vaccinated animals tumors of vaccinated mice showed marked higher infiltrations of CD8<sup>+</sup> T cells. Assuming that the portion of MCMV m38-specific CD8<sup>+</sup> T cells out of all CD8<sup>+</sup> T cells in the blood is transferrable to the portion of MCMV m38-specific CD8<sup>+</sup> T cells in the tumor, effector cells for recruitment and activation by pMHCI-IgG molecules should have been available in the tumor during treatment.

With flow cytometry analyses the phenotype of CD8<sup>+</sup> T cells present in the tumor was analyzed (see chapter 8.4.2.5). CD44 is a cell surface protein, which participates in cell-cell interaction, cell adhesion and cell migration. It has several functions such as lymphocyte activation, recirculation and homing. Expression of CD44 is an indicative marker for effector and memory T cells [NCBI Gene ID: 12505 and 960]. CD62L, also known as L-selectin, is a cell adhesion molecule, which is found on naïve or memory T lymphocytes. As homing factor it facilitates entry of T cells into secondary lymphoid organs by binding to ligands on endothelial cells and thus slowing lymphocyte trafficking through the blood [NCBI Gene ID: 20343] [168]. CD127, also known as Interleukin-7 receptor subunit alpha (IL7R- $\alpha$ ), is involved in development and activation of T lymphocytes [NCBI Gene ID: 16197]. MCMV m38-specific CD8<sup>+</sup> T cells as well as unspecific CD8<sup>+</sup> T cells in the tumor could be characterized as effector cells (CD44<sup>+</sup>/CD62L<sup>-</sup>/CD127<sup>+</sup>). Regardless of whether they were MCMV m38-specific or unspecific, CD8<sup>+</sup> T cells seemed to get a little bit more activated and stimulated to home into the tumor by treatment with pMHCI-IgG molecules or TCB antibody, as they were expressing slightly more CD44 upon treatment. The phenotype of MCMV m38-specific CD8<sup>+</sup> T cells (effector cells: CD44<sup>+</sup>/CD62L<sup>-</sup>/CD127<sup>+</sup>) was mostly independent from treatment and localization (tumor or blood) and therefore mainly caused by vaccination. In this respect, activated

effector cells were present in the tumor during treatment and should have the competence to eliminate tumor cells.

CD8<sup>+</sup> T cells were also checked for expression of PD-1, a marker for activation, but also exhaustion of T cells. PD-1 or CD279 is a cell surface receptor, which is expressed on T and pro-B cells and functions as negative regulator in the immune system [NCBI Gene ID: 18566]. It binds to the ligands PD-L1 (CD274: [NCBI Gene ID: 60533]) and PD-L2. PD-L1 is upregulated on T and B cells upon T or B cell receptor signaling. Interaction of receptor and ligand down regulates activation of T cells, enhances apoptosis of antigen specific T cells and reduces apoptosis of regulatory T cells. As a consequence the mechanism promotes self-tolerance and reduces autoimmunity [169]. PD-1 expression could be found on MCMV m38-specific and unspecific CD8<sup>+</sup> T cells in the tumor. In the blood MCMV m38-specific CD8<sup>+</sup> T cells, but not unspecific CD8<sup>+</sup> T cells showed PD-1 upregulation. As MCMV m38-specific CD8<sup>+</sup> T cells both in the tumor and in the blood expressed PD-1, activation of specific CD8<sup>+</sup> T cells is mainly caused by vaccination. With pMHC1-IgG or TCB treatment PD-1 expression on MCMV m38-specific CD8<sup>+</sup> T cells in the tumor was even slightly higher indicating that treatment with effector molecules additionally activates specific CD8<sup>+</sup> T cells. However, PD-1 upregulation on CTL also leads to suppression of those cells upon interaction with the ligand PD-L1 as described above [57, 59, 72, 170, 171]. PD-L1 expression on APCs or normal tissue cells is caused by IFN- $\gamma$  release of activated CD8<sup>+</sup> T cells [58, 59, 72, 172-174]. Also in a vast amount of tumors PD-L1 is upregulated [57-59], especially when CD8<sup>+</sup> T cells producing IFN- $\gamma$  are infiltrating the tumor. In this way tumors escape surveillance of the immune system and prevent being eliminated by tumor infiltrating CTL [57-59]. In the MC38 tumor model used in this study PD-L1 expression on tumor cells could be detected by flow cytometry analysis (see chapter 8.4.2.6). In pMHC1-IgG and TCB treatment groups PD-L1 expression was considerable higher than in vehicle groups indicating that PD-L1 upregulation on tumor cells took place in response to IFN- $\gamma$  release of CD8<sup>+</sup> T cells activated by treatment. These findings demonstrate that missing tumor growth inhibition under pMHC1-IgG or TCB treatment could be due to inactivation and suppression of effector cells via the PD-1 / PD-L1 axis.

Additionally regulatory T cells could be found in the tumor (see chapter 8.4.2.5). FoxP3 is a specific marker for natural, adaptive and induced T<sub>reg</sub> cells. It is an intracellular protein, which functions as transcriptional regulator in cell nuclei, and plays a critical role in development and function of T<sub>reg</sub> cells [NCBI Gene ID: 20371]. CD25 is the alpha chain of the IL-2 receptor and a less specific

marker for  $T_{reg}$  cells. It is expressed on activated T lymphocytes and constitutively on  $T_{reg}$  cells [NCBI Gene ID: 16184]. In the physiological immune response  $T_{reg}$  cells prevent an overreaction of the immune system by downregulation of effector T cells. IL-2 released by activated effector T cells induces generation and maintenance of  $T_{reg}$  cells, which thereupon secrete IL-10 and other suppressive cytokines [48, 175-180]. Hence regulatory T cells play a crucial role in control of autoimmunity. Infiltrations of  $T_{reg}$  cells in the tumor cause in this case an unwanted, suppressive influence on  $CD8^+$  T cells, which leads to inactivation and loss of effector function of those cells. As complexed IL-2 was administered several times during vaccination in this experiment, it is not surprising that  $T_{reg}$  cells could be found in the tumor.

In summary lack of tumor growth inhibition under pMHC-IgG treatment in solid tumors is probably caused by inactivation of effector cells due to suppressive influences. Basic preconditions, like penetration of molecules and effector cells into the tumor and binding of effector molecules to the target on the tumor cell surface, were met, but effector function of  $CD8^+$  T cells seemed to be compromised. Inactivation of  $CD8^+$  T cells by PD-1 / PD-L1 interactions with tumor cells and by suppressive influences on the basis of  $T_{reg}$  cells probably led to loss of effector function of  $CD8^+$  T cells and thus to lack of tumor growth inhibition.

To overcome these issues a combination therapy with a PD-1 or PD-L1 blocking antibody could be applied. The PD-1 pathway would be interrupted and  $CD8^+$  T cells would no longer be impaired in their effector function [58, 72, 173]. Several antibodies blocking the PD-1 / PD-L1 axis are successful on the market or applied in clinical trials and revealed promising results in melanoma, RCC, NSCLC, colorectal cancer, bladder cancer or Hodgkin's lymphoma [72-79].

To remove suppressive influence on  $CD8^+$  T cells caused by  $T_{reg}$  cells in the mouse model,  $T_{reg}$  cells could be depleted by administration of diphtheria toxin [181, 182] or a  $T_{reg}$  depleting antibody directed against CD25 [183-188]. In patients this approach has to be handled with care as  $T_{reg}$  cells play a crucial role in the control of autoimmunity. However, in some clinical trials depletion of regulatory T cells was accomplished with low-dose cyclophosphamide [189] or docetaxel-based [190] chemotherapy, with an anti-human CCR4 (C-C chemokine receptor type 4) monoclonal antibody [191] or with a recombinant IL-2 diphtheria toxin conjugate [192] showing good tolerability regarding autoimmune responses and an improved outcome in relation to progression of disease.

As mentioned above IL-2 administration during vaccination is most certainly also involved in  $T_{reg}$  infiltration of tumors. Reduction of IL-2 dosing, in a way that specific  $CD8^+$  T cell level is still viable, would probably also contribute to reduction of  $T_{reg}$  cells in the tumor. With this approach unspecific tumor regression as observed in control groups of the study might also be avoided.

Murine models applying  $T_{reg}$  depletion combined with immune checkpoint inhibition were performed before. Combination of  $T_{reg}$  depletion accomplished with an anti-mouse CD25 antibody and CTLA-4 blockage could significantly increase survival in mice bearing B16 tumors [185].  $T_{reg}$  depletion by administration of diphtheria toxin in combination with a PD-L1 blocking and a Tim-3 (T-cell immunoglobulin and mucin-domain containing-3) blocking antibody led to increased virus-specific  $CD8^+$  T cell levels in mice chronically infected with FV (Friend virus) [181].

For successful treatment of solid tumors with pMHCI-IgG or TCB molecules the basic requirement of availability of functional effector  $CD8^+$  T cells has to be met. This might be accomplished with a combination of reduction of IL-2 dosing during vaccination, PD-1 or PD-L1 blockage and  $T_{reg}$  depletion.

## **9.5 COMPARISON OF PEPTIDE-MHC CLASS I-ANTIBODY FUSION MOLECULES WITH CD3-BASED T CELL ENGAGERS**

One main aspect of the study was to compare the anti-tumor efficacy of pMHCI-IgG fusion proteins with CD3-based T cell recruiters. At the moment two T cell engagers recruiting and activating T cells via CD3 have been approved. Catumaxomab is a TCB, that targets EpCAM for the treatment of malignant ascites [87, 88]. It comprises a rat/mouse hybrid monoclonal antibody with an active Fc-domain and is therefore highly immunogenic in humans and causes severe cytokine releases due to Fc $\gamma$ R binding upon systemic administration. Thus only local, peritoneal administration is approved [92]. Blinatumomab overcame those issues by removal of the Fc-part and linkage of the targeting domain with the anti-CD3 domain via a linker. It targets CD19 and is approved for treatment of refractory B-cell acute lymphocytic leukemia [89, 90]. However, lack of FcRn recycling and small size of the molecule lead to a fast drug clearance and require continuous infusion for several weeks. A novel IgG-based TCB, which targets CEA-expressing solid tumors, is currently in phase I clinical trials [91]. It exhibits a similar structure (2+1 format) as the surrogate TCB used in the present study with a full human IgG comprising an engineered Fc-region to abolish Fc $\gamma$ R and

C1q binding (see chapter 8.1.1.4). Therefore it augurs a favourable pharmacokinetic and safety profile compared to earlier TCB formats.

In the present study the TCB as well as the pMHCI-IgG showed comparable outcomes. Both formats could protect mice from lung metastasis in a preventive treatment setting and could reduce metastasis burden in a therapeutic treatment setting (see chapter 8.4.1). However, both molecules lacked mediation of tumor growth inhibition in the solid subcutaneous tumor model probably due to suppression of effector cells (see chapter 8.4.2). By contrast others showed efficacious tumor regression mediated by the human CEA-targeting TCB format in a xenograft mouse model with intraperitoneal transfer of PBMCs [91]. King et al. also compared the in vivo anti-tumor efficacy of pan-T cell recruiters with pMHCI retargeting molecules in a surrogate lymphoma model with endogenous T cell recruitment, whereby all molecules were Fab'-based. It was observed that the CD3-based T cell recruiter and the pMHCI retargeting molecule mediated the same increase of survival, when containing one tumor targeting domain. The pMHCI retargeting molecule comprising two tumor targeting moieties showed even a better outcome [105]. In in vitro assays of the present study the TCB showed a better activation of effector cells and a more rapid and effective target cell killing than the pMHCI-IgG (see chapters 8.2.2 and 8.2.3).

Comparing CD3-based T cell recruiters with pMHCI-IgG fusions several limitations and advantages emerge for each format. For the use of pMHCI-IgG molecules in patients a construct comprising the immunodominant peptide pp65 derived from the human Cytomegalovirus (CMV) would be applied [1, 2, 151]. Chronic CMV infection exists in the large majority of humans [193, 194] and CMV-specific CD8<sup>+</sup> T cells seem to be unique in number and functionality compared with other viral infections [195]. Their phenotype is mostly characterized as effector memory T cells implicating the capability to get rapidly activated and mediate cytotoxicity. A costimulatory signal via interaction of CD28 on effector cells with CD80/86 on tumor cells is not needed, because memory T cells can get activated directly by TCR / peptide-MHC complex interactions without a costimulatory signal via CD28 [196]. Thus redirection of this naturally occurring, highly effective and continuously resupplied subpopulation of CD8<sup>+</sup> T cells [197] for elimination of tumor cells is expected to be very efficacious [1, 2, 151]. Schmittnaegel et al. performed cytotoxicity assays with PBMCs derived from CMV<sup>+</sup> donors and compared human pMHCI-IgG fusion molecules with BiTEs. The CD3-based molecules activated T cells irrespective of their subtype and specificity and induced very rapid killing of target cells even at very low concentrations, whereas pMHCI-IgG fusions mediated a more graded and

more slowly elimination of tumor cells in a concentration-dependent manner. In this study almost identical results could be observed in the in vitro assays with surrogate pMHCI-IgG and TCB molecules (see chapter 8.2.3). The later onset and concentration dependence of target cell killing applying pMHCI-IgG fusions is likely due to the lower number of effector cells activated initially and could pose an advantage as side effects like cytokine release or tumor lysis syndrome could become more manageable [2]. Another aspect, that would broaden the safety window, is the relatively low affinity of TCRs for their cognate pMHC complexes [198]. Peripheral binding to T cells in the circulation is reduced and preferential binding of the molecule to the tumor cell target via avidity is facilitated. Thus no unspecific T cell activation in the absence of simultaneous binding to the tumor cell target in the periphery is expected even at high molecule concentrations [2, 151]. In the human CEA-targeting TCB this issue is addressed by introduction of only one CD3 targeting domain with low affinity [91]. Conclusively, a better safety profile for pMHCI-IgG molecules is expected, as nonspecific cytokine release due to polyclonal T cell activation as observed with CD3-based T cell recruiters is reduced as shown in vitro [2] and in vivo [105]. In addition pMHCI-IgG molecules should not be able to activate CD4<sup>+</sup> T cells, especially regulatory T cells, which is another advantage compared to TCBs. The limiting factor of pMHCI-IgG fusion proteins for the use in patients is the restriction to a specific patient population. One precondition for successful treatment with pMHCI-IgGs is the prior exposure to CMV infection [2]. As the majority of the human population is CMV-positive and prevalence of CMV infection increases with age [193, 194] this should not represent a substantial hurdle. The other, more limiting, prerequisite for application of pMHCI-IgG fusions is the physiological occurrence of a certain HLA-allotype in patients. The immunodominant peptide pp65 derived from CMV is presented on HLA A\*0201, which can be found in 35 % to 40 % of patients [199]. In summary, pMHCI-IgG fusion molecules seem to constitute a good and feasible alternative to CD3-based T cell recruiters in patients with high risks of side effects and in tumor types expressing low levels of antigen.

## 10 REFERENCES

1. Schmittnaegel, M., et al., *A new class of bifunctional major histocompatibility class I antibody fusion molecules to redirect CD8 T cells*. Mol Cancer Ther, 2016.
2. Schmittnaegel, M., et al., *Committing Cytomegalovirus-Specific CD8 T Cells to Eliminate Tumor Cells by Bifunctional Major Histocompatibility Class I Antibody Fusion Molecules*. Cancer Immunol Res, 2015. **3**(7): p. 764-76.
3. Hanahan, D. and R.A. Weinberg, *Hallmarks of cancer: the next generation*. Cell, 2011. **144**(5): p. 646-74.
4. Witsch, E., M. Sela, and Y. Yarden, *Roles for growth factors in cancer progression*. Physiology (Bethesda), 2010. **25**(2): p. 85-101.
5. Cheng, N., et al., *Transforming growth factor-beta signaling-deficient fibroblasts enhance hepatocyte growth factor signaling in mammary carcinoma cells to promote scattering and invasion*. Mol Cancer Res, 2008. **6**(10): p. 1521-33.
6. Amit, I., et al., *A module of negative feedback regulators defines growth factor signaling*. Nat Genet, 2007. **39**(4): p. 503-12.
7. Deshpande, A., P. Sicinski, and P.W. Hinds, *Cyclins and cdks in development and cancer: a perspective*. Oncogene, 2005. **24**(17): p. 2909-15.
8. Lowe, S.W., E. Cepero, and G. Evan, *Intrinsic tumour suppression*. Nature, 2004. **432**(7015): p. 307-15.
9. Fridman, J.S. and S.W. Lowe, *Control of apoptosis by p53*. Oncogene, 2003. **22**(56): p. 9030-40.
10. Grivennikov, S.I., F.R. Greten, and M. Karin, *Immunity, inflammation, and cancer*. Cell, 2010. **140**(6): p. 883-99.
11. Blasco, M.A., *Telomeres and human disease: ageing, cancer and beyond*. Nat Rev Genet, 2005. **6**(8): p. 611-22.
12. Negrini, S., V.G. Gorgoulis, and T.D. Halazonetis, *Genomic instability--an evolving hallmark of cancer*. Nat Rev Mol Cell Biol, 2010. **11**(3): p. 220-8.
13. Hanahan, D. and J. Folkman, *Patterns and emerging mechanisms of the angiogenic switch during tumorigenesis*. Cell, 1996. **86**(3): p. 353-64.
14. Nagy, J.A., et al., *Heterogeneity of the tumor vasculature*. Semin Thromb Hemost, 2010. **36**(3): p. 321-31.
15. Talmadge, J.E. and I.J. Fidler, *AACR centennial series: the biology of cancer metastasis: historical perspective*. Cancer Res, 2010. **70**(14): p. 5649-69.
16. Lu, Z., et al., *The tumor suppressor gene ARHI regulates autophagy and tumor dormancy in human ovarian cancer cells*. J Clin Invest, 2008. **118**(12): p. 3917-29.
17. Demicheli, R., et al., *The effects of surgery on tumor growth: a century of investigations*. Ann Oncol, 2008. **19**(11): p. 1821-8.
18. Barkan, D., J.E. Green, and A.F. Chambers, *Extracellular matrix: a gatekeeper in the transition from dormancy to metastatic growth*. Eur J Cancer, 2010. **46**(7): p. 1181-8.
19. Teng, M.W., et al., *Immune-mediated dormancy: an equilibrium with cancer*. J Leukoc Biol, 2008. **84**(4): p. 988-93.
20. Peinado, H., S. Lavotshkin, and D. Lyden, *The secreted factors responsible for pre-metastatic niche formation: old sayings and new thoughts*. Semin Cancer Biol, 2011. **21**(2): p. 139-46.
21. Kim, M.Y., et al., *Tumor self-seeding by circulating cancer cells*. Cell, 2009. **139**(7): p. 1315-26.

22. DeBerardinis, R.J., et al., *The biology of cancer: metabolic reprogramming fuels cell growth and proliferation*. Cell Metab, 2008. **7**(1): p. 11-20.
23. Vander Heiden, M.G., L.C. Cantley, and C.B. Thompson, *Understanding the Warburg effect: the metabolic requirements of cell proliferation*. Science, 2009. **324**(5930): p. 1029-33.
24. Kennedy, K.M. and M.W. Dewhirst, *Tumor metabolism of lactate: the influence and therapeutic potential for MCT and CD147 regulation*. Future Oncol, 2010. **6**(1): p. 127-48.
25. Egeblad, M., E.S. Nakasone, and Z. Werb, *Tumors as organs: complex tissues that interface with the entire organism*. Dev Cell, 2010. **18**(6): p. 884-901.
26. DeNardo, D.G., P. Andreu, and L.M. Coussens, *Interactions between lymphocytes and myeloid cells regulate pro- versus anti-tumor immunity*. Cancer Metastasis Rev, 2010. **29**(2): p. 309-16.
27. Khong, H.T. and N.P. Restifo, *Natural selection of tumor variants in the generation of "tumor escape" phenotypes*. Nat Immunol, 2002. **3**(11): p. 999-1005.
28. Murphy, K., P. Travers, and M. Walport, *Janeway's Immunobiology*. Seventh ed. 2008: Garland Science, Taylor & Francis Group, LLC.
29. Vukmanovic-Stejic, M., et al., *Human Tc1 and Tc2/Tc0 CD8 T-cell clones display distinct cell surface and functional phenotypes*. Blood, 2000. **95**(1): p. 231-40.
30. Marshall, N.B. and S.L. Swain, *Cytotoxic CD4 T cells in antiviral immunity*. J Biomed Biotechnol, 2011. **2011**: p. 954602.
31. Sallusto, F., et al., *Two subsets of memory T lymphocytes with distinct homing potentials and effector functions*. Nature, 1999. **401**(6754): p. 708-12.
32. Marelli-Berg, F.M., et al., *The highway code of T cell trafficking*. J Pathol, 2008. **214**(2): p. 179-89.
33. Lilleri, D., et al., *Human cytomegalovirus-specific memory CD8+ and CD4+ T cell differentiation after primary infection*. J Infect Dis, 2008. **198**(4): p. 536-43.
34. Dunn, G.P., L.J. Old, and R.D. Schreiber, *The immunobiology of cancer immunosurveillance and immunoediting*. Immunity, 2004. **21**(2): p. 137-48.
35. Finn, O.J., *Immuno-oncology: understanding the function and dysfunction of the immune system in cancer*. Ann Oncol, 2012. **23 Suppl 8**: p. viii6-9.
36. Mittal, D., et al., *New insights into cancer immunoediting and its three component phases--elimination, equilibrium and escape*. Curr Opin Immunol, 2014. **27**: p. 16-25.
37. Schreiber, R.D., L.J. Old, and M.J. Smyth, *Cancer immunoediting: integrating immunity's roles in cancer suppression and promotion*. Science, 2011. **331**(6024): p. 1565-70.
38. Dranoff, G., *Cytokines in cancer pathogenesis and cancer therapy*. Nat Rev Cancer, 2004. **4**(1): p. 11-22.
39. Koebel, C.M., et al., *Adaptive immunity maintains occult cancer in an equilibrium state*. Nature, 2007. **450**(7171): p. 903-7.
40. Algarra, I., T. Cabrera, and F. Garrido, *The HLA crossroad in tumor immunology*. Hum Immunol, 2000. **61**(1): p. 65-73.
41. Hicklin, D.J., F.M. Marincola, and S. Ferrone, *HLA class I antigen downregulation in human cancers: T-cell immunotherapy revives an old story*. Mol Med Today, 1999. **5**(4): p. 178-86.
42. Maeurer, M.J., et al., *Tumor escape from immune recognition: lethal recurrent melanoma in a patient associated with downregulation of the peptide transporter protein TAP-1 and loss of expression of the immunodominant MART-1/Melan-A antigen*. J Clin Invest, 1996. **98**(7): p. 1633-41.
43. Ogino, T., et al., *Association of tapasin and HLA class I antigen down-regulation in primary maxillary sinus squamous cell carcinoma lesions with reduced survival of patients*. Clin Cancer Res, 2003. **9**(11): p. 4043-51.

44. Algarra, I., A. Collado, and F. Garrido, *Altered MHC class I antigens in tumors*. Int J Clin Lab Res, 1997. **27**(2): p. 95-102.
45. Maeda, H. and A. Shiraiishi, *TGF-beta contributes to the shift toward Th2-type responses through direct and IL-10-mediated pathways in tumor-bearing mice*. J Immunol, 1996. **156**(1): p. 73-8.
46. Yang, L., Y. Pang, and H.L. Moses, *TGF-beta and immune cells: an important regulatory axis in the tumor microenvironment and progression*. Trends Immunol, 2010. **31**(6): p. 220-7.
47. Mougiakakos, D., et al., *Regulatory T cells in cancer*. Adv Cancer Res, 2010. **107**: p. 57-117.
48. Jung, Y.J. and J.Y. Seoh, *Feedback loop of immune regulation by CD4+CD25+ Treg*. Immunobiology, 2009. **214**(4): p. 291-302.
49. Curiel, T.J., et al., *Specific recruitment of regulatory T cells in ovarian carcinoma fosters immune privilege and predicts reduced survival*. Nat Med, 2004. **10**(9): p. 942-9.
50. Srivastava, M.K., et al., *Myeloid-derived suppressor cells inhibit T-cell activation by depleting cystine and cysteine*. Cancer Res, 2010. **70**(1): p. 68-77.
51. Ostrand-Rosenberg, S. and P. Sinha, *Myeloid-derived suppressor cells: linking inflammation and cancer*. J Immunol, 2009. **182**(8): p. 4499-506.
52. Comito, G., et al., *Cancer-associated fibroblasts and M2-polarized macrophages synergize during prostate carcinoma progression*. Oncogene, 2014. **33**(19): p. 2423-31.
53. Schwartz, R.H., *Costimulation of T lymphocytes: the role of CD28, CTLA-4, and B7/BB1 in interleukin-2 production and immunotherapy*. Cell, 1992. **71**(7): p. 1065-8.
54. Staveley-O'Carroll, K., et al., *Induction of antigen-specific T cell anergy: An early event in the course of tumor progression*. Proc Natl Acad Sci U S A, 1998. **95**(3): p. 1178-83.
55. Allison, J.P. and M.F. Krummel, *The Yin and Yang of T cell costimulation*. Science, 1995. **270**(5238): p. 932-3.
56. June, C.H., et al., *The B7 and CD28 receptor families*. Immunol Today, 1994. **15**(7): p. 321-31.
57. Abiko, K., et al., *PD-L1 on tumor cells is induced in ascites and promotes peritoneal dissemination of ovarian cancer through CTL dysfunction*. Clin Cancer Res, 2013. **19**(6): p. 1363-74.
58. Blank, C., et al., *PD-L1/B7H-1 inhibits the effector phase of tumor rejection by T cell receptor (TCR) transgenic CD8+ T cells*. Cancer Res, 2004. **64**(3): p. 1140-5.
59. Shi, F., et al., *PD-1 and PD-L1 upregulation promotes CD8(+) T-cell apoptosis and postoperative recurrence in hepatocellular carcinoma patients*. Int J Cancer, 2011. **128**(4): p. 887-96.
60. Motz, G.T., et al., *Tumor endothelium FasL establishes a selective immune barrier promoting tolerance in tumors*. Nat Med, 2014. **20**(6): p. 607-15.
61. Farkona, S., E.P. Diamandis, and I.M. Blasutig, *Cancer immunotherapy: the beginning of the end of cancer?* BMC Med, 2016. **14**: p. 73.
62. Kohrt, H.E., et al., *Immunodynamics: a cancer immunotherapy trials network review of immune monitoring in immuno-oncology clinical trials*. J Immunother Cancer, 2016. **4**: p. 15.
63. Neves, H. and H.F. Kwok, *Recent advances in the field of anti-cancer immunotherapy*. BBA Clin, 2015. **3**: p. 280-8.
64. Sharma, P., et al., *Novel cancer immunotherapy agents with survival benefit: recent successes and next steps*. Nat Rev Cancer, 2011. **11**(11): p. 805-12.
65. Fyfe, G., et al., *Results of treatment of 255 patients with metastatic renal cell carcinoma who received high-dose recombinant interleukin-2 therapy*. J Clin Oncol, 1995. **13**(3): p. 688-96.

66. Kirkwood, J.M., et al., *Interferon alfa-2b adjuvant therapy of high-risk resected cutaneous melanoma: the Eastern Cooperative Oncology Group Trial EST 1684*. J Clin Oncol, 1996. **14**(1): p. 7-17.
67. Yaddanapudi, K., R.A. Mitchell, and J.W. Eaton, *Cancer vaccines: Looking to the future*. Oncoimmunology, 2013. **2**(3): p. e23403.
68. Lowy, D.R. and J.T. Schiller, *Prophylactic human papillomavirus vaccines*. J Clin Invest, 2006. **116**(5): p. 1167-73.
69. Frazer, I.H., D.R. Lowy, and J.T. Schiller, *Prevention of cancer through immunization: Prospects and challenges for the 21st century*. Eur J Immunol, 2007. **37** Suppl 1: p. S148-55.
70. Scott, A.M., J.D. Wolchok, and L.J. Old, *Antibody therapy of cancer*. Nat Rev Cancer, 2012. **12**(4): p. 278-87.
71. Nimmerjahn, F. and J.V. Ravetch, *Fcgamma receptors as regulators of immune responses*. Nat Rev Immunol, 2008. **8**(1): p. 34-47.
72. Topalian, S.L., C.G. Drake, and D.M. Pardoll, *Targeting the PD-1/B7-H1(PD-L1) pathway to activate anti-tumor immunity*. Curr Opin Immunol, 2012. **24**(2): p. 207-12.
73. Lipson, E.J., et al., *Durable cancer regression off-treatment and effective reinduction therapy with an anti-PD-1 antibody*. Clin Cancer Res, 2013. **19**(2): p. 462-8.
74. Chen, R., et al., *Anti-Programmed Cell Death (PD)-1 Immunotherapy for Malignant Tumor: A Systematic Review and Meta-Analysis*. Transl Oncol, 2016. **9**(1): p. 32-40.
75. Marmarelis, M.E., et al., *Tumor control with PD-1 inhibition in a patient with concurrent metastatic melanoma and renal cell carcinoma*. J Immunother Cancer, 2016. **4**: p. 26.
76. Hamid, O., et al., *Safety and tumor responses with lambrolizumab (anti-PD-1) in melanoma*. N Engl J Med, 2013. **369**(2): p. 134-44.
77. Brahmer, J.R., et al., *Safety and activity of anti-PD-L1 antibody in patients with advanced cancer*. N Engl J Med, 2012. **366**(26): p. 2455-65.
78. Ansell, S.M., et al., *PD-1 blockade with nivolumab in relapsed or refractory Hodgkin's lymphoma*. N Engl J Med, 2015. **372**(4): p. 311-9.
79. Topalian, S.L., et al., *Safety, activity, and immune correlates of anti-PD-1 antibody in cancer*. N Engl J Med, 2012. **366**(26): p. 2443-54.
80. Hodi, F.S., et al., *Improved survival with ipilimumab in patients with metastatic melanoma*. N Engl J Med, 2010. **363**(8): p. 711-23.
81. Bartkowiak, T. and M.A. Curran, *4-1BB Agonists: Multi-Potent Potentiators of Tumor Immunity*. Front Oncol, 2015. **5**: p. 117.
82. Ascierto, P.A., et al., *Clinical experiences with anti-CD137 and anti-PD1 therapeutic antibodies*. Semin Oncol, 2010. **37**(5): p. 508-16.
83. Topalian, S.L., G.J. Weiner, and D.M. Pardoll, *Cancer immunotherapy comes of age*. J Clin Oncol, 2011. **29**(36): p. 4828-36.
84. Rosenberg, S.A., et al., *Durable complete responses in heavily pretreated patients with metastatic melanoma using T-cell transfer immunotherapy*. Clin Cancer Res, 2011. **17**(13): p. 4550-7.
85. Gross, G., T. Waks, and Z. Eshhar, *Expression of immunoglobulin-T-cell receptor chimeric molecules as functional receptors with antibody-type specificity*. Proc Natl Acad Sci U S A, 1989. **86**(24): p. 10024-8.
86. Hinrichs, C.S. and S.A. Rosenberg, *Exploiting the curative potential of adoptive T-cell therapy for cancer*. Immunol Rev, 2014. **257**(1): p. 56-71.
87. Ruf, P., et al., *Pharmacokinetics, immunogenicity and bioactivity of the therapeutic antibody catumaxomab intraperitoneally administered to cancer patients*. Br J Clin Pharmacol, 2010. **69**(6): p. 617-25.

88. Heiss, M.M., et al., *The trifunctional antibody catumaxomab for the treatment of malignant ascites due to epithelial cancer: Results of a prospective randomized phase II/III trial*. *Int J Cancer*, 2010. **127**(9): p. 2209-21.
89. Sanford, M., *Blinatumomab: first global approval*. *Drugs*, 2015. **75**(3): p. 321-7.
90. Bargou, R., et al., *Tumor regression in cancer patients by very low doses of a T cell-engaging antibody*. *Science*, 2008. **321**(5891): p. 974-7.
91. Bacac, M., et al., *A Novel Carcinoembryonic Antigen T-Cell Bispecific Antibody (CEA TCB) for the Treatment of Solid Tumors*. *Clin Cancer Res*, 2016. **22**(13): p. 3286-97.
92. Segal, D.M., G.J. Weiner, and L.M. Weiner, *Bispecific antibodies in cancer therapy*. *Curr Opin Immunol*, 1999. **11**(5): p. 558-62.
93. Ogg, G.S., et al., *Sensitization of tumour cells to lysis by virus-specific CTL using antibody-targeted MHC class I/peptide complexes*. *Br J Cancer*, 2000. **82**(5): p. 1058-62.
94. Robert, B., et al., *Antibody-conjugated MHC class I tetramers can target tumor cells for specific lysis by T lymphocytes*. *Eur J Immunol*, 2000. **30**(11): p. 3165-70.
95. Greten, T.F., et al., *Peptide-beta2-microglobulin-MHC fusion molecules bind antigen-specific T cells and can be used for multivalent MHC-Ig complexes*. *J Immunol Methods*, 2002. **271**(1-2): p. 125-35.
96. Lev, A., et al., *Recruitment of CTL activity by tumor-specific antibody-mediated targeting of single-chain class I MHC-peptide complexes*. *J Immunol*, 2002. **169**(6): p. 2988-96.
97. Savage, P., et al., *Anti-viral cytotoxic T cells inhibit the growth of cancer cells with antibody targeted HLA class I/peptide complexes in SCID mice*. *Int J Cancer*, 2002. **98**(4): p. 561-6.
98. Donda, A., et al., *In vivo targeting of an anti-tumor antibody coupled to antigenic MHC class I complexes induces specific growth inhibition and regression of established syngeneic tumor grafts*. *Cancer Immun*, 2003. **3**: p. 11.
99. Lev, A., et al., *Tumor-specific Ab-mediated targeting of MHC-peptide complexes induces regression of human tumor xenografts in vivo*. *Proc Natl Acad Sci U S A*, 2004. **101**(24): p. 9051-6.
100. Oved, K., et al., *Antibody-mediated targeting of human single-chain class I MHC with covalently linked peptides induces efficient killing of tumor cells by tumor or viral-specific cytotoxic T lymphocytes*. *Cancer immunology, immunotherapy : CII*, 2005. **54**(9): p. 867-79.
101. Cesson, V., et al., *Active antiviral T-lymphocyte response can be redirected against tumor cells by antitumor antibody x MHC/viral peptide conjugates*. *Clin Cancer Res*, 2006. **12**(24): p. 7422-30.
102. Mous, R., et al., *Redirection of CMV-specific CTL towards B-CLL via CD20-targeted HLA/CMV complexes*. *Leukemia*, 2006. **20**(6): p. 1096-102.
103. Novak, H., et al., *Selective antibody-mediated targeting of class I MHC to EGFR-expressing tumor cells induces potent antitumor CTL activity in vitro and in vivo*. *Int J Cancer*, 2007. **120**(2): p. 329-36.
104. Savage, P., et al., *Immunotherapy with antibody-targeted HLA class I complexes: results of in vivo tumour cell killing and therapeutic vaccination*. *Tumour Biol*, 2007. **28**(4): p. 205-11.
105. King, B.C., et al., *Antibody-peptide-MHC fusion conjugates target non-cognate T cells to kill tumour cells*. *Cancer immunology, immunotherapy : CII*, 2013. **62**(6): p. 1093-105.
106. Scheiermann, J. and D.M. Klinman, *Clinical evaluation of CpG oligonucleotides as adjuvants for vaccines targeting infectious diseases and cancer*. *Vaccine*, 2014. **32**(48): p. 6377-89.
107. Hartung, E., et al., *Induction of potent CD8 T cell cytotoxicity by specific targeting of antigen to cross-presenting dendritic cells in vivo via murine or human XCR1*. *J Immunol*, 2015. **194**(3): p. 1069-79.

108. Alexopoulou, L., et al., *Recognition of double-stranded RNA and activation of NF-kappaB by Toll-like receptor 3*. *Nature*, 2001. **413**(6857): p. 732-8.
109. Sorensen, M.R., et al., *Quantification of B16 melanoma cells in lungs using triplex Q-PCR--a new approach to evaluate melanoma cell metastasis and tumor control*. *PLoS One*, 2014. **9**(1): p. e87831.
110. Livak, K.J. and T.D. Schmittgen, *Analysis of relative gene expression data using real-time quantitative PCR and the 2(-Delta Delta C(T)) Method*. *Methods*, 2001. **25**(4): p. 402-8.
111. Dobosz, M., et al., *Multispectral Fluorescence Ultramicroscopy: Three-Dimensional Visualization and Automatic Quantification of Tumor Morphology, Drug Penetration, and Antiangiogenic Treatment Response*. *Neoplasia*, 2014. **16**(1): p. 1-W7.
112. Truscott, S.M., et al., *Disulfide bond engineering to trap peptides in the MHC class I binding groove*. *Journal of immunology*, 2007. **178**(10): p. 6280-9.
113. Ridgway, J.B., L.G. Presta, and P. Carter, *'Knobs-into-holes' engineering of antibody CH3 domains for heavy chain heterodimerization*. *Protein engineering*, 1996. **9**(7): p. 617-21.
114. Kabat, E.A., *Sequences of Proteins of Immunological Interest*. Vol. 5th Ed. Public Health Service, National Institutes of Health. 1991: Bethesda.
115. Hezareh, M., et al., *Effector function activities of a panel of mutants of a broadly neutralizing antibody against human immunodeficiency virus type 1*. *J Virol*, 2001. **75**(24): p. 12161-8.
116. Laveran, P., et al., *Immuno-PET and Immuno-SPECT of Rheumatoid Arthritis with Radiolabeled Anti-Fibroblast Activation Protein Antibody Correlates with Severity of Arthritis*. *J Nucl Med*, 2015. **56**(5): p. 778-83.
117. Bacac, M., et al., *Anti-fap antibodies and methods of use*. 2016, Google Patents.
118. Tomlinson, I.M., et al., *The repertoire of human germline VH sequences reveals about fifty groups of VH segments with different hypervariable loops*. *J Mol Biol*, 1992. **227**(3): p. 776-98.
119. Schaefer, W., et al., *Immunoglobulin domain crossover as a generic approach for the production of bispecific IgG antibodies*. *Proc Natl Acad Sci U S A*, 2011. **108**(27): p. 11187-92.
120. Leo, O., et al., *Identification of a monoclonal antibody specific for a murine T3 polypeptide*. *Proc Natl Acad Sci U S A*, 1987. **84**(5): p. 1374-8.
121. Bachem, A., et al., *Expression of XCR1 Characterizes the Batf3-Dependent Lineage of Dendritic Cells Capable of Antigen Cross-Presentation*. *Front Immunol*, 2012. **3**: p. 214.
122. Kroczek, R., *Antibodies to the chemokine receptor xcr1*. 2013, Google Patents.
123. Blattman, J.N., et al., *Estimating the precursor frequency of naive antigen-specific CD8 T cells*. *J Exp Med*, 2002. **195**(5): p. 657-64.
124. Gourley, T.S., et al., *Generation and maintenance of immunological memory*. *Semin Immunol*, 2004. **16**(5): p. 323-33.
125. Badovinac, V.P., B.B. Porter, and J.T. Harty, *Programmed contraction of CD8(+) T cells after infection*. *Nat Immunol*, 2002. **3**(7): p. 619-26.
126. Prlic, M., G. Hernandez-Hoyos, and M.J. Bevan, *Duration of the initial TCR stimulus controls the magnitude but not functionality of the CD8+ T cell response*. *J Exp Med*, 2006. **203**(9): p. 2135-43.
127. Met, O., S. Buus, and M.H. Claesson, *Peptide-loaded dendritic cells prime and activate MHC-class I-restricted T cells more efficiently than protein-loaded cross-presenting DC*. *Cell Immunol*, 2003. **222**(2): p. 126-33.
128. Janssen, E.M., et al., *CD4+ T-cell help controls CD8+ T-cell memory via TRAIL-mediated activation-induced cell death*. *Nature*, 2005. **434**(7029): p. 88-93.

129. Huck, S.P., et al., *Activation and route of administration both determine the ability of bone marrow-derived dendritic cells to accumulate in secondary lymphoid organs and prime CD8+ T cells against tumors*. *Cancer Immunol Immunother*, 2008. **57**(1): p. 63-71.
130. Andre, F., et al., *Exosomes as potent cell-free peptide-based vaccine. I. Dendritic cell-derived exosomes transfer functional MHC class I/peptide complexes to dendritic cells*. *J Immunol*, 2004. **172**(4): p. 2126-36.
131. Hao, S., et al., *Mature dendritic cells pulsed with exosomes stimulate efficient cytotoxic T-lymphocyte responses and antitumor immunity*. *Immunology*, 2007. **120**(1): p. 90-102.
132. Sterzik, A., *Charakterisierung der Wirkung von Gemcitabin auf die Immuntherapie mittels dendritischer Zellen in einem autologen Pankreaskarzinommodell der Maus*. 2012, Ludwig-Maximilians-Universität München.
133. Sheasley-O'Neill, S.L., et al., *Dendritic cell immunization route determines integrin expression and lymphoid and nonlymphoid tissue distribution of CD8 T cells*. *J Immunol*, 2007. **178**(3): p. 1512-22.
134. Creusot, R.J., et al., *Lymphoid-tissue-specific homing of bone-marrow-derived dendritic cells*. *Blood*, 2009. **113**(26): p. 6638-47.
135. Okada, N., et al., *Administration route-dependent vaccine efficiency of murine dendritic cells pulsed with antigens*. *Br J Cancer*, 2001. **84**(11): p. 1564-70.
136. Mullins, D.W., et al., *Route of immunization with peptide-pulsed dendritic cells controls the distribution of memory and effector T cells in lymphoid tissues and determines the pattern of regional tumor control*. *J Exp Med*, 2003. **198**(7): p. 1023-34.
137. Aihara, H. and J. Miyazaki, *Gene transfer into muscle by electroporation in vivo*. *Nat Biotechnol*, 1998. **16**(9): p. 867-70.
138. Akbari, O., et al., *DNA vaccination: transfection and activation of dendritic cells as key events for immunity*. *J Exp Med*, 1999. **189**(1): p. 169-78.
139. Paster, W., et al., *In vivo plasmid DNA electroporation generates exceptionally high levels of epitope-specific CD8+ T-cell responses*. *Gene Ther*, 2003. **10**(9): p. 717-24.
140. Davis, H.L., R.G. Whalen, and B.A. Demeneix, *Direct gene transfer into skeletal muscle in vivo: factors affecting efficiency of transfer and stability of expression*. *Hum Gene Ther*, 1993. **4**(2): p. 151-9.
141. Raz, E., et al., *Intradermal gene immunization: the possible role of DNA uptake in the induction of cellular immunity to viruses*. *Proc Natl Acad Sci U S A*, 1994. **91**(20): p. 9519-23.
142. Condon, C., et al., *DNA-based immunization by in vivo transfection of dendritic cells*. *Nat Med*, 1996. **2**(10): p. 1122-8.
143. Kalat, M., et al., *In vivo plasmid electroporation induces tumor antigen-specific CD8+ T-cell responses and delays tumor growth in a syngeneic mouse melanoma model*. *Cancer Res*, 2002. **62**(19): p. 5489-94.
144. Bergman, P.J., et al., *Development of a xenogeneic DNA vaccine program for canine malignant melanoma at the Animal Medical Center*. *Vaccine*, 2006. **24**(21): p. 4582-5.
145. Seo, S.H., et al., *Optimal induction of HPV DNA vaccine-induced CD8+ T cell responses and therapeutic antitumor effect by antigen engineering and electroporation*. *Vaccine*, 2009. **27**(42): p. 5906-12.
146. Soong, R.S., et al., *Xenogeneic human p53 DNA vaccination by electroporation breaks immune tolerance to control murine tumors expressing mouse p53*. *PLoS One*, 2013. **8**(2): p. e56912.
147. Peng, S., et al., *Control of HPV-associated tumors by innovative therapeutic HPV DNA vaccine in the absence of CD4+ T cells*. *Cell Biosci*, 2014. **4**(1): p. 11.

148. Paster, W., et al., *Structural elements of a protein antigen determine immunogenicity of the embedded MHC class I-restricted T cell epitope*. J Immunol, 2002. **169**(6): p. 2937-46.
149. Schultz, J., et al., *A tetravalent single-chain antibody-streptavidin fusion protein for pretargeted lymphoma therapy*. Cancer Res, 2000. **60**(23): p. 6663-9.
150. Robert, B., et al., *Redirecting anti-viral CTL against cancer cells by surface targeting of monomeric MHC class I-viral peptide conjugated to antibody fragments*. Cancer Immun, 2001. **1**: p. 2.
151. Schmittnaegel, M., et al., *Activation of cytomegalovirus-specific CD8+ T-cell response by antibody-mediated peptide-major histocompatibility class I complexes*. Oncoimmunology, 2016. **5**(1): p. e1052930.
152. Yuan, F., et al., *Vascular permeability in a human tumor xenograft: molecular size dependence and cutoff size*. Cancer Res, 1995. **55**(17): p. 3752-6.
153. Zahnd, C., et al., *Efficient tumor targeting with high-affinity designed ankyrin repeat proteins: effects of affinity and molecular size*. Cancer Res, 2010. **70**(4): p. 1595-605.
154. Schmittnaegel, M., *Rekombinante Viruspeptid-MHCI-Antikörperfusionen zur Induktion von Tumorzelllyse durch Zytomegalievirus-spezifische, zytotoxische T-Zellen*. 2015, Friedrich-Alexander Universität Erlangen-Nürnberg.
155. Paganelli, G., et al., *The three-step pretargeting approach reduces the human anti-mouse antibody response in patients submitted to radioimmunoscintigraphy and radioimmunotherapy*. Eur J Nucl Med, 1997. **24**(3): p. 350-1.
156. Weiden, P.L., et al., *Pretargeted radioimmunotherapy (PRIT) for treatment of non-Hodgkin's lymphoma (NHL): initial phase I/II study results*. Cancer Biother Radiopharm, 2000. **15**(1): p. 15-29.
157. Lanzavecchia, A., G. Iezzi, and A. Viola, *From TCR engagement to T cell activation: a kinetic view of T cell behavior*. Cell, 1999. **96**(1): p. 1-4.
158. Bromley, S.K., et al., *The immunological synapse*. Annu Rev Immunol, 2001. **19**: p. 375-96.
159. Ge, Q., et al., *Soluble peptide-MHC monomers cause activation of CD8+ T cells through transfer of the peptide to T cell MHC molecules*. Proc Natl Acad Sci U S A, 2002. **99**(21): p. 13729-34.
160. Mottez, E., et al., *Cells expressing a major histocompatibility complex class I molecule with a single covalently bound peptide are highly immunogenic*. J Exp Med, 1995. **181**(2): p. 493-502.
161. White, J., et al., *Soluble class I MHC with beta2-microglobulin covalently linked peptides: specific binding to a T cell hybridoma*. J Immunol, 1999. **162**(5): p. 2671-6.
162. Wu, C., et al., *Simultaneous targeting of multiple disease mediators by a dual-variable-domain immunoglobulin*. Nature biotechnology, 2007. **25**(11): p. 1290-7.
163. Qin, H., et al., *Eradication of B-ALL using chimeric antigen receptor-expressing T cells targeting the TSLPR oncoprotein*. Blood, 2015. **126**(5): p. 629-39.
164. Rodgers, D.T., et al., *Switch-mediated activation and retargeting of CAR-T cells for B-cell malignancies*. Proc Natl Acad Sci U S A, 2016. **113**(4): p. E459-68.
165. Kammertoens, T. and T. Blankenstein, *It's the peptide-MHC affinity, stupid*. Cancer Cell, 2013. **23**(4): p. 429-31.
166. Glennie, M.J., et al., *Preparation and performance of bispecific F(ab' gamma)2 antibody containing thioether-linked Fab' gamma fragments*. J Immunol, 1987. **139**(7): p. 2367-75.
167. French, R.R., *How to make bispecific antibodies*. Methods Mol Med, 2000. **40**: p. 333-9.
168. Marchesi, V.T. and J.L. Gowans, *THE MIGRATION OF LYMPHOCYTES THROUGH THE ENDOTHELIUM OF VENULES IN LYMPH NODES: AN ELECTRON MICROSCOPE STUDY*. Proc R Soc Lond B Biol Sci, 1964. **159**: p. 283-90.

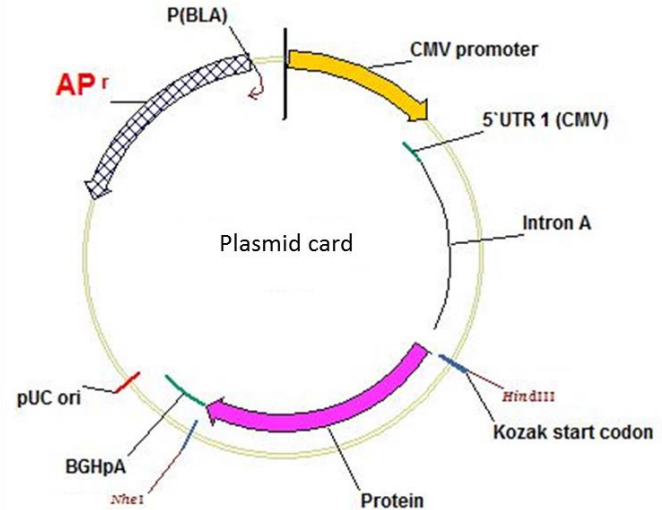
169. Keir, M.E., et al., *PD-1 and its ligands in tolerance and immunity*. *Annu Rev Immunol*, 2008. **26**: p. 677-704.
170. Freeman, G.J., et al., *Engagement of the PD-1 immunoinhibitory receptor by a novel B7 family member leads to negative regulation of lymphocyte activation*. *J Exp Med*, 2000. **192**(7): p. 1027-34.
171. Latchman, Y.E., et al., *PD-L1-deficient mice show that PD-L1 on T cells, antigen-presenting cells, and host tissues negatively regulates T cells*. *Proc Natl Acad Sci U S A*, 2004. **101**(29): p. 10691-6.
172. Spranger, S., et al., *Up-regulation of PD-L1, IDO, and T(regs) in the melanoma tumor microenvironment is driven by CD8(+) T cells*. *Sci Transl Med*, 2013. **5**(200): p. 200ra116.
173. Maekawa, N., et al., *Expression of PD-L1 on canine tumor cells and enhancement of IFN-gamma production from tumor-infiltrating cells by PD-L1 blockade*. *PLoS One*, 2014. **9**(6): p. e98415.
174. Abiko, K., et al., *IFN-gamma from lymphocytes induces PD-L1 expression and promotes progression of ovarian cancer*. *Br J Cancer*, 2015. **112**(9): p. 1501-9.
175. Thornton, A.M. and E.M. Shevach, *Suppressor effector function of CD4+CD25+ immunoregulatory T cells is antigen nonspecific*. *J Immunol*, 2000. **164**(1): p. 183-90.
176. Levings, M.K., R. Sangregorio, and M.G. Roncarolo, *Human cd25(+)/cd4(+) t regulatory cells suppress naive and memory T cell proliferation and can be expanded in vitro without loss of function*. *J Exp Med*, 2001. **193**(11): p. 1295-302.
177. Malek, T.R., et al., *CD4 regulatory T cells prevent lethal autoimmunity in IL-2Rbeta-deficient mice. Implications for the nonredundant function of IL-2*. *Immunity*, 2002. **17**(2): p. 167-78.
178. de la Rosa, M., et al., *Interleukin-2 is essential for CD4+CD25+ regulatory T cell function*. *Eur J Immunol*, 2004. **34**(9): p. 2480-8.
179. Malek, T.R. and A.L. Bayer, *Tolerance, not immunity, crucially depends on IL-2*. *Nat Rev Immunol*, 2004. **4**(9): p. 665-74.
180. Moon, B.I., T.H. Kim, and J.Y. Seoh, *Functional Modulation of Regulatory T Cells by IL-2*. *PLoS One*, 2015. **10**(11): p. e0141864.
181. Dietze, K.K., et al., *Combining regulatory T cell depletion and inhibitory receptor blockade improves reactivation of exhausted virus-specific CD8+ T cells and efficiently reduces chronic retroviral loads*. *PLoS Pathog*, 2013. **9**(12): p. e1003798.
182. Akeus, P., et al., *Treg-cell depletion promotes chemokine production and accumulation of CXCR3(+) conventional T cells in intestinal tumors*. *Eur J Immunol*, 2015. **45**(6): p. 1654-66.
183. Onizuka, S., et al., *Tumor rejection by in vivo administration of anti-CD25 (interleukin-2 receptor alpha) monoclonal antibody*. *Cancer Res*, 1999. **59**(13): p. 3128-33.
184. Shimizu, J., S. Yamazaki, and S. Sakaguchi, *Induction of tumor immunity by removing CD25+CD4+ T cells: a common basis between tumor immunity and autoimmunity*. *J Immunol*, 1999. **163**(10): p. 5211-8.
185. Suttmuller, R.P., et al., *Synergism of cytotoxic T lymphocyte-associated antigen 4 blockade and depletion of CD25(+) regulatory T cells in antitumor therapy reveals alternative pathways for suppression of autoreactive cytotoxic T lymphocyte responses*. *J Exp Med*, 2001. **194**(6): p. 823-32.
186. Tuve, S., et al., *Combination of tumor site-located CTL-associated antigen-4 blockade and systemic regulatory T-cell depletion induces tumor-destructive immune responses*. *Cancer Res*, 2007. **67**(12): p. 5929-39.
187. Setiady, Y.Y., J.A. Coccia, and P.U. Park, *In vivo depletion of CD4+FOXP3+ Treg cells by the PC61 anti-CD25 monoclonal antibody is mediated by Fc gammaRIII+ phagocytes*. *Eur J Immunol*, 2010. **40**(3): p. 780-6.

188. Jarry, U., et al., *Treg depletion followed by intracerebral CpG-ODN injection induce brain tumor rejection*. J Neuroimmunol, 2014. **267**(1-2): p. 35-42.
189. Cao, Y., et al., *CD4+FOXP3+ regulatory T cell depletion by low-dose cyclophosphamide prevents recurrence in patients with large condylomata acuminata after laser therapy*. Clin Immunol, 2010. **136**(1): p. 21-9.
190. Li, J.Y., et al., *Selective depletion of regulatory T cell subsets by docetaxel treatment in patients with nonsmall cell lung cancer*. J Immunol Res, 2014. **2014**: p. 286170.
191. Kurose, K., et al., *Phase Ia Study of FoxP3+ CD4 Treg Depletion by Infusion of a Humanized Anti-CCR4 Antibody, KW-0761, in Cancer Patients*. Clin Cancer Res, 2015. **21**(19): p. 4327-36.
192. Dannull, J., et al., *Enhancement of vaccine-mediated antitumor immunity in cancer patients after depletion of regulatory T cells*. J Clin Invest, 2005. **115**(12): p. 3623-33.
193. Dowd, J.B., A.E. Aiello, and D.E. Alley, *Socioeconomic disparities in the seroprevalence of cytomegalovirus infection in the US population: NHANES III*. Epidemiol Infect, 2009. **137**(1): p. 58-65.
194. Hecker, M., et al., *Continuous cytomegalovirus seroconversion in a large group of healthy blood donors*. Vox Sang, 2004. **86**(1): p. 41-4.
195. van Leeuwen, E.M., et al., *Human virus-specific CD8+ T cells: diversity specialists*. Immunol Rev, 2006. **211**: p. 225-35.
196. Flynn, K. and A. Mullbacher, *Memory alloreactive cytotoxic T cells do not require costimulation for activation in vitro*. Immunol Cell Biol, 1996. **74**(5): p. 413-20.
197. Snyder, C.M., *Buffered memory: a hypothesis for the maintenance of functional, virus-specific CD8(+) T cells during cytomegalovirus infection*. Immunologic research, 2011. **51**(2-3): p. 195-204.
198. Matsui, K., et al., *Low affinity interaction of peptide-MHC complexes with T cell receptors*. Science, 1991. **254**(5039): p. 1788-91.
199. Solberg, O.D., et al., *Balancing selection and heterogeneity across the classical human leukocyte antigen loci: a meta-analytic review of 497 population studies*. Human immunology, 2008. **69**(7): p. 443-64.

# 11 APPENDIX

## DNA vector for production of proteins and DNA vaccination:

- CMV (Cytomegalovirus) promoter
- 5' UTR 1 (CMV)
- Intron A
- Kozak start codon
- Endonucleolytic cleavage sites  
HindIII and NheI
- Protein, which should be expressed
- BGHpA (bovine growth hormone polyadenylation signal)
- pUC ori (origin of replication)
- AP<sup>r</sup> (ampicillin resistance)
- P(BLA) (beta-lactamase gene promoter)



## Amino acid sequences of engineered antibodies and fusion molecules:

(Mutations: EU-Index Kabat numbering scheme [114])

### • *Peptide-MHC class I-IgG fusion molecule:*

#### Peptide-MHC class I fused antibody heavy chain:

**Amino acid 1 to 19:** Signal peptide, **20 to 27:** Peptide (specified below), **28 to 42:** Linker 1 (G<sub>4</sub>S)<sub>3</sub> (disulfide-stabilization linker 1 / MHC class I complex: **29:** G10C), **43 to 141:** Murine β<sub>2</sub>M, **142 to 161:** Linker 2 (G<sub>4</sub>S)<sub>4</sub>, **162 to 435:** α1 – α3 H-2K<sup>b</sup> (disulfide-stabilization linker 1 / MHC class I complex: **245:** Y84C), **436 to 437:** Linker 3 (GS), **438 to 553:** Variable domain of the heavy chain of the murine FAP binder (VH), **559 to 651:** CH1 IgG2c, **675 to 778:** CH2 IgG2c (silent Fc-part: LALA mutation: **675:** L234A / **676:** L235A, DAPG mutation: **711:** D270A / **770:** P329G), **787 to 883:** CH3 IgG2c (disulfide-stabilization pMHC I-HC / HC: **790:** Y349C, hole-mutation: **807:** T366S / **809:** M368A / **848:** Y407V)

```

1   MGWSCIILFL VATATGVHSX XXXXXXXXGCG GSGGGGSGGG GSIQKTPQIQ
51  VYSRHPPENG KPNILNCYVT QFHPPHIEIQ MLKNGKKIPK VEMSDMSFSK
101 DWSFYILAHT EFTPTETDTY ACRVKHASMA EPKTVYWDRD MGGGGSGGGG
151 SGGGGSGGGG SGPHSLRYFV TAVSRPGLGE PRYMEVGYVD DTEFVRFDSG
201 AENPRYEPRA RWMEQEGPEY WERETQKAKG NEQSFRVDLR TLLGCYNQSK
251 GGSHTIQVIS GCEVGS DGR LRGYQQYAYD GCDYIALNED LKTWTAADMA
301 ALITKHKWEQ AGEAERLRAY LEGTCVEWLR RYLKNGNATL LRTDSPKAHV
351 THHSRPEDKV TLRCWALGFY PADITLTWQL NGEELIQDME LVETRPAGDG

```

401 TFQKWASVVV PLGKEQYYTC HVYHQGLPEP LTLRWGSEVQ LLESGGGLVQ  
 451 PGGSLRLSCA ASGFTFSSHA MSWVRQAPGK GLEWVSAIWA SGEQYYADSV  
 501 KGRFTISRDN SKNTLYLQMN SLRAEDTAVY YCAKGWLGNF DYWGQGTLVT  
 551 VSSAKTTAPS VYPLAPVCGG TTGSSVTLGC LVKGYFPEPV TLTWNSGSL  
 601 SGVHTFPALL QSGLYTLSSS VTVTSNTWPS QTITCNVAHP ASSTKVDDKI  
 651 EPRVPITQNP CPPLKECPPC AAPDAAGGPS VFIFPPKIKD VLMISLSPMV  
 701 TCVVVDVSED APDVQISWFV NNVEVHTAQT QTHREDYNST LRVVSALPIQ  
 751 HQDWMSGKEF KCKVNNRALG SPIEKTISKP RGPVVRAPQVC VLPPPAEEMT  
 801 KKEFSLSCAI TGFLPAEIAV DWTSNGRTEQ NYKNTATVLD SDGSYFMVSK  
 851 LRVQKSTWER GSLFACSVVH EGLHNHLTTK TISRSLGK

**MCMV m38 peptide:**

1 SSPPMFRV

**MCMV IE3 peptide:**

1 RALEYKNL

**OVA<sub>257-264</sub> peptide:**

1 SIINFEKL

**Unfused antibody heavy chain:**

**Amino acid 1 to 19:** Signal peptide, **20 to 135:** Variable domain of the heavy chain of the murine FAP binder (VH), **141 to 233:** CH1 IgG2c, **257 to 360:** CH2 IgG2c (silent Fc-part: LALA mutation: **257:** L234A / **258:** L235A, DAPG mutation: **293:** D270A / **352:** P329G), **369 to 465:** CH3 IgG2c (disulfide-stabilization pMHCI-HC / HC: **377:** P354C, knob-mutation: **389:** T366W, HL->RF mutation: **458:** H435R / **459:** L436F)

1 MGWSCIILFL VATATGVHSE VQLLESGGGL VQPGGSLRLS CAASGFTFSS  
 51 HAMS WVRQAP GKGLEWVSAI WASGEQYYAD SVKGRFTISR DNSKNTLYLQ  
 101 MNSLRAEDTA VYYCAKGWLG NFDYWGQGT LVTVSSAKTTA PSVYPLAPVC  
 151 GGTGSSVTL GCLVKGYFPE PVTTLWNSGS LSSGVHTFPA LLQSGLYTSL  
 201 SSVTVTSNTW PSQTITCNVA HPASSTKVDD KIEPRVPITQ NPCPPLKECP  
 251 PCAAPDAAGG PSVFIFPPKI KDVL M ISLSP MVTCVVVDVS EDAPDVQISW  
 301 FVNNVEVHTA QTQTHREDYN STLRVVSALP IQHQDWMSGK EFKCKVNNRA  
 351 LGSPIEKTIS KPRGPVVRAPQ VYVLPPCAEE MTKKEFSLWC MITGFLPAEI  
 401 AVDWTSNGRT EQNYKNTATV LDSDGSYFMY SKLRVQKSTW ERGSLFACSV  
 451 VHEGLHNRFT TKTISRSLGK

**Antibody light chain:**

**Amino acid 1 to 19:** Signal peptide, **20 to 127:** Variable domain of the light chain of the murine FAP binder (VL), **131 to 230:** Constant domain of the light chain (C $\kappa$ )

```

1   MGWSCIILFL VATATGVHSE IVLTQSPGTL SLSPGERATL SCRASQSVSR
51  SYLAWYQQKP GQAPRLLIIG ASTRATGIPD RFSGSGSGTD FTLTISRLEP
101 EDFAVYYCQQ GQVIPPTFGQ GTKVEIKRAD APTVSIFPP SSEQLTSGGA
151 SVVCFLLNFY PKDINVKWKI DGSRQNGVL NSWTDQDSKD STYSMSSTLT
201 LTKDEYERHN SYTCEATHKT STSPIVKSFN RNEC

```

**Non-binding control antibody (DP47):****Variable domain of the heavy chain (VH):**

```

1   EVQLLESGGG LVQPGGSLRL SCAASGFTFS SYAMSWVRQA PGKGLEWVSA
51  ISGSGGSTYY ADSVKGRFTI SRDNSKNTLY LQMNSLRAED TAVYYCAKGS
101 GFDYWGQGTL VTVSS

```

**Variable domain of the light chain (VL):**

```

1   EIVLTQSPGT LSLSPGERAT LSCRASQSVS SSYLAWYQQK PGQAPRLLIY
51  GASSRATGIP DRFSGSGSGT DFTLTISRLE PEDFAVYYCQ QYGSSPLTFG
101 QGTKVEIK

```

- ***T cell bispecific antibody:***

**Antibody light chain with CD3 $\epsilon$  binding domain (CrossMAb format):**

**Amino acid 1 to 19:** Signal peptide, **20 to 126:** Variable domain of the light chain of the murine CD3 $\epsilon$  binder (VL), **129 to 225:** CH1 IgG1

```

1   MGWSCIILFL VATATGVHSD IQMTQSPSSL PASLGDRVTI NCQASQDISN
51  YLNWYQQKPG KAPKLLIYYT NKLADGVPSR FSGSGSGRDS SFTISSLESE
101 DIGSYQCQQY YNYPWTFGPG TKLEIKSSAK TTPPSVYPLA PGSAAQTNSM
151 VTLGCLVKGY FPEPVTVTWN SGLSSGVHT FPAVLQSDLY TLSSSVTVPS
201 SPRPSETVTC NVAHPASSTK VDKKIVPRDC

```

**Antibody heavy chain with CD3 $\epsilon$  binding domain (CrossMAb format) and FAP binding domain:**

**Amino acid 1 to 19:** Signal peptide, **20 to 135:** Variable domain of the heavy chain of the murine CD3 $\epsilon$  binder (VH), **139 to 238:** Constant domain of the light chain (C $\kappa$ ), **143 to 252:** Linker (G $_4$ S) $_2$ , **253 to 368:** Variable domain of the heavy chain of the murine FAP binder (VH), **269 to 465:** CH1 IgG1, **479 to 585:** CH2 IgG1 (silent Fc-part: DAPG mutation: **510:** D270A / **574:** P329G), **586 to 692:** CH3 IgG1 (mutations for heterodimerization not shown)

```

1   MGWSCIILFL VATATGVHSE VQLVESGGGL VQPGKSLKLS CEASGFTFSG

```

```

51   YGMHWVRQAP GRGLESVAYI TSSSINIKYA DAVKGRFTVS RDNAKNLLFL
101  QMNILKSEDT AMYYCARFDW DKNYWGQGTM VTVSSASDAA PTVSIFPPSS
151  EQLTSGGASV VCFLNNFYPK DINVKWKIDG SERQNGVLNS WTDQDSKDST
201  YSMSSTLTLT KDEYERHNSY TCEATHKTST SPIVKSFNRN ECGGGGSGGG
251  GSEVQLLESG GGLVQPGGSL RLSCAASGFT FSSHAMSWVR QAPGKGLEWV
301  SAIWASGEQY YADSVKGRFT ISRDNSKNTL YLQMNSLRAE DTAVYYCAKG
351  WLGNFDYWGQ GTLVTVSSAK TTPPSVYPLA PGSAAQTNSM VTLGCLVKGY
401  FPEPVTVTWN SGSLSSGVHT FPAVLQSDLY TLSSSVTVPS SPRPSETVTC
451  NVAHPASSTK VDKKIVPRDC GCKPCICTVP EVSSVFIFPP KPKDVLITIL
501  TPKVTCVVVA ISKDDPEVQF SWFVDDVEVH TAQTQPREEQ FNSTFRSVSE
551  LPIMHQDWLN GKEFKCRVNS AAFGAPIEKT ISKTKGRPKA PQVYTIPPPK
601  EQMAKDKVSL TCMITDFFPE DITVEWQWNG QPAENYKNTQ PIMNTNGSYF
651  VYSKLVNQQS NWEAGNTFTC SVLHEGLHNN HTEKSLSHSP GK

```

#### **Antibody heavy chain with FAP binding domain:**

**Amino acid 1 to 19:** Signal peptide, **20 to 135:** Variable domain of the heavy chain of the murine FAP binder (VH), **136 to 232:** CH1 IgG1, **246 to 352:** CH2 IgG1 (silent Fc-part: DAPG mutation: **277:** D270A / **341:** P329G), **353 to 459:** CH3 IgG1 (mutations for heterodimerization not shown)

```

1   MGWSCIILFL VATATGVHSE VQLLESGGGL VQPGGSLRLS CAASGFTFSS
51  HAMSWSVRQAP GKGLEWVSAI WASGEQYYAD SVKGRFTISR DNSKNTLYLQ
101 MNSLRAEDTA VYYCAKGWLG NFDYWGQGTL VTVSSAKTTP PSVYPLAPGS
151 AAQTNSMVTL GCLVKGYFPE PVTVTWNSGS LSSGVHTFPA VLQSDLYTLS
201 SSVTVPSSPR PSETVTCNVA HPASSTKVDK KIVPRDCGCK PCICTVPEVS
251 SVFIFPPKPK DVLITITLTPK VTCVVVAISK DDPEVQFSWF VDDVEVHTAQ
301 TQPREEQFNS TFRSVSELP MHQDWLNGKE FKCRVNSAAF GAPIEKTISK
351 TKGRPAPQV YTIPPPKEQM AKDKVSLTCM ITDFFPEDIT VEWQWNGQPA
401 ENYKNTQPI NTNGSYFVYS KLVNQQSNWE AGNTFTCSVL HEGLNHHTE
451 KSLSHSPGK

```

#### **Antibody light chain with FAP binding domain:**

**Amino acid 1 to 19:** Signal peptide, **20 to 127:** Variable domain of the light chain of the murine FAP binder (VL), **131 to 230:** Constant domain of the light chain (Ck)

```

1   MGWSCIILFL VATATGVHSE IVLTQSPGTL SLSPGERATL SCRASQSVSR
51  SYLAWYQQKPK GQAPRLLIIG ASTRATGIPD RFSGSGSGTD FTLTISRLEP
101 EDFAVYYCQQ GQVIPPTFGQ GTKVEIKRAD AAPTVSIFPP SSEQLTSGGA
151 SVVCFLNNFY PKDINVKWKI DGSERQNGVL NSWTDQDSKD STYSMSSTLT
201 LTKDEYERHN SYTCEATHKT STSPIVKSFN RNEC

```

- **Anti-XCR1 antibody:**

**Antibody heavy chain:**

**Amino acid 1 to 19:** Signal peptide, **20 to 135:** Variable domain of the heavy chain of the murine XCR1 binder (VH), **141 to 233:** CH1 IgG2c, **257 to 360:** CH2 IgG2c (silent Fc-part: LALA mutation: **257:** L234A / **258:** L235A, DAPG mutation: **293:** D270A / **352:** P329G), **369 to 465:** CH3 IgG2c, **470 to 479:** Sortase-tag, **480 to 489:** Poly-histidine-tag

```

1   MGWSCIILFL VATATGVHSQ VQLQQPGAEL VKPGASVKLS CKASGYTFTN
51  YWIHWMKQRP GQGLEWIGMI HPNSDNTKYN EKFKAKAILT VDKSSSTAYM
101 QLSSLTSEDS AVYYCARFAN DGAYWGQGTL VTVSAAKTTA PSVYPLAPVC
151 GGTGSSVTL  GCLVKGYFPE PVTLTWNSGS LSSGVHTFPA LLQSGLYTLS
201 SSVTVTSNTW PSQTITCNVA HPASSTKVDK KIEPRVPITQ NPCPPLKECP
251 PCAAPDAAGG PSVFIFPPKI KDVLMIKSLP MVTCTVVDVS EDAPDVQISW
301 FVNNVEVHTA QTQTHREDYN STLRVVSALP IQHQDWMSGK EFKCKVNNRA
351 LGSPIEKTIS KPRGPVRAEQ VYVLPPEAE MTKKEFSLTC MITGFLPAEI
401 AVDWTSNGRT EQNYKNTATV LDSDGSYFMY SKLRVQKSTW ERGSLFACSV
451 VHEGLHNHLT TKTISRSLGG GGGSLPETGG SGSHHHHHH

```

**Antibody light chain:**

**Amino acid 1 to 19:** Signal peptide, **20 to 131:** Variable domain of the light chain of the murine XCR1 binder (VL), **135 to 234:** Constant domain of the light chain (Ck)

```

1   MGWSCIILFL VATATGVHSD VVVTQTPLSL PVSLGDPASI SCKSSQSLVH
51  SNGNTYLHWY LQKPGQSPKL LIYKISNRFK GVPDRFSGSG SGTDFTLKIS
101 RVEAEDLGVY FCSQNTHPY TFGGGTKLEI KRADAAPTQS IFPPSSEQLT
151 SGGASVVCFL NNFYPKDINV KWKIDGSERQ NGVLNSWTDQ DSKDSTYSMS
201 STLTLTKDEY ERHNSYTCEA THKTSTSPIV KSFNRNEC

```

## 12 DANKSAGUNG

An erster Stelle danke ich meinem Mentor Dr. Hendrik Knötgen für die hervorragende Betreuung der Dissertation sowie für die Überlassung einer sehr interessanten Promotions-Thematik. Durch seine Unterstützung und Förderung konnte ich mir auf dem Gebiet der Biotechnologie und der Immunonkologie ein breites Wissen aneignen.

Außerdem möchte ich mich herzlich bei Dr. Frank Herting bedanken, der es mir ermöglicht hat, diese Arbeit in der Abteilung Pharmakologie durchzuführen und die Dissertation vor allem im Rahmen der in vivo Studien betreut hat.

Ein großer Dank geht desweiteren an Prof. Dr. Eckhard Wolf für die akademische Betreuung der Doktorarbeit und für die Bereitschaft, diese gegenüber der Tierärztlichen Fakultät der Ludwig-Maximilians-Universität München zu vertreten.

Ohne die Unterstützung von den Kollegen aus der Pharmakologie wäre meine Arbeit sicher nicht in diesem Umfang realisierbar gewesen. Ein großer Dank geht hierbei an das Labor von Dr. Yvonne Kienast für meine Aufnahme in die Arbeitsgruppe. Besonders möchte ich Carsten Wolter, Stefan Hört und Christa Bayer für die tatkräftige Unterstützung bei den in vivo Arbeiten danken. Auch für die Hilfe von den Praktikanten Marco Gründl und Anne-Kathrin Winter möchte ich mich an dieser Stelle herzlich bedanken. Weiterhin danke ich Stefan Bissinger und Dr. Michael Dobosz aus der Arbeitsgruppe von Dr. Thomas Pöschinger für die Bereitstellung von bereits etablierten Technologien und die kompetente Hilfestellung bei den bildgebenden Verfahren. Auch bei meinen Laborkollegen Monika Lechner und Marco Friedrich aus der Arbeitsgruppe von Dr. Esther Weinberger möchte ich mich für das gute Arbeitsklima und ihre Hilfe bei Fragen aller Art bedanken. Einen besonderen Dank möchte ich Verena Brand aussprechen, die mir nicht nur bei der Immunhistochemie sondern auch bei so manchen Enttäuschungen während der Doktorarbeit mit Rat und Tat zur Seite stand und in der Zeit bei Roche zu einer sehr guten Freundin wurde.

Einen Dank richte ich ebenfalls an Dr. Tobias Schnitzer und Dr. Helmut Niersbach, die vor allem bei tierversuchskundlichen Fragestellungen und beim Genehmigungsverfahren der Tierversuche eine große Unterstützung waren. Außerdem bedanke ich mich bei den Tierpflegern für die optimale Betreuung der Tiere, wodurch ein reibungsloser Ablauf der in vivo Studien gewährleistet war.

Ein großer Dank gebührt auch dem pMHC1-IgG Projektteam. Hierbei möchte ich vor allem Dr. Martina Schmittnägel für die Übergabe des Projektes und die anfängliche Unterstützung sowohl

in wissenschaftlicher als auch in freundschaftlicher Hinsicht danken. Desweiteren danke ich Dr. Sabine Imhof-Jung und ihrer Arbeitsgruppe, im Besonderen Katrin Krause, für die Hilfe bei den molekularbiologischen Arbeiten für die Herstellung der Fusionsmoleküle und Dr. Eike Hoffmann und ihrer Arbeitsgruppe mit Michael Tischler und Dominik Weigl für die Aufreinigung der pMHCI-IgG Proteine. Außerdem möchte ich Dr. Georg Drabner und seiner Arbeitsgruppe für die Analytik der Antikörperfusionen und Dr. Guy Georges für das Modeling der Proteinstrukturen und seine Hilfe bei allen Struktur-relevanten Fragen danken.

Ich danke weiterhin Dr. Christian Klein und Dr. Pablo Umana für ihre Unterstützung in wissenschaftlichen Fragestellungen und bei der Weiterentwicklung der pMHCI-IgG Fusionsmoleküle.

Außerdem danke ich Dr. Claudio Sustmann und Dr. Martin Steegmaier für die Betreuung innerhalb der Abteilung LMR Discovery und die Unterstützung bei organisatorischen und themenbezogenen Fragen.

Bei Dr. Maria Mertens möchte ich mich für die Überprüfung der Arbeit von der patentrechtlichen Seite bedanken.

Außerdem bedanke ich mich bei Brigitta Reger für die enorme Hilfsbereitschaft, nicht nur bei den Bestellungen.

Nicht zuletzt möchte ich mich bei allen Mitarbeitern von Roche pRED bedanken, die durch eine freundliche Atmosphäre und ein sehr gutes Arbeitsklima zum Gelingen dieser Arbeit beigetragen haben.

Auch den Kollaborationspartnern, die in dieses Projekt involviert sind, möchte ich einen Dank aussprechen. Zum einen geht ein großer Dank an Prof. Dr. Richard Kroczeck vom Robert-Koch-Institut in Berlin, der es ermöglichte die XCR1-vermittelte Vakzinierung im Rahmen des pMHCI-IgG-Projektes anzuwenden. Zum anderen möchte ich den Kollaborationspartnern Dr. Ann Hill and Dr. Michael Munks vom Department of Molecular Microbiology & Immunology der Oregon Health & Science University, die ebenfalls mit den pMHCI-IgG Fusionsmolekülen arbeiten, für ihre Unterstützung und Mitarbeit bei diesem Projekt danken.

Abschließend gilt mein tiefster Dank meinen lieben Eltern, die immer an meiner Seite stehen und mich fortwährend unterstützen. Sie haben es überhaupt erst ermöglicht, dass diese Arbeit zustande kommt.